UNIVERSIDAD COMPLUTENSE DE MADRID

FACULTAD DE FARMACIA

DEPARTAMENTO DE FARMACIA GALÉNICA Y TECNOLOGÍA ALIMENTARIA

TESIS DOCTORAL

Development of lipid nanocapsules as a strategy to overcome the passage across the blood-brain barrier of drug substances acting on the central nervous system

Desarrollo de nanocápsulas lipídicas como estrategia para facilitar el paso a través de la barrera hematoencefálica de fármacos que actúan a nivel del sistema nervioso central

MEMORIA PARA OPTAR AL GRADO DE DOCTOR

PRESENTADA POR

Juan Aparicio Blanco

DIRECTORA

Ana Isabel Torres Suárez

Madrid, 2019

UNIVERSIDAD COMPLUTENSE MADRID

Facultad de Farmacia

Departamento de Farmacia Galénica y Tecnología Alimentaria

DESARROLLO DE NANOCÁPSULAS LIPÍDICAS COMO ESTRATEGIA PARA FACILITAR EL PASO A TRAVÉS DE LA BARRERA HEMATOENCEFÁLICA DE FÁRMACOS QUE ACTÚAN A NIVEL DEL SISTEMA NERVIOSO CENTRAL

DEVELOPMENT OF LIPID NANOCAPSULES AS A STRATEGY TO OVERCOME THE PASSAGE ACROSS THE BLOOD-BRAIN BARRIER OF DRUG SUBSTANCES ACTING ON THE CENTRAL NERVOUS SYSTEM

MEMORIA

Presentada para optar al grado de Doctor en Farmacia con Mención Internacional por la Universidad Complutense de Madrid por

Juan Aparicio Blanco

Tesis doctoral dirigida por

Ana Isabel Torres Suárez

Profesora Titular de Universidad

Madrid, 2018

UNIVERSIDAD COMPLUTENSE DE MADRID

Facultad de Farmacia

Departamento de Farmacia Galénica y Tecnología Alimentaria

Tesis doctoral

DESARROLLO DE NANOCÁPSULAS LIPÍDICAS COMO ESTRATEGIA PARA FACILITAR EL PASO A TRAVÉS DE LA BARRERA HEMATOENCEFÁLICA DE FÁRMACOS QUE ACTÚAN A NIVEL DEL SISTEMA NERVIOSO CENTRAL

DEVELOPMENT OF LIPID NANOCAPSULES AS A STRATEGY TO OVERCOME THE PASSAGE ACROSS THE BLOOD-BRAIN BARRIER OF DRUG SUBSTANCES ACTING ON THE CENTRAL NERVOUS SYSTEM

Juan Aparicio Blanco

Madrid, 2018

Ana Isabel Torres Suárez, Profesora Titular del Departamento de Farmacia Galénica y Tecnología Alimentaria de la Facultad de Farmacia de la Universidad Complutense de Madrid

CERTIFICA

que la presente memoria titulada "**Desarrollo de nanocápsulas lipídicas como estrategia para facilitar el paso a través de la barrera hematoencefálica de fármacos que actúan a nivel del sistema nervioso central**" presentada por **Juan Aparicio Blanco** para optar al **grado de Doctor en Farmacia**, ha sido elaborada bajo su dirección en el Departamento de Farmacia Galénica y Tecnología Alimentaria; y que una vez revisada, autoriza su presentación a fin de que pueda ser juzgada por el tribunal constituido a tal efecto.

La memoria se presenta como compendio de publicaciones, que cumplen la normativa vigente de la Facultad de Farmacia de la Universidad Complutense de Madrid

Y para que así conste, firma el presente certificado en Madrid, a 8 de Junio de 2018

Profa. Dra. Ana Isabel Torres Suárez

Madrid, 2018

Las investigaciones realizadas en el presente trabajo se han llevado a cabo gracias al apoyo económico recibido de diferentes organismos públicos:

- Concesión de un contrato dentro del programa de Formación del Profesorado Universitario (FPU) del Ministerio de Educación, Cultura y Deporte en la convocatoria de 2013 con referencia FPU13/02325 (Septiembre 2014-Septiembre 2018)
- Concesión de una ayuda complementaria para la realización de una estancia breve en l'Université d'Angers dentro del programa de Formación del Profesorado Universitario (FPU) del Ministerio de Educación, Cultura y Deporte en la convocatoria de 2014 con referencia EST14/00229 (Septiembre 2015-Noviembre 2015)
- Concesión de dos ayudas complementarias para la realización de sendas estancias breves en The Open University dentro del programa de Formación del Profesorado Universitario (FPU) del Ministerio de Educación, Cultura y Deporte en las convocatorias de 2015 y 2016 con referencias EST15/00534 y EST16/00556 (Septiembre 2016-Diciembre 2016; Junio 2017-Agosto 2017)
- Concesión de la ayuda PR26/16-20311 para la financiación del proyecto de investigación Santander-Universidad Complutense de Madrid "Desarrollo de nanopartículas funcionalizadas con cannabidiol y evaluación de su biodistribución en sistema nervioso central" (IP: Ana Isabel Torres Suárez) en la convocatoria de 2016
- Fondo Específico de Investigación de la Universidad Complutense de Madrid FEI16/83 "Desarrollo de sistemas de liberación prolongada y de vectorización de fármacos de administración por vía oral y parenteral" (IP: Ana Isabel Torres Suárez).
- Financiación del programa de Grupos de Investigación Santander-Universidad Complutense de Madrid GR35/10, Grupo: Administración parenteral de medicamentos.

“Lo esencial es invisible a los ojos”

“What is essential is invisible to the eye”

„Das Wesentliche ist für die Augen unsichtbar“

« L’essentiel est invisible pour les yeux »

Le petit prince

Antoine de Saint-Éxupery

A mis padres, por su disponibilidad y paciencia infinitas

Agradecimientos

A la Dra. Anabel Torres Suárez, por haberme acogido en su grupo de investigación y haber avalado y dirigido el presente proyecto de tesis. Gracias por proporcionarme una formación multidisciplinar.

A los Dres. Nacho Romero y Jean Pierre Benoit, por su interés en el proyecto de tesis al haber aceptado y avalado mi solicitud de estancia en sus centros de investigación (School of Life, Health and Chemical Sciences (LHCS, The Open University) y L'unité Micro et Nanomédecines Biomimétiques (MINT, Université d'Angers), respectivamente).

A todos los miembros de los equipos de investigación en los que he desempeñado mi labor investigadora durante mi tesis doctoral, con especial mención al Grupo de Investigación Administración Parenteral de Medicamentos de la Universidad Complutense de Madrid, a los profesores del Departamento de Farmacia Galénica y Tecnología Alimentaria que han supervisado mi colaboración docente en prácticas, al Dr. David K. Male, a la Dra. Giovanna Lollo, a la Dra. Lina Formica, a Ana Isabel Fraguas, a Rebeca Simancas, a Miguel Rodríguez, a Héctor García, a Mónica Pérez, a Shereen Nizari, a Conor McQuaid, a Edu Frías, a David Roig, a Sonia Azzegagh, a Perla Pucci, a la Dra. Laura Contu, a la Dra. Ana Cadete, a la Dra. Bathabile Ramalapa, a la Dra. Chantal Valcourt y a Ester Baixauli.

Al Ministerio de Educación, Cultura y Deporte del Gobierno de España por la financiación de este proyecto de tesis mediante la concesión del contrato de Formación del Profesorado Universitario FPU13/02325 y de las ayudas a la movilidad para estancias breves EST14/00229, EST15/00534 y EST16/00556.

Al Dr. Víctor Sebastián Cabeza, por su inestimable ayuda con el microscopio electrónico de transmisión.

Al Servicio de Cultivos Celulares del Centro de Investigaciones Biológicas, especialmente a Carmen Doñoro, por su cercanía y profesionalidad.

A los profesores de otros departamentos de la Facultad de Farmacia que han contribuido a mi formación doctoral y/o al desarrollo del presente proyecto de tesis (con especial mención a los Dres Juan Carlos Doadrio, Luis García, Pilar Gómez-

Serranillos, Elena González, Pilar Iniesta, María de la O López-Vázquez, Antonia Martín y Karla Slowing).

Al Spanish-Portuguese Local Chapter de la Controlled Release Society, por haberme permitido formar parte del comité organizador como sección joven de la "XII Spanish-Portuguese Conference on Controlled Drug Delivery: Tailoring drug delivery systems to the patients' needs" celebrado en Coimbra en enero de 2018, en especial a su Junta Directiva (João Nuno, Dolores Torres, Manuela Gaspar, María Blanco y Manoli Igartua) y a mis compañeros Simón Pascual, Pedro Fonte, Sonia Vicente-Ruiz y Sandra Jesus.

A mis familiares y amigos que me han acompañado, apoyado y comprendido durante este periodo. Subrayo especialmente mi agradecimiento a mis padres, a los cuales dedico esta tesis, porque este mérito es también suyo; a Paquita, por ser mi oráculo en momentos bajos; a Pablo, por ser mis manos artísticamente hablando además de un buen amigo; a Martin, ich danke dir dafür, eine nahe persönliche und berufliche Unterstützung aus der Ferne zu sein; y a mis ases, por apostar por mí, desde antes incluso de que yo mismo lo hiciese.

A todos vosotros y a todos los que habéis posibilitado de algún modo la realización de esta tesis, gracias.

Índice de contenidos

Índice de contenidos

Resumen

Desarrollo de nanocápsulas lipídicas como estrategia para facilitar el paso a través de la barrera hematoencefálica de fármacos que actúan a nivel del sistema nervioso central

Introducción

Las patologías que afectan al sistema nervioso central representan un desafío terapéutico de primer orden por su incidencia creciente y la falta de tratamientos eficaces ante la limitación del acceso a sistema nervioso central de la mayoría de fármacos administrados por vía sistémica por parte de la barrera hematoencefálica. Algunas de las estrategias descritas para sortear esta barrera, incluyendo la administración intracerebral o la disrupción artificial de sus uniones estrechas, suponen un elevado riesgo de daño neurológico. Por ello, actualmente se persigue diseñar transportadores de fármacos capaces de atravesar de manera eficiente el endotelio cerebral tras su administración intravenosa. En concreto, la vectorización de agentes antineoplásicos en nanotransportadores para el tratamiento de tumores cerebrales supondría un sustancial avance en terapéutica por la reducción de efectos secundarios derivados de su distribución sistémica. Dado que la distribución de transportadores a sistema nervioso central no puede depender en exclusiva de la vectorización pasiva, a fin de favorecer su paso a través de la barrera hematoencefálica, se está investigando la incorporación de distintos ligandos a estos sistemas.

Objetivos

El objetivo global de esta tesis doctoral es diseñar, desarrollar y evaluar a nivel preclínico un nanotransportador lipídico que sea capaz de atravesar la barrera hematoencefálica para vectorizar fármacos a nivel del sistema nervioso central tras una administración sistémica. Este objetivo general se desglosa en tres objetivos específicos:

1. Estudiar los parámetros experimentales determinantes en la obtención de nanocápsulas lipídicas mediante el método térmico de inversión de fases para, en último término, habilitar la producción de nanocápsulas lipídicas bajo demanda.

2. Desarrollar una novedosa estrategia de funcionalización de nanocápsulas lipídicas con cannabidiol para favorecer su distribución a sistema nervioso central y evaluar su potencial in vitro e in vivo.

3. Encapsular cannabidiol en el núcleo oleoso de las nanocápsulas lipídicas y evaluar in vitro su eficacia como sistemas de liberación prolongada con actividad frente a la línea celular U373MG de glioblastoma humano y, en último término, superar los problemas de formulación tradicionalmente asociados con estos agentes achacables a su elevada lipofilia que han venido limitando su potencial terapéutico. Asimismo, se persigue evaluar la estrategia de funcionalización con cannabidiol para potenciar la captación por células de glioma.

Esta tesis se presenta como compendio de publicaciones con entidad propia. Se estructura en capítulo, cada uno de los cuales aborda uno de los objetivos específicos descritos. Además, cada capítulo está precedido por una minuciosa introducción acerca del estado actual de cada tema. En conjunto, el trabajo de tesis comprende un capítulo de libro, tres publicaciones en revistas indexadas en el JCR (dos en el primer decil y el uno en el primer cuartil de la categoría “Ciencia de los materiales, biomateriales”), y otros tres artículo aún no publicados.

Resultados

Los principales resultados se sintetizan en los siguientes puntos:

1. La obtención de nanocápsulas lipídicas con tamaños de partícula predeterminados para aumentar las posibilidades de éxito de tratamientos de patologías del sistema nervioso central puede conseguirse mediante el método térmico de inversión de fases, pues el diámetro volumen se ajusta a un modelo matemático en una variable: el cociente másico entre la fase interna oleosa y el tensioactivo. Este modelo es válido para nanocápsulas blancas y cargadas con fármaco.

2. El tamaño de las nanocápsulas lipídicas condiciona la capacidad de paso a través de la barrera hematoencefálica en el intervalo 20-60 nm: en concreto, una disminución de tamaño incrementa en 2,5 y 1,6-2,5 veces su paso a través de la barrera hematoencefálica *in vitro* e *in vivo*, respectivamente. Por otra parte, la funcionalización de las nanocápsulas lipídicas con el fitocannabinoide cannabidiol aumenta el paso a través de barrera hematoencefálica 4,3 y 2,5 veces *in vitro* e *in vivo*, respectivamente.

3. El tamaño de las nanocápsulas lipídicas también condiciona la captación por células de glioma: en concreto, una disminución de tamaño incrementa 3-3,5 veces la captación por células de glioma. Asimismo, el tamaño de las nanocápsulas lipídicas condiciona la liberación de fármacos: nanocápsulas de 20 nm cargadas con cannabidiol reducen invariablemente 3 veces los valores de CI_{50} en comparación con sus homólogas de 50 nm. Además, la funcionalización de nanocápsulas lipídicas con el fitocannabinoide cannabidiol aumenta la captación por células de glioma 3,4 veces en comparación con sus homólogos del mismo tamaño no funcionalizados.

Conclusiones

El paso a través de barrera hematoencefálica y la captación por células de glioma, así como la velocidad de liberación de fármacos pueden modularse variando el tamaño particular de las nanocápsulas lipídicas. El método térmico de inversión de fases posibilita su obtención bajo demanda en términos de tamaño particular. Además, el cannabidiol representa una molécula no inmunogénica para la vectorización activa a cerebro y glioma, con potencial para el tratamiento de gliomas dados sus sinergias con los protocolos de quimio y radioterapia. En conjunto, las nanocápsulas lipídicas, cargadas y funcionalizadas con cannabidiol, constituyen prometedores candidatos con capacidad de vectorización a través de barrera hematoencefálica y de células de glioma. Su potencial terapéutico debe ser evaluado en modelos animales de glioma.

Summary

Development of lipid nanocapsules as a strategy to overcome the passage across the blood-brain barrier of drug substances acting on the central nervous system

Introduction

Diseases affecting the central nervous system (CNS) should be regarded as a major health challenge due to their steadily rising incidences and to the current lack of effective treatments given the hindrance to brain drug delivery imposed by the blood-brain barrier (BBB). Some of the described delivery strategies to circumvent the BBB such as the direct intracerebral administration and the artificial disruption of the tight junctions involve high risk of neurological damage. Hence, every effort is currently being devoted to achieving efficient transport across the brain endothelium with targeted drug carriers following minimally-invasive intravenous injection. In particular, nanomedicine is chiefly germane to the field of chemotherapy wherein dose availability at the target site cannot be enhanced by dose increase for fear of severe side effects. Since efficient brain targeting should not solely rely on passive targeting, brain active targeting of nanomedicines into the CNS is being explored.

Aims

The global aim of this thesis is to design, develop and evaluate pre-clinically a BBB-targeted lipid nanocarrier for brain targeting after its intravenous administration. This global aim can be broken down into these specific aims:

1. To ascertain the parameters that drive the formation of lipid nanocapsules (LNCs) by the phase inversion temperature (PIT) method to eventually allow obtaining size-tailored LNCs.

2. To develop LNCs functionalized with CBD as a pioneering non-immunogenic BBB-targeting strategy and to evaluate their brain targeting ability both *in vitro* and *in vivo*.

3. To encapsulate CBD in the oily core of LNCs at high drug loading to test their *in vitro* efficacy as extended-release carriers against a human glioblastoma cell line to ultimately overcome the dosing problems associated with cannabinoids that have constrained their therapeutic potential, and to evaluate the *in vitro* glioma-targeting ability of LNCs functionalized with CBD.

This thesis is presented as a compendium of research articles with stand-alone entity for publication. It is structured in chapter, each of which deals with a specific aim of the thesis project. Each chapter is preceded with a thorough introduction on the state-of-the-art of each issue. Altogether, the thesis encompasses a chapter of a book, three published articles (two in D1 journals and the third one in a Q1 journal in the category “Materials science, biomaterials”), and three other articles that have not yet been published.

The main results can be summarized in the following highlights:

1. Fine size-tailoring of LNCs to increase the chances of success for the treatment of CNS diseases can be achieved by the PIT method. The particle size of LNCs can be accurately predicted beforehand by a validated univariate mathematical model as a function of the internal oily phase: surfactant mass ratio for various oily phase-surfactant combinations. Importantly, this univariate mathematical model serves to obtain not only size-tailored blank LNCs but also drug-loaded LNCs.

2. Particle size certainly influences the BBB-transcytosis ability of LNCs within the range 20-60 nm: in particular, a decrease in the particle size of LNCs yields a 2.5- and 1.6-2.5-fold increase in the transcytosis extent across the BBB *in vitro* and *in vivo*, respectively. Moreover, the functionalization of LNCs with the phytocannabinoid cannabidiol (CBD) increases their brain targeting properties by 4.3- and 2.5-fold *in vitro* and *in vivo*, respectively.

3. Particle size also plays a pivotal role in the *in vitro* glioma targeting ability of LNCs: in particular, a decrease in the particle size of LNCs yields a 3.0-3.5-fold increase in *in vitro* uptake by human glioblastoma cells. Likewise, the size of LNCs influences the extent of CBD release: 20 nm-sized CBD-loaded LNCs reduce by 3.0-fold the IC_{50} value of 50-nm sized CBD-loaded LNCs. Furthermore, the functionalization of LNCs with CBD also enhanced their *in vitro* glioma targeting properties by 3.4-fold in comparison with their equally-sized undecorated counterparts.

Conclusions

Both the BBB and glioma targeting ability and the drug release rate can be tailored by varying the particle size of LNCs. The PIT method enables size-tailored LNCs to be obtained on demand. Additionally, CBD represents a pioneering exogenous and non-immunogenic targeting molecule for brain and glioma targeting of LNCs that may well serve to widen the therapeutic armamentarium against malignant brain tumors thanks to its synergistic effects with the currently available chemo- and radiotherapy. Altogether, LNCs prepared by the PIT method, loaded and functionalized with CBD arise as auspicious dually-targeted (both across the brain endothelia and the brain tumor cells) candidates for intravenous treatment of glioma. Consequently, these formulations deserve subsequent *in vivo* evaluation in an animal model of disease.

Objetivos

Las patologías que afectan al sistema nervioso central constituyen un grupo heterogéneo que comprende no sólo las alteraciones psiquiátricas y neurológicas, dentro de las que se encuadran las enfermedades neurodegenerativas; sino también los ictus isquémicos, los tumores cerebrales y algunos procesos infecciosos. Desafortunadamente, la eficacia de los tratamientos actuales de estas enfermedades es, en muchos casos, cuestionable, ya que la barrera hematoencefálica limita el acceso a sistema nervioso central de la mayoría de fármacos administrados por vía sistémica. Esto hace de las patologías que afectan al sistema nervioso central no sólo el área clínica con mayor crecimiento, sino también el grupo con más necesidades terapéuticas no cubiertas.

La utilización de sistemas transportadores de fármacos con elevada capacidad de paso a través de la barrera hematoencefálica representa una prometedora estrategia para aumentar la eficacia de los tratamientos de las patologías que afectan al sistema nervioso central, ya que podrían favorecer la liberación selectiva del fármaco a este nivel, reduciendo los efectos secundarios asociados a la distribución sistémica del fármaco libre. Particularmente, la vectorización de agentes antineoplásicos en nanotransportadores para el tratamiento de tumores cerebrales supondría un sustancial avance en terapéutica por la reducción de efectos secundarios derivados de su distribución sistémica.

De entre los nanotransportadores en investigación, los vectores lipídicos se erigen como prometedores candidatos alternativos a los vectores poliméricos por su biocompatibilidad y biodegradabilidad. A fin de favorecer su paso a través de la barrera hematoencefálica, se está investigando la incorporación de ligandos específicos a estos sistemas.

En este contexto, y continuando con la línea del grupo de investigación relativa al desarrollo de sistemas de liberación modificada de fármacos de administración por vía parenteral para distintas patologías del sistema nervioso central, el objetivo global de esta tesis doctoral es diseñar, desarrollar y evaluar a nivel preclínico un nanotransportador lipídico que sea capaz de atravesar la barrera hematoencefálica para vectorizar el fármaco a nivel del sistema nervioso central tras una administración

sistémica. Este objetivo general se desglosa en tres objetivos específicos, que se abordarán en los tres primeros capítulos de esta memoria, cada uno de los cuales irá precedido por una minuciosa introducción acerca del estado actual de cada uno de los temas. Estos objetivos específicos son:

1. Diseñar, elaborar y caracterizar nanocápsulas lipídicas obtenidas por el método térmico de inversión de fases desde un planteamiento racional basado en los requisitos que los nanotransportadores han de satisfacer para desarrollar terapias destinadas a tratar patologías del sistema nervioso central. Se seleccionan las nanocápsulas lipídicas por la elevada capacidad de encapsulación de su núcleo oleoso (frente a otros transportadores lipídicos, a saber liposomas y nanopartículas lipídicas sólidas), así como por la estabilidad conferida por su cubierta sólida. Asimismo, la elección del método térmico de inversión de fases para su obtención se fundamenta en su carácter energéticamente eficiente que cumple las premisas para su implementación a nivel industrial, hecho que constituye un requisito imprescindible para el acceso al mercado de toda nueva formulación. Se realiza un estudio exhaustivo de dicha técnica: por un lado, los parámetros experimentales que conducen a la obtención de nanocápsulas de tamaños específicos, y por otro lado, cómo afecta al proceso la modificación de la naturaleza de la fase oleosa y/ o del tensioactivo, para, en último término, habilitar la producción de nanocápsulas lipídicas “a la carta” a tenor de las características impuestas por el fin terapéutico específico.

La parte relativa a la caracterización morfológica de los nanotransportadores por microscopía electrónica de transmisión se ha realizado en colaboración con el profesor Víctor Sebastián Cabeza, del Departamento de Ingeniería Química y Tecnologías del Medio Ambiente del Instituto Universitario de Investigación en Nanociencia de Aragón (Universidad de Zaragoza).

El desarrollo de este objetivo específico de la tesis doctoral se aborda en el primer capítulo, del que forman parte las publicaciones científicas “Managing CNS Tumors: The Nanomedicine Approach”, (“New Approaches to the Management of Primary and Secondary CNS Tumors”, ISBN 978-953-51-3052-9, Editor: Lee Roy Morgan, Publisher: InTech, March 2017) y “Size-tailored nanocapsules by a single step energy-efficient procedure: the phase inversion temperature method revisited”.

2. Desarrollar una estrategia de funcionalización de nanocápsulas lipídicas con cannabidiol (el principal fitocannabinoide desprovisto de acción psicoativa) para favorecer su distribución a sistema nervioso central. Esta estrategia tiene su fundamento en los datos farmacocinéticos de dicho cannabinoide en sangre y cerebro, obtenidos previamente en colaboración con el equipo del profesor Aron Lichtman (Virginia Commonwealth University, EEUU). A tal efecto, se realizan ensayos de viabilidad celular, captación y permeabilidad sobre la línea de endotelio cerebral humano hCMEC/D3. Este modelo celular para la evaluación del paso de las nanocápsulas a través de la barrera hematoencefálica se valida con ensayos de biodistribución en ratones. El objetivo es evaluar la influencia del tamaño de las nanocápsulas y de su funcionalización con cannabinoides en el paso a través de la barrera hematoencefálica *in vitro* e *in vivo*.

La parte correspondiente a la evaluación *in vitro* de este objetivo específico se ha realizado en colaboración con el grupo del profesor Ignacio Romero, posibilitada gracias a la concesión de dos ayudas complementarias para la realización de sendas estancias breves en School of Life, Health and Chemical Sciences (LHCS), The Open University, dentro del programa de Formación del Profesorado Universitario (FPU) del Ministerio de Educación, Cultura y Deporte en las convocatorias de 2015 y 2016 con referencias EST15/00534 y EST16/00556 (Septiembre 2016-Diciembre 2016; Junio 2017-Agosto 2017).

El desarrollo de este objetivo específico de la tesis doctoral se aborda en el segundo capítulo, del que forman parte las publicaciones científicas "*In vitro* screening of nanomedicines through the blood brain barrier: a critical review", (Biomaterials 103 (2016) 229-255, IF (2016): 8,402, D1 en las categorías "Engineering, biomedical" y "Materials science, biomaterials", ISSN: 0142-9612) y "Cannabidiol-targeted lipid nanocapsules across the blood-brain barrier: *in vitro* and *in vivo* evaluation".

3. Evaluar *in vitro* la eficacia de las nanocápsulas desarrolladas sobre una línea celular de glioma humano. Como agente antitumoral, se emplea el cannabidiol, con actividad antiproliferativa en modelos xenográficos de glioma en ratón acreditada por nuestro grupo de investigación con anterioridad en colaboración con el profesor Guillermo Velasco del Departamento de Bioquímica y Biología Molecular de la Facultad de Ciencias Biológicas de la Universidad Complutense de Madrid. En este sentido, se evalúa la influencia del tamaño de las nanocápsulas, así como la estrategia de funcionalización (desarrollada en el objetivo específico anterior) mediante estudios de captación y de viabilidad sobre la línea celular U373MG. La incorporación del cannabinoide en el núcleo oleoso de las nanocápsulas posibilita su administración por vía intravenosa, superando así los problemas de formulación tradicionalmente asociados con estos agentes achacables a su elevada lipofilia, y que en gran medida han venido limitando su potencial terapéutico.

Parte del trabajo relativo a este objetivo específico se ha realizado gracias a la concesión de una ayuda complementaria para la realización de una estancia breve en L'unité Micro et Nanomédecines Biomimétiques (MINT) (Université d'Angers) bajo la supervisión del profesor Jean Pierre Benoit, dentro del programa de Formación del Profesorado Universitario (FPU) del Ministerio de Educación, Cultura y Deporte en la convocatoria de 2014 con referencia EST14/00229 (Septiembre 2015-Noviembre 2015).

El desarrollo de este objetivo específico de la tesis doctoral se aborda en el tercer capítulo, del que forman parte las publicaciones científicas "Glioblastoma multiforme and lipid nanocapsules: a critical review", (Journal of Biomedical Nanotechnology 11 (2015) 1283-1311, IF (2015): 3,929, Q1 en la categoría "Materials science, biomaterials", ISSN: 1550-7033) y "The potential of lipid nanocapsules decorated and loaded with cannabidiol for the treatment of malignant gliomas: in vitro evaluation".

Para finalizar la presente memoria, y con el fin de dibujar para dibujar las líneas futuras en el campo de la nanomedicina aplicada a la terapia de neoplasias del

sistema nervioso central, se incluye un estudio acerca de las posibilidades que ofrecen los nanotransportadores para un seguimiento personalizado de los tumores cerebrales mediante el teragnósitico, tendencia en investigación que aúna tratamiento y diagnóstico por imagen. Dicho estudio lleva por título “Towards tailored management of malignant brain tumors with nanotheranostics” y ha sido publicado en Acta Biomaterialia 73 (2018) 52-63, IF (2016): 6.319, D1 en las categorías “Engineering, biomedical” y “Materials science, biomaterials”, ISSN: 1742-7061).

Aims

Diseases affecting the central nervous system (CNS) represent a heterogeneous group that encompasses not only mental and neurological disorders (including neurodegenerative diseases), but also ischemic strokes, brain tumors and some infectious diseases. Unfortunately, the efficacy of the current standard of care for these diseases remains, in most cases, questionable, since the blood-brain barrier (BBB) truly hinders the distribution to the CNS of the vast majority of drug substances administered systemically. Hence, brain diseases do not only represent the fastest-growing but also the largest area of unmet medical needs.

The use of drug carriers arises as an auspicious alternative to enhance the passage across the BBB, thereby promoting a selective distribution to the CNS with the ensuing reduction in adverse effects caused by peripheral distribution of the drug and improvement in the efficacy of the treatment of many of these diseases. Particularly, brain targeting of nanocarriers would be chiefly germane to the field of brain chemotherapy wherein dose availability at the target site cannot be enhanced by dose increase for fear of severe side effects.

Among the nanocarriers under investigation, lipid-based carriers arise as alternative candidates for brain drug delivery given their inherent low toxicity, biocompatibility and biodegradability. Indeed, the conjugation of many lipid-based nanocarriers with ligands that bind to receptors overexpressed on the brain endothelium is being explored with the purpose of effectivey improving the selective distribution of the therapeutic across the BBB.

Against this background of hindrance to brain delivery, and in line with the research area of the group focused on the development of sustained-release carriers for the treatment of brain diseases, the global aim of the present thesis is to design, develop and evaluate pre-clinically a BBB-targeted lipid nanocarrier for brain targeting after its intravenous administration. This global aim can be broken down into three specific aims, which will be addressed in the first three chapters of this dissertation. Each chapter will be preceded with a thorough introduction on the state-of-the-art of each issue. These specific aims are:

1. To design, obtain and characterize lipid nanocapsules prepared by the phase inversion temperature (PIT) method following a disease-driven approach, in particular the requisites imposed by CNS pathologies. Lipid nanocapsules are chosen according both to the high drug loading potential within their oily core (unlike other lipid carriers, namely liposomes and solid lipid nanoparticles), and to their kinetic stability provided by their solid shell. Likewise, the PIT method was selected on the grounds of their energetically efficient features that meet the requirements for a future implementation at an industrial level and which constitutes a requisite to achieve broad market access. On the one hand, we attain a comprehensive understanding of the role played by the experimental parameters that eventually drive the formation of size-tailored monodisperse lipid nanocapsules, and, on the other hand, we ascertain how the PIT process is affected by changes in the nature of both the oily phase and the surfactant, to ultimately allow obtaining lipid nanocapsules with features thoroughly designed beforehand on the basis of the pathophysiology of a specific disease.

The morphological analysis by transmission electron microscopy of the nanocapsules has been conducted in collaboration with Professor Víctor Sebastián Cabeza, from Department of Chemical Engineering and Environmental Technology and Institute of Nanoscience of Aragon (INA), University of Zaragoza (Spain).

The first chapter of this thesis tackles this specific aim and encompasses the scientific publications “Managing CNS Tumors: The Nanomedicine Approach”, (“New Approaches to the Management of Primary and Secondary CNS Tumors”, ISBN 978-953-51-3052-9, Editor: Lee Roy Morgan, Publisher: InTech, March 2017) and “Size-tailored nanocapsules by a single step energy-efficient procedure: the phase inversion temperature method revisited”.

2. To develop a functionalization strategy of lipid nanocapsules with cannabidiol (the main non-psychotropic phytocannabinoid) to enhance brain targeting. The rationale behind this strategy relies on previous pharmacokinetic data of cannabidiol in blood and brain of mice, with partition favorable to brain, obtained previously by the research group in collaboration with Professor Aron Lichtman from the Virginia Commonwealth University (EEUU). To this end, cell viability, uptake and permeability experiments with the human brain endothelial cell line hCMEC/D3 will be conducted. This cell-based model to evaluate the passage of nanocarriers across the BBB will be validated with results obtained from biodistribution studies in mice. Both the role played by particle size and functionalization with cannabinoids in the extent of passage across the BBB will be evaluated *in vitro* and *in vivo*.

The *in vitro* evaluation of this specific aim has been achieved thanks to two scholarships (EST15/00534 and EST16/00556) by the Spanish Ministry of Education within the Professor Training Programm (FPU) that enabled two research stays at the School of Life, Health and Chemical Sciences (LHCS), The Open University under the supervision of Professor Ignacio Romero (September 2016-December 2016; June 2017-August 2017).

The second chapter of this thesis tackles this specific aim and encompasses the scientific publications “*In vitro* screening of nanomedicines through the blood brain

barrier: a critical review", (Biomaterials 103 (2016) 229-255, IF (2016): 8.402, D1 in the categories "Engineering, biomedical" and "Materials science, biomaterials", ISSN: 0142-9612) and "Cannabidiol-targeted lipid nanocapsules across the blood-brain barrier: *in vitro* and *in vivo* evaluation".

3. To evaluate *in vitro* the efficacy of lipid nanocapsules on a human glioma cell line. As antitumor agent, cannabidiol will be used given its antiproliferative activity in xenografic models of glioma-bearing mice already tested by our research group in collaboration with Professor Guillermo Velasco from Complutense University (Spain). In this regard, both the role played by particle size and functionalization with cannabidiol will be evaluated *in vitro* on the U373MG cell line with uptake and cell viability experiments. The encapsulation of the cannabinoid within the oily core enables its intravenous administration, overcoming in this way formulation issues classically linked to these agents due to their high lipophilicity and that ultimately have constrained their therapeutic potential.

Part of this specific aim has been achieved thanks to a scholarship (EST14/00229) by the Spanish Ministry of Education within the Professor Training Programm (FPU) that enabled a research stay at L'unité Micro et Nanomédecines Biomimétiques (MINT) (Université d'Angers) under the supervision of Professor Jean Pierre Benoit (September 2015-November 2015).

The third chapter of this thesis tackles this specific aim and encompasses the scientific publications "Glioblastoma multiforme and lipid nanocapsules: a critical review", (Journal of Biomedical Nanotechnology 11 (2015) 1283-1311, IF (2015): 3.929, Q1 in the category "Materials science, biomaterials", ISSN: 1550-7033) and "The potential of lipid nanocapsules decorated and loaded with cannabidiol for the treatment of malignant gliomas: in vitro evaluation".

To conclude the present dissertation with an outline on future research directions within the field of the nanomedicine applied to the treatment of CNS neoplasms, a fourth chapter is included on the possibilities that nanocarriers offer to achieve a personalized follow-up of brain tumors by means of theranostics, a research hotspot that integrates treatment with imaging diagnosis. This chapter consists of a review article entitled "Towards tailored management of malignant brain tumors with nanotheranostics" and published in Acta Biomaterialia (Acta Biomaterialia 73 (2018) 52-63, IF (2016): 6.319, D1 in the categories "Engineering, biomedical" y "Materials science, biomaterials", ISSN: 1742-7061).

Chapter 1: Nanomedicine and central nervous system: on-demand development of lipid nanocapsules

Introduction

According to the *Mental health: new understanding, new hope* report by the World Health Organization, one in four people will be affected by mental or neurological disorders at some point in their lives, with approximately 450 million people worldwide currently suffering from such conditions. These prevalence data are expected to increase further due to the increase in life expectancy, emphasizing the need to face mental and neurological disorders as the greatest health challenge of the twenty-first century. Moreover, one-third of all health-related expenses are caused by brain disorders (these figures exceed those for diabetes or heart diseases) [1].

However, stricter regulations for drugs that act on the central nervous system (CNS) result in an average of 13 years and more than $1 billion needed to develop a brain treatment. This, in addition to the high failure rate in the late development process and insufficient funding, has impeded progress in achieving efficient therapies for most brain diseases.

With around a quarter of a million new cases of brain and other CNS tumors being diagnosed every year, these pathologies illustrate the best archetype of brain disorders with questionable treatment. Brain tumors are stratified according to a 'malignancy scale' closely related to clinical prognosis. The current standard approach in high grade brain tumors (grade IV) combines maximal surgical resection (if eligible) with radiotherapy and chemotherapy; as well as symptomatic treatment. The first line chemotherapy consists of temozolomide, whereas carmustine represents the second line treatment. Unfortunately, the efficacy of this treatment remains questionable, since recurrence happens within months after diagnosis, with a poor median survival of 14.6 months and 2-year survival rate of 26.5% [2].

This poor prognosis results from the lack of successful drug delivery across the blood–brain barrier (BBB) to the tumor bed, since the exposure of the tumor to sub-lethal drug concentrations helps select the drug-resistant tumor cells.

Indeed, primary brain tumors account for 2% of all cancers, while brain metastases occur in 10-30% of all cancer patients. This high incidence of intracranial metastases is primarily due to the fact that whereas new chemotherapeutic agents have improved prognosis for many cancers, they have failed to prevent spread of neoplasms into the CNS given their low penetration through the BBB [3].

Therefore, brain drug delivery must be properly addressed, as otherwise, new therapies will continue to fail. For this reason, innovative delivery strategies are emerging to attain therapeutically meaningful levels at the entire diseased brain area and ultimately improve treatment outcomes. In the late 1990s, Gliadel®, a biodegradable wafer that steadily delivers carmustine over three weeks, was approved by the FDA for patients with malignant gliomas. However, Gliadel® can only be implanted at the time of surgery, being thus limited to those patients for whom surgical tumor resection is indicated. Its approval laid the foundations for the engineering of biomaterials to develop drug delivery systems that can effectively overcome the brain delivery issues.

In this regard, nanomedicine, defined as the application of nanotechnology for medical purposes, represents the next generation of systems with potential for brain drug delivery, since colloid carriers could be targeted to enhance the availability of therapeutic agent at the CNS and reduce toxicity by preventing distribution to peripheral tissues [4]. In so doing, nanocarriers would contribute to overcome drug pharmacokinetic limitations that currently account for treatment failure. Indeed, nanomedicine is chiefly germane to the field of chemotherapy wherein dose availability at the target site cannot be enhanced by dose increase for fear of severe side effects. Moreover, whereas most anticancer drugs are hydrophobic and often require to be solubilized in organic solvents for administration, nanomedicines provide alternative formulations to administer chemotherapy without the need to use toxic solvents. Furthermore, nanomedicine opens new avenues for drugs with short half-lives *in vivo.* Nanocarriers not only shield such drugs from enzymatic and chemical degradation, but also can sustain and/or trigger drug release at a specific rate at the target site, resulting in maintenance of drug levels within a therapeutically desirable range.

Nanomedicine for brain drug delivery is compatible with local and systemic administration. Localized delivery can be applied to bypass the BBB. Nevertheless, the mechanical breach of this barrier might also allow neurotoxic compounds to enter the brain, increase the risk of infection, or, in the case of gliomas, even promote tumor dissemination. Moreover, this administration involves neurosurgical procedures, which truly hinders the implementation of regimens of multiple doses [5, 6].

Alternatively, intravenous administration represents a less invasive route that is suitable for multiple dosing regimens [7]. Nonetheless, the development of nanocarriers that can effectively cross the brain endothelium and unambiguously target the diseased cells remains a major challenge. With nanomedicine, brain tumor targeting can be accomplished by passive, active or external physical stimuli-responsive targeting. In the case of brain tumors, as occurs with many distinct solid tumors, the rationale of passive targeting relies on the diffusion of intravascularly administered

nanotheranostics through the interendothelial gaps of the disordered neovasculature of tumor tissue (the blood-brain tumor barrier (BBTB)). This singularity is termed the enhanced retention and permeation (EPR) effect. Active targeting with ligands that bind to receptors overexpressed on the brain endothelium and/or tumor cell membranes could further improve the selective distribution of the therapy in the first instance across the BBB/BBTB and eventually to the tumor cells [8]. Finally, nanocarriers can also be guided to the brain tumor site by external stimuli-responsive targeting. Impotantly, as physical phenomena, this targeting does not rely on the idiosyncrasy of the tumor but can be controlled on-demand in a spatial and temporal manner [9].

Notably, as described in Table 1, on the basis of the promising results gathered from preclinical studies with nanomedicine-based therapies, some nanomedicines have already been approved for phase I/II clinical trials in a variety of CNS tumor conditions for determining their safety, tolerability, toxicity and efficacy. Their outcome will steer the research directions for further improvements towards clinical translation of nanotherapy. The clinical trials launched heretofore mainly evaluate lipid-based nanocarriers [10], since these are highly suitable for CNS drug delivery given the fact that the commercially available lipid-based formulations made of biocompatible and biodegradable lipids show a solid track record of clinical safety.

Unfortunately, the global translational impact of nanomedicine remains modest: the empirical development of delivery systems and later assignment to an existing clinical challenge has led to high attrition rates in clinical trials. Therefore, this formulation-driven research should progressively transition to a disease-driven rational approach, whereby the features of the nanocarriers are thoroughly designed beforehand on the basis of the pathophysiology of a specific disease.

As the effect of nanomedicines mainly relies on the unique interactions of materials at the nanoscale with biological structures, one of the major features that certainly influence the *in vivo* performance of nanomedicines is precisely particle size. Firstly, small particle size is a prerequisite for intravenous administration, to avoid capillary blockade. Moreover, the size of nanomedicines determines their plasma shelf-life. On the one hand, particles above 100 nm are removed more rapidly from the bloodstream than smaller ones due to the higher extent of recognition by the reticuloendothelial system. On the other hand, particles below 10 nm are likely to undergo complete renal clearance. Furthermore, the size of nanomedicines can account for the release rate of their payloads: whereas smaller carriers are expected to release their cargos faster, bigger particles are likely to extend the release over longer timeframes.

Particle size also plays a pivotal role in drug targeting. Traditionally, a size-driven extravasation at the target site based on the disease pathophysiological features has been sought. For instance, if provided enough circulation time, nanocarriers with particle size coarsely below 200 nm could take advantage of the EPR effect to achieve drug targeting to some diseased areas. However, the efficiency of this passive targeting highly relies on the idiosyncrasy of the disease (as the EPR effect in CNS disorders such as gliomas and/or inflammatory diseases is relatively weak, with a cut-

off size of only 10-100 nm [11]) and on the disease stage (with a nearly intact endothelium at early stages). In all these cases, a finer control on particle size is needed to certainly improve the potential therapeutic benefits. Moreover, particle size reversely correlates with the attained extravasation distance and interstitial diffusion and the mechanisms that mediate the internalization of nanocarriers in target cells often follow a size-dependent pattern within the range 10-100 nm [12].

Nanocarrier	**Drug**	**Route of administration**	**Combination therapy (if applicable)**	**Phase of clinical trial (status)**	**Identifier**
Liposomes	Cytarabine (DepoCyt®)	Intrathecal	-	Phase I (unknown)	NCT00003073
			Oral temozolomide	Phase I/II (completed)	NCT01044966
			Intravenous methotrexate	Phase II (completed)	NCT00992602
			Radiotherapy	Phase I (completed)	NCT00854867
	Irinotecan	Convection enhanced delivery	-	Phase I (recruiting)	NCT03086616 NCT02022644
		Intravenous	-	Phase I (completed)	NCT00734682
	Doxorubicin (Myocet®)	Intravenous	-	Phase I (completed)	NCT02861222
	Doxorubicin (Lipodox®)	Intravenous	-	Phase I (completed)	NCT00019630
	Doxorubicin (Caelyx®)	Intravenous	Oral temozolomide and radiotherapy	Phase I/II (completed)	NCT00944801
	Doxorubicin (2B3-101)	Intravenous	Intravenous trastuzumab	Phase I/II (completed)	NCT01386580
	Vincristine (Marqibo®)	Intravenous	-	Phase I/II (completed)	NCT01222780
	Wild type p53 gene	Intravenous	Oral temozolomide	Phase II (recruiting)	NCT02340156
	Rhenium	Convection enhanced delivery	-	Phase I/II (recruiting)	NCT01906385
Albumin-nanoparticles	Paclitaxel (Abraxane®)	Intravenous	Oral lapatinib	Phase I (completed)	NCT00313599
Polymer conjugate	Irinotecan	Intravenous	-	Phase II (completed)	NCT01663012
Gold nanoparticles	Nucleic acids	Intravenous	-	Phase I (recruiting)	NCT03020017

Table 1.0.1: An overlook on the already launched clinical trials with nanomedicines for different CNS tumor conditions

Therefore, the size of nanomedicines conspicuously influences their safety and efficacy profile and should be carefully tailored to each therapeutic purpose. Consequently, for efficient disease-driven design of nanomedicines, their size must be accurately adjusted, which can only be achieved with comprehensive understanding of the fundamental principles of nanomedicine. Otherwise, the formulation procedure will represent the limiting step hindering the development of promising nanotherapies. Hence, the ascertainment of the parameters controlling the size distribution of nanocarriers is crucial to fully exploit their therapeutic potential following a rational approach rather than a trial-and-error process.

In this chapter, we follow the aforementioned disease-driven design of nanocarriers. Firstly, in the review entitled “Managing CNS Tumors: The Nanomedicine Approach”, we address the clinical challenges for developing effective therapies for CNS pathologies and the features that nanomedicines aimed at doing so should accomplish. Subsequently, in the original article entitled “Size-tailored lipid nanocapsules by a single step energy-efficient method: the phase inversion temperature revisited”, we develop and validate a methodology to prepare highly monodisperse lipid nanocapsules with in-advance accurately tailored sizes according to the disease needs. This tailoring is attained for several tandems of oily phase and surfactant, which ultimately enables the concomitant adjustment of the formulation composition to both solubility and toxicological issues imposed by the drug substance in each case. Importantly, we utilize a low-energy method to prepare the lipid nanocapsules that fits the criteria for industrial-scale manufacturing, a feature commonly overlooked when developing nanomedicines but necessary for them to achieve broad market access [13]. The establishment of a mathematical model that can describe the nanocarrier formation by an energetically-efficient procedure will eventually enable nanomedicines to be obtained on demand and on a large scale.

References:

[1] Gustavsson A, Svensson M, Jacobi F, Allgulander C, Alonso J, Beghi E, et al. Cost of disorders of the brain in Europe 2010. Eur Neuropsychopharmacol. 2011;21:718-79.

[2] Alifieris C, Trafalis DT. Glioblastoma multiforme: Pathogenesis and treatment. Pharmacol Ther. 2015;152:63-82.

[3] Au K, Meng Y, Suppiah S, Nater A, Jalali R, Zadeh G. Current Management of Brain Metastases: Overview and Teaching Cases. In: Morgan LR, editor. New Approaches to the Management of Primary and Secondary CNS Tumors. Rijeka: InTech; 2017. p. Ch. 06.

[4] Shi JJ, Kantoff PW, Wooster R, Farokhzad OC. Cancer nanomedicine: progress, challenges and opportunities. Nat Rev Cancer. 2017;17:20-37.

[5] del Burgo LS, Hernandez RM, Orive G, Pedraz JL. Nanotherapeutic approaches for brain cancer management. Nanomed-Nanotechnol Biol Med. 2014;10:905-19.

[6] Miranda A, Blanco-Prieto M, Sousa J, Pais A, Vitorino C. Breaching barriers in glioblastoma. Part I: Molecular pathways and novel treatment approaches. Int J Pharm. 2017;531:372-88.

[7] Orive G, Ali OA, Anitua E, Pedraz JL, Emerich DF. Biomaterial-based technologies for brain anti-cancer therapeutics and imaging. Biochim Biophys Acta-Rev Cancer. 2010;1806:96-107.

[8] Oller-Salvia B, Sanchez-Navarro M, Giralt E, Teixido M. Blood-brain barrier shuttle peptides: an emerging paradigm for brain delivery. Chem Soc Rev. 2016;45:4690-707.

[9] Chen Q, Ke HT, Dai ZF, Liu Z. Nanoscale theranostics for physical stimulus-responsive cancer therapies. Biomaterials. 2015;73:214-30.

[10] Miranda A, Blanco-Prieto MJ, Sousa J, Pais A, Vitorino C. Breaching barriers in glioblastoma. Part II: Targeted drug delivery and lipid nanoparticles. Int J Pharm. 2017;531:389-410.

[11] van Tellingen O, Yetkin-Arik B, de Gooijer MC, Wesseling P, Wurdinger T, de Vries HE. Overcoming the blood-brain tumor barrier for effective glioblastoma treatment. Drug Resist Update. 2015;19:1-12.

[12] Overchuk M, Zheng G. Overcoming obstacles in the tumor microenvironment: Recent advancements in nanoparticle delivery for cancer theranostics. Biomaterials. 2018;156:217-37.

[13] Hare JI, Lammers T, Ashford MB, Puri S, Storm G, Barry ST. Challenges and strategies in anti-cancer nanomedicine development: An industry perspective. Adv Drug Deliv Rev. 2017;108:25-38.

Chapter 4

Managing CNS Tumors: The Nanomedicine Approach

Juan Aparicio-Blanco and Ana-Isabel Torres-Suárez

Additional information is available at the end of the chapter

http://dx.doi.org/10.5772/66131

Abstract

Albeit the rapidly evolving knowledge about tumor biochemistry enables various new drug molecules to be designed as treatments, malignant central nervous system (CNS) tumors remain untreatable due to the failure to expose the entire tumor to such therapeutics at pharmacologically meaningful quantities. Therefore, drug delivery in CNS tumors must be properly addressed, as otherwise, novel therapies will continue to fail. In this regard, nanomedicine poses an appealing platform for efficient drug delivery to the CNS, since it may be targeted to improve the drug availability in the site of action, which would be translated into lower drug doses and fewer side effects. Hence, the accumulation of data about the CNS physiology and their relevant receptors, the widening therapeutic armamentarium of drugs potentially useful in CNS chemotherapy and the alternative routes for administration may envisage nanomedicines as a forthcoming routine approach. Indeed, on the basis of the promising results gathered from preclinical studies of nanomedicine-based therapy both systemically and locally administered, some nanomedicines have already been approved for clinical trials in a variety of CNS tumor conditions to serve as the first steps in the translation of nanotherapy to clinic. Their outcome will steer research directions for further improvements.

Managing CNS Tumors: The Nanomedicine Approach

Juan Aparicio-Blanco and Ana-Isabel Torres-Suárez

Department of Pharmaceutical Technology, Faculty of Pharmacy, Complutense University, 28040, Madrid, Spain

Abstract

Albeit the rapidly evolving knowledge about tumor biochemistry enables various new drug molecules to be designed as treatments, malignant CNS tumors remain untreatable due to the failure to expose the entire tumor to such therapeutics at pharmacologically meaningful quantities. Therefore, drug delivery in CNS tumors must be properly addressed, as otherwise, novel therapies will continue to fail.

In this regard, nanomedicine poses an appealing platform for efficient drug delivery to the CNS, since it may be targeted to improve the drug availability in the site of action, which would be translated into lower drug doses and fewer side-effects. Hence, the accumulation of data about the CNS physiology and their relevant receptors, the widening therapeutic armamentarium of drugs potentially useful in CNS chemotherapy and the alternative routes for administration may envisage nanomedicines as a forthcoming routine approach.

Indeed, on the basis of the promising results gathered from preclinical studies of nanomedicine-based therapy both systemically- and locally-administered, some nanomedicines have already been approved for clinical trials in a variety of CNS tumor conditions to serve as the first steps in translation of nanotherapy to clinic. Their outcome will steer research directions for further improvements.

Keywords

Central nervous system tumors, chemotherapy, brain targeting, nanomedicine, clinical trials, local delivery, systemic delivery

1. Introduction

Primary central nervous system (CNS) tumors represent 2% of all cancers in adults, whereas this percentage rises to 15 to 25% in children. Primary brain tumors are stratified by the World Health Organization (WHO) according to a 'malignancy scale'. The WHO grade is closely related to clinical prognosis, ranging from grade I (with low proliferative potential and the possibility of cure following surgical resection alone) to grade IV (with widespread invasion of the surrounding healthy tissue, high proliferative potential, recurrence and fatal outcome). Unfortunately, many low-grade gliomas eventually often show progression to a higher histologic grade [1].

Gliomas represent approximately 80% of all malignant primary brain tumors. Glioblastomas (WHO grade IV) are the most frequent (54.4%) and aggressive type of glioma [2], although, in terms of treatment, WHO grade III brain tumors and glioblastomas are clustered together and treated similarly.

Although the management of brain tumors depends on the time of diagnosis, new onset or recurrence, the performance status and the age of the patient, the current standard approach in high grade brain tumors combines maximal surgical resection (if eligible) with radiotherapy and concomitant and adjuvant chemotherapy; as well as symptomatic treatment [3].

Available chemotherapy for high grade brain tumors includes temozolomide, nitrosureas (carmustine (BCNU) and lomustine (CCNU)), topoisomerase inhibitors (etoposide, irinotecan), platinum agents (carboplatin), procarbazine and vincristine. The first line chemotherapy for newly diagnosed glioblastoma multiforme consists of temozolomide, whereas carmustine represents the second line treatment. After the approval of temozolomide in 1999, irinotecan, etoposide and platinum agents are mostly used only as adjuvant chemotherapy of bevacizumab (FDA approved in 2009 in monotherapy) for recurrent glioblastomas. In the case of WHO grade III gliomas (anaplastic astrocytomas and oligodendrogliomas), the first line treatment is the PCV combination (procarbazine-lomustine-vincristine) [4].

Unfortunately, the efficacy of the treatment of brain tumors is questionable, since recurrence happens within 6.9 months of initial diagnosis. As a result, despite the combination of surgical resection, radiotherapy and concomitant temozolomide, glioblastoma multiforme remains incurable, with a poor survival median survival of 14.6 months and 2-year survival rate of 26.5% [5]. This poor prognosis results from chemotherapy tumor resistance [6].

One of the chemoresistance mechanism best characterized relates to the expression of O^6-methylguanine-DNA methyltransferase (MGMT), a repair gene that removes alkyl groups from the O^6 position of guanine and consequently counteracts the alkylating agents (temozolomide or nitrosureas). Methylation of the promoter of this gene, which occurs in 35–45% of the cases, makes glioblastoma more sensitive to alkylating agents [7, 8].

Likewise, the existence of glioma stem-cells greatly accounts for tumor recurrence, since they upregulate the expression level of P-gycoprotein [9], which is responsible for active efflux of many chemotherapy agents, including temozolomide.

The overexpression of epidermal growth factor receptor (EGFR), which ultimately triggers the activation of complex alternative signaling pathways aimed at inhibiting apoptosis, also contributes to resistance to standard chemotherapy. Unfortunately, none of the receptor tyrosine kinase inhibitors and signal transduction inhibitors tested in clinical trials prolonged the mean survival, mainly due to the lack of successful drug delivery across the blood–brain tumor barrier (BBTB), since the exposure of the tumor to sub-lethal drug concentrations helps select the drug-resistant tumor cells [10].

The BBTB consists of the endothelium of existing and abnormal angiogenic blood vessels that deliver nutrients and oxygen to the tumor and enable widespread glioma migration to brain areas where the function of the barrier is still intact. Therefore, even though the BBTB is considered dysfunctional, the truth is that in low grade and in the infiltrative parts of high grade gliomas, often responsible for the recurrence, the BBTB closely resembles the tight blood brain barrier (BBB) typical of healthy brain capillaries [11]. Hence, the BBTB greatly accounts for the failure rate of the brain tumor therapy, since the hindrance to brain delivery of chemotherapeutic agents at pharmacologically-effective levels conferred by this barrier cannot be offset by dose increase for fear of systemic toxicity. Furthermore, drug efflux pumps of the BBB can also be expressed in endothelium at the BBTB, representing an additional constraint to the achievement of adequate drug levels at the target site [12].

Since the therapeutic potential of chemotherapy greatly depends on its ability to attain pharmacologically effective levels at the entire diseased brain area, novel strategies to enhance drug delivery at the tumor site are strongly needed.

2. The Nanomedicine Approach

Conventional chemotherapy has failed to improve the prognosis of CNS tumors; hence novel drug-delivery technologies have emerged under the assumption that targeted drug delivery could contribute to expose the entire tumor to therapeutically meaningful levels and ultimately improve treatment outcomes for brain tumors. An example of the success achievable thanks to advances in pharmaceutical technology is Gliadel®, the first FDA-approved brain cancer treatment to deliver chemotherapy directly to the tumor site in patients with malignant glioma for whom surgical resection is indicated. Gliadel® is a biodegradable wafer implanted on the surface of the resected tumor beds at the time of surgery that delivers carmustine steadily for about three weeks directly to the tumor site minimizing drug exposure to other areas of the body. Gliadel® contributes to eradicate the residual tumor cells at the resection margin and complements other standard therapies for brain tumors (surgery and radiotherapy) [13].

Nanomedicine represents an encouraging trend within the field of novel drug-delivery technology with potential to preferentially delivering the drug at the target site and consequently overcoming biodistribution and pharmacokinetic limitations that eventually account for treatment failure of brain tumors. Nanomedicine is the application of nanotechnology in view of making a medical diagnosis or treating or preventing diseases. It exploits the improved and often novel properties of materials at nanoscale. Nanomedicines are colloidal structures that act as drug carriers in which the drug substance is dissolved, entrapped, or encapsulated, or to which the drug substance is adsorbed or attached [14]. Unlike monolithic implants such as Gliadel®, colloidal carriers can be administered with conventional needles and therefore are not limited to those brain tumors where surgical resection is indicated.

Nanomedicine is especially relevant for chemotherapeutic agents, whose low dose availability at the tumor site cannot be counterbalanced by dose increase for fear of severe systemic side effects. Targeted nanomedicines would improve the availability of the drug at the scattered tumor bed and would allow obtaining therapeutic effects with lower drug doses and concomitantly minimizing the side effects of chemotherapy not only in unwanted peripheral tissues, but even on healthy brain cells. Therefore, the therapeutic index of drugs would be greatly enhanced thanks to nanomedicine. Targeted drug delivery to the site of action can be achieved through passive and active targeting or even through external physical stimuli. Passive targeting exploits the specific anatomical and functional features of the target tissues or cells to deliver drugs to the site of action. Active targeting requires the conjugation of tissue or cell-specific ligands on the surface of nanocarriers, whose recognition would eventually allow preferential accumulation of the drug at the diseased site. External stimuli such as a magnetic field, focused ultrasounds, light and heat can also help selectively release the drug payload of nanomedicines at the target site [15].

Moreover, whereas most anticancer drugs are hydrophobic and often require to be solubilized in organic solvents for conventional administration, nanomedicines provide alternative formulations to administer chemotherapy without the need to use toxic solvents. Furthermore, nanomedicine is opening new therapeutic opportunities for easily degradable drug substances that cannot be used effectively as conventional formulations due to their short half-lives in vivo. Nanomedicines not only shield such drugs from enzymatic and chemical drug cleavage that accounts for the loss of pharmacological effect, but also can sustain and/or trigger drug release at a specific rate at the target site, resulting in maintenance of drug levels within a therapeutically desirable range. Thanks to this controlled release profile, undesirable pharmacokinetic properties of drug substances can be overcome with the use of nanocarriers and the dosing frequency can be improved to prescribe more comfortable dose regimens for patients.

The nanomedicine approach to enhance drug delivery to CNS tumors is highly versatile, since it would allow the co-administration of different anticancer agents and is compatible with both local and systemic routes of administration. In the current scenario, this approach must be directed towards surpassing acquired resistance to

conventional chemotherapy and implementing strategies to boost the distribution across the brain endothelium in the case of systemic administration [16].

Nevertheless, nanomedicines might likewise cause unexpected toxicities as the other excipients also reach target tissues along with the drug. Non-degradable nanomedicines used for drug delivery would accumulate at the tumor site and would ultimately result in chronic inflammatory response, because, as colloidal systems, there is no chance of removing them after completion of the treatment. Albeit toxicity concerns of nanomedicines greatly relies on the relatively unexplored size-dependent properties and interaction with biological structures that strikingly differ from those of the bulk material, it is broadly agreed that the safety profile of brain-targeted nanomedicines would be improved with biocompatible excipients devoid of any short or long-term toxic effects [17]. Consequently, despite the vast number of available biomaterials for nanomedicines preparation, only a few are suitable for brain tumor treatment because the CNS requires conservative choices with proven track record of clinical safety. Nanomedicines developed for brain delivery mainly belong to three categories: polymer-based, lipid-based or metal-based, according to their major excipient (Table 1).

Overall, lipid-based nanomedicines may well be the most suitable for CNS drug delivery; insofar as lipids have very low toxicity, are biocompatible and biodegradable by nature and the commercially available lipid-based formulations show a solid track record of clinical safety [18-20], whereas at present, only a few of the studied polymers for the development of polymer-based nanomedicines for brain drug delivery have demonstrated biocompatible, biodegradable and non-toxic properties to be approved by the FDA for clinical use [21-23]. On the other hand, since the lack of biodegradation may not be appropriate for long- term administration, most metal-based nanomedicines (such as magnetic nanoparticles and gold nanoparticles) have been made more biocompatible and water-soluble with polymer coating [24].

3. Local delivery of nanomedicines

The local delivery of anticancer drugs serves to overcome the lack of specificity of conventional chemotherapy. Higher drug levels at the tumor site and lower drug distribution to healthy tissues account for the reduction of the systemic side effects with local routes of administration. Moreover, in the case of CNS tumors, local chemotherapy bypasses the major hurdle for systemic brain drug delivery: the blood–brain tumor barrier. However, the mechanical breach of this barrier may act as a double-edged sword since this might allow neurotoxic blood components to enter the brain or even enhance tumor dissemination.

Nanomedicines offer several advantages over conventional chemotherapy with regards to local CNS delivery: they can extend the exposure to short-brain-half-life drugs and provide long-lasting drug release that ultimately maintains therapeutic levels at the target site over longer periods. Moreover, nanomedicines show potential to enhancing antitumor activity via several pathways. Firstly, locally administered nanomedicines can promote passive diffusion of the anticancer agent to the brain

tumor tissue by raising the local drug concentration gradient. Furthermore, nanomedicines can be actively targeted to the brain tumor cells by conjugating specific ligands that bind to the receptors that are overexpressed or uniquely expressed on the tumor surface (a mutant form of the epidermal growth factor receptor (EGFRvIII), interleukin receptors for interleukins 4 and 13…) to efficiently trigger cellular uptake at the tumor site.

Category	Nanomedicine	Description	Size (nm)	Phase of development
Polymer-based	Polymeric nanoparticles	Solid matrix-like or reservoir-like nanostructures made up of biocompatible and biodegradable polymers or copolymers	20-1000	Preclinical
	Polymeric micelles	Nanostructures of amphiphilic diblock copolymers with a core of hydrophobic blocks stabilized by a corona of hydrophilic blocks	50-200	Preclinical
	Dendrimers	Highly branched tree-like nanostructures composed of a central core, internal branches and reactive terminal groups	1-10	Preclinical
Lipid-based	Liposomes	Vesicles of amphipathic lipids structured in concentric bilayers surrounding an equal number of central aqueous compartments	80-200	Phase I, II clinical trials
	Solid lipid nanoparticles	Solid lipid matrixes at room and body temperatures that are stabilized by surfactant(s)	50-1000	Preclinical
	Lipid nanocapsules	Reservoir nanomedicines with a liquid oily core, surrounded by a shell of surfactants	20-100	Preclinical
Metal-based	Magnetic nanoparticles	Nanostructures composed of magnetic elements that can be manipulated using magnetic fields	10-50	Clinical
	Gold nanoparticles	Nanostructures that can serve as drug carriers and even convert absorbed electromagnetic radiation to heat	5-50	Preclinical

Table 1.1.1- Main types of nanomedicines that are currently under investigation for the treatment of CNS tumors

Similarly, locally administered nanomedicines can also help overcome some of the most troublesome chemoresistance mechanisms that are eventually responsible for tumor recurrence. In this sense, the upregulated expression of P-gycoprotein in drug-resistant cancer stem-cells, which accounts for active efflux of most anticancer agents from the tumor area and reduces the effectiveness of chemotherapy, can be overcome thanks to nanomedicine. Indeed, the coating with nonionic surfactants seems to confer the nanocarrier itself with efflux-pump blockage properties [25]. Additionally, along with

chemotherapy, nanomedicines can serve to deliver irreversible MGMT inhibitors (such as O^6-benzyl guanine) and/or receptor tyrosine kinase inhibitors, to sensitize brain tumor cells to alkylating agents and to counteract the inhibition of apoptosis mediated by the overexpression of the receptor of the epidermal growth factor (EGFR), respectively.

Several local routes of administration may be exploited by nanomedicines for handling of CNS tumors.

- The intracranial administration involves drug delivery directly into the brain parenchyma. Nonetheless, intraoperative infusion of anticancer drugs into brain tumors has experienced minor success given the diffusion-limited drug distribution, which does not allow the drug to reach the infiltrative area of recurrence. Moreover, the high interstitial fluid pressure and the presence of edemas often observed in intracranial tumors may further hinder the diffusion of the infused agent.

Alternatively, convection enhanced delivery (CED), another method for intracranial administration, achieves larger distribution volumes in the brain, for more homogeneous distribution within the tumor tissue, since it uses positive pressure to supplement simple diffusion with fluid convection. CED continuously delivers a bulk flow under a pressure gradient via a stereotactically-guided catheter connected to a syringe pump. Drug leakage away from the tumor site (especially into the subarachnoid space with the subsequent drug spreading via the circulating cerebrospinal fluid (CSF)) should be avoided to minimize side effects such as chemical meningitis. In this regard, the suitable placement of catheters often prevents the leakage and helps spare healthy tissue.

CED can likewise deliver nanocarriers loaded with antineoplastic agents for CNS tumor therapy [26]. When combined with CED, the encapsulation of the drug infused into nanocarriers further reduces the potential side effects caused by drug leakage, while extends the brain half-life of anticancer agents by preventing them from being rapidly metabolized and/or eliminated by capillaries from the injection site. However, for efficient CED through the brain interstitium, the physicochemical properties of the colloidal systems must be optimized.

Firstly, CED-injected nanomedicines must diffuse through interstitial spaces of the brain tissue. Hence, the size of the colloidal systems is a critical parameter to achieve optimal distribution volume with full coverage of the brain tumor tissue. Particles larger than 100 nm do not move readily through the brain interstitium, are retained near the administration site and do not distribute over clinically relevant volumes of brain tissue. Hence, in terms of size, the ideal nanocarrier for CED should be about 20–50 nm.

Moreover, to achieve optimal distribution volumes to cover both the tumor bed and the outlying cancer stem cells, it is convenient to provide nanocarriers with a hydrophilic coating (mostly polyethylene glycol –PEG- [27]). The hydrophilic coating could help mask the hydrophobic structures, which would reduce the eventual binding to brain cells or to proteins in the interstitial space and ultimately enable greater

diffusion. However, hydrophilic coating of nanocarriers also has the drawback of reducing the interactions with tumor cells, required for the loaded anticancer drug to eradicate the tumor. Alternatively, distribution volumes can be enhanced with the presence of co-infusates that serve to saturate the potential binding sites along the track of the infused nanomedicines. Furthermore, the ideal CED-administered nanocarrier should have a global neutral or negative charge to prevent non-specific binding to negatively charged structures in the brain parenchyma and to achieve larger distribution volumes [27].

In addition, the infusion of viscous and hyperosmolar suspensions of nanocarriers would help reduce the risk of drug leakage and enhance the distribution volume by means of osmosis-mediated dilatation of the interstitial space through which nanocarriers could transit, respectively.

Nonetheless, despite its remarkable potential to improving clinical outcomes for CNS tumors, intracranial CED is an invasive neurosurgical procedure, which truly hinders its widespread use and limits the number of dosing cycles to be applied to eligible patients.

- The intrathecal administration involves the injection of anticancer drugs into the intrathecal space, which is the space that holds the cerebrospinal fluid (CSF). This can be achieved either with the implantation of an Ommaya reservoir (a dome-shaped container that is placed subcutaneously under the scalp during surgery, holds the chemotherapy and delivers it into the cerebral ventricles through a small catheter) or with direct injection into the CSF through a numbed area of the lower part of the spinal cord. Despite the significantly less invasive character of the second approach, intrathecal delivery fails to accumulate drugs in the brain parenchyma due to the bulk flow rate of CSF into the venous system, making this route optimal for the treatment of spinal tumors and disseminated meningeal metastases but not for parenchymal tumors like glioblastoma. Indeed, since meningeal gliomatosis remain protected by the blood brain barrier, intrathecal delivery is widely considered a treatment approach for achieving improved outcomes for these patients [28].

Unfortunately, not all anticancer agents are suitable for intrathecal delivery, as drug spread along the spinal canal can cause dose-limiting chemical arachoniditis. For those irritant drug substances, intrathecal delivery can take great advantage of nanomedicine, since their encapsulation into nanostructures could minimize drug exposure to toxic levels. As a proof of it, intrathecally-administered liposomal cytarabine (Depocyt®) has been approved for clinical use in lymphomatous meningitis. Nonetheless, the cytotoxicity of cytarabine against a wide spectrum of tumors makes Depocyt® a promising candidate for treating the above mentioned forms of CNS cancer.

- More recently, the intranasal delivery has been proposed as an alternative local route of administration. Its non-invasive nature would allow self-administration by nasal inhalation and would enable the sterilization procedures of the drug dosage form to be avoided. This delivery route exploits the fact that trigeminal and olfactory nerves that innervate the nasal epithelium represent the only direct connection between the

external environment and the brain [29]. However, this route appears to be relatively inefficient in delivering inhaled drugs to distant brain structures, mainly due to drug loss via systemic absorption.

In regard to brain tumor therapy, intranasal administration has received minor attention, with most applications of this approach being focused on the treatment of neurodegenerative diseases.

Numerous locally-administered drug-loaded nanomedicines have already been assayed for efficacy in rodent models of brain tumors: liposomes, polymer nanoparticles, lipid nanocapsules, dendrimers, magnetic nanoparticles and polymeric micelles, as summarized in Table 2. Although results are highly variable depending on various parameters, namely the tumor lineage and the onset, dose and regimen of treatment, some general conclusions can be drawn from these preclinical studies. Overall, liposomes exhibited the most noticeable survival benefit and the presence of the highest percentage of long-term survivors [30, 31], partly because their potential as drug carriers was acknowledged earlier than any other alternative nanomedicine; hence research on nanomedicines for local CNS anticancer therapy has largely focused on liposomes.

Likewise, in some preclinical studies in rodent models, it was even evidenced that CED outperformed the survival benefit of the same formulation administered by a peripheral intravascular route [32]. Furthermore, the versatility of CED has enabled the co-administration of different liposomal formulations to enhance the effect of the anticancerous agents [33, 34]. Concerning CED, numerous nanomedicines were formulated with a hydrophilic coating of polyethylene glycol and administered as slightly viscous suspensions to achieve optimal distribution volumes that cover the whole brain tumor tissue [35]. In fact, the deprivation of the hydrophilic coating, albeit increased median overall survival in comparison with untreated controls, significantly differed from efficacy findings reported for animals receiving the pegylated nanomedicines [36]. Nevertheless, it has been postulated the existence of a “threshold extent of pegylation”, over which the hindrance conferred by polyethylene glycol to interact with the tumor cells counterbalances the increase in CED distribution volume provided by slight pegylation [37]. On the other hand, the addition of active targeting moieties that preferentially bind to receptors that are overexpressed on brain tumor cells to promote the delivery of nanomedicines to their target cells is controversial: whereas the attachment of OX26 or a cell-penetrating peptide showed enhanced both tumor and healthy tissue internalization, which led to the appearance of side effects and high morbidity [38], the attachment of chlorotoxin or antibodies that selectively bind to the epidermal growth factor receptor mutant (EGFRvIII) present on human glioblastoma cells achieved significant survival benefits [35, 39, 40]. The different response could be explained by the choice of the ligand: ligands that preferentially bind to receptors on the cerebral endothelial are pointless in local delivery, whereas ligands that bind to receptors overexpressed on the brain tumor cells are those to be used for active targeting in local delivery.

Moreover, some studies [41-43] evidenced the importance of an adequate drug release to achieve a therapeutic response: the covalent linkage of methotrexate [42] and cisplatin [43] to dendrimer structures did not lead to any improvement in the median survival time of F98-bearing rats due to a release failure, while the survival benefit achieved with micellar doxorubicin in 9L-bearing rats was significantly relevant compared with CED of liposomal doxorubicin at the same dose due to the lack of release of doxorubicin from the liposomal formulation [41].

Importantly, CED-administered nanocarriers have been designed to overcome the MGMT-related chemoresistance to alkylating agents. O^6-benzyl guanine has been loaded in iron oxide nanoparticles provided with a biocompatible chitosan-polyethylene glycol coating and actively targeted by chlorotoxin. The concurrent CED administration of these magnetic nanoparticles with oral temozolomide in mice implanted with a GBM6 clinically relevant xenograft extended by 2-fold the survival times in comparison with mice treated without the MGMT inhibitor and greatly mitigated the severe myelosuppression associated with systemic administration of free O6-benzyl guanine [35].

With regards to intranasal administration, polymeric micelles are the only nanomedicine type tested in rodent brain tumor models [44, 45]. The attachment of the cell-penetrating peptide Tat on their surface for actively enhancing the penetration rate across the nasal epithelium extended survival times [44].

4. Systemic delivery of nanomedicines

Thanks to the high brain perfusion rate, systemic intravascular administration is a very convenient strategy in the clinical management of cancer for compatibility with repeated drug administration and for its lower invasiveness in comparison with most local delivery routes. However, despite being considered disrupted to some extent, the presence of the BBTB has motivated the failure of conventional systemic chemotherapy for CNS tumors, since in low grade and along the infiltrating areas of high grade gliomas where recurrences tend to occur, the BBTB closely resembles the non-fenestrated endothelial cells typical of healthy brain capillaries. Hence, the BBTB restricts the paracellular permeation of most anticancer agents into the CNS. As a result, conventional systemic chemotherapy must be administered at high drug doses, which cause severe dose-dependent side effects in healthy non-target tissues.

Encapsulated drug	System	Model	Route of administration	Ref
Irinotecan	Liposomes	U87-bearing rats	CED	[14]
Irinotecan	Liposomes	GBM43-/ SF7796-bearing mice	CED	[15]

Encapsulated drug	System	Model	Route of administration	Ref
Topotecan	Liposomes	U251-/U87MG-bearing rats	CED	[16, 17]
Topotecan + Doxorubicin	Liposomes	U87MG-bearing rats	CED	[18]
Irinotecan + Doxorubicin	Liposomes	U251-/U87MG-bearing rats	CED	[19]
Camptothecin	Polymer nanoparticles	9L-bearing rats	CED	[20]
Temozolomide	Polymer nanoparticles	U87-bearing rats	CED	[21]
HSVtk (+ intraperitoneal Ganciclovir)	Polymeric nanoparticles	9L-bearing rats	CED	[22]
Paclitaxel (+ radiotherapy)	Lipid nanocapsules	9L-bearing rats	CED	[23]
Ferrociphenol	Lipid nanocapsules	9L-bearing rats	CED	[24-26]
Ferrociphenol (+ radiotherapy)	Lipid nanocapsules	9L-bearing rats	CED	[27]
Metothrexate	Fifth-generation dendrimers	F98-bearing rats	CED	[28]
Cisplatin	Fifth-generation dendrimers	F98-bearing rats	CED	[29]
EGFRvIII antibody	Magnetic nanoparticles	U87 glioma-bearing mice	CED	[30]

Encapsulated drug	System	Model	Route of administration	Ref
Cetuximab	Magnetic nanoparticles	NO8-30, U87 and LN229-bearing mice	CED	[31]
O^6-Benzyl guanine (+ oral temozolomide)	Magnetic nanoparticles	GBM6-bearing mice	CED	[32]
Doxorubicin	Polymeric micelles	9L gliosarcoma-bearing rats	CED	[33]
Synthetic retinoid Am80 (+ intraperitoneal temozolomide)	Polymeric micelles	U87 glioma-bearing rats	CED	[34]
Camptothecin	Polymeric micelles	C6 glioma-bearing rats	Intranasal	[35]
Camptothecin + siRNA (Raf-1)	Polymeric micelles	C6 glioma-bearing rats	Intranasal	[36]

Table 1.1.2- Locally-administered nanomedicines already tested for efficacy in vivo against orthotopic rodent brain tumor models.

Against this background of hindrance to brain tumor delivery, nanomedicine may enhance the distribution of poorly brain-distributed anticancer agents across the brain endothelium, since nanocarriers may well serve to target brain tumors through passive and active targeting or even through external physical stimuli [53]. Passive targeting occurs with the diffusion of nanomedicines through the inter-endothelial gaps of the highly vascularized leaky BBTB in the case of high grade brain tumors, a phenomenon known as the enhanced retention and permeation (EPR) effect [54]. Moreover, surface-modified brain actively-targeted nanomedicines may also enhance CNS delivery across the intact brain endothelium of infiltrative parts and low grade brain tumors by triggering transcytosis either by ligand-receptor binding or by electrostatic interactions [55]. Therefore, nanomedicines can be useful for the treatment of different malignancy grades of brain tumors. In addition, the use of stimulus-sensitive groups to control drug release within the brain in a therapeutically relevant concentration could further enhance the specificity of the treatment effect to the brain tumor area. Alternatively, nanomedicines can block the active drug efflux back into the bloodstream.

For optimal passive targeting of brain tumors, systemic nanomedicines should have sufficient circulation time [56] to take advantage of the hyper-vascularized, leaky,

and compromised lymphatic drainage system in a CNS tumor and selectively accumulate in the tumor tissue through the EPR effect. When given intravascularly, the larger the nanomedicines, the more susceptible to opsonization and removal by cells of the reticuloendothelial system (RES) [57]. Hence, to reduce opsonization in plasma and increase their plasma circulation time, the size of nanomedicines should be maintained below 100-200 nm. Additionally, the surface coating with hydrophilic polymers such as polyethylene glycol (PEG) to develop “stealth” nanomedicines creates a hydration layer that prevents protein adsorption and evades RES clearance [58], and consequently prolongs their circulation half-life.

Therefore, if properly designed, nanomedicines could cross the leaky BBTB in highly malignant brain tumors by passive targeting. Moreover, the BBTB can be artificially further disrupted to enable a wider distribution of nanomedicines to the brain tumor site. This disruption can be achieved via infusion of a hyperosmotic solution [59] or through the administration of vasoactive agents [60]. Hyperosmotic mannitol infusions cause a transient shrinkage of cerebrovascular endothelial cells, resulting in an enlargement of the tight junctions and BBTB leakiness. However, mannitol infusions also increase the permeability of healthy brain tissue, thereby increasing the risk of neurotoxicity. Conversely, the tumor vasculature is more sensitive than healthy brain vasculature to infusions with vasoactive agents (leukotrienes, bradykinin, and RMP-7, an analogue of bradykinin) through the transient activation of B2 receptors. Nevertheless, delivery of vasoactive agents requires intraarterial infusion, which increases the invasiveness of the procedure, and thereby creates a barrier for clinical translation of this approach. Alternatively, a local, transient and reversible disruption of the BBTB can be generated by low-frequency focused ultrasound without permanent neuronal injury or other undesired long-term effects [61]. However, the artificial transient disruption of the BBTB is increasingly being considered undesirable since this might lead to widespread tumor dissemination and/or to the development of seizures due to the overexposure to neurotoxic blood components that enter the brain.

Additionally, optimal active targeting of nanomedicines would enable anticancer agents to be delivered across fully functional BBB of infiltrative areas and low grade brain tumors exploiting carrier-mediated transportation, receptor-mediated or adsorption-mediated transcytosis.

On the one hand, the carrier- and receptor-mediated active targeting involves functionalizing the surface of nanomedicines with moieties that specifically bind to receptors overexpressed on the brain endothelium and/or brain tumor cell membranes [62]. Therefore, different receptors in the brain could be employed:

- Penetration into the brain tumor area can be improved by simply targeting receptors that are normally overexpressed on the brain endothelium (such as transferrin receptors, nicotinic acetylcholine receptors, low-density lipoprotein receptor (LRP1) or carriers responsible for brain nutrient uptake) [62]. To target the transferrin receptor, both physiological ligands (transferrin and lactoferrin) and monoclonal antibodies (OX26 and 8D3) have been attached onto the surface of different types of nanomedicines [63-65]. Overall, physiological ligands ensure biocompatibility and non-

immunogenicity but develop competitive phenomena with endogenous ligands, whereas monoclonal antibodies prevent competitive phenomena with endogenous ligands since they bind to a different epitope. Likewise, nicotinic acetylcholine receptors have been targeted with peptides derived from snake neurotoxins, namely candoxin and Ophiophagus hannah toxin b [66-68]. The peptide Angiopep-2 has also been attached onto the surface of several nanomedicines to target LRP1 [69, 70]. Furthermore, glucose or mannose conjugation to nanomedicines has conferred brain-targeting properties through overexpressed facilitative glucose transporters [71, 72].

- Receptors distributed on proliferating endothelial cells in the tumor vasculature (αVβ3 integrin, aminopeptidase N, nucleolin) represent additional potential sites for active targeting of nanomedicines to brain tumor tissue. In this sense, peptides containing the amino acid sequence Arg-Gly-Asp (RGD) have been coupled to the surface of distinct nanomedicines to bind to αVβ3 integrin [73, 74]. Another tripeptide Asn-Gly-Arg (NGR) has been conjugated to different nanomedicines to target aminopeptidase N (CD 13) [75]. Moreover, the ability of the F3 peptide and the AS1411 aptamer to bind to nucleolin has been exploited to actively target nanomedicines to the brain tumor tissue [76, 77].

- Nanomedicines could also incorporate targeting moieties that bind to receptors that are overexpressed on tumor cells, to reduce the side effects of the anti-tumor agent on healthy brain cells after bypassing the BBTB. Apart from the already mentioned LRP1 and αVβ3 integrin, these tumor targets include the receptor of the epidermal growth factor (EGFR) and its malignant isoform EGFRvIII, receptors for interleukins 13 (IL-13Rα2) and 4 (IL-4R), the folate and the insulin receptors, and even the membrane-bound matrix metalloproteinase-2 (MMP-2). Consequently, antibodies to EGFR or EGFRvIII have been conjugated to several nanomedicines for brain tumor targeting. Likewise, anti-IL13Rα2 antibodies and IL-13 or IL-4-derived peptides (PEP-1 or AP-1, respectively) have been attached onto the surface of nanomedicines to selectively bind to interleukin receptors [78, 79]. To target the folate receptor, folid acid has been used, whereas to target the insulin receptor, the monoclonal antibody 83-14 has been incorporated to nanomedicines, since the use of the physiological ligand in this case was truly restricted by its biological effect on non-target regions (namely hypoglycemia) [63]. Furthermore, MMP-2 has been widely targeted with nanomedicines coupled to a peptide derived from scorpion venom: chlorotoxin [65, 80].

Since any ligand for which a receptor exists on the cerebral endothelial cells or on the tumor cells might be used for active targeting, the enrichment of knowledge about the transport systems present on the BBB/BBTB and the glioma-specific receptors would enable novel practical approaches for improving the passage of nanomedicines to be designed with the purpose of exposing the entire diseased brain tumor area to pharmacologically meaningful quantities.

On the other hand, the adsorption-mediated active targeting takes advantage of electrostatic interactions between positively-charged ligands and the negatively-charged sialic acid residues in membrane glycoproteins of brain endothelial cells to trigger transcytosis. Hence, this type of active targeting involves modifying the surface

of nanomedicines to make them positively charged, namely functionalization with cationic serum albumin and cell-penetrating peptides. The most frequently used cell-penetrating peptide for functionalization of nanomedicines is the transactivator of transcription peptide derived from HIV (TAT).

Subsequently, nanomedicines can also be designed to target simultaneously the BBB, the BBTB and the brain tumor cells by either attaching multiple targeting moieties, or by conjugating a single ligand that targets both the brain endothelia and the brain tumor cells [81]. In this case, nanomedicine could indeed represent a potential platform for targeting heterogeneous brain tumors [15].

Lastly, nanomedicines can increase intratumoral concentration of systemically administered anticancer agents by inhibiting the efflux pump function of P-glycoprotein that is present at the BBTB and at the infiltrative tumor cells and that actively removes these drugs, accounting to a great extent for resistance to chemotherapy. A localized inhibition on brain efflux transporters can be achieved by co-loading pharmacological efflux pump inhibitors (such as tamoxifen) or by the nanomedicine itself, since the coating with nonionic surfactants seems to provide the nanocarrier itself with efflux-pump blockage properties.

Besides tailoring the size and surface properties of nanomedicines to influence intratumoral accumulation, external forces such as a magnetic field, light and heat can also help selectively release the loaded drug of systemically administered nanomedicines at the tumor site [82]. Magnetic targeting has been applied under the assumption that magnetic nanoparticles can accumulate within a tumor area after systemic administration with a locally applied magnetic field. Another external force such as heat can be also used to control drug release in the case of nanomedicines whose excipients exhibit thermosensitive properties. Apart from enhancing tumor blood flow and vascular permeability, the application of local hyperthermia enables the drug to be easily released from thermosensitive nanomedicines when heating over the phase-transition temperature of the excipients.

Numerous intravenously-administered drug-loaded nanomedicines have already been assayed for efficacy in rodent models of brain tumors: liposomes, polymer nanoparticles, lipid nanocapsules, dendrimers, polymeric micelles, magnetic nanoparticles and gold nanoparticles (Table 3). Albeit results extremely depend on the tumor lineage and the onset, dose and regimen of treatment, some general conclusions can be drawn. In broad terms, following intravenous administration, similar results were obtained with most types of nanomedicines.

Most nanomedicines intended for preclinical evaluation following intravenous administration were designed to exploit passive and/or active targeting. Overall, stealth properties alone do not appear sufficient for enabling a nanoparticle-mediated transport into the brain, since in most cases of passively-non-actively targeted nanomedicines survival benefits remained extremely modest [83-85]. This could be due to the fact that PEG coating also reduces the tumor cell uptake of nanomedicines.

Additional active targeting using moieties that preferentially bind to receptors on the cerebral endothelial cells or overexpressed on brain tumor cells did indeed improve the therapeutic potential of nanomedicines due to preferential distribution to and within the brain tumor area: in all the studies with intravenously-administered actively-targeted nanomedicines, the median survival times were longer than their actively-untargeted counterparts and noticeably longer than the untreated controls [75, 86-88].

However, most of these receptors are ubiquitously expressed to some degree. Hence, in order to prevent the occurrence of non-specific side effects, dual-actively-targeted have already been designed for achieving optimal targeting after systemic administration. In broad terms, the preclinical studies with these dual-targeted nanomedicines showed more extended survival times over their mono-targeted counterparts [65, 73, 78].

Encapsulated drug	System	Strategy	Model	Ref
Paclitaxel	Liposomes	None	9L gliosarcoma-bearing rats	[37]
Paclitaxel	Liposomes	- Polyethylene glycol coating [a] - RGD peptide [b] - Histidine rich TH peptide [c]	C6 glioma-bearing mice	[38]
Irinotecan	Liposomes	- Polyethylene glycol coating [a]	U87MG glioblastoma-bearing mice	[39]
Topotecan	Liposomes	- Polyethylene glycol coating [a] - Wheat germ agglutinin [b] - Tamoxifen [d]	C6 glioma-bearing rats	[40]
Topotecan	Liposomes	- Polyethylene glycol coating [a]	U87M/GBM-43/GBM-6 glioblastoma-bearing mice	[41]
Doxorubicin	Liposomes	- Polyethylene glycol coating [a] - Folate [b] - Transferrin [b]	C6 glioma-bearing rats	[42]
Doxorubicin	Liposomes	- Lactoferrin [b] - Nanocarrier cationization [c]	C6 glioma-bearing rats	[43]
Doxorubicin	Liposomes	- Polyethylene glycol coating [a] - ^{D}CDX peptide [b]	U87MG glioblastoma-bearing mice	[44]
Doxorubicin	Liposomes	- Polyethylene glycol coating [a] - AP-1 peptide [b] - Focused ultrasound [e]	GBM8401 glioblastoma-bearing mice	[45]

Encapsulated drug	System	Strategy	Model	Ref
Doxorubicin	Liposomes	- Polyethylene glycol coating [a] - Glutathione [b]	U87MG glioblastoma-bearing mice	[46]
Doxorubicin	Liposome	- Polyethylene glycol coating [a] - Hyperthermia [e]	C6 glioma-bearing mice	[47]
Epirubicin	Liposomes	- Polyethylene glycol coating [a] - Transferrin [b] - Tamoxifen [d]	C6 glioma-bearing rats	[48]
Daunorubicin	Liposomes	- Polyethylene glycol coating [a] - Mannose [b] - Transferrin [b]	C6 glioma-bearing rats	[49]
RNA antiEGFR	Liposomes	- Polyethylene glycol coating [a] - 83-14 [b] - 8D3 [b]	U87MG glioblastoma-bearing mice	[50]
siRNA antiEGFR	Liposomes	- Polyethylene glycol coating [a] - T7 peptide [b]	U87MG glioblastoma-bearing mice	[51]
DNA (pC27)	Liposomes	- Polyethylene glycol coating [a] - OX26 [b] - Chlorotoxine [b]	C6 glioma-bearing rats	[52]
Paclitaxel	Polymeric nanoparticles	- Polyethylene glycol coating [a] - AS1411 aptamer [b]	C6 glioma-bearing rats	[53]
Paclitaxel	Polymeric nanoparticles	- Polyethylene glycol coating [a] - Peptide 22 [b]	C6 glioma-bearing mice	[54]
Paclitaxel	Polymeric nanoparticles	- Polyethylene glycol coating [a] - F3 peptide [b]	C6 glioma-bearing mice	[55]
Paclitaxel	Polymeric nanoparticles	- Polyethylene glycol coating [a] - PEP-1 [b]	C6 glioma-bearing mice	[56]
Paclitaxel	Polymeric nanoparticles	- Polyethylene glycol coating [a] - Glucose [b]	RG-2 glioma-bearing mice	[57]
Paclitaxel	Polymeric nanoparticles	- Polyethylene glycol coating [a] - APT peptide [b]	U87MG glioblastoma-bearing mice	[58]
Paclitaxel	Polymeric nanoparticles	- Polyethylene glycol coating [a] - iNGR peptide [b]	U87MG glioblastoma-bearing mice	[59]
Paclitaxel	Polymeric nanoparticles	- Polyethylene glycol coating [a] - RGD peptide [b]	U87MG glioblastoma-bearing mice	[60]
Paclitaxel	Polymeric nanoparticles	- Polyethylene glycol coating [a] - Angiopep [b]	U87MG glioblastoma-bearing mice	[61]
Gemcitabine	Polymeric nanoparticles	- Polysorbate-80 coating [a]	C6 glioma-bearing rats	[62]

Encapsulated drug	System	Strategy	Model	Ref
Aclarubicin	Polymeric nanoparticles	- Polyethylene glycol coating [a] - Cationic serum albumin [c]	C6 glioma-bearing rats	[63]
Camptothecin	Polymeric nanoparticles	None	GL261 glioma-bearing mice	[64]
Doxorubicin	Polymeric nanoparticles	- Polysorbate-80 coating [a]	101-8 glioblastoma-bearing rats	[65]
Doxorubicin	Polymeric nanoparticles	- Polysorbate-80/Poloxamer-188/Poloxamer-908 coating [a]	101-8 glioblastoma-bearing rats	[66]
Doxorubicin	Polymeric nanoparticles	- Polysorbate-80/Poloxamer-188 coating [a]	101-8 glioblastoma-bearing rats	[67]
Docetaxel	Polymeric nanoparticles	- Polyethylene glycol coating [a] - TGN peptide [b] - AS1411 aptamer [b]	C6 glioma-bearing mice	[68]
Docetaxel	Polymeric nanoparticles	- Polyethylene glycol coating [a] - IL-13 peptide [b]	U87MG glioblastoma-bearing mice	[69]
Porphyrin	Polymeric nanoparticles	- Polyethylene glycol coating [a] - F3 peptide [b] - Photodynamic therapy [e]	9L gliosarcoma-bearing rats	[70]
Ferrociphenol	Lipid nanocapsules	- Polyethylene glycol coating [a]	9L gliosarcoma-bearing rats	[71]
Doxorubicin	Dendrimers	- Polyethylene glycol coating [a] - RGD peptide [b]	C6 glioma-bearing mice	[72]
RNA antiEGFR (miR-7)	Dendrimers	- Folate [b]	U251 glioma-bearing mice	[73]
DNA (TRAIL)	Dendrimers	- Polyethylene glycol coating [a] - Chlorotoxin [b]	C6 glioma-bearing mice	[74]
DNA (TRAIL)	Dendrimers	- Polyethylene glycol coating [a] - Angiopep [b]	C6 glioma-bearing mice	[75]
DNA (TRAIL)	Dendrimers	- Polyethylene glycol coating [a] - RGD peptide [b]	U87MG glioblastoma-bearing mice	[76]
Paclitaxel	Polymeric micelles	- Polyethylene glycol coating [a] - CDX peptide (candoxin) [b]		
Paclitaxel	Polymeric micelles	- Polyethylene glycol coating [a] - RGD peptide [b] - Transferrin [b]	U87MG glioblastoma-bearing mice	[77]
Paclitaxel	Polymeric micelles	- Polyethylene glycol coating [a] - KC2S peptide [b]	U87MG glioblastoma-bearing mice	[78]
Paclitaxel	Polymeric micelles	- Polyethylene glycol coating [a] - RGD peptide [b]	U87MG glioblastoma-bearing mice	[79]

Encapsulated drug	System	Strategy	Model	Ref
Paclitaxel	Polymeric micelles	- Polyethylene glycol coating [a] - CDX peptide [b]	U87MG glioblastoma-bearing mice	[80]
Doxurubicin + Paclitaxel	Polymeric micelles	- Polyethylene glycol coating [a] - RGD peptide [b]	U87MG glioblastoma-bearing mice	[81]
SN-38 (camptothecin derivative)	Polymeric micelles	- Polyethylene glycol coating [a]	U87MG glioblastoma-bearing mice	[82, 83]
Paclitaxel	Magnetic nanoparticles	- Magnetic fields [e]	C6 glioma-bearing rats	[84]
Doxorubicin	Gold nanoparticles	- Polyethylene glycol coating [a] - TAT peptide [c]	U87MG glioblastoma-bearing mice	[85]

Table 1.1.3- Intravenously-administered nanomedicines already tested for efficacy in vivo against orthotopic rodent brain tumor models. Strategies: a: passive targeting; b: carrier/receptor-mediated active targeting; c: adsorption-mediated active targeting; d: inhibition of efflux pump function; e: targeting caused by external physical stimuli.

5. Conclusions

Despite the tremendous efforts thus far, malignant CNS tumors still represent an unmet medical need. Albeit the rapidly evolving knowledge about tumor biochemistry enables various new drug molecules to be designed as treatments, drug delivery in CNS tumors deserves explicit attention, as otherwise, novel therapies will continue to fail to expose the entire tumor and the infiltrate cells that are not located in the tumor bed to such therapeutics at pharmacologically meaningful quantities. In this regard, nanomedicine poses an appealing platform for efficient drug delivery to the CNS, since it may be targeted to improve the availability of the drugs in their site of action, which could be translated into lower drug doses and fewer side-effects.

The BBTB restricts the permeation of most anticancer agents into the CNS, especially in areas where the BBTB more closely resembles the BBB. Therefore, one major challenge in the field of systemic chemotherapy is the development of nanomedicines that can effectively overcome the BBTB and allow specific targeting of brain cancer cells. Overall, the features of nanomedicines dictate their biological fate: size and surface charge, the surface hydration and/or the presence of targeting ligands on the surface. Concerning brain endothelium permeation, an ideal systemic nanomedicine for CNS drug delivery should be around or smaller than 100 nm; be provided with a hydrophilic coating to avoid removal by the RES, extend its plasma half-life and indirectly increase the likelihood of crossing the brain endothelium; have targeting moieties to selectively enhance the distribution across the BBTB to the CNS and even be able to inhibit the drug efflux transporters at the BBTB.

Alternatively, nanomedicines can be locally administered to bypass the BBTB. However, CED and intrathecal delivery remain invasive approaches that carry

significant risks for patients. An optimal nanomedicine for CED should be below 100 nm, neutral or negatively charged, conjugated to specific ligands that bind the tumor cell receptors and be infused in a slight viscous and hyperosmolar solution.

Overall, nanomedicines intended for brain delivery either for systemic or local delivery should ideally be biocompatible and biodegradable, have a controllable release profile to trigger drug release at the site of action, be able to be sterilized and have a feasible industrial production for clinical implementation.

On the basis of the promising results gathered from preclinical studies of nanomedicine-based therapy, some nanomedicines have already been approved for clinical trials in a variety of CNS tumors conditions to serve as the first steps in translation of nanotherapy to clinic (Table 4). Therefore, their outcome will steer further research directions and when successful, will provide handles for further improvements. Unfortunately, the results of the already completed clinical trials are not yet available on clinicaltrials.gov.

It is worth underlining the fact that current clinical trials using nanomedicines for brain tumors are conducted on patients who have failed conventional therapy and have very poor prognosis (mostly recurrent high-grade glioma or brain metastases). However, expanding the application of nanomedicine to less aggressive forms of brain cancer is challenging, as long as the long-term side effects due to the interactions of colloids with biological structures are not yet known and, consequently, the regulatory agencies have not yet developed comprehensive regulatory guidelines for nanomedicines.

In view of the approved clinical trials, some general conclusions can be drawn. On the one hand, whereas several liposomal formulations are already under clinical trials, the rest of types of nanomedicines are lagging behind. The investigation of nanomedicines for CNS delivery has focused largely on liposomal preparations mostly due to the fact that their potential as drug carriers was already acknowledged back in the 1970s, much earlier than any other alternative nanocarrier.

On the other hand, most liposomes that reached clinical trials for the treatment of brain tumors are passively-targeted, avoiding the ligand-receptor interaction. Despite of the promising preclinical results, translation of active targeting to clinical trials pose some challenges, since most targeted receptors are not exclusively present at the BBTB and/or brain tumor cells, which may give raise to side effects. Additionally, nanomedicines conjugated with physiological ligands can develop competitive phenomena with endogenous ligands and dysregulate their homeostasis, whereas nanomedicines that incorporate monoclonal antibodies must be able of interacting with human receptors to not cause immunogenic reactions; hence, presumably different from those antibodies assayed in rodent preclinical models. Nonetheless, two actively-targeted liposomes have recently made their way to clinical trials to cross the BBB after intravenous injection for achieving higher and efficacious brain drug levels: 2B3-101 is a PEGylated liposomal doxorubicin formulation conjugated with glutathione, and SGT-53 is a cationic liposome conjugated to an anti-transferrin receptor single-chain antibody and encapsulating a normal human wild type p53 DNA sequence to restore

the wild type p53 function and down-modulate MGMT activity in order to increase the sensitivity of tumor cells to alkylating agents.

Concerning the different routes of administration, intravenous among the systemic routes and CED and intrathecal delivery among the local routes have even made its way into clinical trials for nanoparticle administration.

Identifier	Condition	Treatment	Nanomedicine	Route	Targeting approach
00003073	CNS tumors	Cytarabine	Liposome (DepoCyt®)	Intrathecal	None
00029523	Neoplastic meningitis	Cytarabine	Liposome (DepoCyt®)	Intrathecal	None
00313599	CNS tumors	Paclitaxel (+ oral lapatinib)	Albumin nanoparticles (Abraxane®)	Intravenous	None
00019630	Brain tumors (Children)	Doxorubicin	Pegylated liposome (Lipodox®)	Intravenous	Passive
00465673	Brain metastases	Doxorubicin	Pegylated liposome (Lipodox®)	Intravenous	Passive
00734682	Glioblastoma Gliosarcoma Anaplastic astrocytoma Anaplastic oligodendroglioma	Irinotecan	Pegylated liposome	Intravenous	Passive
00854867	Neoplastic meningitis	Cytarabine (+ concomitant/ sequential radiotherapy)	Liposome (DepoCyt®)	Intrathecal	None
00944801	Glioblastoma	Doxorubicin (+ temozolomide + radiotherapy)	Pegylated liposome (Caelix®)	Intravenous	Passive
00964743	Neoplastic meningitis	Cytarabine (+ oral sorafenib)	Liposome (DepoCyt®)	Intrathecal (Ommaya reservoir)	None
00992602	Leptomeningeal metastases	Cytarabine (+ intravenous methotrexate)	Liposome (DepoCyt®)	Intrathecal	None

Identifier	Condition	Treatment	Nanomedicine	Route	Targeting approach
01044966	Glioblastoma multiforme Glioma Astrocytoma Brain tumor	Cytarabine (+ oral temozolomide)	Liposome (DepoCyt®)	Intrathecal	None
01222780	Brain tumors (Children)	Vincristine	Liposome (Marqibo®)	Intravenous	None
01386580	Recurrent malignant glioma Brain metastases	Doxorubicin	Glutathione pegylated liposome	Intravenous	Passive + Active
01563614	Leptomeningeal metastases	Cytarabine (+ oral lomustine + radiotherapy)	Liposome (DepoCyt®)	Intrathecal	None
01818713	Leptomeningeal metastases	Doxorubicin	Glutathione pegylated liposome	Intravenous	Passive + Active
02022644	High grade glioma	Irinotecan	Pegylated liposome	CED	Passive
02340156	Glioblastoma	Normal human wild type p53 DNA sequence (+ oral temozolomide)	Anti-transferrin receptor single-chain antibody cationic liposome	Intravenous	Active

Table 1.1.4- Nanomedicines that have already reached the clinical trials stage for the treatment of CNS tumors.

In conclusion, clinical implementation of nanomedicines for patients with brain tumors is still in its infancy. However, further clinical studies of brain-targeted nanomedicines are warranted in the future, with rising incidences of CNS cancers, many of which being terrible rapidly progressing and so-far untreatable tumors. Hence, the accumulation of data about the CNS physiology and about relevant receptors, the widening therapeutic armamentarium of drugs potentially useful in CNS chemotherapy, the alternative routes for administration and the estimation of the brain permeability with in vitro BBB models to early triage the potential of nanomedicines for optimum therapy of brain tumors envisage nanomedicines as a forthcoming routine approach [114].

Acknowledgements

This work was partially funded by the Research Group GR35/10 Santander-UCM, Group: Parenteral Administration of Drugs. Juan Aparicio-Blanco thanks the

Spanish Ministry of Education for the Contract within the Professor Training Program FPU (Ref. FPU13/02325).

References:

[1] Louis DN, Ohgaki H, Wiestler OD, Cavenee WK, Burger PC, Jouvet A, et al. The 2007 WHO classification of tumours of the central nervous system. Acta Neuropathol. 2007;114:97-109.

[2] Schwartzbaum JA, Fisher JL, Aldape KD, Wrensch M. Epidemiology and molecular pathology of glioma. Nat Clin Pract Neurol. 2006;2:494-503.

[3] Wen PY, Kesari S. Malignant gliomas in adults. N Engl J Med. 2008;359:492-507.

[4] Alifieris C, Trafalis DT. Glioblastoma multiforme: Pathogenesis and treatment. Pharmacol Ther. 2015;152:63-82.

[5] Stupp R, Mason WP, van den Bent MJ, Weller M, Fisher B, Taphoorn MJB, et al. Radiotherapy plus concomitant and adjuvant temozolomide for glioblastoma. N Engl J Med. 2005;352:987-96.

[6] Messaoudi K, Clavreul A, Lagarce F. Toward an effective strategy in glioblastoma treatment. Part I: resistance mechanisms and strategies to overcome resistance of glioblastoma to temozolomide. Drug Discov Today. 2015;20:899-905.

[7] Esteller M, Garcia-Foncillas J, Andion E, Goodman SN, Hidalgo OF, Vanaclocha V, et al. Inactivation of the DNA-repair gene MGMT and the clinical response of gliomas to alkylating agents. N Engl J Med. 2000;343:1350-4.

[8] Hegi ME, Diserens A, Gorlia T, Hamou M, de Tribolet N, Weller M, et al. MGMT gene silencing and benefit from temozolomide in glioblastoma. N Engl J Med. 2005;352:997-1003.

[9] de Faria GP, de Oliveira JA, de Oliveira JGP, Romano SD, Neto VM, Maia RC. Differences in the Expression Pattern of P-Glycoprotein and MRP1 in Low-Grade and High-Grade Gliomas. Cancer Invest. 2008;26:883-9.

[10] Holohan C, Van Schaeybroeck S, Longley DB, Johnston PG. Cancer drug resistance: an evolving paradigm. Nat Rev Cancer. 2013;13:714-26.

[11] van Tellingen O, Yetkin-Arik B, de Gooijer MC, Wesseling P, Wurdinger T, de Vries HE. Overcoming the blood-brain tumor barrier for effective glioblastoma treatment. Drug Resist Update. 2015;19:1-12.

[12] Schinkel AH. P-glycoprotein, a gatekeeper in the blood-brain barrier. Adv Drug Deliv Rev. 1999;36:179-94.

[13] Westphal M, Hilt DC, Bortey E, Delavault P, Olivares R, Warnke PC, et al. A phase 3 trial of local chemotherapy with biodegradable carmustine (BCNU) wafers (Gliadel wafers) in patients with primary malignant glioma. Neuro-Oncology. 2003;5:79-88.

[14] Davis ME, Chen Z, Shin DM. Nanoparticle therapeutics: an emerging treatment modality for cancer. Nat Rev Drug Discov. 2008;7:771-82.

[15] Cheng Y, Morshed RA, Auffinger B, Tobias AL, Lesniak MS. Multifunctional nanoparticles for brain tumor imaging and therapy. Adv Drug Deliv Rev. 2014;66:42-57.

[16] Karim R, Palazzo C, Evrard B, Piel G. Nanocarriers for the treatment of glioblastoma multiforme: Current state-of-the-art. J Control Release. 2016;227:23-37.

[17] Cupaioli FA, Zucca FA, Boraschi D, Zecca L. Engineered nanoparticles. How brain friendly is this new guest? Prog Neurobiol. 2014;119:20-38.

[18] Lai F, Fadda AM, Sinico C. Liposomes for brain delivery. Expert Opin Drug Deliv. 2013;10:1003-22.

[19] Gastaldi L, Battaglia L, Peira E, Chirio D, Muntoni E, Solazzi I, et al. Solid lipid nanoparticles as vehicles of drugs to the brain: Current state of the art. Eur J Pharm Biopharm. 2014;87:433-44.

[20] Aparicio-Blanco J, Torres-Suarez AI. Glioblastoma Multiforme and Lipid Nanocapsules: A Review. J Biomed Nanotechnol. 2015;11:1283-311.

[21] Patel T, Zhou JB, Piepmeier JM, Saltzman WM. Polymeric nanoparticles for drug delivery to the central nervous system. Adv Drug Deliv Rev. 2012;64:701-5.

[22] Costantino L, Boraschi D. Is there a clinical future for polymeric nanoparticles as brain-targeting drug delivery agents? Drug Discov Today. 2012;17:367-78.

[23] Mishra V, Kesharwani P. Dendrimer technologies for brain tumor. Drug Discov Today. 2016;21:766-78.

[24] Singh D, McMillan JM, Kabanov AV, Sokolsky-Papkov M, Gendelman HE. Bench-to-bedside translation of magnetic nanoparticles. Nanomedicine. 2014;9:501-16.

[25] Jabr-Milane LS, van Vlerken LE, Yadav S, Amiji MM. Multi-functional nanocarriers to overcome tumor drug resistance. Cancer Treat Rev. 2008;34:592-602.

[26] Allard E, Passirani C, Benoit JP. Convection-enhanced delivery of nanocarriers for the treatment of brain tumors. Biomaterials. 2009;30:2302-18.

[27] MacKay JA, Deen DF, Szoka FC. Distribution in brain of liposomes after convection enhanced delivery; modulation by particle charge, particle diameter, and presence of steric coating. Brain Res. 2005;1035:139-53.

[28] Serwer LP, James CD. Challenges in drug delivery to tumors of the central nervous system: An overview of pharmacological and surgical considerations. Adv Drug Deliv Rev. 2012;64:590-7.

[29] Mistry A, Stolnik S, Illum L. Nanoparticles for direct nose-to-brain delivery of drugs. Int J Pharm. 2009;379:146-57.

[30] Noble CO, Krauze MT, Drummond DC, Yamashita Y, Saito R, Berger MS, et al. Novel nanoliposomal CPT-11 infused by convection-enhanced delivery in intracranial tumors: Pharmacology and efficacy. Cancer Res. 2006;66:2801-6.

[31] Saito R, Krauze MT, Noble CO, Drummond DC, Kirpotin DB, Berger MS, et al. Convection-enhanced delivery of Ls-TPT enables an effective, continuous, low-dose chemotherapy against malignant glioma xenograft model. Neuro-Oncology. 2006;8:205-14.

[32] Chen PY, Ozawa T, Drummond DC, Kalra A, Fitzgerald JB, Kirpotin DB, et al. Comparing routes of delivery for nanoliposomal irinotecan shows superior anti-tumor activity of local administration in treating intracranial glioblastoma xenografts. Neuro-Oncology. 2013;15:189-97.

[33] Yamashita Y, T Krauze M, Kawaguchi T, Noble CO, Drummond DC, Park JW, et al. Convection-enhanced delivery of a topoisomerase I inhibitor (nanoliposomal topotecan) and a topoisomerase II inhibitor (pegylated liposomal doxorubicin) in intracranial brain tumor xenografts. Neuro-Oncology. 2007;9:20-8.

[34] Krauze MT, Noble CO, Kawaguchi T, Drummond D, Kirpotin DB, Yamashita Y, et al. Convection-enhanced delivery of nanoliposomal CPT-11 (irinotecan) and PEGylated liposomal doxorubicin (Doxil) in rodent intracranial brain tumor xenografts. Neuro-Oncology. 2007;9:393-403.

[35] Stephen ZR, Kievit FM, Veiseh O, Chiarelli PA, Fang C, Wang K, et al. Redox-Responsive Magnetic Nanoparticle for Targeted Convection-Enhanced Delivery of O-6-Benzylguanine to Brain Tumors. ACS Nano. 2014;8:10383-95.

[36] Grahn AY, Bankiewicz KS, Dugich-Djordjevic M, Bringas JR, Hadaczek P, Johnson GA, et al. Non-PEGylated liposomes for convection-enhanced delivery of topotecan and gadodiamide in malignant glioma: initial experience. J Neuro-Oncol. 2009;95:185-97.

[37] Huynh NT, Passirani C, Allard-Vannier E, Lemaire L, Roux J, Garcion E, et al. Administration-dependent efficacy of ferrociphenol lipid nanocapsules for the treatment of intracranial 9L rat gliosarcoma. Int J Pharm. 2012;423:55-62.

[38] Laine AL, Huynh NT, Clavreul A, Balzeau J, Bejaud J, Vessieres A, et al. Brain tumour targeting strategies via coated ferrociphenol lipid nanocapsules. Eur J Pharm Biopharm. 2012;81:690-3.

[39] Hadjipanayis CG, Machaidze R, Kaluzova M, Wang LY, Schuette AJ, Chen HW, et al. EGFRvIII Antibody-Conjugated Iron Oxide Nanoparticles for Magnetic Resonance Imaging-Guided Convection-Enhanced Delivery and Targeted Therapy of Glioblastoma. Cancer Res. 2010;70:6303-12.

[40] Kaluzova M, Bouras A, Machaidze R, Hadjipanayis CG. Targeted therapy of glioblastoma stem-like cells and tumor non-stem cells using cetuximab-conjugated iron-oxide nanoparticles. Oncotarget. 2015;6:8788-806.

[41] Inoue T, Yamashita Y, Nishihara M, Sugiyama S, Sonoda Y, Kumabe T, et al. Therapeutic efficacy of a polymeric micellar doxorubicin infused by convection-enhanced delivery against intracranial 9L brain tumor models. Neuro-Oncology. 2009;11:151-7.

[42] Wu G, Barth RF, Yang WL, Kawabata S, Zhang LW, Green-Church K. Targeted delivery of methotrexate to epidermal growth factor receptor-positive brain tumors by means of cetuximab (IMC-C225) dendrimer bioconjugates. Mol Cancer Ther. 2006;5:52-9.

[43] Barth RF, Wu G, Meisen WH, Nakkula RJ, Yang W, Huo T, et al. Design, synthesis, and evaluation of cisplatin-containing EGFR targeting bioconjugates as potential therapeutic agents for brain tumors. OncoTargets Ther. 2016;9:2769-81.

[44] Taki H, Kanazawa T, Akiyama F, Takashima Y, Okada H. Intranasal delivery of camptothecin-loaded tat-modified nanomicells for treatment of intracranial brain tumors. Pharmaceuticals (Basel, Switzerland). 2012;5:1092-102.

[45] Kanazawa T, Morisaki K, Suzuki S, Takashima Y. Prolongation of Life in Rats with Malignant Glioma by Intranasal siRNA/Drug Codelivery to the Brain with Cell-Penetrating Peptide-Modified Micelles. Mol Pharm. 2014;11:1471-8.

[46] Sawyer AJ, Saucier-Sawyer JK, Booth CJ, Liu J, Patel T, Piepmeier JM, et al. Convection-enhanced delivery of camptothecin-loaded polymer nanoparticles for treatment of intracranial tumors. Drug Deliv Transl Res. 2011;1:34-42.

[47] Bernal GM, LaRiviere MJ, Mansour N, Pytel P, Cahill KE, Voce DJ, et al. Convection-enhanced delivery and in vivo imaging of polymeric nanoparticles for the treatment of malignant glioma. Nanomed-Nanotechnol Biol Med. 2014;10:149-57.

[48] Mangraviti A, Tzeng SY, Kozielski KL, Wang Y, Jin YK, Gullotti D, et al. Polymeric Nanoparticles for Nonviral Gene Therapy Extend Brain Tumor Survival in Vivo. ACS Nano. 2015;9:1236-49.

[49] Vinchon-Petit S, Jarnet D, Paillard A, Benoit JP, Garcion E, Menei P. In vivo evaluation of intracellular drug-nanocarriers infused into intracranial tumours by

convection-enhanced delivery: distribution and radiosensitisation efficacy. J Neuro-Oncol. 2010;97:195-205.

[50] Allard E, Huynh NT, Vessieres A, Pigeon P, Jaouen G, Benoit JP, et al. Dose effect activity of ferrocifen-loaded lipid nanocapsules on a 9L-glioma model. Int J Pharm. 2009;379:317-23.

[51] Allard E, Jarnet D, Vessieres A, Vinchon-Petit S, Jaouen G, Benoit JP, et al. Local Delivery of Ferrociphenol Lipid Nanocapsules Followed by External Radiotherapy as a Synergistic Treatment Against Intracranial 9L Glioma Xenograft. Pharm Res. 2010;27:56-64.

[52] Yokosawa M, Sonoda Y, Sugiyama S, Saito R, Yamashita Y, Nishihara M, et al. Convection-Enhanced Delivery of a Synthetic Retinoid Am80, Loaded into Polymeric Micelles, Prolongs the Survival of Rats Bearing Intracranial Glioblastoma Xenografts. Tohoku J Exp Med. 2010;221:257-64.

[53] Peluffo H, Unzueta U, Negro-Demontel ML, Xu ZK, Vaquez E, Ferrer-Miralles N, et al. BBB-targeting, protein-based nanomedicines for drug and nucleic acid delivery to the CNS. Biotechnol Adv. 2015;33:277-87.

[54] Maeda H, Wu J, Sawa T, Matsumura Y, Hori K. Tumor vascular permeability and the EPR effect in macromolecular therapeutics: a review. J Control Release. 2000;65:271-84.

[55] Beduneau A, Saulnier P, Benoit JP. Active targeting of brain tumors using nanocarriers. Biomaterials. 2007;28:4947-67.

[56] Alyautdin R, Khalin I, Nafeeza MI, Haron MH, Kuznetsov D. Nanoscale drug delivery systems and the blood-brain barrier. Int J Nanomed. 2014;9:795-811.

[57] Dobrovolskaia MA, McNeil SE. Immunological properties of engineered nanomaterials. Nat Nanotechnol. 2007;2:469-78.

[58] Gref R, Luck M, Quellec P, Marchand M, Dellacherie E, Harnisch S, et al. 'Stealth' corona-core nanoparticles surface modified by polyethylene glycol (PEG): influences of the corona (PEG chain length and surface density) and of the core composition on phagocytic uptake and plasma protein adsorption. Colloid Surf B-Biointerfaces. 2000;18:301-13.

[59] Rapoport SI, Robinson PJ. Tight-junctional modification as the basis of osmotic opening of the blood-brain barrier. Ann NY Acad Sci. 1986;481:250-67.

[60] Nakano S, Matsukado K, Black KL. Increased brain tumor microvessel permeability after intracarotid bradykinin infusion is mediated by nitric oxide. Cancer Res. 1996;56:4027-31.

[61] Hynynen K, McDannold N, Vykhodtseva N, Raymond S, Weissleder R, Jolesz FA, et al. Focal disruption of the blood-brain barrier due to 260-kHz ultrasound bursts: a method for molecular imaging and targeted drug delivery. J Neurosurg. 2006;105:445-54.

[62] Oller-Salvia B, Sanchez-Navarro M, Giralt E, Teixido M. Blood-brain barrier shuttle peptides: an emerging paradigm for brain delivery. Chemical Society reviews. 2016;45:4690-707.

[63] Zhang Y, Zhang YF, Bryant J, Charles A, Boado RJ, Pardridge WM. Intravenous RNA interference gene therapy targeting the human epidermal growth factor receptor prolongs survival in intracranial brain cancer. Clin Cancer Res. 2004;10:3667-77.

[64] Wei L, Guo X-Y, Yang T, Yu M-Z, Chen D-W, Wang J-C. Brain tumor-targeted therapy by systemic delivery of siRNA with Transferrin receptor-mediated core-shell nanoparticles. Int J Pharm. 2016;510:394-405.

[65] Yue PJ, He L, Qiu SW, Li Y, Liao YJ, Li XP, et al. OX26/CTX-conjugated PEGylated liposome as a dual-targeting gene delivery system for brain glioma. Mol Cancer. 2014;13:13.

[66] Wei XL, Zhan CY, Shen Q, Fu W, Xie C, Gao J, et al. A D-Peptide Ligand of Nicotine Acetylcholine Receptors for Brain-Targeted Drug Delivery. Angew Chem-Int Edit. 2015;54:3023-7.

[67] Zhan CY, Wei XL, Qian J, Feng LL, Zhu JH, Lu WY. Co-delivery of TRAIL gene enhances the anti-glioblastoma effect of paclitaxel in vitro and in vivo. J Control Release. 2012;160:630-6.

[68] Zhan CY, Yan ZQ, Xie C, Lu WY. Loop 2 of Ophiophagus hannah Toxin b Binds with Neuronal Nicotinic Acetylcholine Receptors and Enhances Intracranial Drug Delivery. Mol Pharm. 2010;7:1940-7.

[69] Huang SX, Li JF, Han L, Liu SH, Ma HJ, Huang RQ, et al. Dual targeting effect of Angiopep-2-modified, DNA-loaded nanoparticles for glioma. Biomaterials. 2011;32:6832-8.

[70] Xin HL, Sha XY, Jiang XY, Zhang W, Chen LC, Fang XL. Anti-glioblastoma efficacy and safety of paclitaxel-loading Angiopep-conjugated dual targeting PEG-PCL nanoparticles. Biomaterials. 2012;33:8167-76.

[71] Jiang XY, Xin HL, Ren QY, Gu JJ, Zhu LJ, Du FY, et al. Nanoparticles of 2-deoxy-D-glucose functionalized poly(ethylene glycol)-co-poly(trimethylene carbonate) for dual-targeted drug delivery in glioma treatment. Biomaterials. 2014;35:518-29.

[72] Ying X, Wen H, Lu WL, Du J, Guo J, Tian W, et al. Dual-targeting daunorubicin liposomes improve the therapeutic efficacy of brain glioma in animals. J Control Release. 2010;141:183-92.

[73] Shi KR, Long Y, Xu CQ, Wang Y, Qiu Y, Yu QW, et al. Liposomes Combined an Integrin alpha(v)beta(3)-Specific Vector with pH-Responsible Cell-Penetrating Property for Highly Effective Antiglioma Therapy through the Blood-Brain Barrier. ACS Appl Mater Interfaces. 2015;7:21442-54.

[74] Jiang XY, Sha XY, Xin HL, Xu XM, Gu JJ, Xia WY, et al. Integrin-facilitated transcytosis for enhanced penetration of advanced gliomas by poly(trimethylene carbonate)-based nanoparticles encapsulating paclitaxel. Biomaterials. 2013;34:2969-79.

[75] Kang T, Gao XL, Hu QY, Jiang D, Feng XY, Zhang X, et al. iNGR-modified PEG-PLGA nanoparticles that recognize tumor vasculature and penetrate gliomas. Biomaterials. 2014;35:4319-32.

[76] Hu QY, Gu GZ, Liu ZY, Jiang MY, Kang T, Miao DY, et al. F3 peptide-functionalized PEG-PLA nanoparticles co-administrated with tLyp-1 peptide for anti-glioma drug delivery. Biomaterials. 2013;34:1135-45.

[77] Guo JW, Gao XL, Su LN, Xia HM, Gu GZ, Pang ZQ, et al. Aptamer-functionalized PEG-PLGA nanoparticles for enhanced anti-glioma drug delivery. Biomaterials. 2011;32:8010-20.

[78] Gao HL, Qian J, Cao SJ, Yang Z, Pang ZQ, Pan SQ, et al. Precise glioma targeting of and penetration by aptamer and peptide dual-functioned nanoparticles. Biomaterials. 2012;33:5115-23.

[79] Yang FY, Wong TT, Teng MC, Liu RS, Lu M, Liang HF, et al. Focused ultrasound and interleukin-4 receptor-targeted liposomal doxorubicin for enhanced targeted drug delivery and antitumor effect in glioblastoma multiforme. J Control Release. 2012;160:652-8.

[80] Huang RQ, Ke WL, Han LA, Li JF, Liu SH, Jiang C. Targeted delivery of chlorotoxin-modified DNA-loaded nanoparticles to glioma via intravenous administration. Biomaterials. 2011;32:2399-406.

[81] Liu Y, Lu WY. Recent advances in brain tumor-targeted nano-drug delivery systems. Expert Opin Drug Deliv. 2012;9:671-86.

[82] Liu HL, Hua MY, Yang HW, Huang CY, Chu PC, Wu JS, et al. Magnetic resonance monitoring of focused ultrasound/magnetic nanoparticle targeting delivery of therapeutic agents to the brain. Proc Natl Acad Sci U S A. 2010;107:15205-10.

[83] Wang CX, Huang LS, Hou LB, Jiang L, Yan ZT, Wang YL, et al. Antitumor effects of polysorbate-80 coated gemcitabine polybutylcyanoacrylate nanoparticles in vitro and its pharmacodynamics in vivo on C6 glioma cells of a brain tumor model. Brain Res. 2009;1261:91-9.

[84] Householder KT, DiPerna DM, Chung EP, Wohlleb GM, Dhruv HD, Berens ME, et al. Intravenous delivery of camptothecin-loaded PLGA nanoparticles for the treatment of intracranial glioma. Int J Pharm. 2015;479:374-80.

[85] Huynh NT, Morille M, Bejaud J, Legras P, Vessieres A, Jaouen G, et al. Treatment of 9L Gliosarcoma in Rats by Ferrociphenol-Loaded Lipid Nanocapsules Based on a Passive Targeting Strategy via the EPR Effect. Pharm Res. 2011;28:3189-98.

[86] Gaillard PJ, Appeldoorn CCM, Dorland R, van Kregten J, Manca F, Vugts DJ, et al. Pharmacokinetics, Brain Delivery, and Efficacy in Brain Tumor-Bearing Mice of Glutathione Pegylated Liposomal Doxorubicin (2B3-101). PLoS One. 2014;9:10.

[87] Zhang B, Sun XY, Mei H, Wang Y, Liao ZW, Chen J, et al. LDLR-mediated peptide-22-conjugated nanoparticles for dual-targeting therapy of brain glioma. Biomaterials. 2013;34:9171-82.

[88] Zhang LH, Zhu SJ, Qian LL, Pei YY, Qiu YM, Jiang YY. RGD-modified PEG-PAMAM-DOX conjugates: In vitro and in vivo studies for glioma. Eur J Pharm Biopharm. 2011;79:232-40.

[89] Zhou R, Mazurchuk RV, Tamburlin JH, Harrold JM, Mager DE, Straubinger RM. Differential Pharmacodynamic Effects of Paclitaxel Formulations in an Intracranial Rat Brain Tumor Model. J Pharmacol Exp Ther. 2010;332:479-88.

[90] Noble CO, Krauze MT, Drummond DC, Forsayeth J, Hayes ME, Beyer J, et al. Pharmacokinetics, tumor accumulation and antitumor activity of nanoliposomal irinotecan following systemic treatment of intracranial tumors. Nanomedicine. 2014;9:2099-108.

[91] Du J, Lu WL, Ying X, Liu Y, Du P, Tian W, et al. Dual-Targeting Topotecan Liposomes Modified with Tamoxifen and Wheat Germ Agglutinin Significantly Improve Drug Transport across the Blood-Brain Barrier and Survival of Brain Tumor-Bearing Animals. Mol Pharm. 2009;6:905-17.

[92] Serwer LP, Noble CO, Michaud K, Drummond DC, Kirpotin DB, Ozawa T, et al. Investigation of intravenous delivery of nanoliposomal topotecan for activity against orthotopic glioblastoma xenografts. Neuro-Oncology. 2011;13:1288-95.

[93] Gao JQ, Lv Q, Li LM, Tang XJ, Li FZ, Hu YL, et al. Glioma targeting and blood-brain barrier penetration by dual-targeting doxorubincin liposomes. Biomaterials. 2013;34:5628-39.

[94] Chen HL, Qin Y, Zhang QY, Jiang W, Tang L, Liu J, et al. Lactoferrin modified doxorubicin-loaded procationic liposomes for the treatment of gliomas. Eur J Pharm Sci. 2011;44:164-73.

[95] Gong W, Wang ZY, Liu N, Lin W, Wang XP, Xu D, et al. Improving Efficiency of Adriamycin Crossing Blood Brain Barrier by Combination of Thermosensitive Liposomes and Hyperthermia. Biol Pharm Bull. 2011;34:1058-64.

[96] Tian W, Ying X, Du J, Guo J, Men Y, Zhang Y, et al. Enhanced efficacy of functionalized epirubicin liposomes in treating brain glioma-bearing rats. Eur J Pharm Sci. 2010;41:232-43.

[97] Wang BY, Lv LY, Wang Z, Jiang Y, Lv W, Liu X, et al. Improved anti-glioblastoma efficacy by IL-13R alpha 2 mediated copolymer nanoparticles loaded with paclitaxel. Sci Rep. 2015;5:13.

[98] Gu GZ, Hu QY, Feng XY, Gao XL, Jiang ML, Kang T, et al. PEG-PLA nanoparticles modified with APT(EDB) peptide for enhanced anti-angiogenic and anti-glioma therapy. Biomaterials. 2014;35:8215-26.

[99] Lu W, Wan J, Zhang Q, She ZJ, Jiang XG. Aclarubicin-loaded cationic albumin-conjugated pegylated nanoparticle for glioma chemotherapy in rats. Int J Cancer. 2007;120:420-31.

[100] Steiniger SCJ, Kreuter J, Khalansky AS, Skidan IN, Bobruskin AI, Smirnova ZS, et al. Chemotherapy of glioblastoma in rats using doxorubicin-loaded nanoparticles. Int J Cancer. 2004;109:759-67.

[101] Ambruosi A, Gelperina S, Khalansky A, Tanski S, Theisen A, Kreuter J. Influence of surfactants, polymer and doxorubicin loading on the anti-tumour effect of poly(butyl cyanoacrylate) nanoparticles in a rat glioma model. J Microencapsul. 2006;23:582-92.

[102] Gelperina S, Maksimenko O, Khalansky A, Vanchugova L, Shipulo E, Abbasova K, et al. Drug delivery to the brain using surfactant-coated poly(lactide-co-glycolide) nanoparticles: Influence of the formulation parameters. Eur J Pharm Biopharm. 2010;74:157-63.

[103] Gao HL, Yang Z, Zhang S, Cao SJ, Shen S, Pang ZQ, et al. Ligand modified nanoparticles increases cell uptake, alters endocytosis and elevates glioma distribution and internalization. Sci Rep. 2013;3:8.

[104] Reddy GR, Bhojani MS, McConville P, Moody J, Moffat BA, Hall DE, et al. Vascular targeted nanoparticles for imaging and treatment of brain tumors. Clin Cancer Res. 2006;12:6677-86.

[105] Liu XZ, Li G, Su ZG, Jiang ZM, Chen L, Wang JF, et al. Poly(amido amine) is an ideal carrier of miR-7 for enhancing gene silencing effects on the EGFR pathway in U251 glioma cells. Oncol Rep. 2013;29:1387-94.

[106] Zhang PC, Hu LJ, Yin Q, Feng LY, Li YP. Transferrin-Modified c RGDfK -Paclitaxel Loaded Hybrid Micelle for Sequential Blood-Brain Barrier Penetration and Glioma Targeting Therapy. Mol Pharm. 2012;9:1590-8.

[107] Zhan CY, Gu B, Xie C, Li J, Liu Y, Lu WY. Cyclic RGD conjugated poly(ethylene glycol)-co-poly(lactic acid) micelle enhances paclitaxel anti-glioblastoma effect. J Control Release. 2010;143:136-42.

[108] Zhan CY, Li B, Hu LJ, Wei XL, Feng LY, Fu W, et al. Micelle-Based Brain-Targeted Drug Delivery Enabled by a Nicotine Acetylcholine Receptor Ligand. Angew Chem-Int Edit. 2011;50:5482-5.

[109] Huang YK, Liu WC, Gao F, Fang XL, Chen YZ. c(RGDyK)-decorated Pluronic micelles for enhanced doxorubicin and paclitaxel delivery to brain glioma. Int J Nanomed. 2016;11:1629-41.

[110] Kuroda JI, Kuratsu JI, Yasunaga M, Koga Y, Saito Y, Matsumura Y. Potent antitumor effect of SN-38-incorporating polymeric micelle, NK012, against malignant glioma. Int J Cancer. 2009;124:2505-11.

[111] Kuroda J, Kuratsu J, Yasunaga M, Koga Y, Kenmotsu H, Sugino T, et al. Antitumor Effect of NK012, a 7-Ethyl-10-Hydroxycamptothecin-Incorporating Polymeric Micelle, on U87MG Orthotopic Glioblastoma in Mice Compared with Irinotecan Hydrochloride in Combination with Bevacizumab. Clin Cancer Res. 2010;16:521-9.

[112] Zhao M, Liang C, Li AM, Chang J, Wang HJ, Yan RM, et al. Magnetic Paclitaxel Nanoparticles Inhibit Glioma Growth and Improve the Survival of Rats Bearing Glioma Xenografts. Anticancer Res. 2010;30:2217-23.

[113] Cheng Y, Dai Q, Morshed RA, Fan XB, Wegscheid ML, Wainwright DA, et al. Blood-Brain Barrier Permeable Gold Nanoparticles: An Efficient Delivery Platform for Enhanced Malignant Glioma Therapy and Imaging. Small. 2014;10:5137-50.

[114] Aparicio-Blanco J, Martin-Sabroso C, Torres-Suarez A-I. In vitro screening of nanomedicines through the blood brain barrier: A critical review. Biomaterials. 2016;103:229-55.

Size-tailored nanocapsules by a single step energy-efficient procedure: the phase inversion temperature method revisited

Juan Aparicio-Blanco, Víctor Sebastián, Miguel Rodríguez-Amaro, Héctor García-Díaz, Ana I. Torres-Suárez

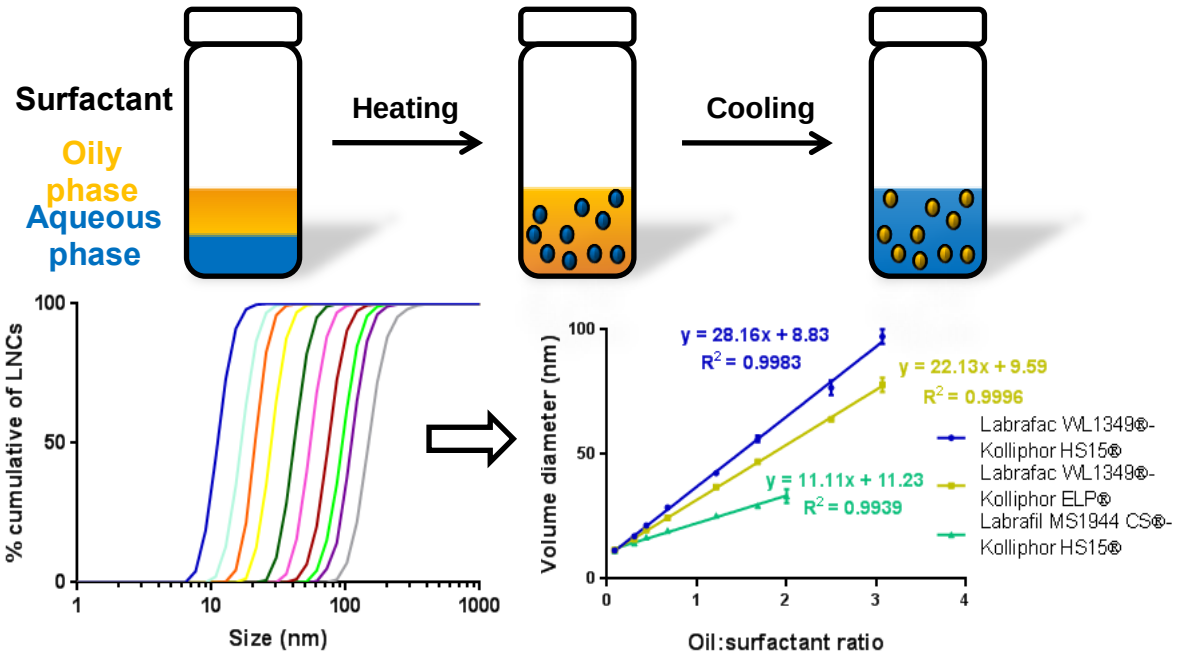

Size-tailored nanocapsules by a single step energetically-efficient procedure: the phase inversion temperature method revisited

Juan Aparicio-Blanco [a], Víctor Sebastián [b,c], Miguel Rodríguez-Amaro [a], Héctor García-Díaz [a], Ana I. Torres-Suárez [a, d]

[a] Department of Pharmaceutics and Food Technology, Complutense University, Madrid, Spain

[b] Department of Chemical Engineering, Aragon Institute of Nanoscience (INA), University of Zaragoza, Zaragoza, Spain

[c] Networking Research Center on Bioengineering, Biomaterials and Nanomedicine (CIBER-BBN), Madrid, Spain

[d] University Institute of Industrial Pharmacy, Complutense University, Madrid, Spain

Abstract

Unfortunately, the empirical development of nanocarriers and later assignment to existing clinical challenges has led to high attrition rates in clinical trials. Therefore, this formulation-driven research is likely to progressively transition to a disease-driven approach, whereby the features of the nanomedicine are thoroughly designed beforehand on the basis of the pathophysiology of a specific disease. Since particle size certainly influences the *in vivo* behavior, rational disease-driven design of nanocarriers, can only be achieved with the ascertainment of the parameters that accurately control their size distribution.

Under this assumption, we have studied in depth the possibilities of the phase-inversion temperature method to obtain kinetically stable and monodisperse lipid nanocapsules. Notably, we have evidenced that the major parameter driving the nanocapsule formation is the oily phase: surfactant ratio, and consequently, have established a linear univariate mathematical model that will bring the implementation of size-tailored nanocapsules imposed by particular pathophysiological features a step closer. Moreover, the nanocapsules have been obtained following a single-step process, with the ensuing relevance for its future scale-up in an energetically-efficient manner. These ascertainments will eventually enable nanomedicines to be obtained "on-demand" to meet the disease-driven criteria in terms of particle size and ultimately increase their chances of success.

Keywords

Phase inversion temperature, low-energy method, lipid nanocapsule, nanomedicine, rational design

1. Introduction

Nanomedicine exploits the tools of nanotechnology to design platforms in the nanoscale range that serve to address unmet clinical challenges [1]. Unfortunately, nanomedicine has not achieved broad market access heretofore: the empirical development of delivery systems and later assignment to an existing clinical challenge has led to high attrition rates in clinical trials [2]. Therefore, this formulation-driven research is highly likely to progressively transition to a disease-driven rational approach, whereby the nanomedicine features are thoroughly designed beforehand on the basis of the pathophysiology of a specific disease [3, 4]. This fine tailoring of the features of colloids entails a profound ascertainment of how these attributes can dictate their in vivo behavior.

As the effect of nanomedicines mainly relies on the unique interactions of materials at the nanoscale with biological structures, one of the major features that certainly influence the in vivo performance of nanomedicines is precisely particle size [5]. Firstly, the intravenous route calls for particle sizes below the caliber of the smallest blood vessels (5 μm) to prevent embolisms. Moreover, the size of nanomedicines determines their plasma circulation time. On the one hand, particles above 100 nm are removed more rapidly from the bloodstream than smaller ones since particle size positively correlates with the extent of recognition by the reticuloendothelial system [6, 7]. On the other hand, particles below 10 nm are likely to undergo complete renal clearance [8]. Furthermore, the size of nanomedicines can account for the release rate of their payloads: whereas smaller carriers are expected to release their cargos faster, bigger particles are likely to extend the release over longer timeframes.

Remarkably, particle size also plays a pivotal role in drug targeting. Traditionally, a size-driven extravasation at the target site based on pathophysiological features has been sought. For instance, if provided enough circulation time, nanocarriers with particle size coarsely below 200 nm can take advantage of the leaky neovasculature and of the impaired lymphatic drainage to be selectively retained at tumor and/or inflammatory sites. This paracellular effect, termed the enhanced permeation and retention (EPR) effect, has become a dogma to explain passive targeting [9]. However, the efficiency of passive targeting highly relies on the stage of the disease (since along the metastatic areas the tumor vasculature closely resembles the physiological endothelium); and on its idiosyncrasy (as the EPR effect in central nervous system disorders such as gliomas and/or inflammatory diseases is relatively weak due to the presence of the blood-brain barrier, with a cut-off size of only 10-100 nm [10, 11]. In all these cases, a much finer control on particle size will certainly improve their potential therapeutic benefits. Moreover, the mechanisms that mediate the internalization of nanocarriers in target cells often follow a size-dependent pattern within the range 10-100 nm.

Therefore, for efficient disease-driven design of nanocarriers, their size must be accurately controlled, which can only be achieved with comprehensive understanding of the fundamental principles of nanoscience. Otherwise, the formulation procedure will represent the limiting step towards the development of promising nanotherapies.

Hence, the ascertainment of the parameters controlling the size distribution of nanocarriers is crucial to fully exploit their therapeutic potential following a rational approach rather than a trial-and-error process. Since nanoparticles are chiefly prepared through polymerization, nano-precipitation and/or lipid crystallization of nanoemulsion templates, understanding the governing phenomena of nanoemulsion formation is of prime interest [12].

Nanoemulsions are, quintessentially, emulsions; namely, thermodynamically unstable liquid-in-liquid dispersions that cannot be formed spontaneously and ultimately tend to separate into the constituent phases. Notably, the energy requirement for nanoemulsification negatively correlates with droplet size in accordance with the Laplace pressure (p) equation for a spherical drop:

$$p = \frac{4\gamma}{d}$$ (Equation 1.2.1)

where d is the droplet diameter and γ the interfacial tension. The methods of nanoemulsification are classified according to the strategies used to overcome this energy penalty.

On the one hand, in the high-energy methods, the energy input is achieved by agitation of the dispersion medium with a mechanical device. Given the huge energy demand, the disruptive shear forces can only be supplied by ultrasonic emulsifiers and high pressure homogenizers. The rationale behind the high-energy nanoemulsification follows the pattern: the higher the energy input, the smaller the droplet size. Nonetheless, high-energy methods exhibit an extremely low energetic yield [13]. Moreover, high-energy methods may give rise to loss of activity of drug substances during processing due to the great shear stresses involved.

On the other hand, in the low-energy methods, the physicochemical properties of surfactants and solvents are exploited to lower the interfacial tension, so that the energy input required can straightforwardly be achieved by simple stirring. Hence, low-energy methods are energetically more efficient and suitable for industrial scale-up. Interestingly, the gentle emulsification conditions also help prevent the potential degradation of drug substances [13]. Accordingly, research focus on low-energy methods has outperformed the interest in the hitherto gold-standard high-energy methods. Low-energy methods exhibit distinct experimental procedures depending on the nature of their excipients. These methods are rigorously classified on the basis of whether or not the surfactant curvature is inverted during emulsification [14]. While positive curvatures are assigned to O/W emulsions, negative curvatures form W/O emulsions.

Spontaneous nanoemulsification, which operates with no change in the surfactant curvature, utilizes the chemical energy released during the prompt diffusion of water-miscible solvents (previously solubilized within the oily phase) towards the aqueous continuous phase, when both phases are mixed [15]. However, this method entails the use of organic solvents, whose removal raise toxicological concerns for nanocarriers intended for biomedical purposes.

Alternatively, phase inversion methods profit from the negligible interfacial tension achieved when the surfactant curvature is inverted to easily drive the emulsification [14, 16]. The surfactant curvature is primarily influenced by the interactions between their polar moieties and the aqueous phase. Hence, several parameters can be modified to customize the surfactant curvature and ultimately lead to phase inversion. Whichever the phase inversion method, an exhaustive knowledge of the behavior of the surfactant in response to changes in those parameters is of the utmost importance.

In the phase inversion composition (PIC) method, the curvature of the surfactant monolayer is inverted by modifying the composition of the system. Whichever the surfactant type, phase inversion can be triggered by altering the ratio between phases: the gradual addition of continuous phase over the dispersed phase leads to a change in the surfactant curvature [17]. For instance, when water is progressively added, the hydration extent of the polar moiety of the surfactant, and therefore its affinity for the aqueous phase, gradually increases until the curvature becomes positive. In the specific case of ionic surfactants, the phase inversion can be driven by a change in the ionic strength: an increase in ionic strength can screen the hydrophilic character of the polar moieties of the surfactant to ultimately generate W/O nanoemulsions, and viceversa. The same trends can be achieved by varying the pH [18].

In the phase inversion temperature (PIT) method, the inversion of the surfactant curvature is driven by changes in temperature. Therefore, surfactants whose hydrophilic-lipophilic balance follows a temperature-dependent pattern must be utilized, namely non-ionic ethoxylated surfactants. Certainly, increasing temperatures reduce the extent of hydration of the poly (oxyethylene) moieties, which ultimately leads to an inversion in the surfactant curvature from positive to negative; and vice versa [19, 20]. At the “phase inversion temperature”, the surfactant curvature is negligible since the affinity for both phases is balanced. Consequently, a minimum in interfacial tension is achieved, whereof this technique takes advantage to promote nanoemulsification. The final formulation is obtained following a thermal quench below the surfactant melting point. Hence, being stabilized by the rigid surfactant shell, nanoemulsion droplets eventually adopt the form of nanocapsules. Notably, the PIT method is the low-energy method with the greatest potential for implementation in industry [21].

In this study, given its auspicious features, we have utilized the PIT method to prepare lipid nanocapsules. We have thoroughly evaluated the parameters that lead to controlled-sized lipid nanocapsules with minimal polydispersity under the assumption that this ascertainment will eventually enable size-tailored nanocapsules to be obtained on a large scale.

2. Experimental section

2.1. Materials. Labrafac lipophile® WL 1349 (caprylic-capric acid triglycerides) and Labrafil® M1944 CS (6-macrogol oleic glycerides) were kindly supplied by Gattefossé S.A. Kolliphor® HS15 ($C_{18}E_{15}$ polyethylene glycol (15) 12-hydroxystearate) and Kolliphor® ELP ($C_{18\Delta9}E_{35}$ polyethylene glycol (35) ricinoleate) were gifts from

BASF. Lipoid® S75 (soybean lecithin with 70% of phosphatidylcholine) was supplied by Lipoid-Gmbh. Henceforth; all chemicals will be referred to by their respective brand names given their complex chemical nature. NaCl and D(+)-trehalose were purchased from Panreac. All chemicals were used as received. De-ionized water was obtained from a MilliQ® Purification System.

2.2. Preparation of the lipid nanocapsules. Lipid nanocapsules were prepared by the phase inversion temperature (PIT) method [19]. Succinctly, all excipients (namely, aqueous and oily phases along with nonionic polyethoxylated surfactants) were mixed in certain proportions under magnetic stirring and progressively heated over the phase inversion temperature of the system. Subsequently, the mixture was gradually cooled down until the phase inversion temperature was reached. Then, a sudden quench with cold water (5 mL) was performed to obtain the final suspension of lipid nanocapsules (Figure 1).

Figure 1.2.1: Scheme of the phase inversion temperature (PIT) method.

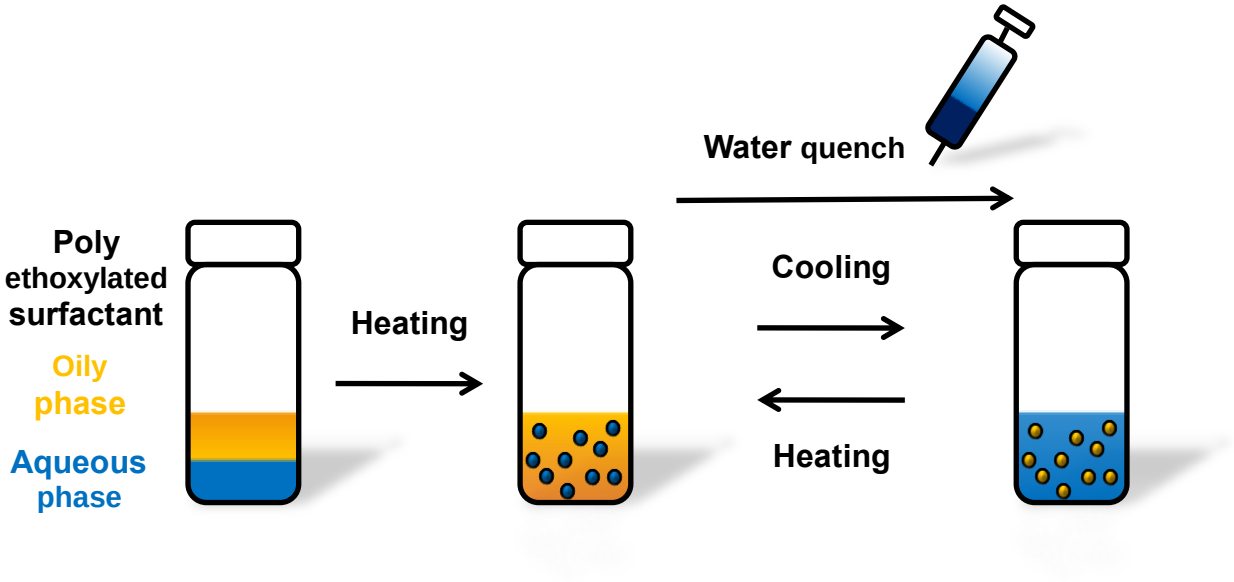

2.3. Characterization of size distribution of lipid nanocapsules. The mean volume diameter and polydispersity index (PdI) of lipid nanocapsules were measured by dynamic light scattering (DLS) using a Microtrac® Zetatrac™ Analyzer (Microtrac Inc., USA). At least triplicates for each condition were determined.

2.4. Morphological examination of lipid nanocapsules. The morphological examination of lipid nanocapsuels was performed by transmission electron microscopy (TEM). TEM images were taken on a T20-FEI Tecnai thermoionic microscope at the Advanced Microscopy Laboratory, LMA, (Zaragoza, Spain). To prepare the samples for TEM, 20μl of lipid nanocapsules suspension was dropped on a carbon copper grid (200 mesh), negatively stained with phosphotungstic acid and dried at room temperature. The microscope was operated at an acceleration voltage of 200 kV.

2.5. Evaluation of the influence of the number of temperature cycles on size distribution. Three formulations of lipid nanocapsules (F3, F5 and F7 in Table 1) were prepared by the PIT method following a variable number of temperature cyclings

(1-5) around the phase inversion temperature to evidence how many of them are required to obtain monodisperse lipid nanocapsules. Experiments were done in triplicate.

2.6. Evaluation of the influence of the composition on size distribution. By varying the relative proportions of their excipients, ten different formulations of lipid nanocapsules were prepared by the PIT method (Table 1) and thoroughly characterized in terms of size distribution to elucidate which ingredients influence both the average volume diameter and the polydispersity index. Experiments were done in triplicate. With the purpose of validating the trend observed for the tandem Labrafac lipophile® WL1349-Kolliphor® HS15, similar experiments were conducted, changing first the nature of the surfactant (to Kolliphor® ELP) and then the oil (to Labrafil® M1944 CS), i.e. changing the surfactant/oil affinities (Tables S1 and S2).

Table 1.2.1: Detailed excipient weights (in mg) for each of the ten different formulations evaluated for the oil-surfactant tandem Kolliphor HS15®-Labrafac lipophile WL1349®.

	F1	F2	F3	F4	F5	F6	F7	F8	F9	F10
Kolliphor HS15®	2950	2478	1934	1390	846	665	484	440	303	220
Lipoïd S75®	75	75	75	75	75	75	75	75	75	75
NaCl	89	89	89	89	89	89	89	89	89	89
Labrafac lipophile WL1349®	250	755	846	937	1028	1118	1209	1350	1300	1480
Water	1636	1603	2055	2509	2962	3053	3143	3046	3233	3136
Oil: surfactant ratio	0.085	0.305	0.437	0.674	1.215	1.681	2.498	3.068	4.290	6.727

2.7. Kinetic stability. After being sterilized by filtration, the kinetic stability of lipid nanocapsules stored in suspension was studied both at 25ºC and at 4ºC over 6 months by monitoring the changes in size distribution with time. Samples (n = 4) were assessed after 0, 2, 4 and 6 months of storage. Their kinetic stability was compared in terms of Ostwald ripening rates, ω, which were determined according to the LSW theory [22].

2.8. Evaluation of the influence of freeze-drying on size distribution. The suspensions of lipid nanocapsules were freeze-dried. Trehalose was added at different concentrations (0, 3 and 5% (w/v)) as a cryoprotectant agent. Slow freezing of the

suspensions was carried out. Freeze-drying was operated in a Telstar Lyoquest laboratory freeze-drier (Telstar Life Sciences, Spain) for 24 hours. The free-dried powder was manually re-suspended in de-ionized water for measurement of the particle size by DLS.

2.9. Stability of the freeze-dried lipid nanocapsules. Freeze-dried lipid nanocapsules were stored at 25 $\pm$ 0.5°C, 75 $\pm$ 2% relative humidity. After 3, 6, 9 and 12 months of storage, the lipid nanocapsules were manually re-suspended in water for measurement of the particle size by DLS.

2.10. Statistics. The data are expressed as mean $\pm$ SD of at least three different experiments. Polydispersity index (PdI) for each size distribution was calculated according to equation 2:

$$PdI = \left(\frac{Standard\ deviation}{Average\ volume\ diameter}\right)^2 \text{ (Equation 1.2.2)}$$

To compare the size distribution profile of two formulations, the similarity factor f_2, defined by equation 3, is utilized. Size distributions were considered identical for f_2-values above 50.

$$f2 = 50 * \log \frac{100}{\sqrt{1+\frac{\sum_{i=1}^{i=n}(R_i - T_i)}{n}}} \text{ (Equation 1.2.3)}$$

Previous verification of the homogeneity of variances with the Bartlett test, one-way ANOVA followed by post-hoc Tukey test were used for multiple group analysis. Statistical significance was fixed as *: $p<0.05$, **: $p<0.01$, ***: $p<0.001$. The statistical signification of the Ostwald ripening rates (ω) was used to elucidate the contribution of the time course to stability. All the data were analyzed using the GraphPad Prism 7 software.

3. Results and discussion

3.1. Evaluation of the influence of the number of temperature cycles on size distribution

Despite holding great promise for improving the efficacy of many drug substances, manufacturing of nanomedicines is still a major obstacle for their market access [21]. This technical challenge for scale-up is greatly due to the lack of comprehensive understanding of the role played by the critical factors involved in the formulation of nanomedicines. Hence, investment in the fundamental principles of nanoscience will help provide clearer guidance for rational scale-up [3]. Currently, nanocarriers are mostly manufactured using high-pressure homogenization. As a result, from an industrial point of view, there is much room for improvement in terms of energetic yield. In this regard, low-energy methods are more appealing for large-scale production owing to the improved formulation yields because emulsification occurs simultaneously in the entire volume of the mixture.

Specifically concerning the nanocapsules prepared by the PIT method, there seems to be some controversy on the relevance of the number of temperature cycles around the phase inversion region. Anton et al. [23] have reported that the number of temperature cycles is associated with a decrease in both particle size and polydispersity index. In a subsequent study, when Malzert-Fréon et al. replaced one of the excipients by Labrasol®, they evidenced that the number of temperature cycles does not improve the size distribution [24]. However, they exclusively attributed this temperature cycle-independence to the presence of Labrasol®. More recently, Klassen et al. switched the nature of both the oily phase and the surfactant to test the role of temperature cycles [25]. This time, they concluded that the contribution of the temperature cycle was only significant at low surfactant concentrations, but had no influence at higher surfactant concentrations. Given these misleading results, we have comprehensively addressed this phenomenon. Indeed, this is not a trivial issue, since as long as the technical complexity of formulation procedures is kept to a minimum; the manufacturing criteria are more likely to be fulfilled.

From the rationale of the mechanism behind the PIT method, we hypothesized that the surfactant concentration at the interface is constant throughout the process and the curvature inversion responsible for driving the emulsification is the same regardless of the number of temperature cycles applied. Hence, there seems not to be scientific support for expecting an improvement in size distribution with the number of cycles for any potential combination of excipients. In this line, we have evaluated the influence of the number of temperature cycles (up to five) on the original composition described by Anton et al. [23]. In particular, we have tested three different sizes that could be categorized into high, medium and low-surfactant formulations.

Results are shown in Figure 2. Monodisperse lipid nanocapsules (PdI < 0.1) were obtained in all cases. Notably, neither average volume diameter (Figure 2a) nor polydispersity index (Figure 2b) were significantly modified with the number of temperature cycles for any of the formulations tested. This evidences that, contrary to the traditionally postulated three temperature cycles necessary to achieve monodisperse populations, only one temperature cycling is required to obtain lipid nanocapsules by the PIT method. These results show great interest for the industrial relevance of the PIT method: the simplification of the formulation procedure paves the way for the encapsulation of thermosensitive cargos thanks to the reduced exposure to heating conditions, increases its energetic yield and greatly shortens preparation times.

Effectively, direct visualization through transmission electron microscopy (TEM) further evidenced that monodisperse nanocapsules were formed in a single-step PIT method (Figure 3) at high (Figure 3a), medium (Figure 3b) and low-surfactant (Figure 3c) concentrations. Moreover, results obtained from DLS analysis highly correlated with particle size observed though TEM.

Figure 1.2.2: Evaluation of the impact of the number of temperature cycles on the size distribution of lipid nanocapsules. (a) Influence on the average volume diameter (nm). (b) Influence on the polydispersity index (PdI). The p-values for one-way ANOVA (factor: number of temperature cycles) for each formulation are shown in the legend.

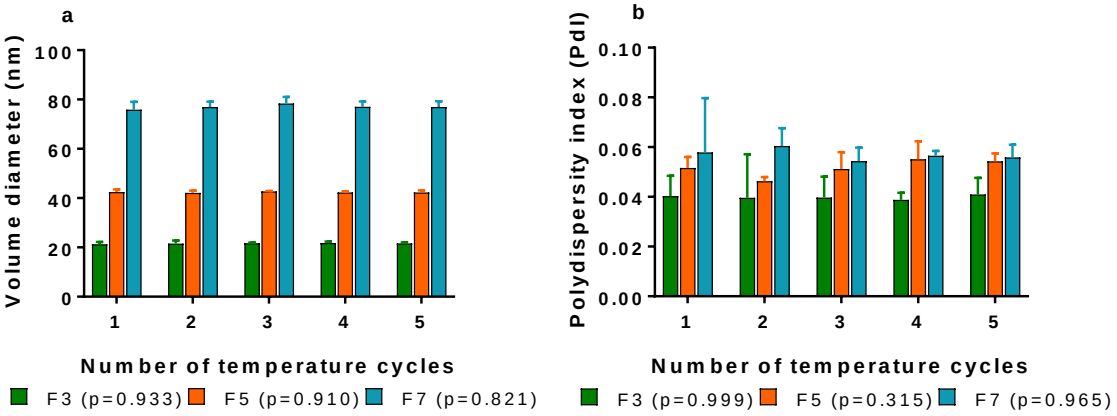

Figure 1.2.3: Comparison of DLS size distribution of lipid nanocapsules and TEM images at different magnifications: F3 (3a), F5 (3b), F7 (3c). Scale bars: 100 nm (center) and 50 nm (right).

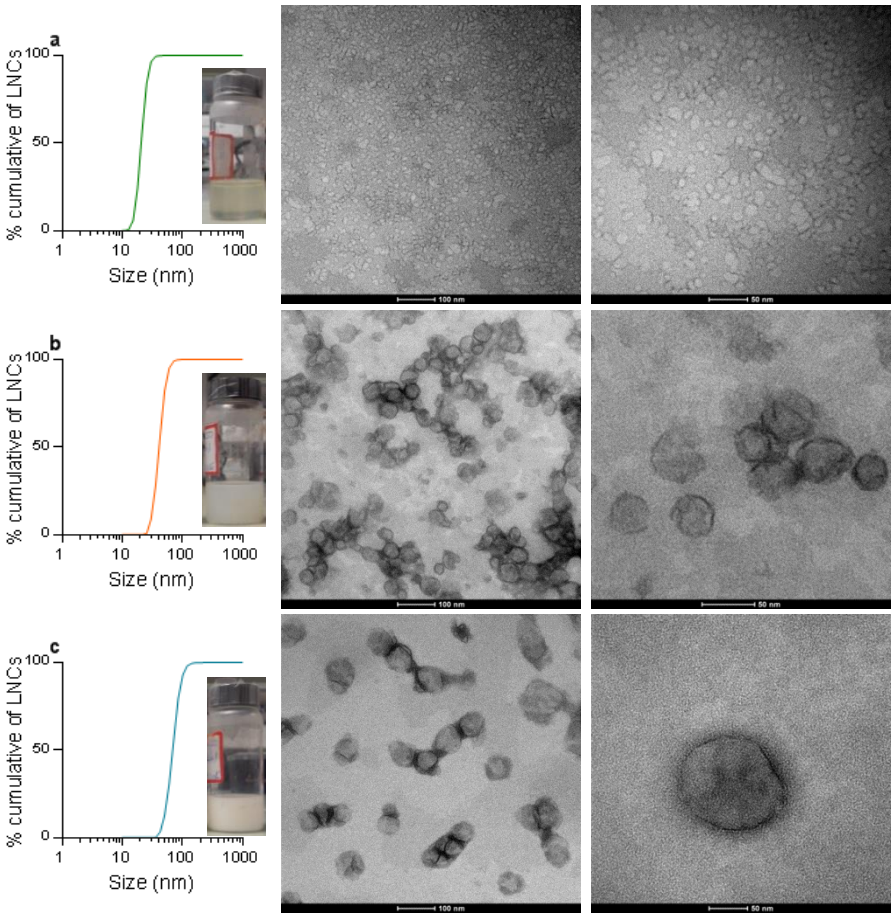

3.2. Evaluation of the influence of the composition on size distribution

Given the importance of the rational design of nanomedicines to achieve efficient disease-driven nanotherapies, we have thoroughly revisited the parameters controlling the size distribution of nanocapsules prepared by the PIT method. Parameters that determine the properties of nanocarriers can be divided into formulation or preparation variables. Nevertheless, for low-energy methods, the formulation variables are the most influencing parameters, since these methods do not rely either on physical energy input or on shear forces [26]. In the case of the PIT method, the most widely studied formulation parameters refer to the relative proportion of their excipients. In this regard, Heurtault et al. [27] predicted the particle diameter as a function of three variables (namely, percentage of surfactant, oil and water in the initial mixture) with a polynomial model. According to the high coefficient of determination (R^2=0.994), the mathematical model was well-suited to predict the size of the nanocarriers. Nevertheless, one major caveat of this model is that the sum of the variables is restrained altogether to 100%; i.e., the selected formulation variables only have two degrees of freedom. Hence, particle size could be better estimated as a function of independent parameters, or even more interestingly, as a function of a relation between them. The latter case would be of the utmost significance since this would provide formulators with a univariate mathematical model that would more intuitively enlighten them on how to tailor particle size with the PIT method.

Since Morales et al. [28] evidenced that the size of O/W nanoemulsions was independent on the water concentration (because water acts as a dilution medium for the dispersed phase), we hypothesized that surfactant and oil should be regarded as the key formulation-driving parameters. On the one hand, the particle size is expected to be reduced with increasing amounts of surfactant due to the decrease in interfacial tension. On the other hand, the particle size is expected to grow with increasing amounts of oil since it represents the liquid core of the colloid capsules. As a result, the mass ratio of oily phase to surfactant seems a suitable variable for prediction of size distribution of nanocapsules prepared by the PIT method. A higher ratio would represent a decrease in surfactant relative concentration, and would ultimately lead to bigger capsules. Nonetheless, the studies that have tested the predictive value of this formulation parameter for the PIT method are rather scarce, and when existing, they have only tested a single oil-surfactant combination [29-32].

In the present work, we have selected in the first instance the system from [27], consisting of Kolliphor HS15®, Labrafac® lipophile WL1349 and water. Figure 4 shows the monodisperse size distributions obtained for the ten formulations tested in terms of the average volume diameters (Figure 4a) and the polydispersity indexes (Figure 4b). Average volume diameters were plotted against the oil/surfactant ratio. In all cases, the particle size increased along with the oil:surfactant ratio, whereas polydispersity indexed was not significantly modified among the different ratios tested contrary to what had been traditionally postulated [33]. Notably, the plot of the volume diameters versus the oil:surfactant ratio was linear for ratios between 0.08 and 3 with an extremely high coefficient of determination (R^2 = 0.9983). To further validate this linear univariate model, we prepared formulations with the same oil:surfactant ratio but

different total amount of both excipients (Table S3) and calculated the similarity factor between the counterparts (Figure 5). The f2 factor calculated was above the 50% similarity threshold (namely, 65.34% for the ratio 0.4374 and 70.25% for the ratio 1.2151). The fact that for a given ratio achieved with different amounts of surfactant and oil, similar volume diameters are obtained is supported by the work of Galindo-Álvarez et al [32]. These results validated that the most relevant parameter for the size distribution of final suspension was the oil:surfactant weight ratio. More precisely, and taking into account the results of Anton and Saulnier [34], who described that it was the water:surfactant ratio which determined the particle size of W/O nanocapsules, the key driving parameter seems to be the dispersed phase:surfactant weight ratio.

Figure 1.2.4: Evaluation of the impact of changes in the formulation composition on the size distribution of lipid nanocapsules for the tandem Labrafac lipophile WL1349 ®-Kolliphor HS15®. (a) Influence on the average volume diameter (nm). (b) Influence on the polydispersity index (p>0.05).

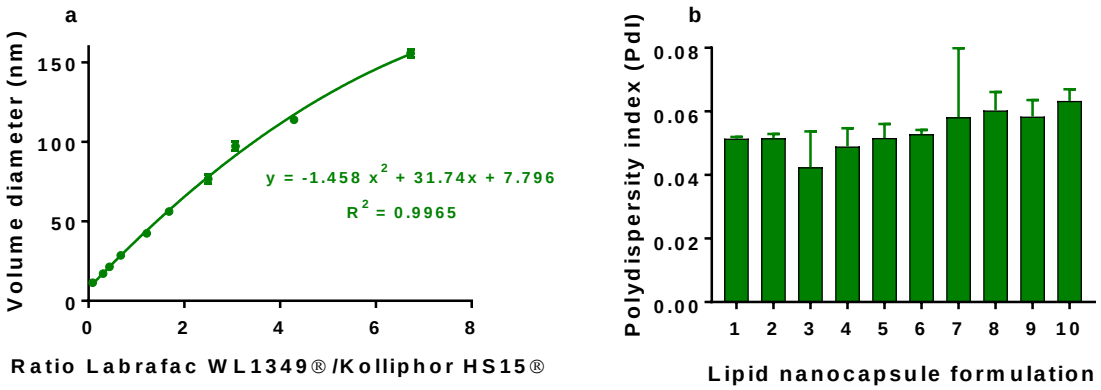

Figure 1.2.5: Comparison of the size distribution profiles of two formulations with the same oil: surfactant ratio but different total amount of both excipients to validate the linear univariate model. (a) Labrafac WL1349®: Kolliphor HS15® ratio=0.4374. (b) Labrafac WL1349®: Kolliphor HS15® ratio=1.2151.

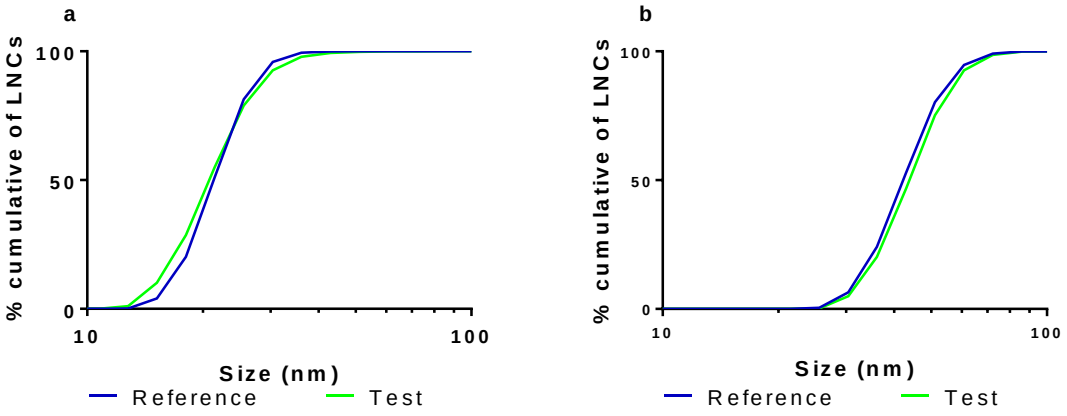

To check if the linear univariate mathematical model describing the nanocarrier formation by the PIT method could be extrapolated to other oil-surfactant tandems, similar experiments were carried out changing the surfactant-oil affinities (namely, first changing the nature of the oily core to Labrafil® MS1944, and subsequently the surfactant to Kolliphor ELP®). Biocompatible excipients were chosen in order to envisage the nanocapsules for parenteral administration. In both cases, a linear region could be defined with coefficient of determinations above 0.99 (Figure 6). Along the linear region the polydispersity indexes continued to be extremely low (<0.06) regardless the particle size (Figure S1).

Figure 1.2.6: Univariate linear regression between the volume diameter and the oil:surfactant ratio for the different combinations tested (namely, Labrafac WL1349®-Kolliphor HS15®, Labrafac WL1349®-Kolliphor ELP®, Labrafil MS 1944 CS®-Kolliphor HS15®).

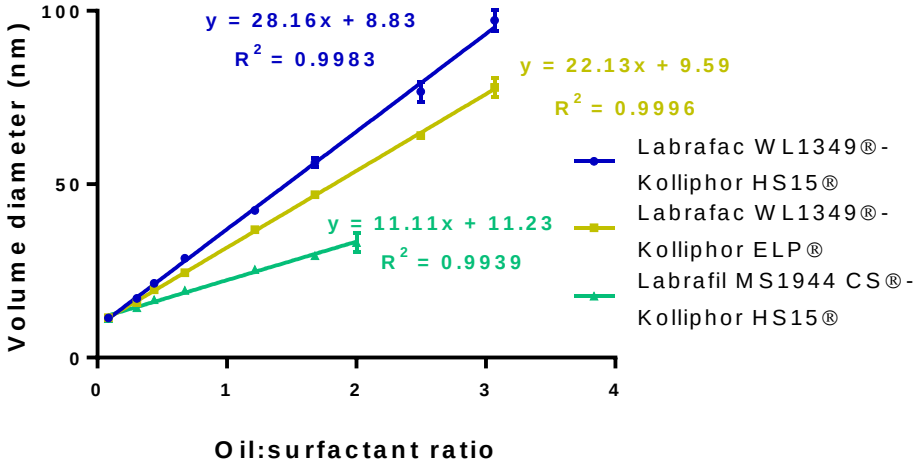

As shown in Figure 6, a comparison among the slopes of the linear plots can be drawn: the highest was achieved for the Labrafac®-Kolliphor HS15® tandem (b = 28.164), whereas the lowest corresponded to the Labrafil®-Kolliphor HS15® (b = 11.11). This difference in the slopes of the linear plots can be attributed to the difference between the HLB values of the surfactants and the triglycerides utilized as oily phase (Table 2). The slopes seem to follow the pattern: the closer the HLB values between the surfactant and the oily phase, the lower the slope of the linear plot.

Table 1.2.2: Hydrophilic-lipophilic balances of the different oily phases and polyethoxylated surfactants as declared by suppliers.

Excipient	HLB value
Labrafac lipophile WL1349®	1
Labrafil M1944 CS®	9
Kolliphor® ELP	12-14
Kolliphor® HS15	14-16

As a result, the global linear trend between particle size and oil:surfactant ratio seems to be consistent through several different compositions. Moreover, this linearization is useful as it accounts for the variation of particle size for a wide variety of experimental data available in the literature originally evaluated following other parameters [29, 35]. Remarkably, this linearization does not only serve to predict the particle size of nanocapsules prepared by the PIT method, but also by the PIC method [36, 37], which further emphasizes the link between the governing phenomena of both techniques.

Accordingly, the size of nanocapsules can be accurately tuned to a well-defined therapeutic purpose. The attainment of this tailoring within the range 10-100 nm for several tandems of oily phase and surfactant ultimately enables the concomitant adjustment of the formulation composition to issues imposed by the drug substance. Solubility issues could be addressed presumably by changing the oily phase to another one that fully solubilizes the drug substance. Toxicological concerns associated with some surfactants could be overcome since it is possible to obtain nanocarriers of the same size at lower surfactant concentrations by switching the emulsifier to another one with a lower HLB value.

3.3. Kinetic stability

As thermodynamically unstable systems, nanoemulsions eventually tend to phase separation to achieve the minimal interfacial area. Nonetheless, given their inherent features, nanoemulsions, and nanocarriers from them derived, can be kinetically stable over several months [12]. The potential breakdown mechanisms are discussed to rule out their contribution in the case of the lipid nanocapsules.

In the first instance, their size on the nanoscale provides stability against sedimentation and creaming as the Brownian motion wherein nanocarriers are involved outweighs the gravity force [16]. In the case of nanocarriers, other breakdown mechanisms that can be precluded are flocculation (namely, the aggregation of particles when the attractive forces between them outstrip the repulsive ones) and coalescence (the subsequent merger of particles) [14]. Certainly, thanks to the steric stabilization provided by the surfactant layer, the repulsive forces are enhanced and the occurrence of a flocculated state is hindered [38]. This steric stabilization is particularly relevant in nanocarriers, where the thickness of the surfactant layer is significantly high in comparison with the particle size [13, 39]. Importantly, around the PIT, given the minimal interfacial tension, coalescence is favored unless the temperature is rapidly removed from the PIT. For this reason, we apply a thermal quench to obtain monodisperse lipid nanocapsules [33].

Finally, Ostwald ripening consists of the diffusion of the liquid core through the dispersion medium from the smaller to the larger particles due to their different Laplace pressures [14]. Hence, this breakdown mechanism arises from the polydispersity in size distribution. The LSW (Lifshitz–Slyozov-Wagner [22]) theory predicts a linear relationship between the cube of particle radius and time:

$$r^3 = \frac{8}{9}\left[\frac{C(\infty)\gamma V_m D}{\rho RT}\right] t \quad \text{(Equation 1.2.4)}$$

where $C(\infty)$ is the solubility of the particle material in the dispersion medium, γ is the interfacial tension, V_m is the molar volume of the particle material, D is the diffusion coefficient in the dispersion medium, ρ is the density of the particle material, R is the gas constant and T is the temperature. The slope of this linear plot is the Ostwald ripening rate (ω_0), which is dependent on temperature since both solubility and diffusivity follows an Arrhenius behavior [40]. In this regard, Ostwald ripening is inferred as breakdown mechanism from linear plots of the cube of particle radius versus time.

Figure 1.2.7: Evaluation of the Ostwald ripening rates of different formulations of lipid nanocapsules over 6 months both at room temperature (7a) and at 4ºC (7b).

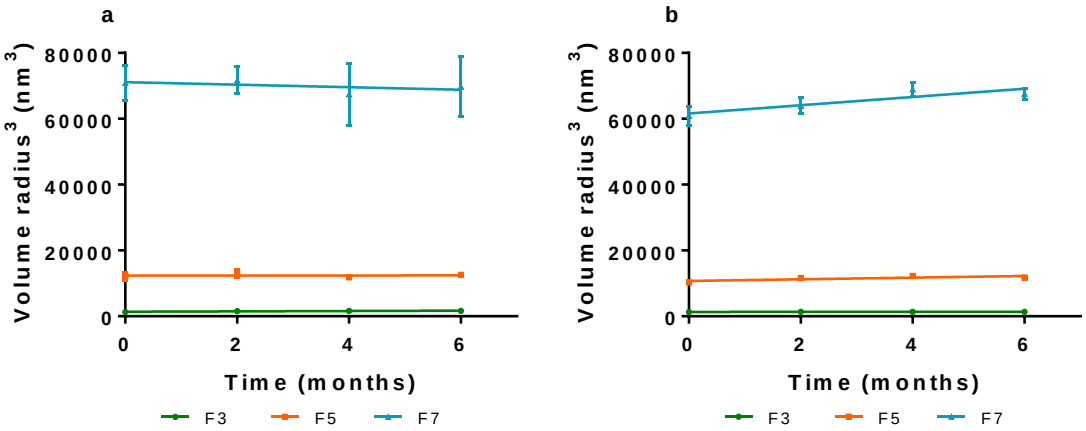

Since Ostwald ripening represents the main breakdown mechanism for nanocarriers, we evaluated the evolution of size distribution of three formulations of lipid nanocapsules prepared by the PIT method over six months both at 25ºC and at 4ºC. The plots of the cube of the particle radius versus time are shown in Figure 7. In no case could Ostwald ripening be inferred as a source of instability because the slopes (ω_0) are not statistically different from zero ($p>0.05$). This is highly relevant, especially if taking into account that our results are evaluated over a much longer period of time than other results reported in the literature [24, 25]. Consequently, it can be concluded that lipid nanocapsules prepared by the PIT method are kinetically stable for longer than six months regardless of the oily core: surfactant ratio. Unlike Malzert-Fréon et al. [24], we have observed high kinetic stability both at room temperature and at 4ºC, which further serves to rule out Ostwald ripening rate as breakdown mechanism of lipid nanocapsules as it does not follow an Arrhenius pattern. The most likely explanation for this high kinetic stability lies, on the one hand, in the presence of a solid thick surfactant layer that noticeably precludes the passage of the liquid oily core through the interface to ultimately reduce the ripening rate, and on the other hand, in the low polydispersity indexes that prevent significant differences in Laplace pressures that could drive the Ostwald ripening. Moreover, as deduced from the LSW theory, low

ripening rates should be expected for oily phases such as Labrafac lipophile WL1349® with negligible solubility in the aqueous dispersion medium.

3.4. Evaluation of the influence of freeze-drying on size distribution

Alternatively, we tested if the size distribution of the lipid nanocapsules was kept unaltered after water removal by freeze-drying and subsequent extemporaneous reconstitution. Trehalose was used as a cryoprotectant as Dulieu and Bazile had previously reported that it preserved the monodisperse features of colloid particles [41]. Nonetheless, it was only for the formulation with the lowest surfactant content (and consequently with the highest particle size) that the addition of trehalose revealed a slight improvement in maintaining the average volume diameter after freeze-drying (Figure 8a). There were no statistically significant differences between the trehalose concentrations tested (namely, 3 and 5%), regardless the particle size ($p>0.05$). With regards to polydispersity, no significant differences were observed upon addition of trehalose for any of the formulations tested ($p>0.05$, Figure 8b). A comparison of the profiles of the size distributions before and after freeze-drying for the three particle sizes is shown in Figure 8c. Only the 20 nm-sized nanocapsules obtained a similarity factor above 50% (f_2 = 72.72); hence, only the nanocapsules with the highest surfactant content were kept unaltered after freeze-drying. The lyophilization process affected the size distribution of the other two formulations: both their volume diameters and particularly their polydispersity dramatically increased (PdI > 0.1).

These results seem to outline that the prevention of leakage of the oily phase during freeze-drying is closely related to the thickness of the surfactant layer relative to the diameter of the colloid capsules. The thickness of the surfactant shell (t) can be calculated as indicated in [41] using the equation:

$$t = \frac{d}{2}\left(1 - \sqrt[3]{F_{oil}}\right) \text{ (Equation 1.2.5)}$$

where F_{oil} is the oil fraction in the nanocapsule and d is the volume diameter of the nanocapsule. Accordingly, an estimation of the thickness of the surfactant shell relative to the capsule diameter represents a 33% for the smallest capsules, with the other two lagging far behind (19.2% and 11.9%, respectively for the formulations 5 and 7). This conclusion is in agreement with the assumption that the surfactant crystallization following the temperature quench of the PIT method below its melting point confers rigidity to the shell of the lipid nanocapsules.

3.5. Stability of the freeze-dried lipid nanocapsules

The stability under storage of the freeze-dried lipid nanocapsules that had been kept unaltered after the freeze-drying process was also tested at 25ºC and 75% relative humidity. Notably, the size distribution features of the lyophilisate were maintained over 12 months ($p > 0.05$, Figure S2) and consequently, the induction of oil leakage during storage was ruled out.

Figure 1.2.8: Influence of freeze-drying on the size distribution of lipid nanocapsules. (a) Evaluation of the impact of trehalose as cryoprotectant agent on the average volume diameter (nm). (b) Evaluation of the impact of trehalose as cryoprotectant agent on the polydispersity index (PdI). (c) Comparison of the size distribution profile before and after freeze-drying.

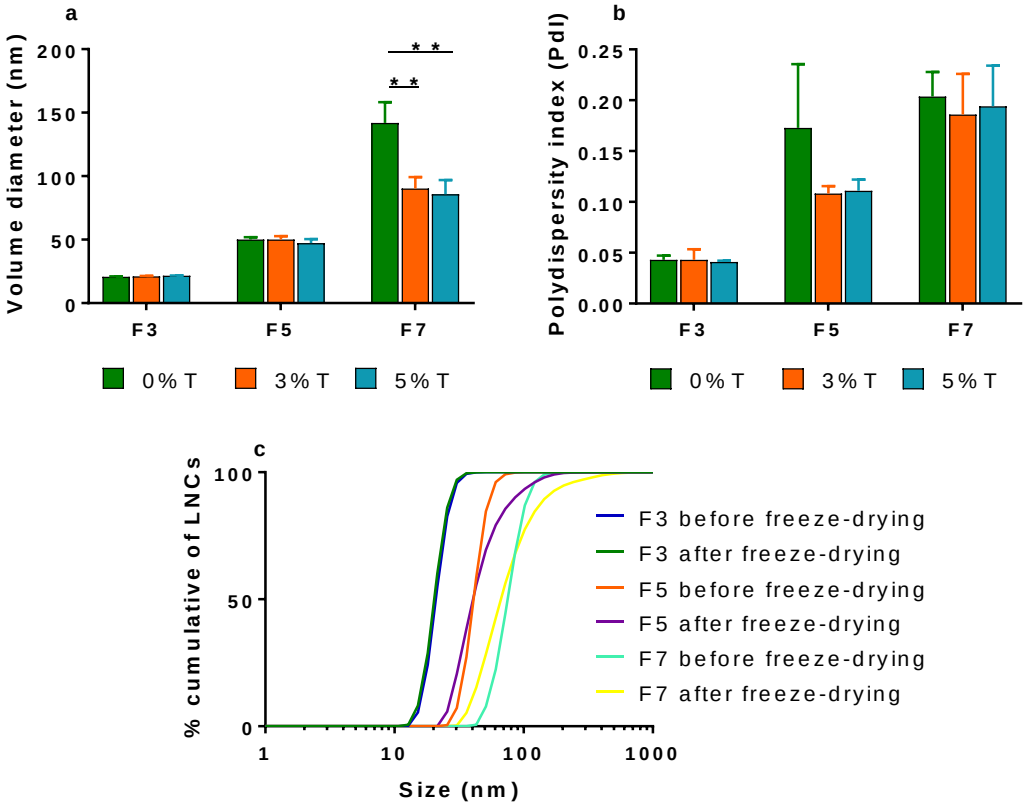

4. Conclusions

Despite holding great promise for improving the efficacy of many drugs, nanomedicine has not achieved broad market access yet: the assignment of delivery systems empirically developed to an existing clinical challenge has led to high attrition rates in clinical trials. Alternatively, a disease-driven rational approach, whereby the nanomedicine features are carefully designed beforehand on the basis of the pathophysiology of a specific disease is more likely to succeed. Since particle size greatly influences the *in vivo* behavior, to fully exploit the disease-driven design of nanocarriers, their size must be accurately controlled. This can only be achieved with a profound ascertainment of the parameters controlling their size distribution.

In this regard, in the present study, we have analyzed the preparation of lipid nanocapsules by the PIT method with a deep insight in the subjacent mechanisms. Notably, these nanocapsules have been obtained in a single-step, as only one temperature cycle was required for their formation as evidenced both by DLS and TEM. This finding will eventually bring a step closer their rational scale-up in an energetically-

efficient manner (often considered as another major obstacle for the market access of nanomedicines). Moreover, we have proved that the particle size can be predicted with a linear univariate mathematical model as a function of the oily phase: surfactant ratio for various oily phase-surfactant combinations, with coefficients of determination above 0.99 in all cases. This will provide formulators with a tool of the utmost significance to implement the rational design of nanocapsules. Importantly, the tailoring can be made not only in terms of the particle size imposed by the particular pathophysiological features of the specific disease to treat, but also in terms of adapting the excipients to the therapeutic needs. For instance, solubility issues imposed by the drug substance could be addressed presumably by changing the oily phase to another one that fully solubilizes the drug substance. Alternatively, toxicological concerns associated with some surfactants could be overcome as nanocarriers of the same size can be obtained at lower surfactant concentration by switching to an emulsifier with lower HLB. This can eventually contribute to increasing the maximum tolerated dose. The lipid nanocapsules were kinetically stable in suspension against the main breakdown mechanisms over six months both at room temperature and at 4ºC.

Altogether, the data presented here serve to envisage these nanocarriers as promising candidates for disease-driven size-tailoring with potential for industrial manufacturing to ultimately achieve broad market access.

Associated content

Supporting Information: Tables with detailed excipient weights for all formulations used to deduce the univariate linear model and its subsequent validation, experimental results on the role of the formulation composition on the polydispersity indexes for the combinations Labrafac lipophile WL1349®-Kolliphor ELP® and Labrafil MS1944 CS®-Kolliphor HS15®, and experimental confirmation of the stability upon storage (25ºC, 75% relative humidity) of freeze-dried lipid nanocapsules over 12 months.

Acknowledgements

This work was supported by the Complutense Research Fund (Ref. 16/83) and by the Research Group GR35/10 Santander-UCM: Parenteral Administration of Drugs. J. A.-B. would like to thank the Spanish Ministry of Education for his contract within the Professor Training Program FPU (Ref. FPU13/02325). V.S. would like to thank CIBER-BBN for support. CIBER-BBN is an initiative funded by the VI National R&D&i Plan 2008–2011 financed by the Instituto de Salud Carlos III with the assistance of the European Regional Development Fund.

References

[1] Shi JJ, Kantoff PW, Wooster R, Farokhzad OC. Cancer nanomedicine: progress, challenges and opportunities. Nat Rev Cancer 2017;17:20-37.

[2] Venditto VJ, Szoka FC. Cancer nanomedicines: So many papers and so few drugs! Adv Drug Deliv Rev 2013;65:80-8.

[3] Hare JI, Lammers T, Ashford MB, Puri S, Storm G, Barry ST. Challenges and strategies in anti-cancer nanomedicine development: An industry perspective. Adv Drug Deliv Rev 2017;108:25-38.

[4] Hartshorn CM, Bradbury MS, Lanza GM, Nel AE, Rao JH, Wang AZ, Wiesner UB, Yang L, Grodzinski P. Nanotechnology Strategies To Advance Outcomes in Clinical Cancer Care. ACS Nano 2018;12:24-43.

[5] Kim BYS, Rutka JT, Chan WCW. Current Concepts: Nanomedicine. N Engl J Med 2010;363:2434-43.

[6] Dufort S, Sancey L, Coll JL. Physico-chemical parameters that govern nanoparticles fate also dictate rules for their molecular evolution. Adv Drug Deliv Rev 2012;64:179-89.

[7] Hirsjarvi S, Dufort S, Gravier J, Texier I, Yan Q, Bibette J, Sancey L, Josserand V, Passirani C, Benoit JP, Coll JL. Influence of size, surface coating and fine chemical composition on the in vitro reactivity and in vivo biodistribution of lipid nanocapsules versus lipid nanoemulsions in cancer models. Nanomed-Nanotechnol Biol Med 2013;9:375-87.

[8] Choi HS, Liu W, Misra P, Tanaka E, Zimmer JP, Ipe BI, Bawendi MG, Frangioni JV. Renal clearance of quantum dots. Nat Biotechnol 2007;25:1165-70.

[9] Bertrand N, Wu J, Xu XY, Kamaly N, Farokhzad OC. Cancer nanotechnology: The impact of passive and active targeting in the era of modern cancer biology. Adv Drug Deliv Rev 2014;66:2-25.

[10] Aparicio-Blanco J, Torres-Suárez AI. Managing CNS Tumors: The Nanomedicine Approach. In: Morgan LR, editor. New Approaches to the Management of Primary and Secondary CNS Tumors: InTech; 2017.

[11] Luo ZM, Jin K, Pang Q, Shen S, Yan ZQ, Jiang T, Zhu XY, Yu L, Pang ZQ, Jiang XG. On-Demand Drug Release from Dual-Targeting Small Nanoparticles Triggered by High-Intensity Focused Ultrasound Enhanced Glioblastoma-Targeting Therapy. ACS Appl Mater Interfaces 2017;9:31612-25.

[12] Anton N, Benoit JP, Saulnier P. Design and production of nanoparticles formulated from nano-emulsion templates - A review. J Control Release 2008;128:185-99.

[13] Fryd MM, Mason TG. Advanced Nanoemulsions. In: Johnson MA, Martinez TJ, editors. Annual Review of Physical Chemistry, Vol 63. Palo Alto: Annual Reviews; 2012. p. 493-518.

[14] Solans C, Sole I. Nano-emulsions: Formation by low-energy methods. Curr Opin Colloid Interface Sci 2012;17:246-54.

[15] Lepeltier E, Bourgaux C, Couvreur P. Nanoprecipitation and the "Ouzo effect": Application to drug delivery devices. Adv Drug Deliv Rev 2014;71:86-97.

[16] Gupta A, Eral HB, Hatton TA, Doyle PS. Nanoemulsions: formation, properties and applications. Soft Matter 2016;12:2826-41.

[17] Sole I, Pey CM, Maestro A, Gonzalez C, Porras M, Solans C, Gutierrez JM. Nano-emulsions prepared by the phase inversion composition method: Preparation variables and scale up. J Colloid Interface Sci 2010;344:417-23.

[18] Maestro A, Sole I, Gonzalez C, Solans C, Gutierrez JM. Influence of the phase behavior on the properties of ionic nanoemulsions prepared by the phase inversion composition method. J Colloid Interface Sci 2008;327:433-9.

[19] Huynh NT, Passirani C, Saulnier P, Benoit JP. Lipid nanocapsules: A new platform for nanomedicine. Int J Pharm 2009;379:201-9.

[20] Machado AHE, Lundberg D, Ribeiro AJ, Veiga FJ, Lindman B, Miguel MG, Olsson U. Preparation of Calcium Alginate Nanoparticles Using Water-in-Oil (W/O) Nanoemulsions. Langmuir 2012;28:4131-41.

[21] Thomas O, Lagarce F. Lipid nanocapsules: a nanocarrier suitable for scale-up process. J Drug Deliv Sci Technol 2013;23:555-9.

[22] Lifshitz IM, Slyozov VV. The kinetics of precipitation from supersaturated solid solutions. J Phys Chem Solids 1961;19:35-50.

[23] Anton N, Gayet P, Benoit JP, Saulnier P. Nano-emulsions and nanocapsules by the PIT method: An investigation on the role of the temperature cycling on the emulsion phase inversion. Int J Pharm 2007;344:44-52.

[24] Malzert-Freon A, Saint-Lorant G, Hennequin D, Gauduchon P, Poulain L, Rault S. Influence of the introduction of a solubility enhancer on the formulation of lipidic nanoparticles with improved drug loading rates. Eur J Pharm Biopharm 2010;75:117-27.

[25] Klassen PL, George Z, Warwick J, Georgiadou S. PIT tuning effects of hydrophobic co-surfactants and drugs. Colloid Surf A-Physicochem Eng Asp 2014;455:1-10.

[26] Gutierrez JM, Gonzalez C, Maestro A, Sole I, Pey CM, Nolla J. Nano-emulsions: New applications and optimization of their preparation. Curr Opin Colloid Interface Sci 2008;13:245-51.

[27] Heurtault B, Saulnier P, Pech B, Venier-Julienne MC, Proust JE, Phan-Tan-Luu R, Benoit JP. The influence of lipid nanocapsule composition on their size distribution. Eur J Pharm Sci 2003;18:55-61.

[28] Morales D, Gutierrez JM, Garcia-Celma MJ, Solans YC. A study of the relation between bicontinuous microemulsions and oil/water nano-emulsion formation. Langmuir 2003;19:7196-200.

[29] Anton N, Vandamme TF. The universality of low-energy nano-emulsification. Int J Pharm 2009;377:142-7.

[30] Roger K, Cabane B, Olsson U. Formation of 10-100 nm Size-Controlled Emulsions through a Sub-PIT Cycle. Langmuir 2010;26:3860-7.

[31] Roger K. Nanoemulsification in the vicinity of phase inversion: Disruption of bicontinuous structures in oil/surfactant/water systems. Curr Opin Colloid Interface Sci 2016;25:120-8.

[32] Galindo-Alvarez J, Boyd D, Marchal P, Tribet C, Perrin P, Marie-Begue E, Durand A, Sadtler V. Miniemulsion polymerization templates: A systematic comparison between low energy emulsification (Near-PIT) and ultrasound emulsification methods. Colloid Surf A-Physicochem Eng Asp 2011;374:134-41.

[33] Koroleva MY, Yurtov EV. Nanoemulsions: the properties, methods of preparation and promising applications. Russ Chem Rev 2012;81:21-43.

[34] Anton N, Saulnier P. Adhesive water-in-oil nano-emulsions generated by the phase inversion temperature method. Soft Matter 2013;9:6465-74.

[35] Izquierdo P, Esquena J, Tadros TF, Dederen JC, Feng J, Garcia-Celma MJ, Azemar N, Solans C. Phase Behavior and nano-emulsion formation by the phase inversion temperature method. Langmuir 2004;20:6594-8.

[36] Caldero G, Garcia-Celma MJ, Solans C. Formation of polymeric nano-emulsions by a low-energy method and their use for nanoparticle preparation. J Colloid Interface Sci 2011;353:406-11.

[37] Pey CM, Maestro A, Sole I, Gonzalez C, Solans C, Gutierrez JM. Optimization of nano-emulsions prepared by low-energy emulsification methods at constant temperature using a factorial design study. Colloid Surf A-Physicochem Eng Asp 2006;288:144-50.

[38] Rahn-Chique K, Puertas AM, Romero-Cano MS, Rojas C, Urbina-Villalba G. Nanoemulsion stability: Experimental evaluation of the flocculation rate from turbidity measurements. Adv Colloid Interface Sci 2012;178:1-20.

[39] Tadros T, Izquierdo R, Esquena J, Solans C. Formation and stability of nano-emulsions. Adv Colloid Interface Sci 2004;108:303-18.

[40] Delmas T, Piraux H, Couffin AC, Texier I, Vinet F, Poulin P, Cates ME, Bibette J. How To Prepare and Stabilize Very Small Nanoemulsions. Langmuir 2011;27:1683-92.

[41] Dulieu C, Bazile D. Influence of lipid nanocapsules composition on their aptness to freeze-drying. Pharm Res 2005;22:285-92.

Supporting Information

Size-tailored nanocapsules by a single step energetically-efficient procedure: the phase inversion temperature method revisited

Juan Aparicio-Blanco [a], Víctor Sebastián [b,c], Miguel Rodríguez-Amaro [a], Héctor García-Díaz [a], Ana I. Torres-Suárez [a, d]

[a] Department of Pharmaceutics and Food Technology, Complutense University, Madrid, Spain

[b] Department of Chemical Engineering, Aragon Institute of Nanoscience (INA), University of Zaragoza, Zaragoza, Spain

[c] Networking Research Center on Bioengineering, Biomaterials and Nanomedicine (CIBER-BBN), Madrid, Spain

[d] University Institute of Industrial Pharmacy, Complutense University, Madrid, Spain

Table 1.2.S1: Detailed excipient weights (in mg) for the different formulations evaluated for the oil-surfactant tandem Kolliphor ELP®-Labrafac lipophile WL1349®.

	F1	F2	F3	F4	F5	F6	F7	F8
Kolliphor ELP®	2950	2478	1934	1390	846	665	484	440
Lipoïd S75®	75	75	75	75	75	75	75	75
NaCl	89	89	89	89	89	89	89	89
Labrafac lipophile WL1349®	250	755	846	937	1028	1118	1209	1350
Water	1636	1603	2055	2509	2962	3053	3143	3046
Oil: surfactant ratio	0.085	0.305	0.437	0.674	1.215	1.681	2.498	3.068

Table 1.2.S2: Detailed excipient weights (in mg) for the different formulations evaluated for the oil-surfactant tandem Kolliphor HS15®-Labrafil M1944 CS®.

	F1	F2	F3	F4	F5	F6	F7
Kolliphor HS15®	2950	2478	1934	1390	846	665	580
Lipoïd S75®	75	75	75	75	75	75	75
NaCl	89	89	89	89	89	89	89
Labrafil M1944 CS®	250	755	846	937	1028	1118	1160
Water	1636	1603	2055	2509	2962	3053	3096
Oil: surfactant ratio	0.085	0.305	0.437	0.674	1.215	1.681	2.000

Table 1.2.S3: Detailed excipient weights (in mg) for the test and reference formulations prepared to validate the univariate linear model for the oil-surfactant tandem Kolliphor HS15®- Labrafac lipophile WL1349®.

	F3 reference	F3 test	F5 reference	F5 test
Kolliphor HS15®	1934	2764	846	995
Lipoïd S75®	75	75	75	75
NaCl	89	89	89	89
Labrafac lipophile WL1349®	846	1209	1028	1209
Water	2055	863	2962	2632
Oil: surfactant ratio	0.437	0.437	1.215	1.215

Figure 1.2.S1: Influence of the formulation composition on the polydispersity index. (a) Labrafac lipophile WL1349®-Kolliphor ELP® ($p>0.05$). (b) Labrafil MS1944 CS®-Kolliphor HS15®.

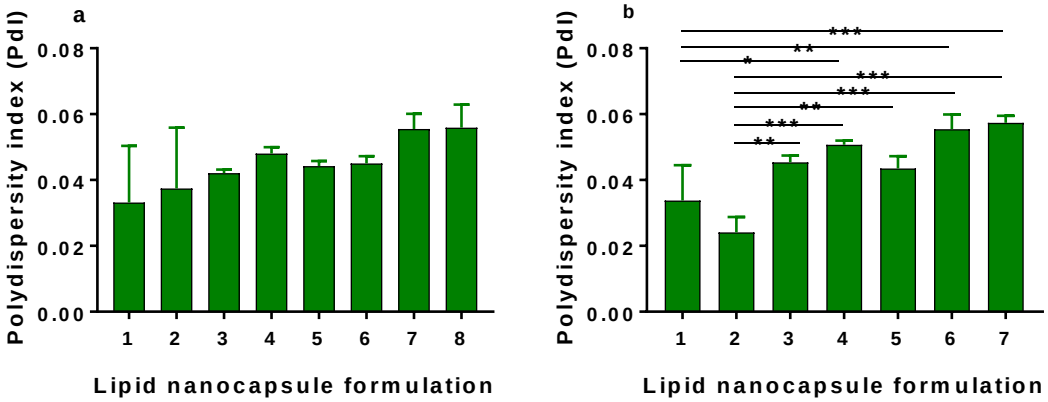

Figure 1.2.S2: Evaluation of the stability of freeze-dried lipid nanocapsules (formulation 3, Table 1) over 12 months (25ºC, 75% relative humidity). (a) Volume radius^3 ($p>0.05$). (b) Polydispersity index ($p > 0.05$)

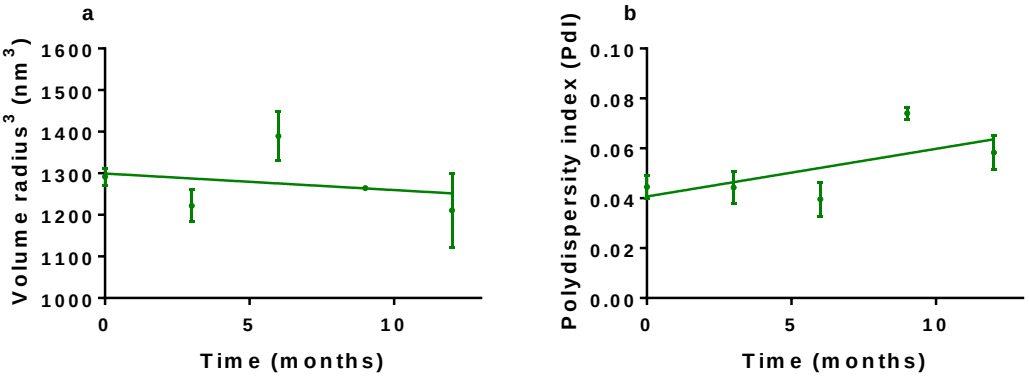

Chapter 2: Cannabidiol-decorated lipid nanocapsules for active targeting across the blood-brain barrier

As outlined in the previous chapter, the efficiency of passive targeting of nanocarriers to brain tumors depends on the stage of the disease: even though the BBTB is considered leaky in the core of high grade gliomas, in the infiltrative areas of glioblastomas and in lower grade gliomas, the BBTB more closely resembles the non-fenestrated BBB and prevents the passage of cancer therapeutics [1, 2]. Accordingly, active targeting with ligands that bind to receptors overexpressed on the brain endothelium and/or tumor cell membranes is being investigated to prolong the median survival times of their actively-untargeted counterparts in rodent models of malignant brain tumors [3-6].

Different receptors in the brain can be used for active targeting of brain tumors. All these receptors are ascribed to at least one of the following categories:

- Receptors normally overexpressed on the brain endothelium to enhance the penetration into the brain area.

- Receptors distributed on proliferating endothelial cells in the tumor vasculature.

- Receptors overexpressed on tumor cells to reduce the side effects of the antitumor agents on healthy brain cells.

- Markers of the tumor microenvironment to retain the carrier at the tumor site.

A summary of the main receptors belonging to each category that have already been exploited for active targeting of nanocarriers are enumerated in Table 1.

In broad terms, distinct receptors should be targeted depending on the administration route. Whereas ligands that preferentially bind to receptors on the cerebral endothelium are futile following local delivery, nanomedicines could be actively targeted to the brain tumor cells by conjugating specific ligands that bind to the receptors that are overexpressed or uniquely expressed on the tumor surface. Alternatively, intravenously administered nanocarriers must be actively targeted across the BBB/BBTB. Likewise, in the case of systemic administration, nanomedicines can be

designed to target simultaneously the BBB, the BBTB and the brain tumor cells by either multiple targeting moieties [3, 4], or by conjugating a single ligand that targets both the brain endothelia and the brain tumor cells to promote the selective distribution of the therapy across the BBB/BBTB and eventually to the tumor cells [7]. In this regard, nanomedicine could represent a potential platform for targeting heterogeneous brain tumors [8].

Receptor location	Receptor name	Targeting moiety	Ref.
Receptors overexpressed on the fully functional endothelium of infiltrative areas	Transferrin receptor	Physiological ligands	[9-11]
		Transferrin-derived peptides	[12-14]
		Monoclonal antibodies (OX26; 8D3)	[15-17]
	Nicotinic receptor	Peptides derived from neurotoxins	[18, 19]
	Low-density lipoprotein receptor	Angiopep-2	[3, 6, 7, 20]
	GLUT1 transporter	Monosaccharides (glucose, mannose)	[21-24]
	Glutathione transporter	Gluthatione	[25]
	GM1 ganglioside	G23 peptide	[26]
Receptors expressed on endothelial cells of neovasculature tumoral	$\alpha_V\beta_3$ integrin	RGD peptide	[6, 27-29]
	Aminopeptidase N (CD13)	NGR peptide	[30-32]
	Nucleolin	F3 peptide	[33]
		AS1411 aptamer	[5, 34]
	Neuropilin-1	tLyp-1 peptide	[35-37]
Receptors overexpressed on tumor cells	Low-density lipoprotein receptor	Angiopep-2	[3, 6, 7, 20]
	$\alpha_V\beta_3$ integrin	RGD peptide	[6, 27-29]
	EGFRvIII	Monoclonal antibody against EGFRvIII	[38]
	IL-13 receptor α2	PEP-1 peptide	[4, 6, 39]
	IL-4 receptor	AP-1 peptide	[40]
	Folic acid receptor	Folic acid	[41, 42]
	Insulin receptor (HIR)	Monoclonal antibody (83-14)	[16]
	CD133	Anti-CD133 monoclonal antibody	[3, 43]
Markers within the tumor microenvironment	MMP-2	Chlorotoxin	[15, 44, 45]
	Fibrin-fibronectin complex	CREKA	[4, 46, 47]
	Tenascin C	FHK peptide	[35]

Table 2.0.1: An overlook on the active targeting strategies already explored with nanomedicines for different CNS tumor conditions. EGFRvIII: malignant isoform of the epidermal growth factor (EGFR), IL-13, Il-4: interleukins 13 and 4; MMP-2: membrane-bound matrix metalloproteinase-2.

As the BBB accounts for the high attrition rate of the treatments of brain tumors, the evaluation of the BBB permeability of targeted nanomedicines is a key ADME feature. Hence, to prevent later failure due to low drug levels at the target site, researchers have been endeavoring to develop *in vitro* screening methods that, retaining the most relevant features of the BBB, reliably predict the *in vivo* BBB permeability of nanomedicines and help early triage the right active targeting strategies to move forward and rule out poor candidates before reaching clinical stage.

Overall, since any ligand for which a receptor exists on the cerebral endothelial or on the tumor cells might be used for active targeting, the enrichment of knowledge about the transport systems present on the brain endothelium and the glioma-specific receptors would enable novel practical approaches for improving the passage of nanomedicines to be designed with the purpose of exposing the entire diseased brain tumor area to pharmacologically meaningful quantities of the antitumor agent [48].

In particular, several receptors to which cannabinoids bind are located on the BBB. Accordingly, we hypothesized that cannabinoids represent exciting perspectives for active brain targeting. In particular, being the major cannabinoid devoid of psychotropic effects, cannabidiol (CBD) seems to be the lead candidate to test the possibilities of this hypothesis. The rationale for the functionalization of nanocarriers with CBD to enhance brain targeting is supported by pharmacokinetics of CBD in mice following subcutaneous administration obtained in a previous collaboration of our research group with Professor Aron Lichtman from the Virginia Commonwealth University (EEUU). As shown in Figure 1, the comparison of CBD levels in the blood and brain of mice revealed a partition favorable to brain ($\frac{AUC_{brain}}{AUC_{blood}} = 1.29$). The most likely mechanism of brain targeting of CBD is receptor-mediated transcytosis across the brain endothelium. Hence, the promising features of CBD for active targeting of nanomedicines deserve further research.

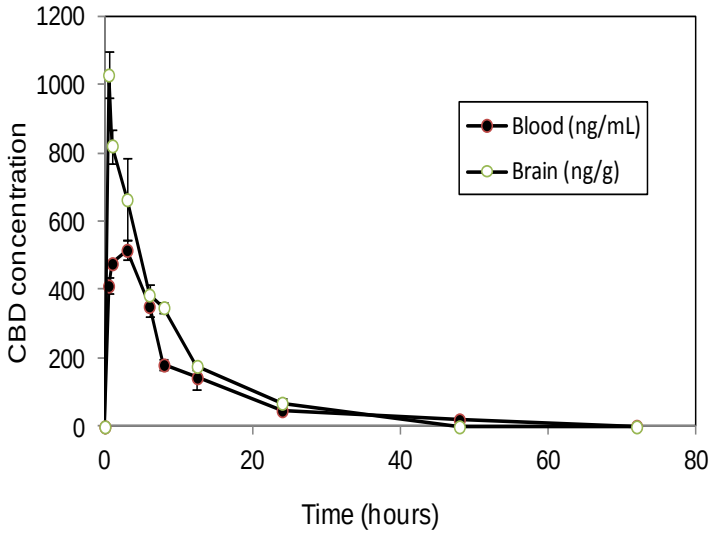

Figure 2.0.1: Pharmacokinetic profile of cannabidiol (CBD) in blood (ng/mL) and brain (ng/g) of mice following subcutaneous administration (unpublished results).

Altogether, this chapter is devoted to the functionalization of the LNCs developed in the first chapter with CBD to ultimately evaluate *in vitro* and *in vivo* the possibilities of this phytocannabinoid as a novel non-immunogenic molecule for brain active targeting. Hence, in the review entitled "*In vitro* screening of nanomedicines through the blood-brain barrier: a critical review" we firstly provide an in-depth analysis of the currently available *in vitro* BBB models. Notably, the relationship between experimental factors and underlying physiological assumptions that ultimately lead to a more predictive capacity of their *in vivo* performance along with the assumptions to derive the permeability coefficients from first principles in each case are comprehensively discussed. Subsequently, in the original article entitled "Cannabidiol-targeted lipid nanocapsules across the blood-brain barrier: *in vitro* and *in vivo* evaluation", we prepare monodisperse LNCs functionalized with CBD and loaded with a fluorescent marker in different sizes, wherewith cell viability, uptake and permeability experiments are conducted on the human brain endothelial cell line hCMEC/D3. The permeability coefficients are validated with the data obtained from biodistribution studies in mice with the same formulations. This validation will ultimately enable an *in vitro* BBB screening method that meets the high-throughput demands in the early stages of drug discovery, provides mechanistic information and lacks ethical constraints to be obtained. Some results from this chapter have likewise been published in the conference paper entitled "Cannabidiol-loaded lipid nanocapsules for glioma therapy across the blood-brain barrier: in vitro assays on human brain endothelial and glioma cell lines", Journal of Cerebral Blood Flow and Metabolism (IF: 5.081, ISSN: 0271-678X).

The *in vitro* evaluation of this chapter has been achieved thanks to two scholarships (EST15/00534 and EST16/00556) awarded by the Spanish Ministry of Education within the Professor Training Programm (FPU) that enabled two research stays at the School of Life, Health and Chemical Sciences (LHCS), The Open University under the supervision of Professor Nacho Romero (September 2016-December 2016; June 2017-August 2017).

References:

[1] van Tellingen O, Yetkin-Arik B, de Gooijer MC, Wesseling P, Wurdinger T, de Vries HE. Overcoming the blood-brain tumor barrier for effective glioblastoma treatment. Drug Resist Update. 2015;19:1-12.

[2] Karim R, Palazzo C, Evrard B, Piel G. Nanocarriers for the treatment of glioblastoma multiforme: Current state-of-the-art. J Control Release. 2016;227:23-37.

[3] Kim JS, Shin DH, Kim JS. Dual-targeting immunoliposomes using angiopep-2 and CD133 antibody for glioblastoma stem cells. J Control Release. 2018;269:245-57.

[4] Wang XZ, Zhang Q, Lv LY, Fu JJ, Jiang Y, Xin HL, et al. Glioma and microenvironment dual targeted nanocarrier for improved antiglioblastoma efficacy. Drug Deliv. 2017;24:1401-9.

[5] Luo ZM, Yan ZQ, Jin K, Pang Q, Jiang T, Lu H, et al. Precise glioblastoma targeting by AS1411 aptamer-functionalized poly (L-gamma-glutamylglutamine)-paclitaxel nanoconjugates. J Colloid Interface Sci. 2017;490:783-96.

[6] Chen CT, Duan ZQ, Yuan Y, Li RX, Pang L, Liang JM, et al. Peptide-22 and Cyclic RGD Functionalized Liposomes for Glioma Targeting Drug Delivery Overcoming BBB and BBTB. ACS Appl Mater Interfaces. 2017;9:5864-73.

[7] Luo ZM, Jin K, Pang Q, Shen S, Yan ZQ, Jiang T, et al. On-Demand Drug Release from Dual-Targeting Small Nanoparticles Triggered by High-Intensity Focused Ultrasound Enhanced Glioblastoma-Targeting Therapy. ACS Appl Mater Interfaces. 2017;9:31612-25.

[8] Cheng Y, Morshed RA, Auffinger B, Tobias AL, Lesniak MS. Multifunctional nanoparticles for brain tumor imaging and therapy. Adv Drug Deliv Rev. 2014;66:42-57.

[9] Ying X, Wen H, Lu WL, Du J, Guo J, Tian W, et al. Dual-targeting daunorubicin liposomes improve the therapeutic efficacy of brain glioma in animals. J Control Release. 2010;141:183-92.

[10] Cui YN, Xu QX, Chow PKH, Wang DP, Wang CH. Transferrin-conjugated magnetic silica PLGA nanoparticles loaded with doxorubicin and paclitaxel for brain glioma treatment. Biomaterials. 2013;34:8511-20.

[11] Gao JQ, Lv Q, Li LM, Tang XJ, Li FZ, Hu YL, et al. Glioma targeting and blood-brain barrier penetration by dual-targeting doxorubincin liposomes. Biomaterials. 2013;34:5628-39.

[12] Cui Y, Zhang M, Zeng F, Jin HY, Xu Q, Huang YZ. Dual-Targeting Magnetic PLGA Nanoparticles for Codelivery of Paclitaxel and Curcumin for Brain Tumor Therapy. ACS Appl Mater Interfaces. 2016;8:32159-69.

[13] Dixit S, Novak T, Miller K, Zhu Y, Kenney ME, Broome AM. Transferrin receptor-targeted theranostic gold nanoparticles for photosensitizer delivery in brain tumors. Nanoscale. 2015;7:1782-90.

[14] Wei L, Guo XY, Yang T, Yu MZ, Chen DW, Wang JC. Brain tumor-targeted therapy by systemic delivery of siRNA with Transferrin receptor-mediated core-shell nanoparticles. Int J Pharm. 2016;510:394-405.

[15] Yue PJ, He L, Qiu SW, Li Y, Liao YJ, Li XP, et al. OX26/CTX-conjugated PEGylated liposome as a dual-targeting gene delivery system for brain glioma. Mol Cancer. 2014;13:13.

[16] Zhang Y, Zhang YF, Bryant J, Charles A, Boado RJ, Pardridge WM. Intravenous RNA interference gene therapy targeting the human epidermal growth factor receptor prolongs survival in intracranial brain cancer. Clin Cancer Res. 2004;10:3667-77.

[17] Johnsen KB, Burkhart A, Melander F, Kempen PJ, Vejlebo JB, Siupka P, et al. Targeting transferrin receptors at the blood-brain barrier improves the uptake of immunoliposomes and subsequent cargo transport into the brain parenchyma. Sci Rep. 2017;7:13.

[18] Wei XL, Zhan CY, Shen Q, Fu W, Xie C, Gao J, et al. A D-Peptide Ligand of Nicotine Acetylcholine Receptors for Brain-Targeted Drug Delivery. Angew Chem-Int Edit. 2015;54:3023-7.

[19] Wei XL, Gao J, Zhan CY, Xie C, Chai ZL, Ran D, et al. Liposome-based glioma targeted drug delivery enabled by stable peptide ligands. J Control Release. 2015;218:13-21.

[20] Gao SQ, Tian HY, Xing ZK, Zhang DW, Guo Y, Guo ZP, et al. A non-viral suicide gene delivery system traversing the blood brain barrier for non-invasive glioma targeting treatment. J Control Release. 2016;243:357-69.

[21] Jiang XY, Xin HL, Ren QY, Gu JJ, Zhu LJ, Du FY, et al. Nanoparticles of 2-deoxy-D-glucose functionalized poly(ethylene glycol)-co-poly(trimethylene carbonate) for dual-targeted drug delivery in glioma treatment. Biomaterials. 2014;35:518-29.

[22] Byeon HJ, Thao LQ, Lee S, Min SY, Lee ES, Shin BS, et al. Doxorubicin-loaded nanoparticles consisted of cationic- and mannose-modified-albumins for dual-targeting in brain tumors. J Control Release. 2016;225:301-13.

[23] Du D, Chang ND, Sun SL, Li MH, Yu H, Liu MF, et al. The role of glucose transporters in the distribution of p-aminophenyl-alpha-D-mannopyranoside modified liposomes within mice brain. J Control Release. 2014;182:99-110.

[24] Li XY, Zhao Y, Sun MG, Shi JF, Ju RJ, Zhang CX, et al. Multifunctional liposomes loaded with paclitaxel and artemether for treatment of invasive brain glioma. Biomaterials. 2014;35:5591-604.

[25] Gaillard PJ, Appeldoorn CCM, Dorland R, van Kregten J, Manca F, Vugts DJ, et al. Pharmacokinetics, Brain Delivery, and Efficacy in Brain Tumor-Bearing Mice of Glutathione Pegylated Liposomal Doxorubicin (2B3-101). PLoS One. 2014;9:10.

[26] Su CH, Tsai CY, Tomanek B, Chen WY, Cheng FY. Evaluation of blood-brain barrier-stealth nanocomposites for in situ glioblastoma theranostics applications. Nanoscale. 2016;8:7866-70.

[27] Belhadj Z, Ying M, Cao X, Hu XF, Zhan CY, Wei XL, et al. Design of Y-shaped targeting material for liposome-based multifunctional glioblastoma-targeted drug delivery. J Control Release. 2017;255:132-41.

[28] You YY, Yang LY, He LZ, Chen TF. Tailored mesoporous silica nanosystem with enhanced permeability of the blood-brain barrier to antagonize glioblastoma. J Mat Chem B. 2016;4:5980-90.

[29] Huang YK, Liu WC, Gao F, Fang XL, Chen YZ. c(RGDyK)-decorated Pluronic micelles for enhanced doxorubicin and paclitaxel delivery to brain glioma. Int J Nanomed. 2016;11:1629-41.

[30] Zhao GJ, Huang Q, Wang F, Zhang X, Hu JG, Tan Y, et al. Targeted shRNA-loaded liposome complex combined with focused ultrasound for blood brain barrier disruption and suppressing glioma growth. Cancer Lett. 2018;418:147-58.

[31] Hu JG, Zhang X, Wen ZH, Tan Y, Huang N, Cheng S, et al. Asn-Gly-Arg-modified polydopamine-coated nanoparticles for dual-targeting therapy of brain glioma in rats. Oncotarget. 2016;7:73681-96.

[32] Kang T, Gao XL, Hu QY, Jiang D, Feng XY, Zhang X, et al. iNGR-modified PEG-PLGA nanoparticles that recognize tumor vasculature and penetrate gliomas. Biomaterials. 2014;35:4319-32.

[33] Hu QY, Gu GZ, Liu ZY, Jiang MY, Kang T, Miao DY, et al. F3 peptide-functionalized PEG-PLA nanoparticles co-administrated with tLyp-1 peptide for anti-glioma drug delivery. Biomaterials. 2013;34:1135-45.

[34] Gao HL, Qian J, Cao SJ, Yang Z, Pang ZQ, Pan SQ, et al. Precise glioma targeting of and penetration by aptamer and peptide dual-functioned nanoparticles. Biomaterials. 2012;33:5115-23.

[35] Kang T, Zhu QQ, Jiang D, Feng XY, Feng JX, Jiang TZ, et al. Synergistic targeting tenascin C and neuropilin-1 for specific penetration of nanoparticles for anti-glioblastoma treatment. Biomaterials. 2016;101:60-75.

[36] Bechet D, Auger F, Couleaud P, Marty E, Ravasi L, Durieux N, et al. Multifunctional ultrasmall nanoplatforms for vascular-targeted interstitial photodynamic therapy of brain tumors guided by real-time MRI. Nanomed-Nanotechnol Biol Med. 2015;11:657-70.

[37] Hu QY, Gao XL, Gu GZ, Rang T, Tu YF, Liu ZY, et al. Glioma therapy using tumor homing and penetrating peptide-functionalized PEG-PLA nanoparticles loaded with paclitaxel. Biomaterials. 2013;34:5640-50.

[38] Hadjipanayis CG, Machaidze R, Kaluzova M, Wang LY, Schuette AJ, Chen HW, et al. EGFRvIII Antibody-Conjugated Iron Oxide Nanoparticles for Magnetic Resonance Imaging-Guided Convection-Enhanced Delivery and Targeted Therapy of Glioblastoma. Cancer Res. 2010;70:6303-12.

[39] Wang BY, Lv LY, Wang ZY, Zhao Y, Wu L, Fang XL, et al. Nanoparticles functionalized with Pep-1 as potential glioma targeting delivery system via interleukin 13 receptor alpha 2-mediated endocytosis. Biomaterials. 2014;35:5897-907.

[40] Yang FY, Wong TT, Teng MC, Liu RS, Lu M, Liang HF, et al. Focused ultrasound and interleukin-4 receptor-targeted liposomal doxorubicin for enhanced targeted drug delivery and antitumor effect in glioblastoma multiforme. J Control Release. 2012;160:652-8.

[41] Zhang J, Chen N, Wang H, Gu W, Liu K, Ai PH, et al. Dual-targeting superparamagnetic iron oxide nanoprobes with high and low target density for brain glioma imaging. J Colloid Interface Sci. 2016;469:86-92.

[42] Chen YC, Chiang CF, Chen LF, Liang PC, Hsieh WY, Lin WL. Polymersomes conjugated with des-octanoyl ghrelin and folate as a BBB-penetrating cancer cell-targeting delivery system. Biomaterials. 2014;35:4066-81.

[43] Tamborini M, Locatelli E, Rasile M, Monaco I, Rodighiero S, Corradini I, et al. A Combined Approach Employing Chlorotoxin-Nanovectors and Low Dose Radiation To Reach Infiltrating Tumor Niches in Glioblastoma. ACS Nano. 2016;10:2509-20.

[44] Stephen ZR, Kievit FM, Veiseh O, Chiarelli PA, Fang C, Wang K, et al. Redox-Responsive Magnetic Nanoparticle for Targeted Convection-Enhanced Delivery of O-6-Benzylguanine to Brain Tumors. ACS Nano. 2014;8:10383-95.

[45] Cho JH, Kim AR, Kim SH, Lee SJ, Chung H, Yoon MY. Development of a novel imaging agent using peptide-coated gold nanoparticles toward brain glioma stem cell marker CD133. Acta Biomater. 2017;47:182-92.

[46] Zhang B, Wang HF, Shen S, She XJ, Shi W, Chen J, et al. Fibrin-targeting peptide CREKA-conjugated multi-walled carbon nanotubes for self-amplified photothermal therapy of tumor. Biomaterials. 2016;79:46-55.

[47] Zhao JJ, Zhang B, Shen S, Chen J, Zhang QZ, Jiang XG, et al. CREKA peptide-conjugated dendrimer nanoparticles for glioblastoma multiforme delivery. J Colloid Interface Sci. 2015;450:396-403.

[48] Oller-Salvia B, Sanchez-Navarro M, Giralt E, Teixido M. Blood-brain barrier shuttle peptides: an emerging paradigm for brain delivery. Chem Soc Rev. 2016;45:4690-707.

Biomaterials 103 (2016) 229–255

Contents lists available at ScienceDirect

Biomaterials

journal homepage: www.elsevier.com/locate/biomaterials

Review

In vitro screening of nanomedicines through the blood brain barrier: A critical review

Juan Aparicio-Blanco [a], Cristina Martín-Sabroso [a], Ana-Isabel Torres-Suárez [a, b, *]

[a] Department of Pharmaceutical Technology, Faculty of Pharmacy, Complutense University, 28040, Madrid, Spain
[b] University Institute of Industrial Pharmacy, Complutense University, 28040, Madrid, Spain

ARTICLE INFO

Article history:
Received 9 May 2016
Received in revised form
14 June 2016
Accepted 20 June 2016
Available online 24 June 2016

Keywords:
Central nervous system
Brain targeting
Nanomedicine
Parallel artificial membrane permeability assay
Cell culture
In vitro blood-brain barrier model

ABSTRACT

The blood-brain barrier accounts for the high attrition rate of the treatments of most brain disorders, which therefore remain one of the greatest health-care challenges of the twenty first century. Against this background of hindrance to brain delivery, nanomedicine takes advantage of the assembly at the nanoscale of available biomaterials to provide a delivery platform with potential to raising brain levels of either imaging or therapeutic agents. Nevertheless, to prevent later failure due to ineffective drug levels at the target site, researchers have been endeavoring to develop a battery of *in vitro* screening procedures that can predict earlier in the drug discovery process the ability of these cutting-edge drug delivery platforms to cross the blood-brain barrier for biomedical purposes.

This review provides an in-depth analysis of the currently available *in vitro* blood-brain barrier models (both cell-based and non-cell-based) with the focus on their suitability for understanding the biological brain distribution of forthcoming nanomedicines. The relationship between experimental factors and underlying physiological assumptions that would ultimately lead to a more predictive capacity of their *in vivo* performance, and those methods already assayed for the evaluation of the brain distribution of nanomedicines are comprehensively discussed.

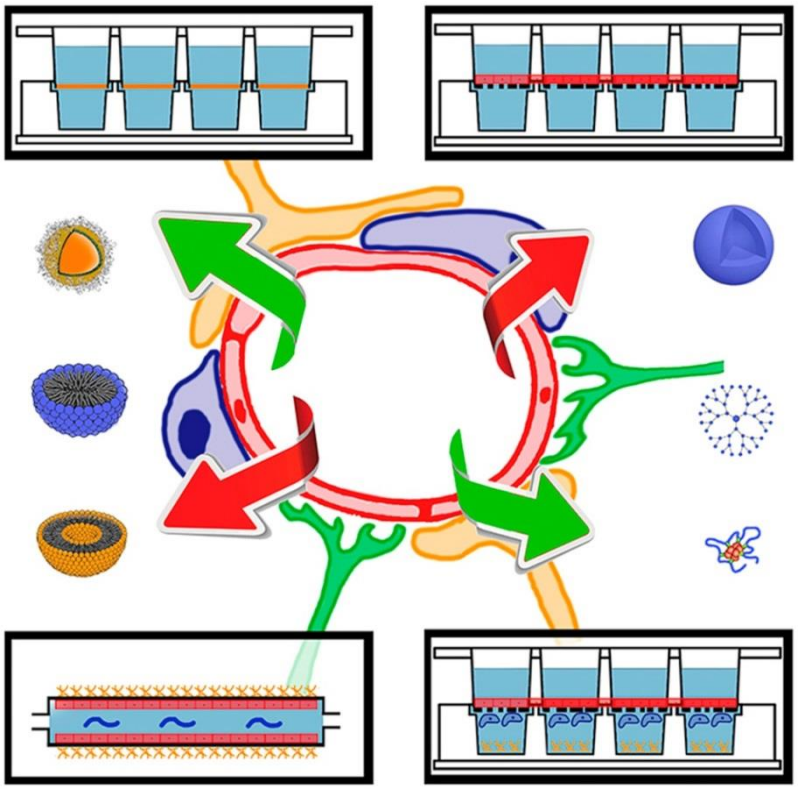

In vitro screening of nanomedicines through the blood-brain barrier: a critical review

Juan Aparicio-Blanco, Cristina Martín-Sabroso, Ana-Isabel Torres-Suárez

Department of Pharmaceutical Technology, Faculty of Pharmacy, Complutense University, 28040, Madrid, Spain

Abstract

The blood-brain barrier accounts for the high attrition rate of the treatments of most brain disorders, which therefore remain one of the greatest health-care challenges of the twenty first century. Against this background of hindrance to brain delivery, nanomedicine takes advantage of the assembly at the nanoscale of available biomaterials to provide a delivery platform with potential to raising brain levels of either imaging or therapeutic agents. Nevertheless, to prevent later failure due to ineffective drug levels at the target site, researchers have been endeavoring to develop a battery of *in vitro* screening procedures that can predict earlier in the drug discovery process the ability of these cutting-edge drug delivery platforms to cross the blood-brain barrier for biomedical purposes.

This review provides an in-depth analysis of the currently available *in vitro* blood-brain barrier models (both cell-based and non-cell-based) with the focus on their suitability for understanding the biological brain distribution of forthcoming nanomedicines. The relationship between experimental factors and underlying physiological assumptions that would ultimately lead to a more predictive capacity of their *in vivo* performance, and those methods already assayed for the evaluation of the brain distribution of nanomedicines are comprehensively discussed.

Keywords

Central nervous system, brain targeting, nanomedicine, parallel artificial membrane permeability assay, cell culture, *in vitro* blood-brain barrier model

1. Introduction

With an average of 13 years and an investment above $1 billion to develop a treatment, disorders of the central nervous system (CNS) represent the disease area whose unmet medical needs call for the most lengthy and resource-consuming procedures [1-4]. Furthermore, the failure rate of treatments for brain disorders is higher than that for other disease areas and occurs later in the development process (at Phase 3 or even after registration [5, 6]). Accordingly, brain disorders represent one of the greatest health-care challenges of the 21st century; a fact that is compounded by the continuously increasing life expectancy [7-9].

The blood-brain barrier (BBB) accounts to a great extent for the high attrition rate of the treatment of most brain disorders, since it hinders free access of most therapeutic molecules to CNS, which leads to insufficient brain exposure for the drug substance to be pharmacologically effective [10-16]. Nevertheless, minimally invasive procedures to reach brain parenchyma with a homogeneous distribution pattern at therapeutic doses would indeed involve crossing the blood-brain barrier [17-19].

Therefore, the right candidates to move forward in the drug discovery process should be adequately selected; the earlier, the better. By the early 1990s, the focus was solely put on the potency and selectivity of the drug substances for the biological target, whereas the role played by pharmacokinetics was underestimated [20]. However, given the high attrition rate due to ineffective drug levels at the target site, by the mid-1990s ADME properties started being addressed earlier in the drug discovery process to rule out poor candidates before reaching clinical stage, as the therapeutic potential of a CNS-acting drug candidate also relies on its ability to attain an effective dose at the CNS [21-24]. Hence, the ability to permeate the BBB is a key ADME features in the case of CNS disorders [25-27]. To evaluate BBB permeability of drug substances, researchers have been endeavoring to develop *in-vitro*, *in-vivo* and *in-silico* methods that, retaining most relevant features of the BBB, reliably predict *in vivo* brain distribution and meet high-throughput demands [20, 28-33]. Nowadays, brain uptake of drug substances is often inferred by combining various screening methods.

Against this background of hindrance to brain delivery, nanomedicine takes advantage of the assembly at the nanoscale of available biomaterials to provide a delivery platform with potential to raising brain levels of drug substances otherwise unable to cross the BBB [34-41]. Consequently, the ability of these cutting-edge drug delivery platforms to cross the blood-brain barrier for biomedical purposes must be screened. Hence, a groundbreaking change in outlook is likely to occur in the near future, since with the purpose of predicting brain distribution, ADME screening methods must be reconsidered for evaluation of novel brain nanomedicines.

Among the screening methods developed to predict the permeability across the BBB, this review focuses on *in vitro* models, since these screening methods, although dependent on *in vivo* data for their validation, meet the high-throughput demands in the early stages of drug discovery, provide mechanistic information, lack ethical constraints and are more economical. Furthermore, once validated, simplified *in vitro* BBB models could represent predictive tools to evaluate batch-to-batch variability (a critical attribute

for the regulation of nanomedicines to promote their translation into the market [42]). In an attempt to gather as many BBB features as possible, two groups of *in vitro* BBB models have been patented: cell-based and non-cell based.

The aim of this review is, on the one hand, to compile the currently available *in vitro* methods for prediction of the BBB permeability [43-47], and, on the other hand, to accomplish an in-depth analysis of the suitability of these methods for ADME screening of forthcoming nanomedicines. Experimental factors that would enable a better *in vivo* prediction are comprehensively discussed and, in this regard, a parallel is drawn between cell-based and non-cell based models for comparison purposes. Likewise, great emphasis is placed on those methods already assayed for the evaluation of brain distribution of nanomedicines.

2. Blood brain barrier

Although it is currently broadly agreed that there are three barriers between the blood and the CNS, neither the epithelial cells of the choroid plexus nor the avascular arachnoid epithelium represent a significant surface for drug exchange between both media. With a total area of between 12 and 18 m^2 in the human adult; hence the largest blood–cerebral parenchyma exchange interface, the brain endothelium represents the physical and metabolic barrier that governs brain uptake [48]. Therefore, this barrier should be mimicked to the greatest extent possible by the screening methods aimed at reliably predicting the cerebral permeability.

The key features of the cerebral endothelial cells are both the lack of fenestrations and the presence of extremely tight intercellular junctions. These features provide the BBB with a transendothelial electrical resistance (TEER) as high as 1500 to 2000 Ωcm^2 [49] (compared with 3.33 Ωcm^2 for peripheral capillaries [50]), causes cell polarization by separating apical and basolateral domains and significantly restricts the permeation of substances into the CNS, particularly via paracellular diffusion pathways. Consequently, most hydrophilic molecules and macromolecules must go through the brain endothelium transcellularly by any of the following pathways: passive diffusion, facilitated diffusion [51] or endo-/transcytosis, (which can be triggered either by ligand-receptor binding or by electrostatic interactions). Once in the brain interstitial fluid, they can still be ejected back into the bloodstream by efflux pumps such as P-glycoprotein, which mediates most of the active efflux at the BBB [52, 53]. One additional transcellular route currently under investigation involves the migration of immune cells to the CNS.

However, not only the blood vessel endothelial cells but also other cell types constitute the BBB: astrocytes, pericytes, microglia and the basal lamina. Astrocytes are glial cells provided with foot processes that surround the basolateral domain of the endothelial cells and release regulatory factors able to upregulate tight junctions and the expression of specialized sets of enzymes and polarized transporters [54, 55]. Pericytes are mural cells separated from the brain endothelium by the basal lamina that induce the polarization of the astrocytic end-feet, thus modulating their signaling over the endothelial cells [56, 57]. The whole unit is referred to as the neurovascular unit.

Thus, in the development of any screening method to predict brain distribution, the unique complexity of the BBB must be considered, since these models should retain as many properties of this physiological environment as possible to reliably infer the BBB permeability [58]. Moreover, another feature that should be taken into account in the design of *in vitro* BBB models is that in some brain disorders, the *in vivo* properties of the BBB are significantly altered, which may ultimately enhance or comprise the permeability of a given entity.

3. Nanocarriers

Against this background of hindrance to brain delivery of most drugs, nanomedicine represents an appealing platform with potential to raising CNS drug and/or imaging agent levels in an effective and safe way [59-63] Nanomedicines consist in the association of unmodified drugs with delivery systems in the nanoscale range [64]. As shown in Table 1, several nanocarriers have already been developed for brain delivery [60, 65, 66]), which mainly belong to three categories: polymer-based, lipid-based or metal-based, according to their major excipient.

Material	Type	Morphology	Size
Polymer-based nanocarriers	Polymeric conjugates	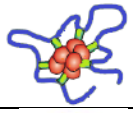	2-25 nm
	Polymer nanoparticles		10-1000 nm
	Polymeric micelles	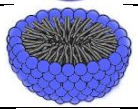	10-200 nm
	Dendrimers	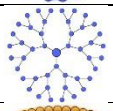	1-10 nm
Lipid-based nanocarriers	Liposomes	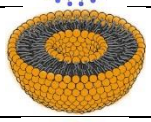	20-5000 nm
	Solid lipid nanoparticles		50-1000 nm
	Lipid nanocapsules	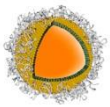	20-100 nm
Metal-based nanocarriers	Magnetite/Gold/Selenium nanoparticles		1-200 nm

Table 2.1.1: An overview of main available nanotechnological platforms to be exploited with the purpose of enhancing brain drug delivery

The inclusion of a known drug in a nanocarrier is regarded as a new chemical entity; hence the availability of a poorly brain-distributed drug can be largely enhanced

thanks to nanotechnology. As a result, the specific properties of the nanodevice (such as its interaction with the biological system or the extent of masking of the physicochemical properties of the loaded drug) should be properly assessed to reliably foresee its therapeutic outcome [67-71].

With the paracellular route truly restricted at the BBB, nanocarriers enhance CNS delivery by promoting any of the transcellular pathways across the brain endothelium [72-75]. In this regard, nanomedicines can potentiate the passive diffusion across the brain endothelium by raising the local drug concentration gradient. Likewise, nanocarriers can trigger transcytosis through the BBB (either by ligand-receptor binding or by electrostatic interactions) thanks to targeting moieties attached on their surface [76]. Alternatively, nanocargos can block the active efflux back into the bloodstream.

Consequently, since the properties of nanomedicines likely dictate their biological fate, with regard to brain endothelium permeation, ideal nanocarriers should gather as many of the following features as possible. Firstly, with the purpose of optimally enabling the transcytosis pathways above outlined, the particle size should be around or smaller than 50 nm [77]. Likewise, lipid-based nanocarriers are assumed to be the most suitable for brain delivery, inasmuch as lipids have very low toxicity, tend to traverse the brain endothelium with ease and are biocompatible and biodegradable by nature, thereby meeting the requirement of a proven track record of clinical safety. Furthermore, with respect to the surface characteristics, it is broadly agreed that the presence of a hydrophilic coating confers long-circulating properties to the nanocarriers, which indirectly increases the likelihood of the brain endothelium being crossed (strategy often known as passive targeting). Additionally, nanomediciones could be further tailored to take advantage of targeting moieties to enhance the biodistribution to the CNS. These moieties would potentiate the entry routes above described, either by binding membrane receptors present at the BBB [78, 79] or by electrostatically triggering endocytosis. In both cases, this strategy is often referred to as active targeting [80, 81]. Lastly, the coating with nonionic surfactants seems to confer the nanocarrier itself with efflux-pump blockage properties, since polyethylene glycol and polypropylene glycol among others have been proven to exhibit intrinsic efflux-pump blocking activity [82].

Therefore, nanomedicines would let brain drug levels otherwise unachievable be obtained [83], insofar as they may enhance the distribution across the brain endothelium, and prevent the peripheral enzymatic drug cleavage that accounts for the loss of pharmacological effect. As a result of this optimized pharmacokinetic profile, the doses and even the dosing frequency can be reduced and the harmful side effects due to distribution into unwanted peripheral targets can be minimized. This fact is of great concern for therapeutic agents whose low dose availability at the target site cannot be counterbalanced by dose increase for fear of severe side effects, as in the case of chemotherapy.

Therefore, the evaluation of the permeability of CNS drug delivery systems with *in vitro* BBB models is of great importance: it allows an estimation of their biodistribution that may well steer the optimization of physicochemical parameters of

nanocarriers to achieve more favorable drug pharmacokinetic and distribution profiles for both brain imaging diagnosis [84-90] and optimum therapy of CNS pathologies [91] (such as neurodegenerative disorders [92-97], ischemic strokes [98], brain tumors [99-103] or viral infections [104]).

4. Non-cell based models

4.1. Parallel Artificial Membrane Permeability Assay (PAMPA)

Firstly described in 1998 by Kansy [105] to predict intestinal absorption, PAMPA is a non-cell based assay used to infer passive transcellular permeability of drugs and nanomedicines in the early phases of research process.

As depicted in Figure 1, PAMPA is carried out in multi-well plates provided with a donor and an acceptor chamber. Both compartments are separated by a lipid artificial membrane that is supported by a low-binding hydrophobic membrane porous filter (usually made of polyvinylidene difluoride –PVDF-). The assay evaluates the extent to which the sample (drug substances or nanomedicines) permeate from the donor to the acceptor chamber after a given incubation time. To this end, sample levels in both compartments after the incubation time has elapsed are quantified to determine the permeability across the lipid artificial membrane. The equations to calculate permeability coefficients depend on the PAMPA design [106, 107].

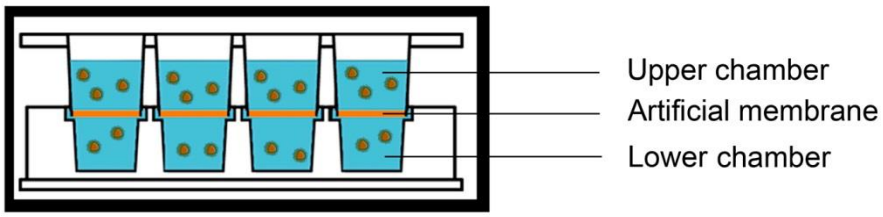

Figure 2.1.1- Scheme of an *in vitro* non-cell based method for prediction of the BBB permeability: the parallel artificial membrane permeability assay (PAMPA)

To draw some conclusions from PAMPA results, a classification range must be first established for high (CNS+) and low (CNS-) BBB permeation into the CNS, based on the PAMPA permeability coefficients obtained for standards with known *in vivo* performance. This discrimination range is then used to divide samples with unknown performance into CNS+ or CNS- categories according to their experimental permeability coefficients [108]. Traditionally, the establishment of this discrimination range stems from an *in vitro-in vivo* comparison between PAMPA permeability coefficients and *in vivo* brain:blood ratio –a parameter that quantifies the extent of permeation- [109]. Nevertheless, both parameters should measure the rate of brain penetration to predict permeability, and consequently, *in situ* brain perfusion has also been used as the *in vivo* parameter [110, 111].

Two aqueous media separated by very thin, pore-free, oily membrane where the sample is retained to a negligible extent represents the simplest PAMPA model.

Equations to calculate apparent permeability under these conditions are here described.

Two analogous expressions describe the flux in a transport model. Defined according to Fick's first law, flux is calculated as follows:

$$J\ (t) = \ P_m\ (C_D(t) - C_A\ (t))$$

where J refers to the flux, in units of mol cm^{-2} s^{-1}, P_m the membrane permeability in units of cm s^{-1}, and C_D and C_A are concentrations in the donor and acceptor compartments, respectively, in units of mol cm^{-3}.

Likewise, taken as the amount of solute that passes through a unit area in a unit of time in a direction perpendicular to the surface, flux is calculated as follows:

$$J\ (t) = \ -\ \frac{V_D}{A}\frac{dC_D(t)}{dt}$$

where J is the flux, in units of mol cm^{-2} s^{-1}, V_D the volume of the donor compartment in units of cm^3, A the membrane area in units of cm^2 and $dC_D(t)/dt$ the disappearance rate from the donor compartment in units of mol cm^{-3} s^{-1}.

A differential equation is obtained if both expressions are equated:

$$\frac{dC_D(t)}{dt} = \ -\ \frac{A}{V_{\ D}}\ P_m\ (C_D(t) - C_A(t))$$

The mass balance requires the total amount of sample be preserved. At the start, all the solute is in the donor compartment, whereas at a later stage, the sample distributes into both compartments:

$$V_D C_D(0) = \ V_D C_D(t) + \ V_A C_A(t)$$

where C_D (0) is the sample concentration placed into the donor compartment at the beginning of the assay, C_D (t) and C_A (t) the sample concentration after the incubation time has elapsed in the donor and acceptor compartment, respectively, and V_D and V_A the volume of buffer solution in the donor and acceptor compartment, respectively.

Under the given simplistic assumptions, mass balance serves to replace C_A (t) with donor-based terms, obtaining thereby another differential equation:

$$\frac{dC_D(t)}{dt} + \frac{AP}{V_D V_A}\ (V_D + V_A)C_D(t) - \frac{AP}{V_A}\ C_D(0) = 0$$

Solving the latter differential equation in terms of C_D (t), the following simplified exponential equation is obtained:

$$\frac{C_D(t)}{C_D(0)} = \frac{V_A}{V_A + V_D}\left(\frac{V_D}{V_A} + exp\left[-\frac{APt}{V_D V_A}(V_D + V_A)\right]\right)$$

This equation serves to describe drug disappearance from the donor compartment as a function of time. Taking into account mass balance, this disappearance equation can be reformulated into another one describing drug appearance in the acceptor compartment as a function of time:

$$\frac{C_A(t)}{C_D(0)} = \frac{V_D}{V_A + V_D}\left(1 - \exp\left[-\frac{APt}{V_D V_A}(V_D + V_A)\right]\right)$$

Since in the simplest model, membrane retention is neglected, apparent permeability (referred to as such given the fact that there are assumptions made on its calculation) is thus given by either disappearance or appearance kinetics equations:

$$P_{app} = -\frac{1}{At(V_D + V_A)} V_D V_A \, ln\left[-\frac{V_D}{V_A} + \left(\frac{V_A + V_D}{V_A}\right)\frac{C_D(t)}{C_D(0)}\right]$$

$$P_{app} = -\frac{1}{At(V_D + V_A)} V_D V_A ln\left[1 - \left(\frac{V_A + V_D}{V_D}\right)\frac{C_A(t)}{C_D(0)}\right]$$

Main variations implemented up to date in PAMPA models with the aim of better evaluating the BBB permeability properties are here compiled and related to underlying physiological assumptions, as outlined in Table 2.

Experimental factor	**Underlying physiological assumption**
Lipid artificial membrane	It should resemble the physiological lipid content of the BBB (18% phosphatidylcholine, 23% phosphatidylethanolamine, 14% phophatidylserine, 1:1.8 negative: zwitterionic lipid ratio) and fill all the internal void volume of the filter to prevent “paracellular” aqueous diffusion. Four microliters of a 22 mg lipid /mL solution achieved the best discriminating features.
Organic solvent	Phospholipids must be dissolved in a non-polar solvent to enable the homogeneous coating of the PAMPA filters. A proper choice of this solvent must be made.
Buffer solutions	Only pH 7.4 must be envisaged since brain penetration occurs at the constant physiological pH of the blood. The establishment of the *sink* conditions should be considered on a case-by-case basis.
Incubation temperature	BBB-PAMPA shows linear dependency on the incubation temperature. Physiological incubation temperature results in a higher correlation with the *in vivo* brain to plasma ratio.
Incubation time	The assay should be conducted before the model reaches a state of equilibrium to represent a kinetic *in vitro* model. In comparison to free drugs, incubation times are expected to be increased with nanocarries, given their size in the nanometric range.
Stirring	Ideal *in vitro* BBB models should achieve negligible unstirred water layer in the donor compartment. For this reason and to shorten the incubation time, stirring should be applied (especially when screening lipophilic entities).
Porosity	Apparent porosity should be included in permeability calculation to accurately compare permeability coefficients regardless of filter porosity and lipid volume.
Physical configuration	The physical configuration in which test samples migrate in a gravitational-fashion from the top to the bottom compartment agrees with physical configuration of cell-based *in vitro* models and optimally matches *in vivo* conditions, where the sample in the bloodstream does not need to permeate against gravity.

Table 2.1.2: PAMPA experimental factors related to their underlying physiological assumptions

4.1.1. Lipid membrane

Given that each tissue has a different lipid composition, the lipid artificial membrane content has been modified to simulate distinct biological barriers, including some surrogates for BBB permeability [112].

The major lipid components of BBB are phosphatidylcholine, phosphatidylethanolamine and phosphatidylserine. Among biological membranes, BBB has the higher negative lipid content ratio.

Four different lipids have been assayed in PAMPA models to predict the BBB permeability, ranging from lipids traditionally used to evaluate gastrointestinal absorption (soy lecithin, phosphatidylcholine, dioleylphosphatidylcholine DOPC), to specific brain lipids (porcine polar brain lipid, PBL). The latter achieved the best outcomes probably owing to its cerebral origin, thus with a higher likelihood of mimicking the lipid composition of brain endothelial cells [108, 109]. The PAMPA assay with the porcine polar brain lipid (PBL) showed the best discriminating attributes between CNS+ and CNS- samples [109] and strongly correlated to *in situ* brain perfusion [111]. As a result, it is assumed that the ideal lipid artificial membrane should exhibit the closest composition to the physiological lipid content.

With regard to membrane properties, the above general equations to calculate BBB permeability should be expanded to include nanocarrier distribution into the membrane. The extent of such distribution would depend on relative lipophilicities of the nanocarrier and the membrane.

In this case, expressions stem from the same premises as in the general case, but the mass balance needs to address the fact that at a given time, the sample distributes not only between acceptor and donor compartments but also into a third compartment: the membrane.

$$V_D C_D(0) = V_A C_A(t) + V_D C_D(t) + V_M C_M(t)$$

This mass balance can be greatly simplified if the retention fraction parameter (R), defined as the fraction distributed into the membrane, is taken into account:

$$V_D C_D(0)(1 - R) = V_A C_A(t) + V_D C_D(t)$$

Likewise, t=0 and t=t should be replaced as integration limits by t= t_{lag} and t=t, where t_{lag} represents the time at which membrane is saturated with sample and permeation starts to occur.

Factoring out C_A (t) thanks to the new mass balance, the modified differential equation is solved in terms of C_D (t) with the new integration limits to obtain the following expressions that describe drug disappearance from the donor compartment or drug appearance in the acceptor compartment as a function of time:

$$\frac{C_D(t)}{C_D(0)} = \frac{V_A(1-R)}{V_A + V_D}\left(\frac{V_D}{V_A} + \exp\left[\frac{AP\left(t_{lag} - t\right)}{V_D V_A}\ (V_A\ +\ V_D)\right]\right)$$

$$\frac{C_A(t)}{C_D(0)} = \frac{V_D(1-R)}{V_A+V_D}\left(1-\exp\left[\frac{AP(t_{lag}-t)}{V_D V_A}(V_A+V_D)\right]\right)$$

Since in this model, membrane retention is not neglected, effective permeability (referred to as such given the fact that no assumptions are made on its calculation) is thus given in cm s^{-1} by either disappearance or appearance kinetics equations:

$$P_{eff} = -\left(\frac{1}{A\left(t-t_{lag}\right)(V_D+V_A)}\right)V_D V_A ln\left[-\frac{V_D}{V_A}+\left(\frac{V_A+V_D}{V_A(1-R)}\right)\frac{C_D(t)}{C_D(0)}\right]$$

$$P_{eff} = -\left(\frac{1}{A\left(t-t_{lag}\right)(V_D+V_A)}\right)V_D V_A ln\left[1-\left(\frac{V_A+V_D}{V_D(1-R)}\right)\frac{C_A(t)}{C_D(0)}\right]$$

where A is the filter area (cm^2), V_D and V_A are the volumes in the donor and acceptor phase (cm^3), t is the incubation time, t_{lag} is the time required to saturate the membrane (s), $C_D(t)$ is the sample concentration (mol cm^{-3}) in the donor phase at time t, C_A (t) is the sample concentration (mol cm^{-3}) in the acceptor phase at time t, $C_D(0)$ is the sample concentration (mol cm^{-3}) in the donor phase at time 0 and R is the retention fraction.

As PAMPA assay correlates with the ability of nanocarriers to traverse the modeled membrane barrier, the higher the membrane permeability, the higher the likelihood of reaching the brain.

Tsinman's group unveiled that the volume of lipid solution added onto the PAMPA filter matrix is closely related to the presence of aqueous pores in the artificial membrane [113]: only models with enough lipid to fill all the internal void volume (2,6 µL for 70% porosity PVDF filters [114]) can suitably predict BBB permeability. Thinner artificial membranes would possess water channels through which "paracellular" aqueous diffusion would occur, contrary to the *in vivo* BBB situation. Moreover, the higher the water channel porosity, the greater the extent of "paracellular" diffusion.

On the other hand, the higher the volume of lipid solution, the higher the percentage of sample trapped in the membrane, parameter defined previously as the retention fraction (R) [114].

Among PAMPA-BBB assays conducted, a concentration of 22 mg lipid /mL solvent and a volume of 4 µL (representing a slight excess over the internal volume capacity of the filter) achieved the best separation for CNS+ and CNS- [112], very close values to initial metrics postulated by Kansky [105].

4.1.2. Organic solvent

Most phospholipids are solids that do not homogeneously disperse into PAMPA filters; hence they are dissolved in a non-polar solvent to enable filter coating. Consequently, a proper choice of the solvent must be made [115]. Most researchers focus on hydrocarbon solvents, such as n-dodecane (the most broadly used up to date) [109], hexane [108, 116], n-hexadecane or other viscous alkanes [113].

Bigogno's group studied the BBB-PAMPA in the presence and in the absence of PBL, so as to better understand the role played on the *in vitro* permeability assay by the organic solvent in which phospholipids are dissolved [116]. For compounds with medium permeability, dodecane itself was not able to properly determine permeability values. In those cases, the addition of phospholipids was required to correctly shift CNS- drugs to CNS+. A 1:1 dodecane:hexane solution allowed the greatest differences between permeability values measured with and without phospholipids to be obtained.

Another study conducted on the role of the organic solvent [113] outlined that the presence of hexadecane as solvent lowered the reliability of predictions.

4.1.3. Buffer solutions

Another factor to be taken into account for BBB permeability prediction by means of PAMPA assay is the composition of buffer solutions in donor and acceptor wells. Buffer solutions most broadly used so far include phosphate buffer solution (PBS) [116-118], brain sink buffer (BSB) [113] and universal buffer [112].

When it comes to PAMPA-BBB assay, only neutral pH 7.4 must be considered, due to the fact that brain penetration occurs at the constant physiological pH of the blood and the optimal PAMPA model should reflect as closely as possible the *in vivo* pH conditions [106].

The maintenance of *sink* conditions in the BBB-PAMPA model is controversial. Under the term "*sink* condition", it is to be understood any process that maintains a concentration gradient with low sample levels in the acceptor well so that it serves as the driving force for transport. Traditionally, *sink* conditions have been disregarded in BBB-PAMPA models in comparison with gastrointestinal PAMPA, where the bloodstream represents the acceptor compartment and consequently samples are quickly swept away from the absorption site or highly bound to serum proteins [106]. Nevertheless, in BBB-PAMPA, the acceptor compartment, represented by the CNS interstitial fluid also experiences *in vivo* a drainage into the cerebrospinal fluid (circulating through the ventricles after being produced by choroid plexus) and then into the venous system through the arachnoid granulations [119] which may well maintain low sample levels in the interstitial fluid. Moreover, high affinity values and/or high uptake rate of the nanomedicines into the brain tissue coupled with high diffusivity within the brain tissue may well likewise reduce the sample levels in the fluid of the receiver compartment and ultimately trigger the permeability through the blood-brain barrier. As a result, the establishment of the *sink* conditions in the BBB-PAMPA should be at best made taking all these factors into account on a case-by-case basis.

If *sink* conditions are applicable, the reverse flux due to $C_A(t)$ is nil and therefore should be neglected in the permeability equations. In this case, equations stem from the following premise:

$$\frac{dC_D(t)}{dt} = -\frac{A}{V_D} P_m C_D(t)$$

where $dC_D(t)/dt$ refers to the disappearance rate from the donor compartment in units of mol cm^{-3} s^{-1}, A is the membrane area in units of cm^2, V_D the volume of the donor compartment in units of cm^3, P_m the membrane permeability in units of cm s^{-1} and C_D to the concentration in the donor compartment in units of mol cm^{-3}.

Solving the latter differential equation, the following simplified exponential equation describing drug disappearance from the donor compartment as a function of time is obtained:

$$\frac{C_D(t)}{(1-R)C_D(0)} = exp\left[-\frac{AP_m(t-t_{lag})}{V_D}\right]$$

Under these circumstances, apparent permeability (referred to as such given the fact that there are assumptions made on its calculation) will be given by:

$$P_{app} = -\frac{V_D}{A(t-t_{lag})} ln\left[\frac{C_D(t)}{(1-R)C_D(0)}\right]$$

where A is the filter area (cm^2), V_D is the volume in the donor phase (cm^3), t is the incubation time, t_{lag} is the time required to saturate the membrane (s), $C_D(t)$ is the sample concentration (mol cm^{-3}) in the donor phase at time t, $C_D(0)$ is the sample concentration (mol cm^{-3}) in the donor phase at time 0 and R is the retention fraction.

4.1.4. Incubation temperature

Given the influence of temperature on other physico-chemical parameters, membrane permeability has a temperature dependence to be addressed among factors influencing PAMPA.

Membrane permeability is defined according to Fick's first law as a composite parameter that lumps the drug membrane diffusivity, the drug membrane partition coefficient and the thickness of the membrane:

$$P_m = \frac{D_m K}{h}$$

Since both diffusivity and membrane partition coefficient are temperature-dependent parameters (as described by Stoke-Einstein and van't Hoff equations, respectively), it seems logical to assume temperature dependence of membrane permeability.

Membrane permeability measured with various PAMPA methods proved to be linearly dependent on the incubation temperature [120]. Should the slope of such linear relation be taken as a measure of the temperature effect on permeability, the BBB-PAMPA model showed the lowest effect on temperature raise, which could be attributed to the higher phase transition temperatures of lipid mixtures used in this method unlike mono-component systems (100% phosphatidylcholine), typical of GIT-PAMPA.

Nevertheless, when it comes to *in vitro*/*in vivo* correlations, identical incubation temperatures resulted in a higher correlation between effective permeability measured with BBB-PAMPA and *in vivo* brain to plasma ratio. Hence, the relevance of a proper selection of the incubation temperature is highlighted, since the closer to the bio-relevant incubation conditions in *in vitro* assays, the better the *in vivo* BBB permeability prediction.

4.1.5. Incubation time

In PAMPA assay each well is a one-point-in-time sample. Hence, to meet high-throughput demands and to retain reliability of predictions all at once, some compromises must be implemented.

If a state of equilibrium is reached in the PAMPA assay, then the sample distributes into both compartments and the membrane solely based on effective membrane-buffer partition coefficient. Under these conditions, the PAMPA assay does no longer represent a kinetic *in vitro* model, preventing permeability coefficients from being determined [106]. Nevertheless, if *sink* conditions are maintained in the receiver chamber, the equilibrium would be shifted and consequently a steady-state would never be achieved.

Therefore, the assay should better be conducted before the model reaches a state of equilibrium. In the case of drug substances, this has been translated into periods of time below 20 hours, although such incubation times might be increased in the case of nanocarries, given their size in the nanometric range.

Further reduction of incubation time would shorten the assay time, thereby enhancing the high throughput nature of this *in vitro* screening method. In fact, negligible differences have been observed in permeability coefficients measured with PAMPA-BBB models after 5 hours of incubation [118].

4.1.6. Stirring

Since both sides of the membrane in a PAMPA assay contact with a domain of buffer that is not stirred by convection of the bulk aqueous phase, passive transport across its artificial membrane involves diffusion not only through the lipid membrane but also through the static adjacent layer on each side of the barrier [106, 121]. The artificial membrane represents the rate-limiting barrier for hydrophilic entities; whereas for lipophilic entities, it is the unstirred water layer (UWL) which constitutes the rate-limiting barrier, especially if UWL is thicker than the phospholipid membrane.

Hence, the *in vitro* permeability data must be corrected for the UWL effect that tends to lower effective permeability; otherwise, *in vitro* assays of lipophilic entities would rather indicate water permeability than lipid membrane permeation.

Given that series resistances are additive, to correct *in vitro* permeability data for the UWL effect, the total resistance to passive transport across an unstirred PAMPA model is assumed to be the sum of those of the lipid membrane and the UWL in both

compartments. Furthermore, taking into account that resistance is the inverse of permeability,

$$\frac{1}{P_{eff}} = \frac{1}{P_m} + \frac{1}{P_u}$$

where P_{eff} stands for the measured effective permeability, P_u for the total UWL permeability, and P_m is the permeability of the artificial membrane.

The UWL permeability can be determined experimentally by a method based on the transport across a high-porous lipid-free microfilter [122]. Under these circumstances, the stagnant water layers on both compartments are the only barrier to be overcome by permeants, and the effective permeability would precisely represent the UWL permeability.

The total thickness of the UWL (h), taken as the sum of the UWL thickness from the two sides of the membrane barrier, is often determined from Fick's first law of diffusion,

$$P_u = \frac{D_{aq}}{h}$$

where D_{aq} is the aqueous diffusivity. According to the Stokes-Einstein equation, D_{aq} is expected to depend on the inverse square root of the molecular weight of the solute [113].

In vitro permeability assays at best should match the dimensions of the *in vivo* UWL. However, the *in vivo* UWL tends to be significantly smaller than the *in vitro* UWL. In fact, in brain capillaries the UWL may be neglected, given that the diameter of the capillaries is about 7 μm and that there is an efficient mixing near the surface due to the constant blood flow. Therefore, ideal *in vitro* BBB models should achieve negligible UWL in the donor compartment. Nevertheless, in unstirred PAMPA, the UWL may vary from 2000 to 4000 μm thick [106].

Fortunately, the thickness of the UWL decreases with the extent of stirring of the bulk solution [121]. The total UWL permeability coefficient is composed of the permeability coefficient of the UWL on the donor and acceptor sides, whose values may be equal or unequal depending on the symmetry of hydrodynamics in the donor and receiver chambers:

$$\frac{1}{P_u} = \frac{1}{P_u^D} + \frac{1}{P_u^A} = \frac{P_u^D + P_u^A}{P_u^D P_u^A}$$

where P_u stands for the total UWL permeability, P_u^D and P_u^A for the UWL permeability on the donor and acceptor sides, respectively.

Stirring is usually accomplished either by orbital plate shakers (a vibrating platform device on which the permeation plate is placed) or by magnetic stirring. In both cases, the stirring produces asymmetric hydrodynamics. On the one hand, with orbital shakers, the solution at the top is efficiently stirred, whereas the stirring of the

bottom compartment, entirely filled with buffer and enclosed by the filter, is considerably dampened. On the other hand, with magnetic stirring, the thickness of the UWL decreases to a greater extent in the stirred chamber [121, 123].

To match *in vivo* BBB, the stirring should be applied with the purpose of making negligible the UWL in the donor compartment, which would be translated into a higher UWL permeability on the donor side (P_u^D). Based on the previous equation, if under stirring, P_u^D exceeds P_u^A by more than tenfold ($P_u^D >> P_u^A$), it could be assumed that only the resistance of the acceptor UWL contributes to transport kinetics, and consequently,

$$P_u \approx P_u^A$$

Orbital shakers have been reported to lower the thickness of the stagnant water layer to 300 μm [124], whereas individual-well magnetic stirring has been demonstrated to lower the UWL thickness to the *in vivo* range [121].

On the other hand, if a *sink* state is maintained in the receiver chamber, only the resistance of the unstirred water layer from the donor compartment would contribute to the kinetics of transport, since the *sink* effect would always promote the diffusion in the acceptor chamber to take place.

In addition to matching *in vivo* UWL, stirring also shortens greatly the incubation time of lipophilic entities, since their rate-limiting barrier is circumvented. In fact, stirred PAMPA models are reported to be incubated for 1 hour in the case of lipophilic entities, meeting to a greater extent the desirable high throughput demands. Conversely, stirring had better not be applied to hydrophilic entities, because it might well increase the aqueous channel porosity of the artificial lipid membrane, allowing thereby to some extent “paracellular” diffusion, absent *in vivo* in BBB. As a result, incubation time up to 15 hours has been described for hydrophilic samples [121].

Nevertheless, permeability results gained so far with stirred BBB-PAMPA models to diminish the UWL effect (referred to as BBB-PAMPA-UWL) have revealed some discrepancies with the *in vivo* ability of the samples to traverse the BBB [109].

4.1.7. Porosity

With the purpose of assuring that permeability values from PAMPA assays are comparable regardless of the filter porosity, the filter area should be multiplied by the filter porosity (ε) in the calculation of effective permeability [124].

Moreover, Nielsen and Avdeef incorporated the concept of apparent filter porosity (ε_a) [114]: if lipid volume fills all filter pores and still remains some leftover lipid covering the filter surface on both sides, the total thickness of the PAMPA membrane is:

$$h_m^{TOT} = 2h_m + h_m^F$$

where h_m is the thickness of the donor or acceptor layer and h_m^F, the layer in the filter pores.

Permeation through the donor/acceptor layer ($P_m^{D/A}$) is greater than the total membrane permeability as described by

$$P_m^D = \left(\frac{h_m^{TOT}}{h_m}\right) P_m$$

Permeation through the filter pores must address the fact that the filter surface is only available for permeation to the extent of the nominal porosity (ε):

$$P_m^F = \left(\frac{h_m^{TOT}}{h_m^F}\right) \varepsilon \, P_m$$

Since series resistances are additive, the apparent permeability is

$$P_{app} = \left(\frac{h_m^{TOT}}{2h_m + \frac{h_m^F}{\varepsilon}}\right) P_m = \varepsilon_a P_m$$

where ε_a stands for the apparent porosity.

Alternatively, the thickness of the donor/acceptor layer can be given by the following expression

$$h_m = \frac{\frac{V_m}{A} - h_m^F \varepsilon}{2}$$

where V_m is the lipid volume (cm^3), A the filter geometrical area (cm^2), h_m^F the filter thickness (cm) and ε the nominal filter porosity.

Factoring out h_m from the definition of apparent porosity produces an equation directly related to measurable parameters:

$$\varepsilon_a = \frac{\frac{V_m}{A} + h_m^F(1-\varepsilon)}{\frac{V_m}{A} + h_m^F(\frac{1}{\varepsilon} - \varepsilon)}$$

wich allows predicting that increasing the lipid volume (V_m) makes the apparent porosity tend to unity. As a result, if lipid volume added on the filter exceeds the volume of the pores, the leftover lipid layer on both sides of the lipophilic filter increases the apparent porosity.

In UWL rate-limited transport, the more the lipid excess, the lower the resistance of the artificial membrane to the passage and the higher the permeability coefficient.

In membrane rate-limited transport, in addition to raising apparent porosity (thereby increasing permeability), increasing lipid volume leads to enhanced resistance owing to the lipid itself, hence contributing simultaneously to lowering permeability coefficients.

For the mentioned reasons, apparent porosity should be included in permeability calculation. Thanks to apparent porosity, PAMPA results can be accurately compared regardless of not only filter porosity but also lipid volume.

4.1.8. Model configuration

Two physical configuration of the PAMPA permeation cell have been described by PAMPA practitioners.

Kansy defined a PAMPA model consisting of a donor compartment placed on top of the "sandwich" assembly [105], whereas the acceptor compartment was placed at the bottom of the microtitre plate. Such physical configuration agrees with physical configuration of cell-based *in vitro* models, where test samples are supposed to migrate in a gravitational-fashion from the top compartment to the bottom compartment through the cell monolayer. In this model configuration, stirring by means of orbital shakers enables the UWL effect in the donor chamber to be reduced for better *in vivo* emulation.

Conversely, Avdeef implemented a PAMPA model in which the top compartment represented the acceptor well whereas the test sample was deposited into the bottom chamber [106]. This disposition does not rely on gravity to trigger sample permeation. Stirring to lower the UWL thickness of the donor compartment could be applied in this case by magnetic stirring.

Presumably, the effective permeability coefficients measured from the flux will contain contributions from the physical configuration of the model assembly. Nevertheless, when it comes to evaluating permeability of nanocarriers, the former assembly seems to be optimal, given the fact that *in vivo*, nanosystems are dynamically distributed by the bloodstream, a situation that does not match with a static compartment where diffusion through the artificial membrane and through the unstirred water layer must be overcome against gravity.

4.1.9. Concluding remarks on the PAMPA assay

Unfortunately, the simplistic PAMPA assay will never exactly mimic the complex brain endothelial membranes due to the presence of an organic solvent and the lack of a bilayer-structure in the artificial membrane [112].

The inability to generate a full description of transport mechanisms governing BBB permeability accounts for another of the major shortcomings of PAMPA method, since as a physicochemical barrier devoid of influx/efflux transporters and metabolizing enzymes, at most it can only adequately predict transcellular passive diffusion [125]. Samples undergoing active efflux or metabolic processes will exhibit overestimated PAMPA permeability values, whereas those affected by uptake phenomena or paracellular passive diffusion will be underestimated.

With regard to the evaluation of BBB permeability of nanomedicines, PAMPA could serve to evaluate the extent of contribution of transcellular passive diffusion to the global *in vivo* permeation rate and to determine the role played by different

excipients on passive diffusion. Nonetheless, the lack of transport mechanisms would limit the application of PAMPA for *in vitro* studies aimed at testing different targeting strategies as BBB permeation enhancers of nanomedicines, such as the comparison of active targeting moieties, the determination of the optimal ligand density or the synergic effect of a dual targeting strategy.

To the best of our knowledge, only Giralt's group has already conducted studies on the prediction of BBB permeation of nanomedicines using the PAMPA technique: firstly, this assay served to evidence the permeability enhancement of GABA, nipecotic acid and aminolevulinic acid when linked to peptide moieties [126], and later, to rule out the contribution of passive diffusion to the global permeation rate of transferrin-targeted gold nanoparticles [127]. However, the PAMPA assay has found so far greater acceptance for gastrointestinal tract passive transport prediction, since a broader spectrum of nanomedicines has already been tested, such as polymeric micelles [128], polymeric nanoparticles [129, 130], liposomes [131, 132], solid lipid nanoparticles [133] and solid self-nanoemulsifying drug delivery systems [134, 135]. Overall, results pointed out that inclusion in nanocarriers may significantly alter the passive diffusion pattern of the free drug. These first-in-a-new-class results are likely to promote more research in the field of CNS drug discovery in the near future, given the recent advantages in nanomedicine, which seem to call for high throughput screening methods.

4.2. Phospholipid vesicle-based permeation assay (PVPA)

To palliate some of the PAMPA limitations, another *in vitro* non-cell based method for evaluation of passive permeability has recently been outlined: phospholipid vesicle-based permeation assay (PVPA) [136]. Therefore, it could also be used for prediction of brain delivery for new drug delivery systems in early drug development.

This model uses for transport studies a permeation barrier made of a tight layer of phospholipid vesicles. To this end, a liposomal suspension is added on filter supports and liposomes are fused following evaporation of the solvent, so that a phospholipid bilayer within the filter pores is ultimately obtained.

Importantly, unlike PAMPA, in PVPA no organic solvents are used since it only consists of phospholipids, which mimics more accurately the *in vivo* situation consisting of hydrated phospholipid bilayers. Moreover, PVPA studies performed so far have thoroughly assessed the barrier integrity, thereby ensuring that alterations in barrier structure do not account for the experimental permeability coefficients [137].

However, as also happens with PAMPA, this model has only proven useful for the prediction of transcellular passive diffusion.

5. In vitro cell-based models

To overcome limitations of *in vitro* non-cell based models, cell-based models are often integrated as screening tools to give a more comprehensive insight into the mechanisms involved in the passage through the BBB [138-140].

Emerged in the 1980s, cell-based models to screen BBB permeability represent a more physiologically relevant tool over PAMPA to obtain mechanistic information since they account for both transcellular passive diffusion and active transport devoid of additional physiological factors that exist *in vivo* [141, 142]. Likewise, these models can evaluate to some extent the role played by metabolism. Nevertheless, under the non-physiological culture conditions, cell-based models do not necessarily show the same relevant cell biological transporters as *in vivo*, which calls for previous validation with *in vivo* data to guarantee the potential of cell-based models for BBB permeability screening tools [143].

Like PAMPA, cell-based models are carried out in multi-well plates provided with a donor compartment simulating the blood and an acceptor compartment representing the CNS. Both compartments contain physiological buffer. Nevertheless, instead of a lipid artificial membrane, the permeability process is governed in this case by a cell monolayer seeded onto a porous filter support that separates both compartments [141]. Therefore, the ability of the cells to grow in a confluent monolayer with analogous features to the BBB *in vivo* on some semipermeable support is a prerequisite for it to be a suitable permeation model. Since all BBB features absent in non-neuronal capillaries act as BBB markers, these can serve to evaluate endothelial properties of each *in vitro* cell model.

Similarly, the cell-based permeability assays evaluate the extent to which the sample (drug substances or nanomedicines) permeate from the apical to the basolateral chamber after a given incubation time. To this end, sample levels in both compartments after the incubation time has elapsed are quantified to determine the permeability across the cell monolayer. The equations to calculate permeability coefficients depend on the model design and can be extrapolated from equations described for different PAMPA designs by bearing in mind that retention fraction accounts now for the drug fraction distributed into the cell monolayer [107]. Variations on this basic design involve the type of filter used, the presence of matrix, the mechanisms for agitation and the configuration of the diffusion cell [123].

As cell-based models correlates with the ability of drug delivery systems to traverse the BBB, the higher the permeability coefficient, the more likely the brain uptake *in vivo*.

Main criteria to be considered for an appropriate design of a cell-based model to be predictive of BBB permeability are here reviewed and related to physiological conditions in Figure 2 and in Table 3, following the pattern above mentioned in the case of PAMPA.

5. 1. Cell type

Similarly to what happened with the nature of the artificial lipid membranes in PAMPA, cell-based BBB models differ from each other in the origin, the expression level of transporters, the tightness of the monolayer and the affiliation with a primary or immortalized cell line. All these variables affect the reliability of predictions and make each model generate a specific piece of information on BBB permeability [125].

Experimental factor	Underlying physiological assumption
Cell type	Cell-based BBB models must exhibit restricted paracellular diffusion with TEER values in the order of hundreds of Ωcm^2 and permeability coefficients for paracellular tracers in the order of 10^{-6} cms^{-1}. Primary brain capillary endothelial cultures provide the closest phenotypic resemblance to the *in vivo* BBB, although cell lines provide a stable and homogenous source throughout numerous passages. A minimal seeding density (4×10^5 cells/cm^2) is needed.
Extracellular matrix	A coating with rat tail type I collagen (alone or in combination with type IV collagen) and fibronectin is frequently added to the filter surface to tighten monolayers by mimicking the basal lamina, which *in vivo* contributes to the development of a functional BBB.
Culture medium	Culture medium must mimic the physiological environment of the cell monolayer to prevent dedifferentiation. Therefore, BBB permeability assays must be performed only at neutral pH 7.4. To enhance the barrier properties, glial-secreted soluble factors or serum-free media can be used. To prevent hydrostatic pressure gradients, equal fluid volumes must be used in both chambers.
Incubation temperature	To reliably predict the *in vivo* BBB permeability, assays must be performed at physiological temperature (37ºC). Alternatively, low temperatures can be used to separate the contributions of active and passive transport since they inhibit transport pathways involving energy consumption.
Incubation time	To properly represent a kinetic *in vitro* assay, cell-based models must exhibit an incubation time that do not allow a steady state to be reached. Moreover, cell-based models are often used as multitimepoint assays, by replacing the acceptor medium with fresh medium, namely physically-maintained *sink* conditions, to better outline the kinetic permeability profile.
Stirring	Both compartments in cell-based BBB models are exposed to a stagnant aqueous layer that could act as the rate-limiting barrier. In these cases, effective permeability data must be corrected for the UWL effect. Since UWL in brain capillaries may be neglected, stirring is often applied to *in vitro* cell-based BBB models.
Filter support	Filter composition should not allow non-specific adsorption. Moreover, the pore size must be chosen to allow for free passage of the nanomedicines across the cell-free filters but must still support the cell monolayer to allow confluence to be reached.
Physical configuration	As all elements of the neurovascular unit contribute *in vivo* to the induction and maintenance of BBB phenotype, co-culture systems have been implemented to enhance the BBB properties of monocultures. Likewise, dynamic models have been developed to mimic the *in vivo* shear stress generated by the blood flow on the apical surface of endothelial cells.

Table 2.1.3: Experimental factors of cell-based models related to their underlying physiological assumptions

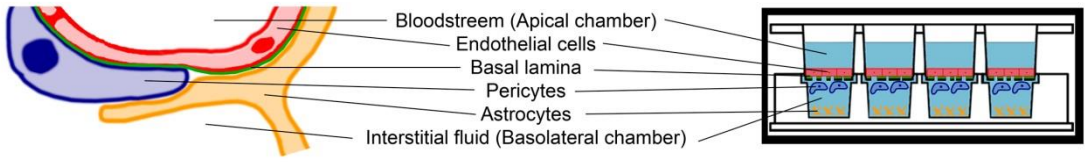

Figure 2.1.2: Scheme of an *in vitro* cell based method for prediction of the BBB permeability: parallelism with the blood-brain barrier *in vivo*

5.1.1. Monolayer integrity

Cell-based BBB models must exhibit paracellular diffusion restricted by tight junctions to mimic this key BBB feature. To this end, the monolayer integrity must be assessed by measuring the transendothelial electrical resistance (TEER) –which indicates the tightness of cell junctions- or the permeability coefficient of hydrophilic paracellular tracers (such as dextran, mannitol or sodium fluorescein) –which evidences the restriction of the paracellular pathway- and by evidencing the tight junction expression level by microscopy techniques [144]. The ideal cellular model should provide values for these parameters as close as possible to the *in vivo* situation. Therefore, for a cell-based BBB model to be considered appropriate for BBB permeability screening, the cell monolayer should display *in vitro* TEER values in the order of hundreds of Ωcm^2 and permeability coefficients for paracellular tracers in the order of 10^{-6} cms^{-1} [47]. Monolayer integrity must likewise be assessed at the end of the assay to confirm that the sample did not alter the barrier properties.

5.1.2. Passage

In spite of the fact that BBB research emerged with isolated brain capillaries [145], these models proved not to be suitable for permeability assays: unlike the *in vivo* situation, in isolated brain capillaries, samples encounter the endothelial cells from the basolateral side, given the strict technical impracticability to access to the luminal surface from the culture medium [146]. Such a major impairment boosted the development of alternative approaches based on *in vitro* cell culture models [147, 148]. Cell models arose when cells mimicking the BBB could be maintained *in vitro* under appropriate culture conditions.

Cells must be subcultured over certain time intervals. This process involves dissociation of cells from each other and from their growth substrate and transfer to a new culture plate. The importance of the passage number depends on the cell type under study, especially primary cells or cell lines [123, 141], as outlined in Table 4.

Primary or low passage brain capillary endothelial cultures provide the closest phenotypic resemblance to the *in vivo* BBB permeability. Notwithstanding, reproducibility is not guaranteed since the number of identical cells per brain is limited, which leads to high batch-to-batch variability and ethical constraints. Furthermore, primary cells tend to dedifferentiate when subcultured, thereby losing features associated with the BBB *in vivo* (including barrier tightness and expression levels of specific transporters); hence, they cannot be stored for an extended period of time. Taken together, these facts prevent the generalized use of primary cells as BBB permeability models [146].

To circumvent the drawbacks related to handling of primary cultures, immortalized endothelial cell lines were developed by either gene or virus transfection. Cell lines are less labor intensive since they are commercially available, thereby exhibiting negligible batch-to-batch variability. Moreover, cell lines provide a stable source with high yield and homogeneity throughout numerous passages. Nevertheless, immortalized brain endothelial cells form incomplete tight junctions [149], which lead to

the formation of leakier monolayers than the primary cultures. As a result, monocultures of immortalized cells are of limited interest to predict BBB permeability [47].

<table>
<tr><th colspan="2">Primary cultures</th></tr>
<tr><th>Advantages</th><th>Disadvantages</th></tr>
<tr><td>Primary cultures represent the closest phenotypic resemblance to the in vivo BBB.</td><td>The isolation of primary brain endothelial cells is time-consuming and needs expertise, since it requires enzymatic digestion steps combined with separation of the microvessels and removal of non-endothelial cells [150].</td></tr>
<tr><td>Primary cultures are the first choice for permeability studies, since cell lines exhibit leakier barrier properties. Primary porcine brain endothelial cells show the tightest paracellular barrier.</td><td>Human primary cultures would be the ideal model to screen human therapies. However, the availability of reliable sources of healthy human brain tissue for the isolation of cells is restricted. Consequently, human brain tissue often originates from autopsy or surgery, whose cell yield is low and suitability for physiological prediction is controversial.</td></tr>
<tr><td>The models based on bovine or porcine endothelial cells are robust and show high yield in terms of amount of cerebral endothelial cells from each animal brain.</td><td>The culture of primary cells gives raise to great batch-to-batch differences. This lack of reproducibility truly impedes the high throughput screening with primary cultures.</td></tr>
<tr><td rowspan="2">The models based on rodent endothelial cells allow syngeneic co-cultures to be easily prepared and in vitro- in vivo correlations to be established with data from pharmacokinetic studies on rodents.</td><td>The cerebral endothelial monolayers tend to lose their barrier phenotype with long-term cultivation or repeated passages.</td></tr>
<tr><td>The primary cultures require the sacrifice of multiple animals, which gives raise to ethical and economic constraints and makes them inconvenient for industrial use</td></tr>
<tr><th colspan="2">Cell lines</th></tr>
<tr><th>Advantages</th><th>Disadvantages</th></tr>
<tr><td>Cell lines represent a stable source with high yield and minimal inter-batches variability.</td><td rowspan="2">The transfection process itself, in addition to removal from the native environment, can account for the non-maintenance of the physiological expression pattern of tight junctions, enzymes and transporters.</td></tr>
<tr><td>Transfection enables immortalized cell lines to keep their features unaltered throughout numerous passages.</td></tr>
<tr><td>Cell lines are less labour-intensive and costly and easier to culture than primary cultures.</td><td rowspan="2">As a result, the barrier properties of cell lines are weaker than those of monolayer of primary cultures, which truly limits their usefulness for permeability screening.</td></tr>
<tr><td>Cell lines are commercially available from trusted sources.</td></tr>
</table>

Table 2.1.4: Comparison of advantages and disadvantages of primary cultures and cell lines to mimic the blood brain barrier *in vitro*

5.1.3 Cell origin

According to cell origin, two tiers of *in vitro* cell-based BBB models have been used: on the one hand, cells of non-cerebral-nor endothelial sources and, on the other hand, cells of cerebral origin from different species of mammals, as outlined in Table 5.

				Monoculture	Coculture											
					Astrocytes							Pericytes			Neurons	
					M	R				P	H	R	P	H	R	H
					PC	PC	CL			PC	PC	PC	PC	PC	PC	PC
							C6	CTX-TNA2	C8-D1A							
BEC	M	PC		[151-155]	[156-158]	[159]										
		CL	b.End3	[154, 160, 161]		[161]	[162]		[163]							
			b.End5	[151, 154, 164, 165]												
			MBEC4	[154, 166]												
			cEnd	[167]												
	R	PC		[150, 168-170]		[150, 168, 171-187]	[178]					[168, 172, 175, 179]			[176, 187]	
		CL	RBE4	[149, 188, 189]		[189]										
			RBE4.B			[190, 191]									[190-192]	
			TR-BBB	[149, 193]		[194]										
	B	PC		[21, 164, 195-206]		[178, 186, 207-219]	[178, 202, 204, 214, 220-223]									
		CL	t-BBEC-117	[224]												
			TBMEC P11	[225]												
	P	PC		[226-231]		[232-234]	[162, 232, 235]	[233]		[236-238]			[238, 239]			
		CL	PBMEC/C1-2	[240, 241]			[242, 243]									

				Monoculture	Coculture											
					Astrocytes							Pericytes			Neurons	
					M	R				P	H	R	P	H	R	H
					PC	PC	CL			PC	PC	PC	PC	PC	PC	PC
							C6	CTX-TNA2	C8-D1A							
BEC	H	PC		[195, 244-246]		[178]	[178]				[178, 186, 245, 247-252]			[247]		[247]
		CL	hCMEC/D3	[165, 246, 253-260]							[261, 262]			[262]		
			BB19	[257, 263]												
			NKIM-6	[264]												
			TY08	[265]												
			HBMEC/ciβ	[266]												
			hBMEC	[257]												
			TY10	[257]												
			SV-HCEC	[267]												

Table 2.1.5: Developed cell-based models of the blood brain barrier. BEC: brain endothelial cells; M: mouse; R: rat; B: bovine; P: porcine; H: human; PC: primary culture; CL: cell line. Triple cocultures: [168, 172, 175, 176, 179, 187, 190, 191, 238, 262] . Quaternary coculture : [247]. Dynamic models: [178, 183-185, 222, 223, 242, 248, 249, 255]. Microfluidic models: [163, 188, 259].

Despite the TEER values close to those of *in vivo* BBB phenotype achieved with some of the non-cerebral models [268], their use as BBB permeability predictors may be comprised compared to cell-based models of cerebral origin, given their distinct morphology, membrane composition (particularly ratios of phospholipid to cholesterol, unsaturated to saturated acyl chains, and phosphatidylcholine to sphingomyelin) and expression pattern of transporters with regard to cerebral endothelia [111, 213, 250, 269].

Alternatively, modified epithelial cell lines of non-cerebral origin have been developed to screen substrates or inhibitors of efflux pumps at the BBB [268, 270]. This screening reaches a further dimension in the case of nanomedicines, since it would evidence if the inclusion of an efflux-pump substrate into the nanocarrier serves to mask the transporter-binding properties of the drug or even to enhance brain delivery thanks to the pump blockage properties of the nanocarrier itself [82]. The main examples include the Madin-Darby canine kidney cell line transfected with the human MDR1 gene that encodes the polarized expression of the P-glycoprotein P (P-gp) -MDR1-MDCK- [271, 272]; the human epithelial colorectal adenocarcinoma cell line Caco-2, with polarized overexpression of P-gp; its vinblastine-treated cell line variant (VB-Caco-2) expressing higher levels of P-gp than native cells [273]; and the human urinary bladder carcinoma cell line -ECV304-.

Since the cell boundary is polarized, the permeability of the drug delivery system across these cell lines must be measured in both directions: apical-to-basolateral (A-B) and basolateral-to-apical (B-A). B-A/A-B permeability ratios above 2 are indicative of P-gp-mediated efflux phenomena.

Therefore, under these circumstances, two different permeability coefficients must be considered: one associated with the apical-to-basolateral transport ($P^{A\rightarrow B}$) and another one linked to the basolateral-to-apical transport ($P^{B\rightarrow A}$). As a result, the two flux expressions to be equated in this case must include both permeability coefficients:

$$J\ (t) = \ P_{eff}^{A\rightarrow B}\ C_A(t) - P_{eff}^{B\rightarrow A} C_B\ (t)$$

where J refers to the flux, in units of mol cm^{-2} s^{-1}, $P^{A\rightarrow B}$ to the apical-to-basolateral permeability in units of cm s^{-1}, $P^{B\rightarrow A}$ to the basolateral-to-apical permeability in units of cm s^{-1} and C_A and C_B are concentrations in the basolateral and apical compartments, respectively, in units of mol cm^{-3},

and

$$J\ (t) = \ -\frac{V_A}{A}\frac{dC_A(t)}{dt}$$

where J is the flux, in units of mol cm^{-2} s^{-1}, V_A the volume of the apical compartment in units of cm^3, A the filter area in units of cm^2 and $dC_A(t)/dt$ the disappearance rate from the apical compartment in units of mol cm^{-3} s^{-1}.

The differential equation obtained in this case when both expressions are equated is:

$$\frac{dC_A(t)}{dt} = -\frac{A}{V_A}\left(P_{eff}^{A\to B}\, C_A(t) - P_{eff}^{B\to A} C_A(t)\right)$$

In this case, the mass balance needs to address the sample fraction distributed into the cell monolayer:

$$V_A C_A(0) = V_B C_B(t) + V_A C_A(t) + V_C C_{\ C}(t)$$

which can be greatly simplified to:

$$V_A C_A(0)(1-R) = V_B C_B(t) + V_A C_A(t)$$

where C_A (0) is the sample concentration placed into the apical compartment at the beginning of the assay, C_A (t), C_B (t), C_C (t) the sample concentration after the incubation time has elapsed in the apical, basolateral and cell monolayer compartment, respectively; V_A, V_B, V_C the volume of media in the apical, basolateral and cell monolayer compartment, respectively; and R the retention fraction to the cell monolayer.

Under the given circumstances, mass balance serves to replace C_B (t) with apical-based terms, obtaining thereby another differential equation:

$$\frac{dC_A(t)}{dt} + \left(A\left[\frac{P_{eff}^{A\to B}}{V_A} + \frac{P_{eff}^{B\to A}}{V_B}\right]\right) C_A(t) - \frac{AP_{eff}^{B\to A}}{V_A}\, C_A(0)(1-R) = 0$$

The latter differential equation is solved in terms of C_A (t) to obtain the following exponential equation that describes the drug disappearance from the apical compartment as a function of time:

$$\frac{C_A(t)}{C_A(0)} = \frac{(1-R)}{V_B\left(\frac{P_{eff}^{A\to B}}{V_A} + \frac{P_{eff}^{B\to A}}{V_B}\right)}\left(P_{eff}^{B\to A} + \frac{V_B P_{eff}^{A\to B}}{V_A}\, exp\left[A\left(\frac{P_{eff}^{A\to B}}{V_A} + \frac{P_{eff}^{B\to A}}{V_B}\right)\left(t_{lag} - t\right)\right]\right)$$

where A is the filter area multiplied by the nominal porosity (cm^2), V_A and V_B are the volumes in the apical and basolateral compartment (cm^3), t (s) is the incubation time, t_{lag} (s) represents the time at which the cell monolayer is saturated with sample and permeation starts to occur, R is the retention fraction to the cell monolayer, $P^{A\to B}$ and $P^{B\to A}$ are the permeability coefficients (apical-to-basolateral and basolateral-to-apical, respectively), C_A(t) is the sample concentration (mol cm^{-3}) in the apical compartment at time t, and C_A(0) is the sample concentration (mol cm^{-3}) in the apical compartment at time 0.

In this model, basolateral-to-apical effective permeability (referred to as such given the fact that no assumptions are made on its calculation) is given in cm s^{-1} by the following equation:

$$P_{eff}^{B\to A} = \frac{r_a V_A}{A\,(1-r_a)\left(t_{lag} - t\right)}\, ln\left[-r_a + \frac{(1+r_a)\, C_A(t)}{(1-R) C_A(0)}\right]$$

where r_a represents the asymmetry ratio, defined as follows:

$$r_a = \frac{V_A}{V_B} \frac{P_{eff}^{B \to A}}{P_{eff}^{A \to B}}$$

Under these circumstances, an assay in the presence of selective inhibitors of the efflux pumps should be previously conducted in order to determine the apical-to-basolateral permeability coefficient by using the equations reported in the PAMPA section.

Furthermore, the possibility of developing cell-based BBB models from human pluripotent stem cells has been postulated recently. To this end, stem cells should be submitted to a differentiation process to obtain endothelial cells [274-277]. Likewise, all other cellular elements of the neurovascular unit could be obtained with appropriate differentiation processes [247]. This approach would solve the ethical concerns related to restricted accessibility to human cerebral sources.

5.1.4. Other cell features

The physical dimensions of the cells making up the monolayer dictate the efficacy of paracellular restriction since junctional density is greater in cells that are narrow or of small diameter than in cells that are wide or spread out on the substrate. Furthermore, the height of the monolayer impacts the path length to be traversed by the nanocarrier and thereby the extent of monolayer retention [123]. Overall, a relatively high minimal seeding density (4×10^5 cells/cm^2) is needed [157].

Likewise, time in culture influences the barrier properties of the cell monolayer, since it determines the extent of both tight junction formation and cell differentiation. With regard to the growth culture curve, the resistance of the monolayer increases with time during the log phase as tight junctions form; reaches a plateau when confluence is achieved and finally decreases during senescence. Optimally, a confluent monolayer must be accomplished to achieve the highest resistance that best mimics the *in vivo* conditions [141].

5.2. Filter support

The filter is solely aimed at serving as mechanical support for the cell monolayer. Nevertheless, as it also happened with PAMPA, when evaluating the permeation of nanocarriers, if parameters as filter composition, porosity and pore size are not properly addressed, the filter support would additionally hamper nanocarrier diffusion.

5.2.1 Filter composition

Filter composition should not allow non-specific adsorption of the drug delivery system to occur. Otherwise, the calculated permeability coefficient would not reflect the proper BBB permeability. The Transwell® filters most frequently used are made of polycarbonate or polyethylene terephthalate. The former shows low non-specific binding properties, while the latter favors the formation of significant tighter monolayers [158].

5.2.2 Pore size and porosity

Overall, the greater the pore size and porosity, the less the hindrance caused by the filter to the passage of nanocarriers. Therefore, the pore size must be chosen to allow for free passage of the nanoparticles across the cell-free filters. Additionally, the greater the nanocarrier size, the higher the likelihood of reaching the pore size. As a result, the filter limits the aptness of a given cell-based model to evaluate the BBB permeability of nanosized carriers below its pore size. Notwithstanding, the pore size should not be enlarged above 1-3 μm to palliate the hindrance, since they must still support the cell monolayer in order to allow confluence to be reached. Otherwise cells could migrate through the pores towards the basolateral domain.

The contribution of all these parameters can be evaluated by conducting the permeability assay in the absence of the cell monolayer. If nanocarrier permeability is truly restricted under these circumstances, equations to calculate effective permeability should include the contribution of the filter support to the overall resistance:

$$\frac{1}{P_{eff}} = \frac{1}{P_M} + \frac{1}{P_F}$$

where P_{eff} stands for the measured effective permeability, P_M for the permeability of the cell monolayer and P_F for the permeability coefficient of the filter, calculated as

$$P_F = \frac{\varepsilon_F D}{h_F}$$

where ε_F stands for the filter porosity, D for the aqueous diffusion coefficient in cm^2/s and h_F for the thickness of the filter in cm.

5.3. Extracellular matrix

A strategy to enhance differentiation of immortalized cell lines into tighter monolayers consists in coating the filter with a substrate able to mimic the basal lamina, which *in vivo* contributes to the development of a functional BBB. Given that type IV collagen, fibronectin and laminin are the major components of the basal lamina *in vivo*, rat tail type I collagen (alone or in combination with type IV collagen) and fibronectin are frequently added to the filter surface [278]. Alternatively, gelatin coating has also been described [279-281], even though its use does not actually rely on any physiological assumption concerning the BBB environment.

It is noteworthy that if the matrix is of significant thickness (collagen mats of thickness up to 0,4 μm have been reported [123]), permeability coefficients might be altered. In those cases, the role of the filter coating should be addressed in the equations to be used by taking into account that the contribution of the matrix as a series resistance with the monolayer is additive:

$$\frac{1}{P_{eff}} = \frac{1}{P_M} + \frac{1}{P_F} + \frac{1}{P_{Mat}}$$

where P_{eff} stands for the measured effective permeability, P_M for the permeability of the cell monolayer, P_F for the permeability coefficient of the filter and P_{Mat} for the permeability of the matrix.

5.4. Culture media

Culture medium in the donor and acceptor wells must mimic as closely as possible the physiological environment of the cell monolayer to prevent dedifferentiation from occurring. Moreover, it should enable permeability coefficients to be determined.

5.4.1. pH

Besides the fact that cells are not stable over a wide pH range, the optimal cell-based model should reflect the constant physiological pH of the blood at which BBB permeation occurs. As a result, BBB permeability assays must be performed only at neutral pH 7.4.

5.4.2. Supplements

Changes in culture media composition are aimed at enhancing the barrier properties of the cell lines (mainly to upregulate expression levels of tight junctions and specific transporters).

5.4.2.1. *Cell-conditioned media*

In vivo, glial–secreted soluble factors account for the induction of the BBB phenotype on brain endothelial cells; hence astrocyte and/or C6 conditioned medium, obtained from growing astrocyte and C6 glioma cultures, have been used [242, 282]. However, in these cases the influence of cerebral endothelial cells themselves on the release of different factors by astrocytes is overlooked.

5.4.2.2. *Serum-free media*

Differentiation media should be serum-free given that the barrier function of the monolayer is seriously altered in the presence of serum [160]. Additionally, serum removal from the acceptor well better matches the BBB physiology, as the basolateral surface of the brain endothelium is exposed *in vivo* to serum-free interstitial fluid [221].

5.4.2.3. *Others*

The monolayer tightness has also proven to be upregulated by the second messenger cAMP (cyclic adenosine monophosphate) [283] and hydrocortisone [226, 284]. For this reason, culture media are often supplemented with cAMP modulators (such as 8-(4-chlorophenylthio)adenosine 3′,5′-cyclic monophosphate -CPT-cAMP-) and/or phosphodiesterase inhibitors (such as 4-(3-butoxy-4 methoxybenzyl)-2-imidazolidinone -RO-20-1724-[195]) to elevate cAMP levels; with hydrocortisone; and sometimes with puromycin [150], which boosts the response of the monolayer to glucocorticoid treatment. Notwithstanding, it should be checked previously that the use of such stimulants does not trigger other processes than an enhancement of monolayer

tightness, that could ultimately give rise to misleading non-physiological BBB phenotypes [146].

5.4.3. Volume of culture medium

To prevent hydrostatic pressure gradients in either direction from occurring, equal fluid volumes must be used in both chambers. The effect of hydrostatic pressure on permeability increases with the extent of monolayer leakiness [123].

5.5. Incubation temperature

To reliably predict the *in vivo* BBB permeability, assays should be performed at physiological temperature (37ºC).

Alternatively, low temperatures (mostly 4ºC) can be used to elucidate the passage mechanisms of nanocarriers, since temperatures below 18ºC inhibit transport pathways involving energy consumption, separating thereby the contributions of active and passive transport [123].

5.6. Incubation time

As in the case of PAMPA, to properly represent a kinetic *in vitro* assay, cell-based models must exhibit an incubation time that do not allow a steady state to be reached. Otherwise, permeability coefficients could not be calculated since distribution would be solely based on monolayer-culture medium partition coefficient and the physiological permeation condition would be misrepresented.

Moreover, cell-based models are versatile, since they are often used as multitimepoint assays, by replacing the acceptor medium with fresh medium, namely physically-maintained *sink* conditions, to better outline the kinetic permeability profile.

In the case of drug-loaded nanomedicines, most reported BBB permeability assays often comprise multiple timepoints of measurement with maximum incubation time around two to four hours in order to prevent steady state from being reached. Only [281] and [285] extended the assay time to 24 hours. Notwithstanding, the prolongation of the permeability assays may raise issues of the validity of the *in vitro* model.

5.7. Stirring

As also happened in PAMPA, both compartments in cell-based BBB models are exposed to a stagnant aqueous layer that could act as the rate-limiting barrier, the unstirred water layer (UWL). In these cases, effective permeability data of cell-based models must also be corrected for the UWL effect.

The effective permeability under these circumstances is composed of the effective coefficients for all the barriers in series. As series resistances are additive and resistance is the inverse of permeability:

$$\frac{1}{P_{eff}} = \frac{1}{P_M} + \frac{1}{P_u}$$

where P_{eff} stands for the measured effective permeability, P_M for the permeability of the cell monolayer ,and P_u represents the total UWL permeability.

Given that the UWL in brain capillaries may be neglected as mentioned above, stirring is often applied to *in vitro* cell-based BBB models. The contributions to P_u of the permeability coefficients of the UWL on the apical and basolateral domains depend on the symmetry of hydrodynamics generated by the stirring method.

Under these circumstances, the total UWL permeability (P_u) can be determined as a function of hydrodynamic conditions imposed by stirring, since P_u (cm/s) is directly proportional to stirring speed (ν, expressed as rpm) raised to the xth power:

$$P_u = \kappa \nu^x$$

where κ is a constant descriptive of the diffusivity of the sample (to the power 2/3), kinematic viscosity (to the power -1/6), unit conversion and geometric factors of the permeation cell [121].

The linearization of the previous equation results in

$$\frac{1}{P_{eff}} = \frac{1}{P_M} + \frac{1}{\kappa \nu^x}$$

which allows $1/P_M$ and $1/\kappa$ to be determined from a linear plot of $1/P_{eff}$ versus 1/v.

In the Transwell® system utilized for BBB permeability assays, stirring is often accomplished by means of an orbital mixer. Therefore, due to asymmetry in the hydrodynamic conditions, the degree of stirring on the apical compartment is greater than in the basolateral, where stirring is seriously dampened by the confined space nearly filled with buffer solution. In this case, the empirical constant “x” ranges from 0.8 to 1.0 [123].

In the side-by-side diffusion cell-system in which stirring is achieved by bubbling O_2-CO_2, the hydrodynamics are symmetrical and the power x is expected to take values between 0.3 and 0.5 [123].

5.8. Model configuration

A summary of the main model configurations that have been described is represented in Figure 3.

Figure 2.1.3: Main different model configurations described for *in vitro* cell-based screening methods of the blood-brain barrier permeability

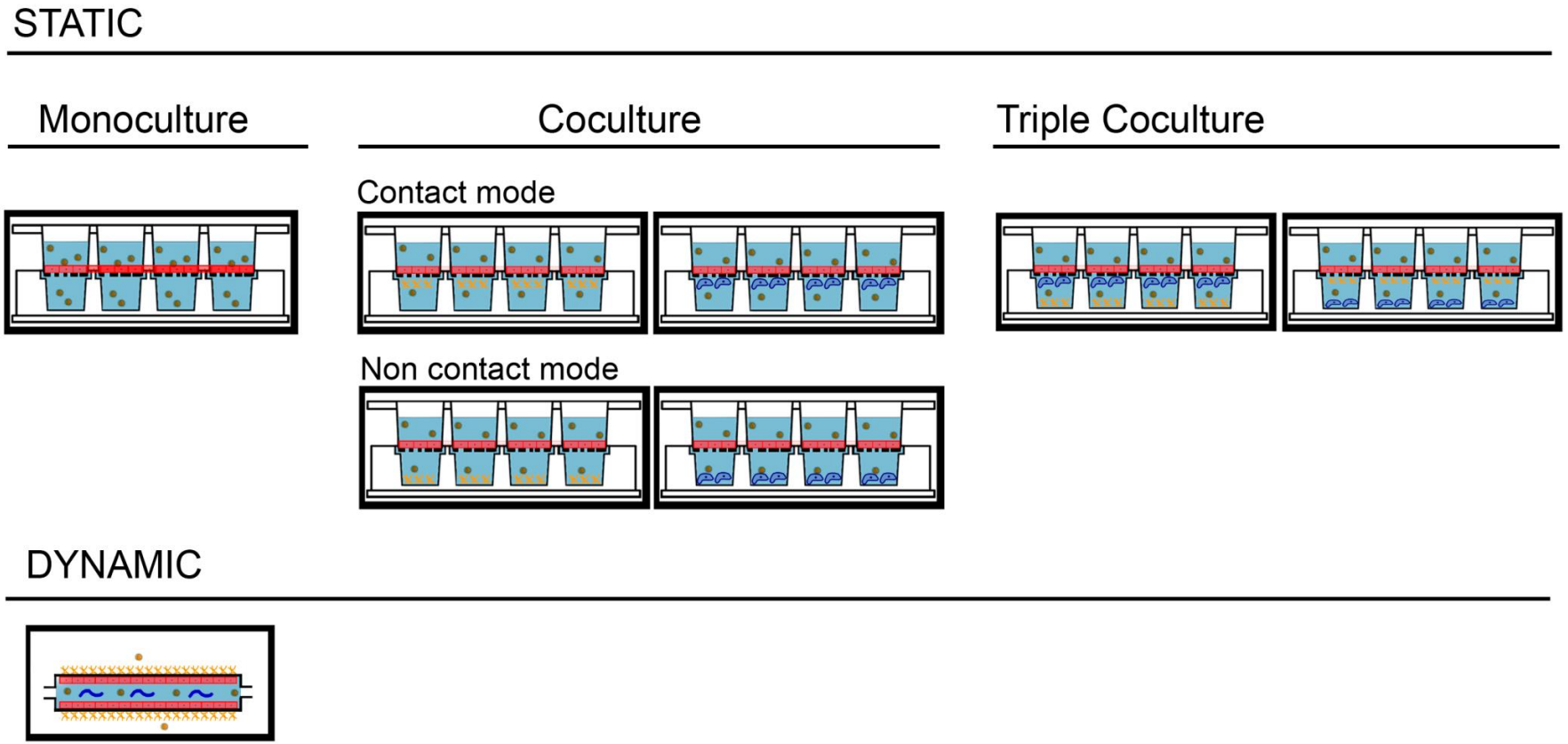

5.8.1. Static models

Most broadly employed cell cultures are based on brain endothelial cells (either primary cultures or cell lines) displayed as a static model on a Transwell® system. Nevertheless, as all elements of the neurovascular unit contribute *in vivo* to the induction and maintenance of BBB phenotype, another strategy pioneered by Dehouck [209] to enhance the BBB properties of monocultures consists of implementing co-culture systems [286, 287], with higher TEER values and lower permeability coefficients of paracellular tracers than the corresponding endothelial monoculture. Several coculture systems and orientation formats have been described.

5.8.1.1 *Coculture systems*

The different combination of cerebral endothelial cells with elements of the neurovascular unit makes coculture systems differ from each other [288-290]. On the one hand, cerebral endothelial cells can be established with either primary cells or cell lines, while glial cells (which can be primary astrocytes, astrocytic cell lines or C6 glioma cell lines), pericytes or even neurons can be included as elements of the neurovascular unit. Additionally, to better mimic the *in vivo* BBB, triple coculture systems with endothelial cells, pericytes and astrocytes have been described [168, 172, 175]. Some models use cells from different species, whereas syngeneic models utilize cells from the same species to prevent interspecific non-recognition problems [181, 286].

5.8.1.2. *Orientation format*

Two main experimental setups for cocultures have been designed: contact or non-contact cocultures [291]. In the former type, endothelial cells are seeded on top of the porous filter, whereas the astrocytes, glial cells or pericytes in each case are cultured at the opposite side of the filter support [208, 291]. In the latter coculture model, astrocytes, glial cells or pericytes are grown on the bottom of the well.

Regarding triple cell coculture methods and taking into account that seeding the endothelial cells on the top of the filter support is a common feature, two further setups are possible since pericytes and astrocytes can be grown on the opposite side of the filter or on the bottom of the well, respectively.

In all these cases, filter thickness and pore size must be thoroughly considered, since astrocytes/pericytes must be restricted to the basolateral side, while allowing soluble secreted factors and astrocytic end-feet to interact with the endothelial cells seeded on the apical side. In this sense, pore sizes of 0.4 µm are preferable to those of 3 µm, which proved unable to retain astrocytes/pericytes in the basolateral chamber. Regarding coculture with astrocytes, better barrier properties were achieved with the non-contact format, since in the contact mode pores were clogged by astrocytic end-feet, which prevented the passage of astrocyte-secreted soluble factors that are responsible for maintenance of BBB phenotype.

5.8.2 Dynamic models

Dynamic models, a further tridimensional configuration of cell-based models, have been developed to better mimic the BBB *in vivo*, as the apical surface of endothelial cells is permanently exposed *in vivo* to a tangential shear stress (5 dyn/cm^2) caused by the blood flow. This shear stress affects the endothelial barrier function by increasing the BBB tightness and the expression of ABC transporters and CYP enzymes [292, 293]. As a result, higher values of TEER have been reported in dynamic models than in the static models previously described [223].

Dynamic models have mostly been built on the basis of the hollow fiber apparatus. In this configuration, brain capillaries are represented by a tube through which the culture medium is pumped at a controllable rate. The tube is placed inside a sealed chamber that mimics the basolateral domain and cerebral endothelial cells are grown intraluminally [178, 222]. In coculture dynamic configuration, glial cells are cocultured extraluminally [255].

Another dynamic model that has been described is based on a transparent plastic chamber with a snapwell insert on which endothelial cells are cultured [249]. More recently, the model has been further improved to mimic venous segments as well [294] by reducing the pressure and adding smooth muscle cells.

Nevertheless, dynamic models do not meet high throughput screening criteria given their specific technical demands. Moreover, a larger number of cells to coat the hollow fibers and longer times to reach constant TEER are required. A comparison between dynamic and static models is delineated in Table 6.

	Transwell ® monoculture	Transwell® coculture	Dynamic model
Transendothelial electric resistance	Low	Moderate	High
Time to steady transendothelial electric resistance	3-4 days	3-4 days	>7 days
Amount of cells required	Low	Moderate	High
Resemblance with the neurovascular unit	Moderate	High	High
Shear stress	No	No	Yes
Suitability for high-throughput screening	High	Moderate	Low

Table 2.1.6: Comparison between cell-based models of the blood brain barrier in terms of high-throughput screening ability and resemblance with the *in vivo* BBB features

5.8.3. Microfluidic models

To downsize the cell-based BBB models and hence reduce the amount of cells required for the assay, microfluidic models have been recently put forward [295, 296]. These models represent a coculture of cells of the neurovascular unit seeded on a porous membrane in contact mode. However, the membrane is housed at the interface of two microchannels of polydimethylsiloxane through which flows the culture medium [163, 188].

5.9. Concluding remarks on cell-based models

The optimal cell-based model to study the BBB permeability of nanocarriers would consist of a human cell line (to palliate interspecies differences) under appropriate culture conditions that allow high TEER and physiological expression levels of functional transporters to be achieved with the purpose of good correlating with *in vivo* results.

Nevertheless, regarding the most sophisticated configurations, with the present degree of development, it is not granted that increasing the model complexity to better replicate the *in vivo* neurovascular unit will be rewarded by substantially higher correlations at the early phases of the drug delivery process.

With regard to the evaluation of BBB permeability of nanomedicines, cell-based models, unlike non-cell based models, could serve to evaluate active transport pathways that contribute to the global *in vivo* permeation rate. Consequently, *in vitro* cell-based models have proven to be useful tools to evaluate the targeting abilities of different moieties attached to the nanocarriers or to determine the optimal ligand density with the purpose of achieving higher CNS drug levels *in vivo*.

Lipid, magnetic and polymeric nanoparticles, liposomes and dendrimers have already been assayed for BBB permeability in an *in vitro* cell-based model, as sketched in Table 7. The main conclusions from the results of the studies presented in Table 7, include the fact that an increase in the size of the nanocarrier yields a decrease in the BBB permeability coefficient [297-305] and that nanoparticle surface plays a key role in BBB permeability (in terms of surface coating [306] and surface charge, with enhanced permeability values for cationic charges [302, 307, 308]). Overall, drug loading onto nanocarriers enhances BBB permeability and this enhancement often follows a time-dependent pattern [309-315].

Moreover, in those cases where active targeting moieties are attached to the surface of the nanocarrier, the permeability enhancement is strongly dependent on the ligand density at the surface interface [305, 316-321]. Furthermore, cell-based models have even been used to establish the efficiency of distinct nanocargos for a given drug, with a focus on the role played by their different excipients [297, 299, 322].

Noteworthy, for the sake of high-throughput screening, static cell-based models were the most broadly used (only one dynamic model has been reported [323]), although additional strategies are often applied to overcome leakiness of Transwell®

monocultures. The tendency towards the use of these models is likely to rise further in the CNS drug discovery field.

Many of these conclusions drawn with BBB cell-based models have been validated with *in vivo* studies, as shown in Table 7. To this end, a plethora of techniques has been used to verify *in vivo* the preliminary results obtained with the cell-based assays, namely scintigraphy [324-326], near-infrared in vivo imaging [327-333], ex vivo optical imaging [301, 334], confocal microscopy [309, 317], chromatographic quantification [307, 312, 315, 335] and pharmacodynamics studies [281, 285, 336]. In all cases, the consistency between the results from *in vitro* and *in vivo* studies was evidenced.

Overall, cell-based models are only suitable for medium throughput screening due to the higher cost than assays with artificial membranes and the elaborate preparation, which is accounted by the fact that primary cultures are labor-intensive *per se* and that no simple cell line is available for BBB prediction since in monoculture they are too leaky.

5.10. Cell-based models and brain pathophysiological conditions

Unlike artificial-membrane-based *in vitro* BBB models, cell-based models are versatile to develop more representative *in vitro* BBB models of brain pathophysiological conditions by modifying the above mentioned experimental factors. These changes (for instance in the filter coating, the composition of culture medium or the coculture configuration) should be implemented to match, for each brain disorder, the *in vivo* properties of the diseased BBB; namely monolayer integrity and the pathophysiological expression pattern of transporters.

As a first attempt to evidence the passage of nanomedicines across the BBB in a pathological microenvironment (mainly for glioma treatment), some *in vitro* studies have implemented changes in the coculture configuration. In these models, the brain endothelial cells are cocultured in a non-contact mode with glioma cell lines at the bottom of the basolateral chamber to resemble the tumor microenvironment that the nanocarrier would face *in vivo*. These studies have proven extremely useful to evidence the synergic effect of a dual targeting strategy to achieve higher CNS drug levels *in vivo* [279-281, 285, 309, 330, 332, 333, 336, 337]. The dual targeting strategy consists in the combination of two different active targeting strategies on the same nanocarrier, one of which is aimed at promoting the passage across the BBB and the other one is aimed at enhancing the preferential localization at the target site. However, these models could be further improved by adapting more experimental factors to better match the diseased BBB in gliomas.

Likewise, many of the in vitro cell-based assays have been validated with pathophysiological *in vivo* models [281, 285, 309, 329-334, 336-339]. In broad terms, qualitative results from both studies are consistent with each other, which demonstrate that cell-based models might be useful as preliminary screening tools to triage promising nanomedicines.

Nanosystem	**Active targeting strategy**	**Load**	**Brain microvascular endothelial cells**	**Strategies to enhance barrier properties**	Ref.
Pluronic® 85/121 polymer conjugate	None	Horseradish peroxidase	Bovine brain endothelial cells	Collagen and fibronectin coating	[324]*#
Peptide conjugates	Small cyclic *N*-methylated peptides	GABA	Bovine brain endothelial cells	Type IV collagen and fibronectin coating Coculture with rat astrocytes cAMP/RO-20-1724	[126]*
		Aminolevulinic acid			
		Nipecotic acid			
Lutensol AP20 micelles	None	Kynurenic acid	Rat brain endothelial cells	Collagen and fibronectin coating Coculture with rat astrocytes Hydrocortisone CPT-cAMP/RO-20-1724	[340]* #
Triton X 100 micelles					
Hydroxypropyl methacrylamide-co-lauryl methacrylate micelles	None	Rhodamine B	Human brain endothelial cells	Fibronectin and type IV collagen coating Serum deprivation Hydrocortisone	[322]*
Pluronic P85 micelles	Insulin	Rhodamine B	Bovine brain endothelial cells	Collagen and fibronectin coating	[341]
Polybutadiene-co-poly (ethylene glycol) micelles	G23 peptide	Fluorescein	hCMEC/D3	Type I collagen coating Hydrocortisone Dexamethasone	[317, 325] #
Poly (ethylene glycol)-G2-polyether-co-polyester dendrimers	None	Rhodamine B	bEnd3	Coculture with U373MG astrocytoma cells	[342]*
Poly (ethylene) imine dendrimers	None	Copper (II)	Human brain endothelial cells	Fibronectin and type IV collagen coating	[343]*
Poly glycerol dendrimers					
Poly (ethylene glycol)-polyamidoamine dendrimers	Rabies virus glycoprotein RVG29	^{125}I and DNA	Mouse brain endothelial cells	Serum deprivation	[327]* #
Poly (ethylene glycol)-G4-polyamidoamine dendrimers	Transferrin and Tamoxifen	Doxorubicin	Murine brain endothelial cells	Gelatin coating	[280]

Nanosystem	**Active targeting strategy**	**Load**	**Brain microvascular endothelial cells**	**Strategies to enhance barrier properties**	Ref.
Poly (ethylene glycol)-G4-polyamidoamine dendrimers	Transferrin and Wheat Germ Agglutinin	Doxorubicin	Murine brain endothelial cells	Gelatin coating	[279]
Poly (ethylene glycol)-polyamidoamine dendrimers	Lactoferrin	^{125}I and DNA	Mouse brain endothelial cells	Serum deprivation	[344]*
Poly (ethylene glycol)-G4-polyamidoamine dendrimers	Angiopep	Doxorubicin	Murine brain endothelial cells	Gelatin coating	[345]
Poly (ethylene glycol)-polyamidoamine dendrimers	Angiopep	^{125}I and DNA	Mouse brain endothelial cells	Serum deprivation	[346]* #
Poly (ethylene glycol)- poly-lysine dendrimers	Leptin-derived peptide	^{125}I and DNA	Mouse brain endothelial cells	Serum deprivation	[328]* #
G3-polyamidoamine dendrimers	Lauryl-chains	Paclitaxel and fluorescein isothiocyanate	Porcine brain endothelial cells	Collagen and fibronectin coating Serum deprivation Hydrocortisone CPT-cAMP/RO-20-1724	[347]*
Quaternary ammonium-β-ciclodextrin nanoparticles	None	Doxorubicin	Bovine brain endothelial cells	Bovine fibronectin coating	[348]*
β-ciclodextrin-poly- aminoester nanoparticles	None	Dichloro-triazinyl-amino-fluorescein	Bovine brain endothelial cells	Fibronectin coating	[349]*
			Huma brain endothelial cells		
Chitosan nanoparticles	None	Dopamine	MDCK	None specified	[319]* #
Chitosan nanoparticles	None	Fluorescein-isothiocyanate dextran 4	MDCK	None specified	[350]*
^{14}C-Radiolabeled polyethylene glycol-co-polyhexadecyl-cyanoacrylate) nanoparticles	None	None	Rat brain endothelial cells	Type IV collagen coating Coculture with rat astrocytes	[306]

Nanosystem	Active targeting strategy	Load	Brain microvascular endothelial cells	Strategies to enhance barrier properties	Ref.
Polybutyl-cyanoacrylate nanoparticles	None	Stavudine	Human brain endothelial cells	Fibronectin and collagen coating	[297]*
Methyl-methacrylate-sulfopropyl-methacrylate nanoparticles		Delavirdine			
		Saquinavir			
Polybutyl-cyanoacrylate nanoparticles	None	Zidovudine	Bovine brain endothelial cells	None specified	[299]*
Methyl-methacrylate-sulfopropy-lmethacrylate nanoparticles		Lamivudine			
Methyl-methacrylate-sulfopropyl-methacrylate nanoparticles	RMP-7 (Cereport®)	Stavudine	Human brain endothelial cells	Coculture with human astrocytes	[298]*
		Delavirdine			
		Saquinavir			
Polybutyl-cyanoacrylate nanoparticles	CRM197	Zidovudine	Human brain endothelial cells	Coculture with human astrocytes	[305]*
Polysorbate 80-coated chitosan nanoparticles	None	Methotrexate	MDCK	None specified	[351]*
Poloxamer 188-coated poly (lactic-co-glycolic) acid-poly (ethylene glycol)-poly (lactic-co-glycolic) acid nanoparticles	None	Loperamide	RBE4	Type IV collagen coating Coculture with C6 cell line	[335] #
Polysorbate 80-coated poly (lactic-co-glycolic) acid-poly (ethylene glycol)-poly (lactic-co-glycolic) acid nanoparticles					
Polysorbate 80-coated poly (lactic-co-glycolic) acid nanoparticles	None	Tissue inhibitor of matrix metalloproteinases	Rat brain endothelial cells	Type IV collagen and fibronectin coating Hydrocortisone Coculture with rat astrocytes	[311] #

Nanosystem	**Active targeting strategy**	**Load**	**Brain microvascular endothelial cells**	**Strategies to enhance barrier properties**	Ref.
Polysorbate 80-coated poly (lactic-co-glycolic) acid nanoparticles	None	Tissue inhibitor of matrix metallo-proteinases	RBE4	Type I collagen coating	[311] #
Poly (ethylene glycol)-coated poly (lactic-co-glycolic) acid nanoparticles	None	Ox-carbazepine	hCMEC/D3	Hydrocortisone	[352]*
		6- Coumarin			
Poly (ethylene glycol)-poly lactic acid nanoparticles	Cationic bovine serum albumin	6- Coumarin	Rat brain endothelial cells	Coculture with rat astrocytes	[307, 308]* #
Poly (ethylene glycol)-co-poly (lactic acid) nanoparticles	Peptide22	Paclitaxel	Mouse brain endothelial cells	None specified	[334] #
Magnetic silica poly (lactic-co-glycolic) acid nanoparticles	Transferrin and external magnetic field	6- Coumarin	bEnd3	Coculture with U87MG human glioblastoma cells	[337] #
Poly (ethylene glycol)-co-poly-ε-caprolactone nanoparticles	Angiopep	Rhodamine B isothiocyanate	Rat brain endothelial cells	Serum deprivation	[353] #
Poly (ethylene glycol)-co-poly-ε-caprolactone nanoparticles	Angiopep	Paclitaxel	Rat brain endothelial cells	Serum deprivation	[329] #
Poly (ethylene glycol)-co-poly-ε-caprolactone nanoparticles	TGN peptide and AS1411 aptamer	6-Coumarin	bEnd3	None specified	[309, 330] #
Poly (ethylene glycol)-co-poly (trimethylene carbonate) nanoparticles	2-deoxy-D-glucose	Paclitaxel	bEnd3	Serum deprivation	[331] #
Polystyrene nanoparticles	Viral peptide gH625	Fluorescent dye	bEnd3	None specified	[354]*
Poly (ethylene glycol)-coated gelatin-siloxane nanoparticles	SynB peptide	None	Rat brain endothelial cells	Coculture with rat astrocytes Serum deprivation	[313] #
Poly (ethylene glycol)-coated silica nanoparticles	None	Rubpy dye	bEnd3	Serum deprivation	[301] #

Nanosystem	**Active targeting strategy**	**Load**	**Brain microvascular endothelial cells**	**Strategies to enhance barrier properties**	Ref.
Silica nanoparticles	None	Fluorescent label	Rat brain endothelial cells	Coculture with rat pericytes	[302]*
Silica nanoparticles	None	Green fluorescent label	hCMEC/D3	Fibronectin and collagen coating Hydrocortisone	[355]*
Silica nanoparticles	None	Green fluorescent label	hCMEC/D3	Type I collagen and fibronectin coating Hydrocortisone	[300]
Silica matrix magnetic nanoparticles	Prion protein	None	hCMEC/D3	Type I collagen coating Hydrocortisone	[356]
Titanium dioxide nanoparticles	None	None	Rat brain endothelial cells	Coculture with rat astrocytes	[357]
Protamine-oligonucleotide nanoparticles	Apo A-I	^{125}I	Porcine brain endothelial cells	Collagen coating Hydrocortisone	[310]*
Poly (ethylene glycol)-coated human serum albumin nanoparticles	Apolipoprotein E	Obidoxime	Porcine brain endothelial cells	Type IV collagen coating Serum deprivation	[358]
		HI-6 oxime			
Human serum albumin nanoparticles	None	Oxime (HI-6)	Porcine brain endothelial cells	Type IV collagen coating Serum deprivation Hydrocortisone	[359]
Multi-walled carbon nanotubes	Diethylene triamine pentaacetate	^{111}In	Porcine brain endothelial cells	Coculture with rat astrocytes Serum deprivation Hydrocortisone CPT-cAMP/RO-20-1724	[360]* #
Multiwalled carbon nanotubes	None	Fluorescein isothiocyanate	cEND	Type IV collagen coating	[361]
Poly (ethylene glycol)-coated liposomes	Mannose and transferrin	Daunorubicin	Murine brain endothelial cells	Gelatin coating	[281] #
Poly (ethylene glycol)-coated liposomes	Cereport ® (RM-7)	Nerve growth factor	Mouse brain endothelial cells	Gelatin coating	[326]* #
Poly (ethylene glycol)-coated liposomes	Tamoxifen and Wheat Germ Agglutinin	Topotecan	Murine brain endothelial cells	Coculture with rat astrocytes	[336] #

Nanosystem	**Active targeting strategy**	**Load**	**Brain microvascular endothelial cells**	**Strategies to enhance barrier properties**	Ref.
Poly (ethylene glycol)-coated liposomes	cRGD and histidine rich tandem peptide	Carboxi-fluorescein	bEnd3	None specified	[333] #
Poly (ethylene glycol)-coated liposomes	Folate and Transferrin	Doxorubicin	bEnd3	None specified	[332] #
Poly (ethylene glycol)-coated liposomes	Transferrin and poly-L-arginine	Indocarbocyanine fluorescent dye (DiI)	bEnd3	Collagen coating Coculture with rat astrocytes	[362]*
Poly (ethylene glycol)-coated liposomes	Transferrin and Tamoxifen	Epirubicin	Rat brain endothelial cells	Gelatin coating Serum deprivation	[285] #
Poly (ethylene glycol)-coated liposomes	^{D}CDX peptide	Rhodamine B	Rat brain endothelial cells	Collagen coating	[339] #
(Procationic) liposomes	Lactoferrin	Coumarin-6	Rat brain endothelial cells	Coculture with rat astrocytes	[315]* #
Poly (ethylene glycol)-coated liposomes	Glucose	Coumarin-6	Rat brain endothelial cells	Coculture with rat astrocytes	[312, 316] #
Poly (ethylene glycol)-coated liposomes	Apo-E derived peptides	^{3}H-Curcumin	RBE4	Type I collagen coating Serum deprivation	[321]*
Magnetic liposomes	External magnetic field	Azido-thymidine 5'-triphosphate	Human brain endothelial cells	Coculture with human astrocytes	[363]*
Magnetic poly (ethylene glycol)-coated liposomes	Transferrin + External magnetic field	Carboxi-fluorescein	Human brain endothelial cells	Coculture with human astrocytes	[364]
Poly (ethylene glycol)-coated liposomes	Apo B100-derived peptide + Statins	Doxorubicin	hCMEC/D3	Type I collagen coating Hydrocortisone	[365]*
Radiolabeled poly (ethylene glycol)-coated liposomes	RI7217 antibody	None	hCMEC/D3	Type I collagen coating	[366]*
Poly (ethylene glycol)-coated liposomes	OX26 antibody	Fluorescent dextran	hCMEC/D3	Type I collagen coating Hydrocortisone	[367]
Poly (ethylene glycol)-coated liposomes	OX26 and anti-amyloid β monoclonal antibodies	Fluorescent dextran	hCMEC/D3	Type I collagen coating Hydrocortisone	[368]

Nanosystem	**Active targeting strategy**	**Load**	**Brain microvascular endothelial cells**	**Strategies to enhance barrier properties**	Ref.
Poly (ethylene glycol)-coated liposomes	Human anti-transferrin receptor antibody	Arsenic trioxide	hCMEC/D3	Type IV collagen and fibronectin coating Hydrocortisone Coculture with medulloblastoma cell lines (VC312R and DAOY)	[369]*
Radiolabeled liposomes	Phosphatidic acid and ApoE-derived peptide	None	hCMEC/D3	Type I collagen coating	[370]* #
Thermosensitive poly (ethylene glycol)-coated liposomes	Hyperthermia	Adriamycin	ECV304	Coculture with rat astrocytes	[338]* #
Poly (ethylene glycol)-coated liposomes	Cyclic RGD peptide	Trefoil-factor 3 and cyanine fluorescent dye	Human brain endothelial cells	Collagen coating	[371] #
Solid lipid nanoparticles	None	Stavudine	Human brain endothelial cells	Fibronectin and collagen coating	[297]*
		Delavirdine			
		Saquinavir			
Cationic solid lipid nanoparticles	None	Saquinavir	Human brain endothelial cells	None specified	[372]*
Poly (ethylene glycol)-coated solid lipid nanoparticles	83-14 monoclonal antibody	Saquinavir	Human brain endothelial cells	Gelatin coating Coculture with human astrocytes	[320]*
Poly (ethylene glycol)-coated solid lipid nanoparticles	83-14 monoclonal antibody	Carmustine	Human brain endothelial cells	Coculture with human astrocytes	[318]*
Iron oxide nanoparticles	None	None	bEnd3	Collagen coating Serum deprivation	[304]*
Poly (ethylene glycol)-poly lactic acid and polyvinyl pyrrolidone-coated iron oxide nanoparticles	None	Curcumin	MDCK	None specified	[373]* #

Nanosystem	**Active targeting strategy**	**Load**	**Brain microvascular endothelial cells**	**Strategies to enhance barrier properties**	Ref.
Poly (isobutylene-maleic anhydride)-coated iron oxide nanoparticles	None	AlexaFluor 660-labeled enfuvirtide	Rat brain endothelial cells	Fibronectin coating Coculture with rat astrocytes	[374] #
Iron oxide nanoparticles	Anti-PECAM-1 antibody	None	hCMEC/D3	Type I collagen coating Hydrocortisone	[375]* #
Oleic acid-coated iron oxide nanoparticles	External magnetic field	None	Human brain endothelial cells	None specified	[376]
Polyvinylamine-coated iron oxide nanoparticles					
Iron oxide nanoparticles	External magnetic field and osmotic BBB disruption	None	bEnd3	None specified	[377]*
Iron oxide nanoparticles	External magnetic field	Morphine antagonist CTOP	Human brain endothelial cells	Coculture with human astrocytes	[378]
Iron oxide nanoparticles	External magnetic field	Tenofovir and vorinostat	Human brain endothelial cells	Coculture with human astrocytes	[379]
Iron oxide nanoparticles	External magnetic field	Brain Derived Neurotrophic Factor	Human brain endothelial cells	Coculture with human astrocytes	[380]
Poly (ethylene glycol)-coated iron oxide nanoparticles	Lactoferrin	None	Porcine brain endothelial cells	Collagen coating Serum deprivation Hydrocortisone	[381] #
Iron oxide nanoparticles	External magnetic field	None	Human brain endothelial cells	Coculture with rat astrocytes	[382]
Poly (ethylene glycol)-coated gold nanoparticles	None	None	Rat brain endothelial cells	Type IV collagen coating Coculture with rat astrocytes	[303]
Gold nanoparticles	Glucose	None	hCMEC/D3	Coculture with human astrocytes	[383]

Nanosystem	**Active targeting strategy**	**Load**	**Brain microvascular endothelial cells**	**Strategies to enhance barrier properties**	Ref.
Gold nanoparticles	THRPPMWSPVWP peptide	CLPFFD peptide	Bovine brain endothelial cells	Fibronectin and type IV collagen coating Coculture with rat astrocytes Serum deprivation CPT-cAMP/RO-20-1724	[127]* #
Selenium nanoparticles	B6 peptide and sialic acid	Rhutenium	bEnd3	Coculture with PC12 cell line Serum deprivation	[384]
Quantum Rods	Transferrin	None	Human brain microvascular endothelial cells	Coculture with human astrocytes	[314]
Quantum Rods	None	None	Rat brain endothelial cells	Coculture with rat pericytes	[302]*
P22 Salmonella typhimurium capside	Tat-peptide	Ziconotide	Human brain endothelial cells	Coculture with human astrocytes Dynamic *in vitro* model	[323]

Table 2.1.7: Cell-based models of the blood brain barrier used to evidence the passage of nanomedicines. *: these references have calculated apparent permeability values expressed in cm/s; #: these references have conducted *in vivo* studies to further evidence the brain delivery, BBB: blood brain barrier; CPT-cAMP: 8-(4-chlorophenylthio) adenosine 3′,5′-cyclic monophosphate; RO-20-1724: 4-(3-butoxy-4 methoxybenzyl)-2-imidazolidinone; PECAM: platelet-endothelial cell adhesion molecule.

6. Conclusion

Screening BBB permeability remains one of the key ADME properties to be addressed early in CNS drug discovery process to triage promising candidates.

Although dependent on *in vivo* data for validation, *in vitro* models developed to predict the BBB permeability, meet the medium-to-high-throughput demands, provide mechanistic information and are more economical. However, each *in vitro* model has limitations that prevent them from mimicking all *in vivo* features of the BBB. Whereas assays with artificial membranes overlook active transport processes, the application of cerebral cell-based models may be comprised by the artificial conditions under which they are maintained *in vitro*. Moreover, non-cerebral cell-based models lack numerous properties of the *in vivo* brain endothelium.

To gain a more comprehensive insight into the mechanisms involved in the passage through the BBB, BBB permeability can be inferred by combining *in vitro*

screening methods, which would enable the contribution of active and passive transport processes to be separated. Consequently, a comparison by plotting of the permeability coefficients from both tests allows three different regions to be defined that help elucidate transport mechanism and thereby the forecast capacity of the methods [385]: samples actively uptaken (high cell-based model permeability versus low artificial-membrane permeability) constitute the first area; samples with passive permeability (similar permeability coefficients for both assays) represent the second one and samples actively effluxed (low cell-based model permeability versus high artificial membrane permeability) constitute the third region, as depicted in Figure 4.

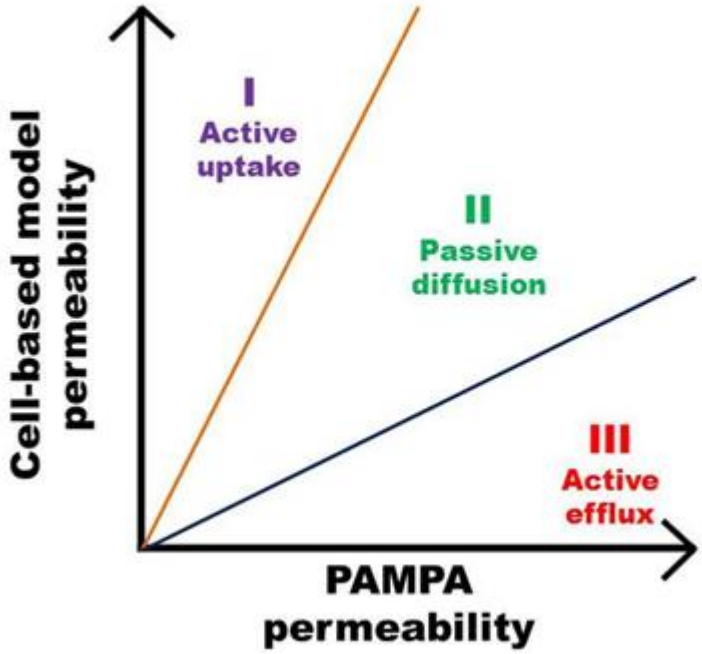

Figure 2.1.4: Comparison of data gained with cell-based and non-cell based screening methods

Given the advances in the field of nanomedicine over the last decade aimed at enhancing the passage across the BBB, another groundbreaking change in outlook is likely to occur in the near future: with the purpose of predicting brain distribution, *in vitro* ADME screening methods must be adapted for evaluation of these new drug delivery platforms to provide information regarding the brain penetration of nanocarriers, and ultimately to establish a relation of causality with the clinical situation [386]. To this end, simplistic *in vitro* models such as artificial-membrane-based cannot represent the complicated absorption of these nanosystems in the human brain and cell-based models may well be the first choice despite their medium-throughput nature, since a compromise between throughput potential and the limitations associated with each model must be met. In accordance with this idea, the vast majority of models that have been currently used and validated for the screening of nanomedicines are *in vitro* cell-based models. Noteworthy, further simplified *in vitro* BBB models may well serve in the future to verify batch-to-batch variability in terms of BBB permeation, a critical attribute for the regulation of nanomedicines to promote their translation into the market.

Much more research is likely to be done in the near future to design more efficient and safer nanomedicines based on their BBB permeability, thereby improving the treatment of CNS-related pathologies.

Acknowledgements

This work was partially funded by the Research Group GR35/10 Santander-UCM, Group: Parenteral Administration of Drugs. Juan Aparicio-Blanco thanks the Spanish Ministry of Education for the Contract within the Professor Training Program FPU (Ref. FPU13/02325).The authors would like to thank Pablo Jiménez-Romero for providing assistance with the figures.

References

[1] Shakir R. Brain health: widening the scope of NCDs. Lancet. 2016;387:518-9.

[2] Cruz M, Jenkins R, Silberberg D. The burden of brain disorders. Science. 2006;312:53-.

[3] Nutt DJ. The full cost and burden of disorders of the brain in Europe exposed for the first time. Eur Neuropsychopharm. 2011;21:715-7.

[4] Ravindranath V, Dang HM, Goya RG, Mansour H, Nimgaonkar VL, Russell VA, et al. Regional research priorities in brain and nervous system disorders. Nature. 2015;527:S198-S206.

[5] Nutt D, Goodwin G. ECNP Summit on the future of CNS drug research in Europe 2011: report prepared for ECNP by David Nutt and Guy Goodwin. Eur Neuropsychopharm. 2011;21:495-9.

[6] Pardridge WM. Why is the global CNS pharmaceutical market so under-penetrated? Drug Discov Today. 2002;7:5-7.

[7] Silberberg D, Anand NP, Michels K, Kalaria RN. Brain and other nervous system disorders across the lifespan - global challenges and opportunities. Nature. 2015;527:S151-S4.

[8] Reynolds EH. Brain and mind: a challenge for WHO. Lancet. 2003;361:1924-5.

[9] Wittchen HU, Jacobi F, Rehm J, Gustavsson A, Svensson M, Jonsson B, et al. The size and burden of mental disorders and other disorders of the brain in Europe 2010. EurNeuropsychopharm. 2011;21:655-79.

[10] Betsholtz C. Double function at the blood-brain barrier. Nature. 2014;509:432-3.

[11] Zlokovic BV. The blood-brain barrier in health and chronic neurodegenerative disorders. Neuron. 2008;57:178-201.

[12] Saunders NR, Ek CJ, Habgood MD, Dziegielewska KM. Barriers in the brain: a renaissance? Trends Neurosci. 2008;31:279-86.

[13] Pardridge WM. Blood-brain barrier delivery. Drug Discov Today. 2007;12:54-61.

[14] Neuwelt E, Abbott N, Abrey L, Banks WA, Blakley B, Davis T, et al. Strategies to advance translational research into brain barriers. Lancet Neurol. 2008;7:84-96.

[15] Neuwelt EA, Bauer B, Fahlke C, Fricker G, Iadecola C, Janigro D, et al. Engaging neuroscience to advance translational research in brain barrier biology. Nat Rev Neurosci. 2011;12:169-82.

[16] Begley DJ. Delivery of therapeutic agents to the central nervous system: the problems and the possibilities. Pharmacol Ther. 2004;104:29-45.

[17] Pardridge WM. Drug and gene delivery to the brain: The vascular route. Neuron. 2002;36:555-8.

[18] Aparicio-Blanco J, Torres-Suarez AI. Glioblastoma Multiforme and Lipid Nanocapsules: A Review. J Biomed Nanotechnol. 2015;11:1283-311.

[19] McCarthy N. Therapy - Through the barricades. Nat Rev Cancer. 2006;6:660-.

[20] Clark DE. In silico prediction of blood-brain barrier permeation. Drug Discov Today. 2003;8:927-33.

[21] Vandenhaute E, Sevin E, Hallier-Vanuxeem D, Dehouck MP, Cecchelli R. Case study: adapting in vitro blood-brain barrier models for use in early-stage drug discovery. Drug Discov Today. 2012;17:285-90.

[22] Gabathuler R. Approaches to transport therapeutic drugs across the blood-brain barrier to treat brain diseases. Neurobiol Dis. 2010;37:48-57.

[23] Regina A, Demeule M, Laplante A, Jodoin J, Dagenais C, Berthelet F, et al. Multidrug resistance in brain tumors: Roles of the blood-brain barrier. Cancer Metastasis Rev. 2001;20:13-25.

[24] Morgan P, Van der Graaf PH, Arrowsmith J, Feltner DE, Drummond KS, Wegner CD, et al. Can the flow of medicines be improved? Fundamental pharmacokinetic and pharmacological principles toward improving Phase II survival. Drug Discov Today. 2012;17:419-24.

[25] Wolka AM, Huber JD, Davis TP. Pain and the blood-brain barrier: obstacles to drug delivery. Adv Drug Deliv Rev. 2003;55:987-1006.

[26] Kingwell K. Drug delivery: New targets for drug delivery across the BBB. Nat Rev Drug Discov. 2016;15:84-5.

[27] Pardridge WM. Drug and gene targeting to the brain with molecular Trojan horses. Nat Rev Drug Discov. 2002;1:131-9.

[28] Pardridge WM. Log(BB), PS products and in silico models of drug brain penetration. Drug Discov Today. 2004;9:392-3.

[29] Vellonen KS, Malinen M, Mannermaa E, Subrizi A, Toropainen E, Lou YR, et al. A critical assessment of in vitro tissue models for ADME and drug delivery. J Control Release. 2014;190:94-114.

[30] Summerfield SG, Dong KC. In vitro, in vivo and in silico models of drug distribution into the brain. J Pharmacokinet Pharmacodyn. 2013;40:301-14.

[31] Norinder U, Haeberlein M. Computational approaches to the prediction of the blood-brain distribution. Adv Drug Deliv Rev. 2002;54:291-313.

[32] Nicolazzo JA, Charman SA, Charman WN. Methods to assess drug permeability across the blood-brain barrier. J Pharm Pharmacol. 2006;58:281-93.

[33] Pardridge WM. Holy grails and in vitro blood-brain barrier models. Drug Discov Today. 2004;9:258-.

[34] Banks WA. From blood-brain barrier to blood-brain interface: new opportunities for CNS drug delivery. Nat Rev Drug Discov. 2016;15:275-92.

[35] Srikanth M, Kessler JA. Nanotechnology-novel therapeutics for CNS disorders. Nat Rev Neurol. 2012;8:307-18.

[36] Silva GA. Neuroscience nanotechnology: Progress, opportunities and challenges. Nat Rev Neurosci. 2006;7:65-74.

[37] Kabanov AV, Gendelman HE. Nanomedicine in the diagnosis and therapy of neuro degenerative disorders. Prog Polym Sci. 2007;32:1054-82.

[38] Blanco E, Shen H, Ferrari M. Principles of nanoparticle design for overcoming biological barriers to drug delivery. Nat Biotechnol. 2015;33:941-51.

[39] Vlieghe P, Khrestchatisky M. Medicinal Chemistry Based Approaches and Nanotechnology-Based Systems to Improve CNS Drug Targeting and Delivery. Med Res Rev. 2013;33:457-516.

[40] Modi G, Pillay V, Choonara YE, Ndesendo VMK, du Toit LC, Naidoo D. Nanotechnological applications for the treatment of neurodegenerative disorders. Prog Neurobiol. 2009;88:272-85.

[41] Patel MM, Goyal BR, Bhadada SV, Bhatt JS, Amin AF. Getting into the Brain Approaches to Enhance Brain Drug Delivery. CNS Drugs. 2009;23:35-58.

[42] Gaspar R. Regulatory issues surrounding nanomedicines: setting the scene for the next generation of nanopharmaceuticals. Nanomedicine. 2007;2:143-7.

[43] Cecchelli R, Berezowski V, Lundquist S, Culot M, Renftel M, Dehouck MP, et al. Modelling of the blood-brain barrier in drug discovery and development. Nat Rev Drug Discov. 2007;6:650-61.

[44] Eddy EP, Maleef BE, Hart TK, Smith PL. In vitro models to predict blood-brain barrier permeability. Adv Drug Deliv Rev. 1997;23:185-98.

[45] Helms HC, Abbott NJ, Burek M, Cecchelli R, Couraud PO, Deli MA, et al. In vitro models of the blood brain barrier: An overview of commonly used brain endothelial cell culture models and guidelines for their use. J Cereb Blood Flow Metab. 2016:1-29.

[46] He YR, Yao Y, Tsirka SE, Cao Y. Cell-Culture Models of the Blood-Brain Barrier. Stroke. 2014;45:2514-26.

[47] Bicker J, Alves G, Fortuna A, Falcao A. Blood-brain barrier models and their relevance for a successful development of CNS drug delivery systems: A review. Eur J Pharm Biopharm. 2014;87:409-32.

[48] Abbott NJ, Patabendige AAK, Dolman DEM, Yusof SR, Begley DJ. Structure and function of the blood-brain barrier. Neurobiol Dis. 2010;37:13-25.

[49] Crone C, Olesen SP. Electrical resistance of brain microvascular endothelium. Brain Res. 1982;241:49-55.

[50] Crone C, Christensen O. Electrical resistance of a capillary endothelium. J Gen Physiol. 1981;77:349-71.

[51] Dobson PD, Kell DB. Carrier-mediated cellular uptake of pharmaceutical drugs: an exception or the rule? Nat Rev Drug Discov. 2008;7:205-20.

[52] Sun HY, Dai HQ, Shaik N, Elmquist WF. Drug efflux transporters in the CNS. Adv Drug Deliv Rev. 2003;55:83-105.

[53] Schinkel AH. P-glycoprotein, a gatekeeper in the blood-brain barrier. Adv Drug Deliv Rev. 1999;36:179-94.

[54] Janzer RC, Raff MC. Astrocytes induce blood-brain barrier properties in endothelial cells. Nature. 1987;325:253-7.

[55] Abbott NJ, Ronnback L, Hansson E. Astrocyte-endothelial interactions at the blood-brain barrier. Nat Rev Neurosci. 2006;7:41-53.

[56] Armulik A, Genove G, Mae M, Nisancioglu MH, Wallgard E, Niaudet C, et al. Pericytes regulate the blood-brain barrier. Nature. 2010;468:557-61.

[57] Peppiatt CM, Howarth C, Mobbs P, Attwell D. Bidirectional control of CNS capillary diameter by pericytes. Nature. 2006;443:700-4.

[58] Li AP. In vitro experimental models for the blood-brain barrier. Drug Discov Today. 2004;9:204-5.

[59] Ali IU, Chen XY. Penetrating the Blood-Brain Barrier: Promise of Novel Nanoplatforms and Delivery Vehicles. Acs Nano. 2015;9:9470-4.

[60] Wong HL, Wu XY, Bendayan R. Nanotechnological advances for the delivery of CNS therapeutics. Adv Drug Deliv Rev. 2012;64:686-700.

[61] Biddlestone-Thorpe L, Marchi N, Guo K, Ghosh C, Janigro D, Valerie K, et al. Nanomaterial-mediated CNS delivery of diagnostic and therapeutic agents. Adv Drug Deliv Rev. 2012;64:605-13.

[62] Kreuter J. Nanoparticulate systems for brain delivery of drugs. Adv Drug Deliv Rev. 2012;64:213-22.

[63] Wohlfart S, Gelperina S, Kreuter J. Transport of drugs across the blood-brain barrier by nanoparticles. J Control Release. 2012;161:264-73.

[64] Davis ME, Chen Z, Shin DM. Nanoparticle therapeutics: an emerging treatment modality for cancer. Nat Rev Drug Discov. 2008;7:771-82.

[65] Blasi P, Glovagnoli S, Schoubben A, Ricci M, Rossi C. Solid lipid nanoparticles for targeted brain drug delivery. Adv Drug Deliv Rev. 2007;59:454-77.

[66] Patel T, Zhou J, Piepmeier JM, Saltzman WM. Polymeric nanoparticles for drug delivery to the central nervous system. Adv Drug Deliv Rev. 2012;64:701-5.

[67] Krol S. Challenges in drug delivery to the brain: Nature is against us. J Control Release. 2012;164:145-55.

[68] Nel A, Xia T, Madler L, Li N. Toxic potential of materials at the nanolevel. Science. 2006;311:622-7.

[69] Bramini M, Ye D, Hallerbach A, Raghnaill MN, Salvati A, Aberg C, et al. Imaging Approach to Mechanistic Study of Nanoparticle Interactions with the Blood-Brain Barrier. Acs Nano. 2014;8:4304-12.

[70] Yildirimer L, Thanh NTK, Loizidou M, Seifalian AM. Toxicological considerations of clinically applicable nanoparticles. Nano Today. 2011;6:585-607.

[71] Hussain SM, Braydich-Stolle LK, Schrand AM, Murdock RC, Yu KO, Mattie DM, et al. Toxicity Evaluation for Safe Use of Nanomaterials: Recent Achievements and Technical Challenges. Adv Mater. 2009;21:1549-59.

[72] Florence AT. "Targeting" nanoparticles: The constraints of physical laws and physical barriers. J Control Release. 2012;164:115-24.

[73] Chen Y, Liu LH. Modern methods for delivery of drugs across the blood-brain barrier. Adv Drug Deliv Rev. 2012;64:640-65.

[74] Sahay G, Alakhova DY, Kabanov AV. Endocytosis of nanomedicines. J Control Release. 2010;145:182-95.

[75] Barua S, Mitragotri S. Challenges associated with penetration of nanoparticles across cell and tissue barriers: A review of current status and future prospects. Nano Today. 2014;9:223-43.

[76] Xu S, Olenyuk BZ, Okamoto CT, Hamm-Alvarez SF. Targeting receptor-mediated endocytotic pathways with nanoparticles: Rationale and advances. Adv Drug Deliv Rev. 2013;65:121-38.

[77] Green E. Blood-brain barrier - Size matters at the blood-brain barrier. Nat Rev Neurosci. 2003;4:525-.

[78] Giacomini KM, Huang SM, Tweedie DJ, Benet LZ, Brouwer KLR, Chu XY, et al. Membrane transporters in drug development. Nat Rev Drug Discov. 2010;9:215-36.

[79] Lee G, Dallas S, Hong M, Bendayan R. Drug transporters in the central nervous system: Brain barriers and brain parenchyma considerations. Pharmacol Rev. 2001;53:569-96.

[80] Muro S. Challenges in design and characterization of ligand-targeted drug delivery systems. J Control Release. 2012;164:125-37.

[81] Bhaskar S, Tian FR, Stoeger T, Kreyling W, de la Fuente JM, Grazu V, et al. Multifunctional Nanocarriers for diagnostics, drug delivery and targeted treatment across blood-brain barrier: perspectives on tracking and neuroimaging. Part Fibre Toxicol. 2010;7:1-25.

[82] Garcion E, Lamprecht A, Heurtault B, Paillard A, Aubert-Pouessel A, Denizot B, et al. A new generation of anticancer, drug-loaded, colloidal vectors reverses multidrug resistance in glioma and reduces tumor progression in rats. Mol Cancer Ther. 2006;5:1710-22.

[83] Kozlovskaya L, Stepensky D. Quantitative analysis of the brain-targeted delivery of drugs and model compounds using nano-delivery systems. J Control Release. 2013;171:17-23.

[84] Kievit FM, Zhang MQ. Cancer Nanotheranostics: Improving Imaging and Therapy by Targeted Delivery Across Biological Barriers. Adv Mater. 2011;23:H217-H47.

[85] Li J, Cai P, Shalviri A, Henderson JT, He CS, Foltz WD, et al. A Multifunctional Polymeric Nanotheranostic System Delivers Doxorubicin and Imaging Agents across the Blood-Brain Barrier Targeting Brain Metastases of Breast Cancer. Acs Nano. 2014;8:9925-40.

[86] Yan HH, Wang L, Wang JY, Weng XF, Lei H, Wang XX, et al. Two-Order Targeted Brain Tumor Imaging by Using an Optical/Paramagnetic Nanoprobe across the Blood Brain Barrier. Acs Nano. 2012;6:410-20.

[87] Veiseh O, Sun C, Gunn J, Kohler N, Gabikian P, Lee D, et al. Optical and MRI multifunctional nanoprobe for targeting gliomas. Nano Lett. 2005;5:1003-8.

[88] Selvi BR, Jagadeesan D, Suma BS, Nagashankar G, Arif M, Balasubramanyam K, et al. Intrinsically Fluorescent Carbon Nanospheres as a Nuclear Targeting Vector: Delivery of Membrane-Impermeable Molecule to Modulate Gene Expression In Vivo. Nano Lett. 2008;8:3182-8.

[89] Ni DL, Zhang JW, Bu WB, Xing HY, Han F, Xiao QF, et al. Dual-Targeting Upconversion Nanoprobes across the Blood-Brain Barrier for Magnetic Resonance/Fluorescence Imaging of Intracranial Glioblastoma. Acs Nano. 2014;8:1231-42.

[90] Patil R, Ljubimov AV, Gangalum PR, Ding H, Portilla-Arias J, Wagner S, et al. MRI Virtual Biopsy and Treatment of Brain Metastatic Tumors with Targeted Nanobioconjugates: Nanoclinic in the Brain. Acs Nano. 2015;9:5594-608.

[91] Shilo M, Motiei M, Hana P, Popovtzer R. Transport of nanoparticles through the blood-brain barrier for imaging and therapeutic applications. Nanoscale. 2014;6:2146-52.

[92] Goldsmith M, Abramovitz L, Peer D. Precision Nanomedicine in Neurodegenerative Diseases. Acs Nano. 2014;8:1958-65.

[93] Fonseca-Santos B, Gremiao MPD, Chorilli M. Nanotechnology-based drug delivery systems for the treatment of Alzheimer's disease. Int J Nanomed. 2015;10:4981-5003.

[94] Crunkhorn S. Neurological disorders: Nanoparticle opens door to cerebral palsy treatment. Nat Rev Drug Discov. 2012;11:440-1.

[95] Pahuja R, Seth K, Shukla A, Shukla RK, Bhatnagar P, Chauhan LKS, et al. Trans-Blood Brain Barrier Delivery of Dopamine-Loaded Nanoparticles Reverses Functional Deficits in Parkinsonian Rats. Acs Nano. 2015;9:4850-71.

[96] Huang M, Hu M, Song QX, Song HH, Huang JL, Gu X, et al. GM1-Modified Lipoprotein-like Nanoparticle: Multifunctional Nanoplatform for the Combination Therapy of Alzheimer's Disease. Acs Nano. 2015;9:10801-16.

[97] Roney C, Kulkarni P, Arora V, Antich P, Bonte F, Wu AM, et al. Targeted nanoparticles for drug delivery through the blood-brain barrier for Alzheimer's disease. J Control Release. 2005;108:193-214.

[98] Kim CK, Kim T, Jang H, Kim D, Hyeon T, Lee SH. Newly Designed Ceria Nanoparticle for the Therapy of Ischemic Stroke. Circulation. 2012;126:2.

[99] Beduneau A, Saulnier P, Benoit JP. Active targeting of brain tumors using nanocarriers. Biomaterials. 2007;28:4947-67.

[100] Koo YEL, Reddy GR, Bhojani M, Schneider R, Philbert MA, Rehemtulla A, et al. Brain cancer diagnosis and therapy with nanoplatforms. Adv Drug Deliv Rev. 2006;58:1556-77.

[101] Lesniak MS, Brem H. Targeted therapy for brain tumours. Nat Rev Drug Discov. 2004;3:499-508.

[102] Rutka JT, Kim B, Etame A, Diaz RJ. Nanosurgical Resection of Malignant Brain Tumors: Beyond the Cutting Edge. Acs Nano. 2014;8:9716-22.

[103] Sharpe MA, Marcano DC, Berlin JM, Widmayer MA, Baskin DS, Tour JM. Antibody-Targeted Nanovectors for the Treatment of Brain Cancers. Acs Nano. 2012;6:3114-20.

[104] Wong HL, Chattopadhyay N, Wu XY, Bendayan R. Nanotechnology applications for improved delivery of antiretroviral drugs to the brain. Adv Drug Deliv Rev. 2010;62:503-17.

[105] Kansy M, Senner F, Gubernator K. Physicochemical high throughput screening: Parallel artificial membrane permeation assay in the description of passive absorption processes. J Med Chem. 1998;41:1007-10.

[106] Avdeef A. Absorption and Drug Development: Solubility, Permeability and the Charge State. In: John Wiley & Sons I, editor. New Jersey2003.

[107] Youdim KA, Avdeef A, Abbott NJ. In vitro trans-monolayer permeability calculations: often forgotten assumptions. Drug Discov Today. 2003;8:997-1003.

[108] Muller J, Esso K, Dargo G, Konczol A, Balogh GT. Tuning the predictive capacity of the PAMPA-BBB model. Eur J Pharm Sci. 2015;79:53-60.

[109] Mensch J, Melis A, Mackie C, Verreck G, Brewster ME, Augustijns P. Evaluation of various PAMPA models to identify the most discriminating method for the prediction of BBB permeability. Eur J Pharm Biopharm. 2010;74:495-502.

[110] Di L, Kerns EH, Carter GT. Strategies to assess blood-brain barrier penetration. Expert Opin Drug Discov. 2008;3:677-87.

[111] Di L, Kerns EH, Bezar IF, Petusky SL, Huang YP. Comparison of Blood-Brain Barrier Permeability Assays: In Situ Brain Perfusion, MDR1-MDCKII and PAMPA-BBB. J Pharm Sci. 2009;98:1980-91.

[112] Di L, Kerns EH, Fan K, McConnell OJ, Carter GT. High throughput artificial membrane permeability assay for blood-brain barrier. Eur J Med Chem. 2003;38:223-32.

[113] Tsinman O, Tsinman K, Sun N, Avdeef A. Physicochemical Selectivity of the BBB Microenvironment Governing Passive Diffusion-Matching with a Porcine Brain Lipid Extract Artificial Membrane Permeability Model. Pharm Res. 2011;28:337-63.

[114] Nielsen PE, Avdeef A. PAMPA - a drug absorption in vitro model - 8. Apparent filter porosity and the unstirred water layer. Eur J Pharm Sci. 2004;22:33-41.

[115] Kansy M, Avdeef A, Fischer H. Advances in screening for membrane permeability: high-resolution PAMPA for medicinal chemists. Drug discovery today Technologies. 2004;1:349-55.

[116] Carrara S, Reali V, Misiano P, Dondio G, Bigogno C. Evaluation of in vitro brain penetration: Optimized PAMPA and MDCKII-MDR1 assay comparison. Int J Pharm. 2007;345:125-33.

[117] Konczol A, Muller J, Foldes E, Beni Z, Vegh K, Kery A, et al. Applicability of a Blood-Brain Barrier Specific Artificial Membrane Permeability Assay at the Early Stage of Natural Product-Based CNS Drug Discovery. J Nat Prod. 2013;76:655-63.

[118] Jhala D, Chettiar SS, Singh JK. Optimization and validation of an *in vitro* blood brain barrier permeability assay using artificial lipid membrane. Journal of Bioequivalence and Bioavailability. 2012;S14.

[119] Palmer A. The role of the blood-CNS barrier in CNS disorders and their treatment. Neurobiol Dis. 2010;37:3-12.

[120] Vizseralek G, Balogh T, Takacs-Novak K, Sinko B. PAMPA study of the temperature effect on permeability. Eur J Pharm Sci. 2014;53:45-9.

[121] Avdeef A, Nielsen PE, Tsinman O. PAMPA - a drug absorption in vitro model 11. Matching the in vivo unstirred water layer thickness by individual-well stirring in microtitre plates. Eur J Pharm Sci. 2004;22:365-74.

[122] Camenisch G, Folkers G, vandeWaterbeemd H. Comparison of passive drug transport through Caco-2 cells and artificial membranes. Int J Pharm. 1997;147:61-70.

[123] Ho NFH, Raub TJ, Burton PS, Barsuhn CL. Quantitative approaches to delineate passive transport mechanisms in cell culture monolayers. In: Amidon GL, Lee PI, Topp EM, editors. Transport Processes in Pharmaceutical Systems. New York: Marcel Dekker; 2000. p. 219-316.

[124] Wohnsland F, Faller B. High-throughput permeability pH profile and high-throughput alkane/water log P with artificial membranes. J Med Chem. 2001;44:923-30.

[125] Passeleu-Le Bourdonnec C, Carrupt PA, Scherrmann JM, Martel S. Methodologies to Assess Drug Permeation Through the Blood-Brain Barrier for Pharmaceutical Research. Pharm Res. 2013;30:2729-56.

[126] Malakoutikhah M, Prades R, Teixido M, Giralt E. N-Methyl Phenylalanine-Rich Peptides as Highly Versatile Blood-Brain Barrier Shuttles. J Med Chem. 2010;53:2354-63.

[127] Prades R, Guerrero S, Araya E, Molina C, Salas E, Zurita E, et al. Delivery of gold nanoparticles to the brain by conjugation with a peptide that recognizes the transferrin receptor. Biomaterials. 2012;33:7194-205.

[128] Mathot F, Schanck A, Van Bambeke F, Arien A, Noppe M, Brewster M, et al. Passive diffusion of polymeric surfactants across lipid bilayers. J Control Release. 2007;120:79-87.

[129] Huerta C, Aberturas MD, Molpeceres J. Nimesulide-loaded nanoparticles for the potential coadjuvant treatment of prostate cancer. Int J Pharm. 2015;493:152-60.

[130] Aberturas MR, Hernan D, Gil ME, Ligresti LA, De Petrocellis L, Torres AI, et al. Anandamide-loaded nanoparticles: Preparation and characterization. J Microencapsul. 2011;28:200-10.

[131] Sandhya KV, Devi GS, Mathew ST. Liposomal formulations of serratiopeptidase: In vitro studies using PAMPA and Caco-2 models. Mol Pharm. 2008;5:92-7.

[132] Yanamandra S, Venkatesan N, Kadajji VG, Wang ZJ, Issar M, Betageri GV. Proliposomes as a drug delivery system to decrease the hepatic first-pass metabolism: Case study using a model drug. Eur J Pharm Sci. 2014;64:26-36.

[133] Righeschi C, Bergonzi MC, Isacchi B, Bazzicalupi C, Gratteri P, Bilia AR. Enhanced curcumin permeability by SLN formulation: The PAMPA approach. LWT - Food Sci Technol. 2016;66:475-83.

[134] Jankovic J, Djekic L, Dobricic V, Primorac M. Evaluation of critical formulation parameters in design and differentiation of self-microemulsifying drug delivery systems (SMEDDSs) for oral delivery of aciclovir. Int J Pharm. 2016;497:301-11.

[135] Krstic M, Popovic M, Dobricic V, Ibric S. Influence of Solid Drug Delivery System Formulation on Poorly Water-Soluble Drug Dissolution and Permeability. Molecules. 2015;20:14684-98.

[136] Flaten GE, Dhanikula AB, Luthman K, Brandl M. Drug permeability across a phospholipid vesicle based barrier: A novel approach for studying passive diffusion. Eur J Pharm Sci. 2006;27:80-90.

[137] Flaten GE, Luthman K, Vasskog T, Brandl M. Drug permeability across a phospholipid vesicle-based barrier - 4. The effect of tensides, co-solvents and pH changes on barrier integrity and on drug permeability. Eur J Pharm Sci. 2008;34:173-80.

[138] deBoer AG, Breimer DD. Reconstitution of the blood-brain barrier in cell culture for studies of drug transport and metabolism. Adv Drug Deliv Rev. 1996;22:251-64.

[139] Lockman PR, Koziara J, Roder KE, Paulson J, Abbruscato TJ, Mumper RJ, et al. In vivo and in vitro assessment of baseline blood-brain barrier parameters in the presence of novel nanoparticles. Pharm Res. 2003;20:705-13.

[140] Rubin LL. The blood-brain barrier in and out of cell culture. Curr Opin Neurobiol. 1991;1:360-3.

[141] Elsheikh MA, Elnaggar YSR, Abdallah OY. Rationale employment of cell culture versus conventional techniques in pharmaceutical appraisal of nanocarriers. J Control Release. 2014;194:92-102.

[142] Wilhelm I, Krizbai IA. In Vitro Models of the Blood-Brain Barrier for the Study of Drug Delivery to the Brain. Mol Pharm. 2014;11:1949-63.

[143] Avdeef A. How well can in vitro brain microcapillary endothelial cell models predict rodent in vivo blood-brain barrier permeability? Eur J Pharm Sci. 2011;43:109-24.

[144] Ye D, Dawson KA, Lynch I. A TEM protocol for quality assurance of in vitro cellular barrier models and its application to the assessment of nanoparticle transport mechanisms across barriers. Analyst. 2015;140:83-97.

[145] Brendel K, Meezan E, Carlson EC. Isolated brain microvessels: a purified, metabolically active preparation from bovine cerebral cortex. Science. 1974;185:953-5.

[146] Lundquist S, Renftel M. The use of in vitro cell culture models for mechanistic studies and as permeability screens for the blood-brain barrier in the pharmaceutical industry - Background and current status in the drug discovery process. Vasc Pharmacol. 2002;38:355-64.

[147] Terasaki T, Ohtsuki S, Hori S, Takanaga H, Nakashima E, Hosoya K. New approaches to in vitro models of blood-brain barrier drug transport. Drug Discov Today. 2003;8:944-54.

[148] Navone SE, Marfia G, Invernici G, Cristini S, Nava S, Balbi S, et al. Isolation and expansion of human and mouse brain microvascular endothelial cells. Nat Protoc. 2013;8:1680-93.

[149] Roux F, Couraud PO. Rat brain endothelial cell lines for the study of blood-brain barrier permeability and transport functions. Cell Mol Neurobiol. 2005;25:41-58.

[150] Perriere N, Demeuse PH, Garcia E, Regina A, Debray M, Andreux JP, et al. Puromycin-based purification of rat brain capillary endothelial cell cultures. Effect on the expression of blood-brain barrier-specific properties. J Neurochem. 2005;93:279-89.

[151] Steiner O, Coisne C, Engelhardt B, Lyck R. Comparison of immortalized bEnd5 and primary mouse brain microvascular endothelial cells as in vitro blood-brain barrier models for the study of T cell extravasation. J Cereb Blood Flow Metab. 2011;31:315-27.

[152] Imaizumi S, Kondo T, Deli MA, Gobbel G, Joo F, Epstein CJ, et al. The influence of oxygen free radicals on the permeability of the monolayer of cultured brain endothelial cells. Neurochem Int. 1996;29:205-11.

[153] Dejana E, Liebner S. *In vitro* model for modulating the blood brain barrier and methods of screening. 2010.

[154] Watanabe T, Dohgu S, Takata F, Nishioku T, Nakashima A, Futagami K, et al. Paracellular Barrier and Tight Junction Protein Expression in the Immortalized Brain Endothelial Cell Lines bEND.3, bEND.5 and Mouse Brain Endothelial Cell 4. Biol Pharm Bull. 2013;36:492-5.

[155] Welser-Alves JV, Boroujerdi A, Milner R. Isolation and Culture of Primary Mouse Brain Endothelial Cells. In: Milner R, editor. Cerebral Angiogenesis: Methods and Protocols: Humana Press Inc, 999 Riverview Dr, Ste 208, Totowa, Nj 07512-1165 USA; 2014. p. 345-56.

[156] Coisne C, Dehouck L, Faveeuw C, Delplace Y, Miller F, Landry C, et al. Mouse syngenic in vitro blood-brain barrier model: a new tool to examine inflammatory events in cerebral endothelium. Lab Invest. 2005;85:734-46.

[157] Wuest DM, Lee KH. Optimization of endothelial cell growth in a murine in vitro blood-brain barrier model. Biotechnol J. 2012;7:409-17.

[158] Wuest DM, Wing AM, Lee KH. Membrane configuration optimization for a murine in vitro blood-brain barrier model. J Neurosci Methods. 2013;212:211-21.

[159] Shayan G, Choi YS, Shusta EV, Shuler ML, Lee KH. Murine in vitro model of the blood-brain barrier for evaluating drug transport. Eur J Pharm Sci. 2011;42:148-55.

[160] Brown RC, Morris AP, O'Neil RG. Tight junction protein expression and barrier properties of immortalized mouse brain microvessel endothelial cells. Brain Res. 2007;1130:17-30.

[161] Li GL, Simon MJ, Cancel LM, Shi ZD, Ji XY, Tarbell JM, et al. Permeability of Endothelial and Astrocyte Cocultures: In Vitro Blood-Brain Barrier Models for Drug Delivery Studies. Ann Biomed Eng. 2010;38:2499-511.

[162] Omidi Y, Campbell L, Barar J, Connell D, Akhtar S, Gumbleton M. Evaluation of the immortalised mouse brain capillary endothelial cell line, b.End3, as an in vitro blood-brain barrier model for drug uptake and transport studies. Brain Res. 2003;990:95-112.

[163] Booth R, Kim H. Characterization of a microfluidic in vitro model of the blood-brain barrier (mu BBB). Lab Chip. 2012;12:1784-92.

[164] Yang T, Roder KE, Abbruscato TJ. Evaluation of bEnd5 cell line as an in vitro model for the blood-brain barrier under normal and hypoxic/aglycemic conditions. J Pharm Sci. 2007;96:3196-213.

[165] Paolinelli R, Corada M, Ferrarini L, Devraj K, Artus C, Czupalla CJ, et al. Wnt Activation of Immortalized Brain Endothelial Cells as a Tool for Generating a Standardized Model of the Blood Brain Barrier In Vitro. PLoS One. 2013;8:e70233.

[166] Tatsuta T, Naito M, Oh-hara T, Sugawara I, Tsuruo T. Functional involvement of P-glycoprotein in blood-brain barrier. J Biol Chem. 1992;267:20383-91.

[167] Burek M, Salvador E, Forster CY. Generation of an Immortalized Murine Brain Microvascular Endothelial Cell Line as an In Vitro Blood Brain Barrier Model. J Vis Exp. 2012;66:6.

[168] Vandenhaute E, Dehouck L, Boucau MC, Sevin E, Uzbekov R, Tardivel M, et al. Modelling the Neurovascular Unit and the Blood-Brain Barrier with the Unique Function of Pericytes. Curr Neurovasc Res. 2011;8:258-69.

[169] Abbott NJ, Hughes CC, Revest PA, Greenwood J. Development and characterisation of a rat brain capillary endothelial culture: towards an in vitro blood-brain barrier. J Cell Sci. 1992;103:23-37.

[170] Ichikawa N, Naora K, Hirano H, Hashimoto M, Masumura S, Iwamoto K. Isolation and primary culture of rat cerebral microvascular endothelial cells for studying drug transport in vitro. J Pharmacol Toxicol Methods. 1996;36:45-52.

[171] Abbott NJ, Dolman DEM, Drndarski S, Fredriksson SM. An Improved In Vitro Blood-Brain Barrier Model: Rat Brain Endothelial Cells Co-cultured with Astrocytes. In: Milner R, editor. Astrocytes: Methods and Protocols: Humana Press Inc, 999 Riverview Dr, Ste 208, Totowa, Nj 07512-1165 USA; 2012. p. 415-30.

[172] Nakagawa S, Deli MA, Kawaguchi H, Shimizudani T, Shimono T, Kittel A, et al. A new blood-brain barrier model using primary rat brain endothelial cells, pericytes and astrocytes. Neurochem Int. 2009;54:253-63.

[173] Hultman K, Bjorklund U, Hansson E, Jern C. Potentiating effect of endothelial cells on astrocytic plasminogen activator inhibitor type-1 gene expression in an in vitro model of the blood-brain barrier. Neuroscience. 2010;166:408-15.

[174] Hansson E, Westerlund A, Bjorklund U, Olsson T. mu-opioid agonists inhibit the enhanced intracellular Ca2+ responses in inflammatory activated astrocytes co-cultured with brain endothelial cells. Neuroscience. 2008;155:1237-49.

[175] Nakagawa S, Deli MA, Nakao S, Honda M, Hayashi K, Nakaoke R, et al. Pericytes from brain microvessels strengthen the barrier integrity in primary cultures of rat brain endothelial cells. Cell Mol Neurobiol. 2007;27:687-94.

[176] Xue Q, Liu Y, Qi HY, Ma Q, Xu L, Chen WH, et al. A Novel Brain Neurovascular Unit Model with Neurons, Astrocytes and Microvascular Endothelial Cells of Rat. Int J Biol Sci. 2013;9:174-89.

[177] Xu DH, Yan M, Li HD, Fang PF, Liu YW. Influence of P-glycoprotein on brucine transport at the in vitro blood-brain barrier. Eur J Pharmacol. 2012;690:68-76.

[178] Stanness KA, Westrum LE, Fornaciari E, Mascagni P, Nelson JA, Stenglein SG, et al. Morphological and functional characterization of an in vitro blood-brain barrier model. Brain Res. 1997;771:329-42.

[179] Toyoda K, Tanaka K, Nakagawa S, Thuy DHD, Ujifuku K, Kamada K, et al. Initial Contact of Glioblastoma Cells with Existing Normal Brain Endothelial Cells Strengthen the Barrier Function via Fibroblast Growth Factor 2 Secretion: A New In Vitro Blood-Brain Barrier Model. Cell Mol Neurobiol. 2013;33:489-501.

[180] Perriere N, Yousif S, Cazaubon S, Chaverot N, Bourasset F, Cisternino S, et al. A functional in vitro model of rat blood-brain barrier for molecular analysis of efflux transporters. Brain Res. 2007;1150:1-13.

[181] Demeuse P, Kerkhofs A, Struys-Ponsar C, Knoops B, Remacle C, de Aguilar PV. Compartmentalized coculture of rat brain endothelial cells and astrocytes: a syngenic model to study the blood-brain barrier. J Neurosci Methods. 2002;121:21-31.

[182] Lacombe O, Videau O, Chevillon D, Guyot AC, Contreras C, Blondel S, et al. In Vitro Primary Human and Animal Cell-Based Blood-Brain Barrier Models as a Screening Tool in Drug Discovery. Mol Pharm. 2011;8:651-63.

[183] Krizanac-Bengez L, Mayberg MR, Cunningham E, Hossain M, Ponnampalam S, Parkinson FE, et al. Loss of shear stress induces leukocyte-mediated cytokine release and blood-brain barrier failure in dynamic in vitro blood-brain barrier model. J Cell Physiol. 2006;206:68-77.

[184] Krizanac-Bengez L, Kapural M, Parkinson F, Cucullo L, Hossain M, Mayberg MR, et al. Effects of transient loss of shear stress on blood-brain barrier endothelium: role of nitric oxide and IL-6. Brain Res. 2003;977:239-46.

[185] Parkinson FE, Friesen J, Krizanac-Bengez L, Janigro D. Use of a three-dimensional in vitro model of the rat blood-brain barrier to assay nucleoside efflux from brain. Brain Res. 2003;980:233-41.

[186] Garberg P, Ball M, Borg N, Cecchelli R, Fenart L, Hurst RD, et al. In vitro models for the blood-brain barrier. Toxicol Vitro. 2005;19:299-334.

[187] Lippmann ES, Weidenfeller C, Svendsen CN, Shusta EV. Blood-brain barrier modeling with co-cultured neural progenitor cell-derived astrocytes and neurons. J Neurochem. 2011;119:507-20.

[188] Prabhakarpandian B, Shen MC, Nichols JB, Mills IR, Sidoryk-Wegrzynowicz M, Aschner M, et al. SyM-BBB: a microfluidic blood brain barrier model. Lab Chip. 2013;13:1093-101.

[189] Roux F, Durieu-Trautmann O, Chaverot N, Claire M, Mailly P, Bourre JM, et al. Regulation of gamma-glutamyl transpeptidase and alkaline phosphatase activities in immortalized rat brain microvessel endothelial cells. J Cell Physiol. 1994;159:101-13.

[190] Schiera G, Bono E, Raffa MP, Gallo A, Pitarresi GL, Di Liegro I, et al. Synergistic effects of neurons and astrocytes on the differentiation of brain capillary endothelial cells in culture. J Cell Mol Med. 2003;7:165-70.

[191] Schiera G, Sala S, Gallo A, Raffa MP, Pitarresi GL, Savettieri G, et al. Permeability properties of a three-cell type in vitro model of blood-brain barrier. J Cell Mol Med. 2005;9:373-9.

[192] Cestelli A, Catania C, D'Agostino S, Di Liegro I, Licata L, Schiera G, et al. Functional feature of a novel model of blood brain barrier: studies on permeation of test compounds. J Control Release. 2001;76:139-47.

[193] Ohtsuki S, Sato S, Yamaguchi H, Kamoi M, Asashima T, Terasaki T. Exogenous expression of claudin-5 induces barrier properties in cultured rat brain capillary endothelial cells. J Cell Physiol. 2007;210:81-6.

[194] Terasaki T, Nakashima E, Iizasa H, Hosoya K, Hattori K. Blood brain barrier reconstruction model prepared by cocultivation. 2001.

[195] Rubin LL, Hall DE, Porter S, Barbu K, Cannon C, Horner HC, et al. A cell culture model of the blood-brain barrier. J Cell Biol. 1991;115:1725-35.

[196] Bowman PD, Ennis SR, Rarey KE, Betz AL, Goldstein GW. Brain microvessel endothelial cells in tissue culture: a model for study of blood-brain barrier permeability. Ann Neurol. 1983;14:396-402.

[197] Rutten MJ, Hoover RL, Karnovsky MJ. Electrical resistance and macromolecular permeability of brain endothelial monolayer cultures. Brain Res. 1987;425:301-10.

[198] Letrent SP, Polli JW, Humphreys JE, Pollack GM, Brouwer KR, Brouwer KLR. P-glycoprotein-mediated transport of morphine in brain capillary endothelial cells. Biochem Pharmacol. 1999;58:951-7.

[199] van Bree JB, de Boer AG, Danhof M, Ginsel LA, Breimer DD. Characterization of an "in vitro" blood-brain barrier: effects of molecular size and lipophilicity on cerebrovascular endothelial transport rates of drugs. J Pharmacol Exp Ther. 1988;247:1233-9.

[200] Gumbleton M, Audus KL. Progress and limitations in the use of in vitro cell cultures to serve as a permeability screen for the blood-brain barrier. J Pharm Sci. 2001;90:1681-98.

[201] Pirro JP, Di Rocco RJ, Narra RK, Nunn AD. Relationship between in vitro transendothelial permeability and in vivo single-pass brain extraction. J Nucl Med. 1994;35:1514-9.

[202] Abbruscato TJ, Davis TP. Combination of hypoxia/aglycemia compromises in vitro blood-brain barrier integrity. J Pharmacol Exp Ther. 1999;289:668-75.

[203] Audus KL, Borchardt RT. Characterization of an in vitro blood-brain barrier model system for studying drug transport and metabolism. Pharm Res. 1986;3:81-7.

[204] Raub TJ, Kuentzel SL, Sawada GA. Permeability of bovine brain microvessel endothelial cells in vitro: barrier tightening by a factor released from astroglioma cells. Exp Cell Res. 1992;199:330-40.

[205] Wang W, Dentler WL, Borchardt RT. VEGF increases BMEC monolayer permeability by affecting occludin expression and tight junction assembly. Am J Physiol-Heart Circul Physiol. 2001;280:H434-H40.

[206] Smith KR, Borchardt RT. Permeability and mechanism of albumin, cationized albumin, and glycosylated albumin transcellular transport across monolayers of cultured bovine brain capillary endothelial cells. Pharm Res. 1989;6:466-73.

[207] Dehouck MP, Méresse S, Dehouck B, Fruchart JC, Cecchelli R. In vitro reconstituted blood-brain barrier. J Control Release. 1992;21:81-91.

[208] Cecchelli R, Dehouck B, Descamps L, Fenart L, Buee-Scherrer V, Duhem C, et al. In vitro model for evaluating drug transport across the blood-brain barrier. Adv Drug Deliv Rev. 1999;36:165-78.

[209] Dehouck MP, Meresse S, Delorme P, Fruchart JC, Cecchelli R. An easier, reproducible, and mass-production method to study the blood-brain barrier in vitro. J Neurochem. 1990;54:1798-801.

[210] Hamm S, Dehouck B, Kraus J, Wolburg-Buchholz K, Wolburg H, Risau W, et al. Astrocyte mediated modulation of blood-brain barrier permeability does not correlate with a loss of tight junction proteins from the cellular contacts. Cell Tissue Res. 2004;315:157-66.

[211] Dehouck MP, Dehouck B, Schluep C, Lemaire M, Cecchelli R. Drug transport to the brain: Comparison between in vitro and in vivo models of the blood-brain barrier. Eur J Pharm Sci. 1995;3:357-65.

[212] van der Sandt ICJ, Vos CMP, Nabulsi L, Blom-Roosemalen MCM, Voorwinden HH, de Boer AG, et al. Assessment of active transport of HIV protease inhibitors in various cell lines and the in vitro blood-brain barrier. Aids. 2001;15:483-91.

[213] Lundquist S, Renftel M, Brillault J, Fenart L, Cecchelli R, Dehouck MP. Prediction of drug transport through the blood-brain barrier in vivo: A comparison between two in vitro cell models. Pharm Res. 2002;19:976-81.

[214] Boveri M, Berezowski V, Price A, Slupek S, Lenfant AM, Benaud C, et al. Induction of blood-brain barrier properties in cultured brain capillary endothelial cells: Comparison between primary glial cells and C6 cell line. Glia. 2005;51:187-98.

[215] Helms HC, Madelung R, Waagepetersen HS, Nielsen CU, Brodin B. In vitro evidence for the brain glutamate efflux hypothesis: Brain endothelial cells cocultured with astrocytes display a polarized brain-to-blood transport of glutamate. Glia. 2012;60:882-93.

[216] Culot M, Lundquist S, Vanuxeem D, Nion S, Landry C, Delplace Y, et al. An in vitro blood-brain barrier model for high throughput (HTS) toxicological screening. Toxicol Vitro. 2008;22:799-811.

[217] Gaillard PJ, Voorwinden LH, Nielsen JL, Ivanov A, Atsumi R, Engman H, et al. Establishment and functional characterization of an in vitro model of the blood-brain barrier, comprising a co-culture of brain capillary endothelial cells and astrocytes. Eur J Pharm Sci. 2001;12:215-22.

[218] Helms HC, Brodin B. Generation of Primary Cultures of Bovine Brain Endothelial Cells and Setup of Cocultures with Rat Astrocytes. In: Milner R, editor. Cerebral Angiogenesis: Methods and Protocols: Humana Press Inc, 999 Riverview Dr, Ste 208, Totowa, Nj 07512-1165 USA; 2014. p. 365-82.

[219] Neuhaus J, Risau W, Wolburg H. Induction of blood-brain barrier characteristics in bovine brain endothelial cells by rat astroglial cells in transfilter coculture. Ann NY Acad Sci. 1991;633:578-80.

[220] Shah KK, Yang L, Abbruscato TJ. In Vitro Models of the Blood-Brain Barrier. In: Milner R, editor. Astrocytes: Methods and Protocols: Humana Press Inc, 999 Riverview Dr, Ste 208, Totowa, Nj 07512-1165 USA; 2012. p. 431-49.

[221] Colgan OC, Collins NT, FeTguson G, Murphy RP, BiTney YA, Cahill PA, et al. Influence of basolateral condition on the regulation of brain microvascular endothelial tight junction properties and barrier function. Brain Res. 2008;1193:84-92.

[222] Cucullo L, McAllister MS, Kight K, Krizanac-Bengez L, Marroni M, Mayberg MR, et al. A new dynamic in vitro model for the multidimensional study of astrocyte-endothelial cell interactions at the blood-brain barrier. Brain Res. 2002;951:243-54.

[223] Santaguida S, Janigro D, Hossain M, Oby E, Rapp E, Cucullo L. Side by side comparison between dynamic versus static models of blood-brain barrier in vitro: A permeability study. Brain Res. 2006;1109:1-13.

[224] Sobue K, Yamamoto N, Yoneda K, Hodgson ME, Yamashiro K, Tsuruoka N, et al. Induction of blood-brain barrier properties in immortalized bovine brain endothelial cells by astrocytic factors. Neurosci Res. 1999;35:155-64.

[225] Yazdanian M, Bormann BJ. Immortalized brain endothelial cells. 2000.

[226] Hoheisel D, Nitz T, Franke H, Wegener J, Hakvoort A, Tilling T, et al. Hydrocortisone reinforces the blood-brain properties in a serum free cell culture system. Biochem Bioph Res Co. 1998;247:312-5.

[227] Patabendige A, Skinner RA, Abbott NJ. Establishment of a simplified in vitro porcine blood-brain barrier model with high transendothelial electrical resistance. Brain Res. 2013;1521:1-15.

[228] Franke H, Galla HJ, Beuckmann CT. An improved low-permeability in vitro-model of the blood-brain barrier: transport studies on retinoids, sucrose, haloperidol, caffeine and mannitol. Brain Res. 1999;818:65-71.

[229] Patabendige A, Abbott NJ. Primary porcine brain microvessel endothelial cell isolation and culture. Curr Protoc Neurosci. 2014;69:3.27.1-3..17.

[230] Fischer S, Renz D, Schaper W, Karliczek GF. Effects of barbiturates on hypoxic cultures of brain derived microvascular endothelial cells. Brain Res. 1996;707:47-53.

[231] Franke H, Galla HJ, Beuckmann CT. Primary cultures of brain microvessel endothelial cells: a valid and flexible model to study drug transport through the blood-brain barrier in vitro. Brain Res Protoc. 2000;5:248-56.

[232] Fischer S, Wobben M, Kleinstuck J, Renz D, Schaper W. Effect of astroglial cells on hypoxia-induced permeability in PBMEC cells. Am J Physiol-Cell Physiol. 2000;279:C935-C44.

[233] Cantrill CA, Skinner RA, Rothwell NJ, Penny JI. An immortalised astrocyte cell line maintains the in vivo phenotype of a primary porcine in vitro blood-brain barrier model. Brain Res. 2012;1479:17-30.

[234] Malina KCK, Cooper I, Teichberg VI. Closing the gap between the in-vivo and in-vitro blood-brain barrier tightness. Brain Res. 2009;1284:12-21.

[235] Smith M, Omidi Y, Gumbleton M. Primary porcine brain microvascular endothelial cells: Biochemical and functional characterisation as a model for drug transport and targeting. J Drug Target. 2007;15:253-68.

[236] Bobilya DJ. A Model for Transport Studies of the Blood-Brain Barrier. Membrane Transporters in Drug Discovery and Development: Methods and Protocols: Humana Press Inc, 999 Riverview Dr, Ste 208, Totowa, Nj 07512-1165 USA; 2010. p. 149-63.

[237] Jeliazkova-Mecheva VV, Bobilya DJ. A porcine astrocyte/endothelial cell co-culture model of the blood-brain barrier. Brain Res Protoc. 2003;12:91-8.

[238] Thomsen LB, Burkhart A, Moos T. A Triple Culture Model of the Blood-Brain Barrier Using Porcine Brain Endothelial cells, Astrocytes and Pericytes. PLoS One. 2015;10:e0134765.

[239] Thanabalasundaram G, Schneidewind J, Pieper C, Galla HJ. The impact of pericytes on the blood-brain barrier integrity depends critically on the pericyte differentiation stage. Int J Biochem Cell Biol. 2011;43:1284-93.

[240] Teifel M, Friedl P. Establishment of the permanent microvascular endothelial cell line PBMEC/C1-2 from porcine brains. Exp Cell Res. 1996;228:50-7.

[241] Neuhaus W, Stessl M, Strizsik E, Bennani-Baiti B, Wirth M, Toegel S, et al. Blood-brain barrier cell line PBMEC/C1-2 possesses functionally active P-glycoprotein. Neurosci Lett. 2010;469:224-8.

[242] Neuhaus W, Lauer R, Oelzant S, Fringeli UP, Ecker GF, Noe CR. A novel flow based hollow-fiber blood-brain barrier in vitro model with immortalised cell line PBMEC/C1-2. J Biotechnol. 2006;125:127-41.

[243] Lauer R, Bauer R, Linz B, Pittner F, Peschek GA, Ecker G, et al. Development of an in vitro blood-brain barrier model based on immortalized porcine brain microvascular endothelial cells. Farmaco. 2004;59:133-7.

[244] Bernas MJ, Cardoso FL, Daley SK, Weinand ME, Campos AR, Ferreira AJG, et al. Establishment of primary cultures of human brain microvascular endothelial cells to provide an in vitro cellular model of the blood-brain barrier. Nat Protoc. 2010;5:1265-72.

[245] Kasa P, Pakaski M, Joo F, Lajtha A. Endothelial cells from human fetal brain microvessels may be cholinoceptive, but do not synthesize acetylcholine. J Neurochem. 1991;56:2143-6.

[246] Urich E, Lazic SE, Molnos J, Wells I, Freskgard PO. Transcriptional Profiling of Human Brain Endothelial Cells Reveals Key Properties Crucial for Predictive In Vitro Blood-Brain Barrier Models. PLoS One. 2012;7:e38149.

[247] Lippmann ES, Al-Ahmad A, Azarin SM, Palecek SP, Shusta EV. A retinoic acid-enhanced, multicellular human blood-brain barrier model derived from stem cell sources. Sci Rep. 2014;4:10.

[248] Cucullo L, Hossain M, Rapp E, Manders T, Marchi N, Janigro D. Development of a humanized in vitro blood-brain barrier model to screen for brain penetration of antiepileptic drugs. Epilepsia. 2007;48:505-16.

[249] Siddharthan V, Kim YV, Liu S, Kim KS. Human astrocytes/astrocyte-conditioned medium and shear stress enhance the barrier properties of human brain microvascular endothelial cells. Brain Res. 2007;1147:39-50.

[250] Mabondzo A, Bottlaender M, Guyot AC, Tsaouin K, Deverre JR, Balimane PV. Validation of In Vitro Cell-Based Human Blood Brain Barrier Model Using Clinical Positron Emission Tomography Radioligands To Predict In Vivo Human Brain Penetration. Mol Pharm. 2010;7:1805-15.

[251] Megard I, Garrigues A, Orlowski S, Jorajuria S, Clayette P, Ezan E, et al. A co-culture-based model of human blood-brain barrier: application to active transport of indinavir and in vivo-in vitro correlation. Brain Res. 2002;927:153-67.

[252] Kuo YC, Lu CH. Effect of human astrocytes on the characteristics of human brain-microvascular endothelial cells in the blood-brain barrier. Colloid Surf B-Biointerfaces. 2011;86:225-31.

[253] Weksler BB, Subileau EA, Perriere N, Charneau P, Holloway K, Leveque M, et al. Blood-brain barrier-specific properties of a human adult brain endothelial cell line. Faseb J. 2005;19:1872-4.

[254] Poller B, Gutmann H, Krahenbuhl S, Weksler B, Romero I, Couraud PO, et al. The human brain endothelial cell line hCMEC/D3 as a human blood-brain barrier model for drug transport studies. J Neurochem. 2008;107:1358-68.

[255] Cucullo L, Couraud PO, Weksler B, Romero IA, Hossain M, Rapp E, et al. Immortalized human brain endothelial cells and flow-based vascular modeling: a marriage of convenience for rational neurovascular studies. J Cereb Blood Flow Metab. 2008;28:312-28.

[256] Weksler B, Romero IA, Couraud P-O. The hCMEC/D3 cell line as a model of the human blood brain barrier. Fluids and barriers of the CNS. 2013;10:16.

[257] Eigenmann DE, Xue G, Kim KS, Moses AV, Hamburger M, Oufir M. Comparative study of four immortalized human brain capillary endothelial cell lines, hCMEC/D3, hBMEC, TY10, and BB19, and optimization of culture conditions, for an in vitro blood-brain barrier model for drug permeability studies. Fluids and barriers of the CNS. 2013;10:33.

[258] Couraud PO, Romero I, Weksler B. Human blood brain barrier model. 2006.

[259] Griep LM, Wolbers F, de Wagenaar B, ter Braak PM, Weksler BB, Romero IA, et al. BBB on chip: microfluidic platform to mechanically and biochemically modulate blood-brain barrier function. Biomed Microdevices. 2013;15:145-50.

[260] Dauchy S, Miller F, Couraud PO, Weaver RJ, Weksler B, Romero IA, et al. Expression and transcriptional regulation of ABC transporters and cytochromes P450 in hCMEC/D3 human cerebral microvascular endothelial cells. Biochem Pharmacol. 2009;77:897-909.

[261] Daniels BP, Cruz-Orengo L, Pasieka TJ, Couraud PO, Romero IA, Weksler B, et al. Immortalized human cerebral microvascular endothelial cells maintain the properties of primary cells in an in vitro model of immune migration across the blood brain barrier. J Neurosci Methods. 2013;212:173-9.

[262] Hatherell K, Couraud PO, Romero IA, Weksler B, Pilkington GJ. Development of a three-dimensional, all-human in vitro model of the blood-brain barrier using mono-, co-, and tri-cultivation Transwell models. J Neurosci Methods. 2011;199:223-9.

[263] Kusch-Poddar M, Drewe J, Fux I, Gutmann H. Evaluation of the immortalized human brain capillary endothelial cell line BB19 as a human cell culture model for the blood-brain barrier. Brain Res. 2005;1064:21-31.

[264] Ketabi-Kiyanvash N, Herold-Mende C, Kashfi F, Caldeira S, Tommasino M, Haefeli WE, et al. NKIM-6, a new immortalized human brain capillary endothelial cell line with conserved endothelial characteristics. Cell Tissue Res. 2007;328:19-29.

[265] Sano Y, Shimizu F, Abe M, Maeda T, Kashiwamura Y, Ohtsuki S, et al. Establishment of a New Conditionally Immortalized Human Brain Microvascular Endothelial Cell Line Retaining an In Vivo Blood-Brain Barrier Function. J Cell Physiol. 2010;225:519-28.

[266] Kamiichi A, Furihata T, Kishida S, Ohta Y, Saito K, Kawamatsu S, et al. Establishment of a new conditionally immortalized cell line from human brain microvascular endothelial cells: A promising tool for human blood-brain barrier studies. Brain Res. 2012;1488:113-22.

[267] Muruganandam A, Herx LM, Monette R, Durkin JP, Stanimirovic DB. Development of immortalized human cerebromicrovascular endothelial cell line as an in vitro model of the human blood-brain barrier. Faseb J. 1997;11:1187-97.

[268] Hellinger E, Veszelka S, Toth AE, Walter F, Kittel A, Bakk ML, et al. Comparison of brain capillary endothelial cell-based and epithelial (MDCK-MDR1, Caco-2, and VB-Caco-2) cell-based surrogate blood-brain barrier penetration models. Eur J Pharm Biopharm. 2012;82:340-51.

[269] Hakkarainen JJ, Jalkanen AJ, Kaariainen TM, Keski-Rahkonen P, Venalainen T, Hokkanen J, et al. Comparison of in vitro cell models in predicting in vivo brain entry of drugs. Int J Pharm. 2010;402:27-36.

[270] Zhang Y, Bachmeier C, Miller DW. In vitro and in vivo models for assessing drug efflux transporter activity. Adv Drug Deliv Rev. 2003;55:31-51.

[271] Pastan I, Gottesman MM, Ueda K, Lovelace E, Rutherford AV, Willingham MC. A retrovirus carrying an MDR1 cDNA confers multidrug resistance and polarized expression of P-glycoprotein in MDCK cells. P Natl Acad Sci USA. 1988;85:4486-90.

[272] Wang Q, Rager JD, Weinstein K, Kardos PS, Dobson GL, Li JB, et al. Evaluation of the MDR-MDCK cell line as a permeability screen for the blood-brain barrier. Int J Pharm. 2005;288:349-59.

[273] Hellinger E, Bakk ML, Pocza P, Karoly T, Vastag M. Drug penetration model of vinblastine-treated Caco-2 cultures. Eur J Pharm Sci. 2010;41:96-106.

[274] Lippmann ES, Azarin SM, Kay JE, Nessler RA, Wilson HK, Al-Ahmad A, et al. Derivation of blood-brain barrier endothelial cells from human pluripotent stem cells. Nat Biotechnol. 2012;30:783-91.

[275] James D, Nam HS, Seandel M, Nolan D, Janovitz T, Tomishima M, et al. Expansion and maintenance of human embryonic stem cell-derived endothelial cells by TGF beta inhibition is Id1 dependent. Nat Biotechnol. 2010;28:161-6.

[276] Levenberg S, Golub JS, Amit M, Itskovitz-Eldor J, Langer R. Endothelial cells derived from human embryonic stem cells. P Natl Acad Sci USA. 2002;99:4391-6.

[277] Choi KD, Yu J, Smuga-Otto K, Salvagiotto G, Rehrauer W, Vodyanik M, et al. Hematopoietic and Endothelial Differentiation of Human Induced Pluripotent Stem Cells. Stem Cells. 2009;27:559-67.

[278] Tilling T, Engelbertz C, Decker S, Korte D, Huwel S, Galla HJ. Expression and adhesive properties of basement membrane proteins in cerebral capillary endothelial cell cultures. Cell Tissue Res. 2002;310:19-29.

[279] He H, Li Y, Jia XR, Du J, Ying X, Lu WL, et al. PEGylated Poly(amidoamine) dendrimer-based dual-targeting carrier for treating brain tumors. Biomaterials. 2011;32:478-87.

[280] Li Y, He H, Jia XR, Lu WL, Lou JN, Wei Y. A dual-targeting nanocarrier based on poly(amidoamine) dendrimers conjugated with transferrin and tamoxifen for treating brain gliomas. Biomaterials. 2012;33:3899-908.

[281] Ying X, Wen H, Lu WL, Du J, Guo J, Tian W, et al. Dual-targeting daunorubicin liposomes improve the therapeutic efficacy of brain glioma in animals. J Control Release. 2010;141:183-92.

[282] Wolburg H, Neuhaus J, Kniesel U, Krauss B, Schmid EM, Ocalan M, et al. Modulation of tight junction structure in blood-brain barrier endothelial cells. Effects of tissue culture, second messengers and cocultured astrocytes. J Cell Sci. 1994;107:1347-57.

[283] Rist RJ, Romero IA, Chan MWK, Couraud PO, Roux F, Abbott NJ. F-actin cytoskeleton and sucrose permeability of immortalised rat brain microvascular endothelial cell monolayers: effects of cyclic AMP and astrocytic factors. Brain Res. 1997;768:10-8.

[284] Weidenfeller C, Schrot S, Zozulya A, Galla HJ. Murine brain capillary endothelial cells exhibit improved barrier properties under the influence of hydrocortisone. Brain Res. 2005;1053:162-74.

[285] Tian W, Ying X, Du J, Guo J, Men Y, Zhang Y, et al. Enhanced efficacy of functionalized epirubicin liposomes in treating brain glioma-bearing rats. Eur J Pharm Sci. 2010;41:232-43.

[286] Deli MA, Abraham CS, Kataoka Y, Niwa M. Permeability studies on in vitro blood-brain barrier models: Physiology, pathology, and pharmacology. Cell Mol Neurobiol. 2005;25:59-127.

[287] Urich E, Patsch C, Aigner S, Graf M, Iacone R, Freskgard PO. Multicellular Self-Assembled Spheroidal Model of the Blood Brain Barrier. Sci Rep. 2013;3:8.

[288] Kirkpatrick CJ, Fuchs S, Unger RE. Co-culture systems for vascularization - Learning from nature. Adv Drug Deliv Rev. 2011;63:291-9.

[289] Zehendner CM, Luhmann HJ, Kuhlmann CRW. Studying the neurovascular unit: an improved blood-brain barrier model. J Cereb Blood Flow Metab. 2009;29:1879-84.

[290] Chou CH, Sinden JD, Couraud PO, Modo M. In vitro modeling of the neurovascular environment by coculturing adult human brain endothelial cells with human neural stem cells. PLoS One. 2014;9:e106346.

[291] Cohen-Kashi Malina K, Cooper I, Teichberg VI. Closing the gap between the in-vivo and in-vitro blood-brain barrier tightness. Brain Res. 2009;1284:12-21.

[292] Cucullo L, Marchi N, Hossain M, Janigro D. A dynamic in vitro BBB model for the study of immune cell trafficking into the central nervous system. J Cereb Blood Flow Metab. 2011;31:767-77.

[293] Cucullo L, Hossain M, Puvenna V, Marchi N, Janigro D. The role of shear stress in Blood-Brain Barrier endothelial physiology. BMC Neurosci. 2011;12:15.

[294] Cucullo L, Hossain M, Tierney W, Janigro D. A new dynamic in vitro modular capillaries-venules modular system: Cerebrovascular physiology in a box. BMC Neurosci. 2013;14:12.

[295] Yeon JH, Na D, Choi K, Ryu SW, Choi C, Park JK. Reliable permeability assay system in a microfluidic device mimicking cerebral vasculatures. Biomed Microdevices. 2012;14:1141-8.

[296] Cho HS, Seo JH, Wong KHK, Terasaki Y, Park J, Bong K, et al. Three-Dimensional Blood-Brain Barrier Model for in vitro Studies of Neurovascular Pathology. Sci Rep. 2015;5:9.

[297] Kuo YC, Su FL. Transport of stavudine, delavirdine, and saquinavir across the blood-brain barrier by polybutylcyanoacrylate, methylmethacrylate-sulfopropylmethacrylate, and solid lipid nanoparticles. Int J Pharm. 2007;340:143-52.

[298] Kuo YC, Lee CL. Methylmethacrylate-sulfopropylmethacrylate nanoparticles with surface RMP-7 for targeting delivery of antiretroviral drugs across the blood-brain barrier. Colloid Surf B-Biointerfaces. 2012;90:75-82.

[299] Kuo YC, Chen HH. Effect of nanoparticulate polybutylcyanoacrylate and methylmethacrylate-sulfopropylmethacrylate on the permeability of zidovudine and lamivudine across the in vitro blood-brain barrier. Int J Pharm. 2006;327:160-9.

[300] Ye D, Raghnaill MN, Bramini M, Mahon E, Aberg C, Salvati A, et al. Nanoparticle accumulation and transcytosis in brain endothelial cell layers. Nanoscale. 2013;5:11153-65.

[301] Liu D, Lin BQ, Shao W, Zhu Z, Ji TH, Yang CY. In Vitro and in Vivo Studies on the Transport of PEGylated Silica Nanoparticles across the Blood-Brain Barrier. ACS Appl Mater Interfaces. 2014;6:2131-6.

[302] Hanada S, Fujioka K, Inoue Y, Kanaya F, Manome Y, Yamamoto K. Cell-Based in Vitro Blood-Brain Barrier Model Can Rapidly Evaluate Nanoparticles' Brain Permeability in Association with Particle Size and Surface Modification. Int J Mol Sci. 2014;15:1812-25.

[303] Etame AB, Smith CA, Chan WCW, Rutka JT. Design and potential application of PEGylated gold nanoparticles with size-dependent permeation through brain microvasculature. Nanomed-Nanotechnol Biol Med. 2011;7:992-1000.

[304] Hoff D, Sheikh L, Bhattacharya S, Nayar S, Webster TJ. Comparison study of ferrofluid and powder iron oxide nanoparticle permeability across the blood-brain barrier. Int J Nanomed. 2013;8:703-10.

[305] Kuo YC, Chung CY. Transcytosis of CRM197-grafted polybutylcyanoacrylate nanoparticles for delivering zidovudine across human brain-microvascular endothelial cells. Colloid Surf B-Biointerfaces. 2012;91:242-9.

[306] Garcia-Garcia E, Gil S, Andrieux K, Desmaele D, Nicolas V, Taran F, et al. A relevant in vitro rat model for the evaluation of blood-brain barrier translocation of nanoparticles. Cell Mol Life Sci. 2005;62:1400-8.

[307] Lu W, Wan J, She ZJ, Jiang XG. Brain delivery property and accelerated blood clearance of cationic albumin conjugated pegylated nanoparticle. J Control Release. 2007;118:38-53.

[308] Lu W, Tan YZ, Hu KL, Jiang XG. Cationic albumin conjugated pegylated nanoparticle with its transcytosis ability and little toxicity against blood-brain barrier. Int J Pharm. 2005;295:247-60.

[309] Gao HL, Yang Z, Zhang S, Pang ZQ, Liu QF, Jiang XG. Study and evaluation of mechanisms of dual targeting drug delivery system with tumor microenvironment assays compared with normal assays. Acta Biomater. 2014;10:858-67.

[310] Kratzer I, Wernig K, Panzenboeck U, Bernhart E, Reicher H, Wronski R, et al. Apolipoprotein A-I coating of protamine-oligonucleotide nanoparticles increases particle uptake and transcytosis in an in vitro model of the blood-brain barrier. J Control Release. 2007;117:301-11.

[311] Chaturvedi M, Molino Y, Sreedhar B, Khrestchatisky M, Kaczmarek L. Tissue inhibitor of matrix metalloproteinases-l loaded poly(lactic-co-glycolic acid) nanoparticles for delivery across the blood-brain barrier. Int J Nanomed. 2014;9:575-88.

[312] Xie FL, Yao N, Qin Y, Zhang QY, Chen HL, Yuan MQ, et al. Investigation of glucose-modified liposomes using polyethylene glycols with different chain lengths as the linkers for brain targeting. Int J Nanomed. 2012;7:163-75.

[313] Tian XH, Wei F, Wang TX, Wang P, Lin XN, Wang J, et al. In vitro and in vivo studies on gelatin-siloxane nanoparticles conjugated with SynB peptide to increase drug delivery to the brain. Int J Nanomed. 2012;7:1031-41.

[314] Xu G, Yong KT, Roy I, Mahajan SD, Ding H, Schwartz SA, et al. Bioconjugated quantum rods as targeted probes for efficient transmigration across an in vitro blood-brain barrier. Bioconjugate Chem. 2008;19:1179-85.

[315] Chen HL, Tang L, Qin Y, Yin YJ, Tang J, Tang WW, et al. Lactoferrin-modified procationic liposomes as a novel drug carrier for brain delivery. Eur J Pharm Sci. 2010;40:94-102.

[316] Qin Y, Fan W, Chen HL, Yao NA, Tang WW, Tang J, et al. In vitro and in vivo investigation of glucose-mediated brain-targeting liposomes. J Drug Target. 2010;18:536-49.

[317] Georgieva JV, Brinkhuis RP, Stojanov K, Weijers C, Zuilhof H, Rutjes F, et al. Peptide-Mediated Blood-Brain Barrier Transport of Polymersomes. Angew Chem-Int Edit. 2012;51:8339-42.

[318] Kuo YC, Shih-Huang CY. Solid lipid nanoparticles carrying chemotherapeutic drug across the blood-brain barrier through insulin receptor-mediated pathway. J Drug Target. 2013;21:730-8.

[319] Trapani A, De Giglio E, Cafagna D, Denora N, Agrimi G, Cassano T, et al. Characterization and evaluation of chitosan nanoparticles for dopamine brain delivery. Int J Pharm. 2011;419:296-307.

[320] Kuo YC, Ko HF. Targeting delivery of saquinavir to the brain using 83-14 monoclonal antibody-grafted solid lipid nanoparticles. Biomaterials. 2013;34:4818-30.

[321] Re F, Cambianica I, Zona C, Sesana S, Gregori M, Rigolio R, et al. Functionalization of liposomes with ApoE-derived peptides at different density affects cellular uptake and drug transport across a blood-brain barrier model. Nanomed-Nanotechnol Biol Med. 2011;7:551-9.

[322] Hemmelmann M, Metz VV, Koynov K, Blank K, Postina R, Zentel R. Amphiphilic HPMA-LMA copolymers increase the transport of Rhodamine 123 across a BBB model without harming its barrier integrity. J Control Release. 2012;163:170-7.

[323] Anand P, O'Neil A, Lin E, Douglas T, Holford M. Tailored delivery of analgesic ziconotide across a blood brain barrier model using viral nanocontainers. SciRep. 2015;5:10.

[324] Batrakova EV, Vinogradov SV, Robinson SM, Niehoff ML, Banks WA, Kabanov AV. Polypeptide point modifications with fatty acid and amphiphilic block copolymers for enhanced brain delivery. Bioconjugate Chem. 2005;16:793-802.

[325] Stojanov K, Georgieva JV, Brinkhuis RP, van Hest JC, Rutjes FP, Dierckx R, et al. In Vivo Biodistribution of Prion- and GM1-Targeted Polymersomes following Intravenous Administration in Mice. Mol Pharm. 2012;9:1620-7.

[326] Xie Y, Ye LY, Zhang XB, Cui W, Lou JN, Nagai T, et al. Transport of nerve growth factor encapsulated into liposomes across the blood-brain barrier: In vitro and in vivo studies. J Control Release. 2005;105:106-19.

[327] Liu Y, Huang RQ, Han L, Ke WL, Shao K, Ye LY, et al. Brain-targeting gene delivery and cellular internalization mechanisms for modified rabies virus glycoprotein RVG29 nanoparticles. Biomaterials. 2009;30:4195-202.

[328] Liu Y, Li JF, Shao K, Huang RQ, Ye LY, Lou JN, et al. A leptin derived 30-amino-acid peptide modified pegylated poly-L-lysine dendrigraft for brain targeted gene delivery. Biomaterials. 2010;31:5246-57.

[329] Xin HL, Jiang XY, Gu JJ, Sha XY, Chen LC, Law K, et al. Angiopep-conjugated poly(ethylene glycol)-co-poly(epsilon-caprolactone) nanoparticles as dual-targeting drug delivery system for brain glioma. Biomaterials. 2011;32:4293-305.

[330] Gao HL, Qian J, Cao SJ, Yang Z, Pang ZQ, Pan SQ, et al. Precise glioma targeting of and penetration by aptamer and peptide dual-functioned nanoparticles. Biomaterials. 2012;33:5115-23.

[331] Jiang XY, Xin HL, Ren QY, Gu JJ, Zhu LJ, Du FY, et al. Nanoparticles of 2-deoxy-D-glucose functionalized poly(ethylene glycol)-co-poly(trimethylene carbonate) for dual-targeted drug delivery in glioma treatment. Biomaterials. 2014;35:518-29.

[332] Gao JQ, Lv Q, Li LM, Tang XJ, Li FZ, Hu YL, et al. Glioma targeting and blood-brain barrier penetration by dual-targeting doxorubincin liposomes. Biomaterials. 2013;34:5628-39.

[333] Shi KR, Long Y, Xu CQ, Wang Y, Qiu Y, Yu QW, et al. Liposomes Combined an Integrin alpha(v)beta(3)-Specific Vector with pH-Responsible Cell-Penetrating Property for Highly Effective Antiglioma Therapy through the Blood-Brain Barrier. ACS Appl Mater Interfaces. 2015;7:21442-54.

[334] Zhang B, Sun XY, Mei H, Wang Y, Liao ZW, Chen J, et al. LDLR-mediated peptide-22-conjugated nanoparticles for dual-targeting therapy of brain glioma. Biomaterials. 2013;34:9171-82.

[335] Chen YC, Hsieh WY, Lee WF, Zeng DT. Effects of surface modification of PLGA-PEG-PLGA nanoparticles on loperamide delivery efficiency across the blood-brain barrier. J Biomater Appl. 2013;27:909-22.

[336] Du J, Lu WL, Ying X, Liu Y, Du P, Tian W, et al. Dual-Targeting Topotecan Liposomes Modified with Tamoxifen and Wheat Germ Agglutinin Significantly Improve Drug Transport across the Blood-Brain Barrier and Survival of Brain Tumor-Bearing Animals. Mol Pharm. 2009;6:905-17.

[337] Cui YN, Xu QX, Chow PKH, Wang DP, Wang CH. Transferrin-conjugated magnetic silica PLGA nanoparticles loaded with doxorubicin and paclitaxel for brain glioma treatment. Biomaterials. 2013;34:8511-20.

[338] Gong W, Wang ZY, Liu N, Lin W, Wang XP, Xu D, et al. Improving Efficiency of Adriamycin Crossing Blood Brain Barrier by Combination of Thermosensitive Liposomes and Hyperthermia. Biol Pharm Bull. 2011;34:1058-64.

[339] Wei XL, Zhan CY, Shen Q, Fu W, Xie C, Gao J, et al. A D-Peptide Ligand of Nicotine Acetylcholine Receptors for Brain-Targeted Drug Delivery. Angew Chem-Int Edit. 2015;54:3023-7.

[340] Hornok V, Bujdoso T, Toldi J, Nagy K, Demeter I, Fazakas C, et al. Preparation and properties of nanoscale containers for biomedical application in drug delivery: preliminary studies with kynurenic acid. J Neural Transm. 2012;119:115-21.

[341] Batrakova EV, Han HY, Miller DW, Kabanov AV. Effects of pluronic P85 unimers and micelles on drug permeability in polarized BBMEC and Caco-2 cells. Pharm Res. 1998;15:1525-32.

[342] Dhanikula RS, Hammady T, Hildgen P. On the Mechanism and Dynamics of Uptake and Permeation of Polyether-Copolyester Dendrimers Across an In Vitro Blood-Brain Barrier Model. J Pharm Sci. 2009;98:3748-60.

[343] Fehse S, Nowag S, Quadir M, Kim KS, Haag R, Multhaup G. Copper Transport Mediated by Nanocarrier Systems in a Blood-Brain Barrier In Vitro Model. Biomacromolecules. 2014;15:1910-9.

[344] Huang RQ, Ke WL, Han L, Liu Y, Shao K, Ye LY, et al. Brain-targeting mechanisms of lactoferrin-modified DNA-loaded nanoparticles. J Cereb Blood Flow Metab. 2009;29:1914-23.

[345] Xu ZJ, Wang Y, Ma ZY, Wang ZJ, Wei Y, Jia XR. A poly(amidoamine) dendrimer-based nanocarrier conjugated with Angiopep-2 for dual-targeting function in treating glioma cells. Polym Chem. 2016;7:715-21.

[346] Ke WL, Shao K, Huang RQ, Han L, Liu Y, Li JF, et al. Gene delivery targeted to the brain using an Angiopep-conjugated polyethyleneglycol-modified polyamidoamine dendrimer. Biomaterials. 2009;30:6976-85.

[347] Teow HM, Zhou ZY, Najlah M, Yusof SR, Abbott NJ, D'Emanuele A. Delivery of paclitaxel across cellular barriers using a dendrimer-based nanocarrier. Int J Pharm. 2013;441:701-11.

[348] Gil ES, Li JS, Xiao HN, Lowe TL. Quaternary Ammonium beta-Cyclodextrin Nanoparticles for Enhancing Doxorubicin Permeability across the In Vitro Blood-Brain Barrier. Biomacromolecules. 2009;10:505-16.

[349] Gil ES, Wu LF, Xu LC, Lowe TL. beta-Cyclodextrin-poly(beta-Amino Ester) Nanoparticles for Sustained Drug Delivery across the Blood-Brain Barrier. Biomacromolecules. 2012;13:3533-41.

[350] Hombach J, Bernkop-Schnurch A. Chitosan solutions and particles: Evaluation of their permeation enhancing potential on MDCK cells used as blood brain barrier model. Int J Pharm. 2009;376:104-9.

[351] Trapani A, Denora N, Iacobellis G, Sitterberg J, Bakowsky U, Kissel T. Methotrexate-Loaded Chitosan- and Glycolchitosan-Based Nanoparticles: A Promising Strategy for the Administration of the Anticancer Drug to Brain Tumors. AAPS PharmSciTech. 2011;12:1302-11.

[352] Lopalco A, Ali H, Denora N, Rytting E. Oxcarbazepine-loaded polymeric nanoparticles: development and permeability studies across in vitro models of the blood-brain barrier and human placental trophoblast. Int J Nanomed. 2015;10:1985-96.

[353] Xin HL, Sha XY, Jiang XY, Chen LC, Law K, Gu JJ, et al. The brain targeting mechanism of Angiopep-conjugated poly(ethylene glycol)-co-poly(epsilon-caprolactone) nanoparticles. Biomaterials. 2012;33:1673-81.

[354] Guarnieri D, Falanga A, Muscetti O, Tarallo R, Fusco S, Galdiero M, et al. Shuttle-Mediated Nanoparticle Delivery to the Blood-Brain Barrier. Small. 2013;9:853-62.

[355] Ragnaill MN, Brown M, Ye D, Bramini M, Callanan S, Lynch I, et al. Internal benchmarking of a human blood-brain barrier cell model for screening of nanoparticle uptake and transcytosis. Eur J Pharm Biopharm. 2011;77:360-7.

[356] Georgieva JV, Kalicharan D, Couraud PO, Romero IA, Weksler B, Hoekstra D, et al. Surface Characteristics of Nanoparticles Determine Their Intracellular Fate in and Processing by Human Blood-Brain Barrier Endothelial Cells In Vitro. Mol Ther. 2011;19:318-25.

[357] Brun E, Carriere M, Mabondzo A. In vitro evidence of dysregulation of blood-brain barrier function after acute and repeated/long-term exposure to TiO2 nanoparticles. Biomaterials. 2012;33:886-96.

[358] Wagner S, Kufleitner J, Zensi A, Dadparvar M, Wien S, Bungert J, et al. Nanoparticulate Transport of Oximes over an In Vitro Blood-Brain Barrier Model. PLoS One. 2010;5:e14213.

[359] Dadparvar M, Wagner S, Wien S, Kufleitner J, Worek F, von Briesen H, et al. HI 6 human serum albumin nanoparticles-Development and transport over an in vitro blood-brain barrier model. Toxicol Lett. 2011;206:60-6.

[360] Kafa H, Wang JTW, Rubio N, Venner K, Anderson G, Pach E, et al. The interaction of carbon nanotubes with an in vitro blood-brain barrier model and mouse brain in vivo. Biomaterials. 2015;53:437-52.

[361] Shityakov S, Salvador E, Pastorin G, Forster C. Blood-brain barrier transport studies, aggregation, and molecular dynamics simulation of multiwalled carbon nanotube functionalized with fluorescein isothiocyanate. Int J Nanomed. 2015;10:1703-13.

[362] Sharma G, Modgil A, Sun CW, Singh J. Grafting of Cell-Penetrating Peptide to Receptor-Targeted Liposomes Improves their Transfection Efficiency and Transport across Blood-Brain Barrier Model. J Pharm Sci. 2012;101:2468-78.

[363] Saiyed ZM, Gandhi NH, Nair MPN. Magnetic nanoformulation of azidothymidine 5 '-triphosphate for targeted delivery across the blood-brain barrier. Int J Nanomed. 2010;5:157-66.

[364] Ding H, Sagar V, Agudelo M, Pilakka-Kanthikeel S, Atluri VSR, Raymond A, et al. Enhanced blood-brain barrier transmigration using a novel transferrin embedded fluorescent magneto-liposome nanoformulation. Nanotechnology. 2014;25:1-14.

[365] Pinzon-Daza ML, Garzon R, Couraud PO, Romero IA, Weksler B, Ghigo D, et al. The association of statins plus LDL receptor-targeted liposome-encapsulated doxorubicin increases in vitro drug delivery across blood-brain barrier cells. Br J Pharmacol. 2012;167:1431-47.

[366] Salvati E, Re F, Sesana S, Cambianica I, Sancini G, Masserini M, et al. Liposomes functionalized to overcome the blood-brain barrier and to target amyloid-beta peptide: the chemical design affects the permeability across an in vitro model. Int J Nanomed. 2013;1749-1758:10.

[367] Markoutsa E, Pampalakis G, Niarakis A, Romero IA, Weksler B, Couraud PO, et al. Uptake and permeability studies of BBB-targeting immunoliposomes using the hCMEC/D3 cell line. Eur J Pharm Biopharm. 2011;77:265-74.

[368] Markoutsa E, Papadia K, Clemente C, Flores O, Antimisiaris SG. Anti-A beta-MAb and dually decorated nanoliposomes: Effect of A beta 1-42 peptides on interaction with hCMEC/D3 cells. Eur J Pharm Biopharm. 2012;81:49-56.

[369] Al-Shehri A, Favretto ME, Ioannou PV, Romero IA, Couraud PO, Weksler BB, et al. Permeability of PEGylated Immunoarsonoliposomes Through In Vitro Blood Brain Barrier-Medulloblastoma Co-culture Models for Brain Tumor Therapy. Pharm Res. 2015;32:1072-83.

[370] Bana L, Minniti S, Salvati E, Sesana S, Zambelli V, Cagnotto A, et al. Liposomes bi-functionalized with phosphatidic acid and an ApoE-derived peptide affect A beta aggregation features and cross the blood-brain-barrier: Implications for therapy of Alzheimer disease. Nanomed-Nanotechnol Biol Med. 2014;10:1583-90.

[371] Qin J, Yang X, Zhang RX, Luo YX, Li JL, Hou J, et al. Monocyte mediated brain targeting delivery of macromolecular drug for the therapy of depression. Nanomed-Nanotechnol Biol Med. 2015;11:391-400.

[372] Kuo YC, Chen HH. Effect of electromagnetic field on endocytosis of cationic solid lipid nanoparticles by human brain-microvascular endothelial cells. J Drug Target. 2010;18:447-56.

[373] Cheng KK, Chan PS, Fan SJ, Kwan SM, Yeung KL, Wang YXJ, et al. Curcumin-conjugated magnetic nanoparticles for detecting amyloid plaques in Alzheimer's disease mice using magnetic resonance imaging (MRI). Biomaterials. 2015;44:155-72.

[374] Fiandra L, Colombo M, Mazzucchelli S, Truffi M, Santini B, Allevi R, et al. Nanoformulation of antiretroviral drugs enhances their penetration across the blood brain barrier in mice. Nanomed-Nanotechnol Biol Med. 2015;11:1387-97.

[375] Dan M, Cochran DB, Yokel RA, Dziubla TD. Binding, Transcytosis and Biodistribution of Anti-PECAM-1 Iron Oxide Nanoparticles for Brain-Targeted Delivery. PLoS One. 2013;8:e81051.

[376] Kenzaoui BH, Bernasconi CC, Hofmann H, Juillerat-Jeanneret L. Evaluation of uptake and transport of ultrasmall superparamagnetic iron oxide nanoparticles by human brain-derived endothelial cells. Nanomedicine. 2012;7:39-53.

[377] Sun ZZ, Worden M, Wroczynskyj Y, Yathindranath V, van Lierop J, Hegmann T, et al. Magnetic field enhanced convective diffusion of iron oxide nanoparticles in an osmotically disrupted cell culture model of the blood-brain barrier. Int J Nanomed. 2014;9:3013-26.

[378] Sagar V, Pilakka-Kanthikeel S, Atluri VSR, Ding H, Arias AY, Jayant RD, et al. Therapeutical Neurotargeting via Magnetic Nanocarrier: Implications to Opiate-Induced Neuropathogenesis and NeuroAIDS. J Biomed Nanotechnol. 2015;11:1722-33.

[379] Jayant RD, Atluri VSR, Agudelo M, Sagar V, Kaushik A, Nair M. Sustained-release nanoART formulation for the treatment of neuroAIDS. Int J Nanomed. 2015;10:1077-93.

[380] Pilakka-Kanthikeel S, Atluri VSR, Sagar V, Saxena SK, Nair M. Targeted Brain Derived Neurotropic Factors (BDNF) Delivery across the Blood-Brain Barrier for Neuro-Protection Using Magnetic Nano Carriers: An In-Vitro Study. PLoS One. 2013;8:e62241.

[381] Qiao RR, Jia QJ, Huwel S, Xia R, Liu T, Gao FB, et al. Receptor-Mediated Delivery of Magnetic Nanoparticles across the Blood-Brain Barrier. Acs Nano. 2012;6:3304-10.

[382] Thomsen LB, Linemann T, Pondman KM, Lichota J, Kim KS, Pieters RJ, et al. Uptake and Transport of Superparamagnetic Iron Oxide Nanoparticles through Human Brain Capillary Endothelial Cells. ACS Chem Neurosci. 2013;4:1352-60.

[383] Gromnicova R, Davies HA, Sreekanthreddy P, Romero IA, Lund T, Roitt IM, et al. Glucose-Coated Gold Nanoparticles Transfer across Human Brain Endothelium and Enter Astrocytes In Vitro. PLoS One. 2013;8:e81043.

[384] Yin TT, Yang LC, Liu YN, Zhou XB, Sun J, Liu J. Sialic acid (SA)-modified selenium nanoparticles coated with a high blood-brain barrier permeability peptide-B6 peptide for potential use in Alzheimer's disease. Acta Biomater. 2015;25:172-83.

[385] Kerns EH, Di L, Petusky S, Farris M, Ley R, Jupp P. Combined application of parallel artificial membrane permeability assay and Caco-2 permeability assays in drug discovery. J Pharm Sci. 2004;93:1440-53.

[386] Mc Carthy DJ, Malhotra M, O'Mahony AM, Cryan JF, O'Driscoll CM. Nanoparticles and the Blood-Brain Barrier: Advancing from In-Vitro Models Towards Therapeutic Significance. Pharm Res. 2015;32:1161-85.

Cannabidiol-targeted lipid nanocapsules across the blood-brain barrier: in vitro and in vivo evaluation

Juan Aparicio-Blanco, Ignacio A. Romero, David K. Male, Karla Slowing, Luis García, Ana I. Torres-Suárez

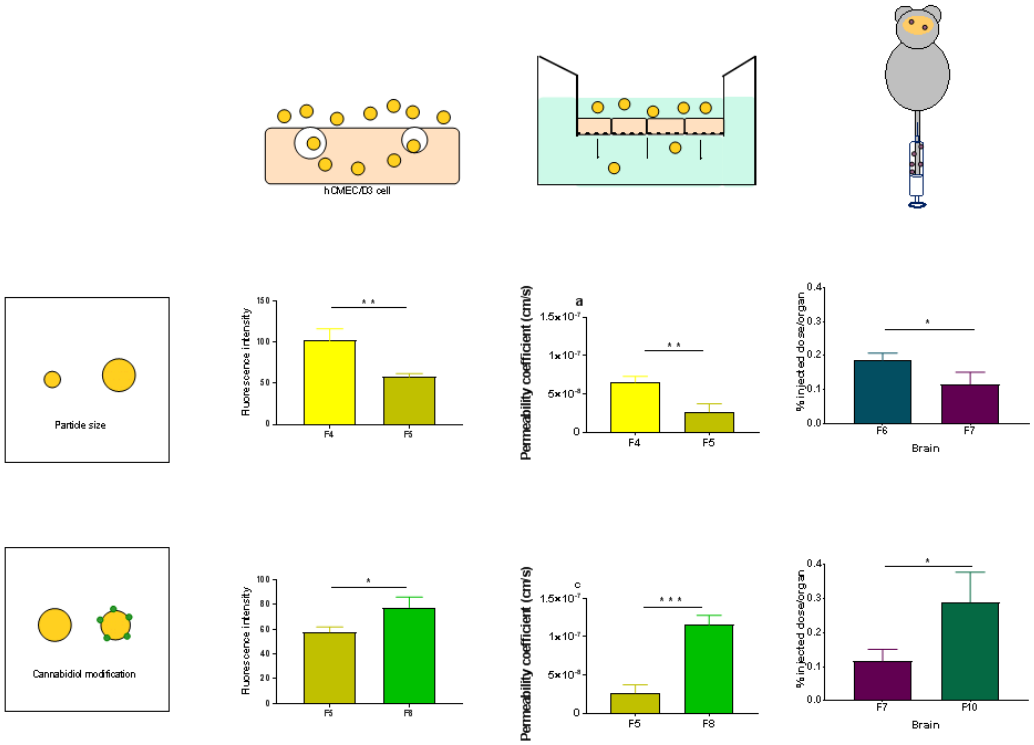

Cannabidiol-targeted lipid nanocapsules across the blood-brain barrier: *in vitro* and *in vivo* evaluation

Juan Aparicio-Blanco [a,b], Ignacio A. Romero [b], David K. Male [b], Karla Slowing [c], Luis García [c], Ana I. Torres-Suárez [a, d]

[a] Department of Pharmaceutics and Food Technology, Complutense University, Madrid, Spain

[b] School of Life, Health and Chemical Sciences, Faculty of Science, The Open University, Milton Keynes, United Kingdom

[c] Department of Pharmacology, Pharmacognosy and Botany, Complutense University, Madrid, Spain

[d] University Institute of Industrial Pharmacy, Complutense University, Madrid, Spain

Abstract

Diseases affecting the central nervous system (CNS) should be regarded as a major health challenge due to their steadily rising incidences and to the current lack of effective treatments given the hindrance to brain drug delivery imposed by the blood-brain barrier (BBB). Nanomedicine holds great promise to enhance the passage across the BBB. Since efficient brain targeting should not solely rely on passive targeting, brain active targeting of nanomedicines into the CNS is being explored.

The present study is devoted to the development of lipid nanocapsules (LNCs) decorated with non-psychotropic cannabinoids as pioneering non-immunogenic brain targeting molecules and to the evaluation of their brain targeting ability both in vitro and in vivo. Noticeably, both the permeability experiments across the hCMEC/D3 cell-based in vitro BBB model and the biodistribution experiments in mice consistently demonstrated that the highest brain targeting ability was achieved with the smallest-sized cannabinoid-modified LNCs. As the transport efficiency across the BBB certainly determines the efficacy of the treatments for brain disorders, small cannabinoid-decorated LNCs represent auspicious platforms for the design and development of novel therapies for CNS diseases.

Keywords

Cannabidiol, brain targeting, central nervous system, in vitro BBB model, permeability, nanomedicine

1. Introduction

According to the Mental health: new understanding, new hope report by the World Health Organization, one in four people will be affected by mental or neurological disorders at some point in their lives, with approximately 450 million people worldwide currently suffering from such conditions. These prevalence data are expected to increase further due to the increase in life expectancy, emphasizing the need to face diseases affecting the central nervous system (CNS) as a major health challenge of the twenty-first century [1]. Unfortunately, the efficacy of the current standard of care for these diseases remains questionable in most cases, since the blood-brain barrier (BBB) truly hinders the distribution to the CNS of the vast majority of drug substances administered systemically. In consequence, high doses are often required to achieve therapeutically meaningful levels in the CNS, and this causes severe toxicity to peripheral tissues. Therefore, there is a dire need for developing effective strategies of brain drug delivery that overcome biodistribution and pharmacokinetic limitations that account for treatment failure [2-4].

The BBB consists of the endothelial cell monolayer of the brain capillaries closely associated with pericytes and astrocytes and is physiologically responsible for the maintenance of CNS homeostasis. The key features of the brain endothelium that account for the severe restriction to brain drug delivery are both the lack of fenestrations and the presence of tight intercellular junctions [5]. Some of the described delivery strategies to circumvent the BBB such as the direct intracerebral administration [6] and the artificial disruption of the tight junctions by chemical or physical stimuli [7] involve high risk of neurological damage. Hence, every effort is currently being devoted to achieving efficient transport across the brain endothelium with targeted drug carriers following minimally-invasive intravenous injection.

In this regard, the use of nanocarriers arises as an alternative to enhance the passage across the BBB [8]. Noticeably, given their low toxicity, biocompatibility and biodegradability, the clinical trials launched heretofore for the treatment of brain conditions with nanomedicines mostly evaluate lipid-based nanocarriers [9]. Since one major feature that certainly influences the in vivo performance of nanomedicines is particle size, a size-controlled extravasation at the target site based on pathophysiological features has traditionally been sought. Nonetheless, although the paracellular permeability of the brain endothelium is altered in most CNS diseases, the BBB dysfunction is typically only substantial in advanced stages of disease and in the most affected sites [10, 11]. Therefore, efficient brain targeting of nanomedicines should not solely rely on passive targeting. To remedy this shortcoming, brain active targeting is being explored with the purpose of boosting transcellularly the delivery efficiency across the BBB [12].

Brain active targeting is based on the modification of nanocarriers with moieties capable of triggering receptor-mediated transcytosis into the CNS through specific binding with endogenous transporters overexpressed on the brain endothelium. Remarkably, the transcytotic mechanisms that mediate the internalization of nanocarriers often follow a size-dependent pattern within the range 10-100 nm. In

these cases, a fine control on particle size will certainly improve their potential therapeutic outcome. Various receptors highly expressed on the cerebral endothelial cells (such as transferrin receptor [13, 14], nicotinic acetylcholine receptor [15, 16], low-density lipoprotein receptor [17, 18] and glucose transporter [19, 20]) have been utilized to develop brain active targeting strategies. However, the translational impact of brain active targeting in clinical trials remains modest, as only three out of the eight liposomes that have made their way to clinical trials for distinct brain conditions following intravenous administration are actively-targeted (ClinicalTrials.gov identifiers: NCT01386580, NCT02048358 and NCT02340156). This is greatly due to the flaws that currently available targeting moieties have: on the one hand, the use of physiological ligands as targeting moieties can develop competitive phenomena with their endogenous counterparts and consequently dysregulate brain homeostasis; whereas on the other hand, the use of targeting peptides must ensure non-immunogenicity [12]. Hence, novel brain targeting moieties are strongly needed.

Since any ligand for which a receptor exists on the cerebral endothelial cells may be potentially used for brain targeting, research on innovative exogenous non-immunogenic ligands are likely to thrive in the near future. In this regard, we hypothesized that cannabinoids hold great promise for brain active targeting. In particular, cannabidiol (CBD), the main phytocannabinoid devoid of psychotropic effects with high BBB transcytosis efficacy, is the appropriate lead candidate to test the possibilities of this hypothesis. Effectively, this cannabinoid has been postulated to bind to various receptors located on the brain endothelium environment [21], namely the CB_1-receptor [22], the serotonin receptor 5-HT_{1A} [23], the transient potential vanilloid receptor type-1 (TPVR-1) [24], the G protein-coupled receptor 55 (GPR55) [25], the adenosine A_{2A} receptor [26] and the dopamine receptor D_2 [27].

On account of the aforementioned considerations, the present study is devoted to the development of CBD-decorated lipid nanocapsules (LNCs) and to the evaluation of their brain targeting ability both in vitro and in vivo. LNCs were selected on the grounds of their high drug loading, their kinetic stability and the energetically efficient features of their formulation procedure (the phase inversion temperature (PIT) method). Cell viability, uptake and permeability experiments were conducted on the human brain endothelial cell line hCMEC/D3. The in vitro permeability coefficients across the hCMEC/D3 monolayer were validated with in vivo data from biodistribution studies in mice. Both the role played by particle size and functionalization with CBD in the extent of passage across the BBB was evaluated.

2. Materials and methods

2.1. Materials

Labrafac lipophile® WL 1349 (caprylic-capric acid triglycerides) was kindly supplied by Gattefossé. Kolliphor® HS15 ($C_{18}E_{15}$ polyethylene glycol (15) 12-hydroxystearate) was a gift from BASF. Lipoid® S75 (soybean lecithin with 70% of phosphatidylcholine) was supplied by Lipoid-Gmbh. NaCl was purchased from Panreac. De-ionized water was obtained from a MilliQ® Purification System. The fluorescent dyes 3,3'-dioctadecyloxacarbocyanine perchlorate (DiO) and 1,1′-

dioctadecyl-3,3,3′,3′-tetramethylindodicarbocyanine 4-chlorobenzenesulfonate salt (DiD) were purchased from Invitrogen Molecular Probes. Cannabidiol (CBD) was provided by THC-Pharma. Endothelial Cell Basal Medium-2 (EBM-2) and culture supplements were purchased from Lonza. Dulbecco's Modified Eagle Medium (DMEM) devoid of phenol red was provided by Gibco. Tetramethyl-rhodamine-isothiocyanate–dextran, type I collagen from calf skin, fibronectin from bovine plasma, Hank's Balanced Salt Solution (HBSS), 3-(4,5-dimethyl-2-thiazolyl)-2,5-diphenyl-2H-tetrazolium bromide (MTT), dimethyl-sulfoxide (DMSO) and sterile Nunc Lab-Tek® chamber slides (8 wells, Permanox® slide, 0.8 cm^2/well) were purchased from Sigma-Aldrich. Vectashield® mounting medium with DAPI (H-1200) was provided by Vector Laboratories. Sterile Millicell® Hanging Cell Culture Inserts were supplied by Millipore (12-well culture plates; membrane: polyethylene terephthalate membrane; pore size: 1.0 μm; membrane surface area: 1.1 cm^2).

2.2. Cell line

The human brain endothelial hCMEC/D3 cells were seeded in collagen-coated flasks and cultured in EBM-2 medium supplemented with 2.5% foetal bovine serum (FBS), 0.025% (v/v) rhEGF, 0.025% (v/v) VEGF 0.025% IGF, 0.1% (v/v) rhFGF, 0.1% (v/v) gentamycin, 0.1% (v/v) ascorbic acid and 0.04% (v/v) hydrocortisone at 37ºC in 95% air and 5% CO_2. For all experiments, cells between passage 25 and 30 were used.

2.3. Animals

Male ICR mice, aging 4-5 weeks and weighting 29 ± 3 g, were purchased from Envigo. The mice were housed in ventilated cages with free water and food in a 12h dark/light cycle. Animals were acclimated for one week before the experiment. All in vivo experiments were approved by the Ethics Committee of the Community of Madrid (Ref. PROEX 111/14) and conducted according to Spanish and European guidelines (Directive 86/609/EEC).

2.4. Preparation and characterization of lipid nanocapsules

2.4.1. Blank lipid nanocapsules (F1, F2, F3)

Lipid nanocapsules (LNCs) were prepared by the phase inversion temperature (PIT) method. Succinctly, Labrafac lipophile® WL 1349,Kolliphor® HS15, Lipoid® S75, NaCl and water were mixed under magnetic stirring and progressively heated over the phase inversion temperature of the system. Subsequently, the mixture was gradually cooled down until the phase inversion temperature was reached. Then, a sudden quench with cold water (5 mL) was performed to obtain the final suspension of LNCs. By varying the relative proportions of the excipients, formulations of blank LNCs indifferent sizes were prepared.

2.4.2. Fluorescently-labeled lipid nanocapsules (F4, F5, F6, F7)

The fluorescent dyes DiO and DiD were encapsulated in LNCs for particle tracking purposes in in vitro and in vivo experiments, respectively. To prepare the dye-

loaded LNCs, the fluorescent dye was firstly dissolved in the oily phase that constitute the core of the LNCs at a weight ratio of 15 mg of dye/ g of Labrafac lipophile® WL1349. Then, the remaining excipients were added and progressively heated and cooled down around the phase inversion temperature as indicated in 2.4.1.

2.4.3. Lipid nanocapsules decorated with cannabidiol (CBD) (F8, F9, F10, F11)

Pre-formed fluorescently-labeled LNCs were incubated with a CBD solution (15 mg/mL) in a 3:1 (v/v) ratio. The mixture was gently stirred overnight until complete solvent evaporation. The contribution of the solvent itself to the size distribution of LNCs was ruled out by incubating LNCs with pure solvent up to above the 3:1 (v/v) ratio.

The detailed excipient weight for each group of LNCs is shown in Table 1: blank LNCs (F1-F3), fluorescently-labelled LNCs (F4-F7), CBD-decorated LNCs (F8-F11). The mean volume diameter and polydispersity index (PdI) of each formulation were measured by dynamic light scattering (DLS) using a Microtrac® Zetatrac™ Analyzer (Microtrac Inc., USA). Measurements were done in triplicate.

Excipient	F1	F2	F3	F4	F5	F6	F7	F8	F9	F10	F11
Kolliphor® HS15	1934	846	484	1934	846	1934	846	645	282	645	282
Lipoid® S75	75	75	75	75	75	75	75	25	25	25	25
NaCl	89	89	89	89	89	89	89	30	30	30	30
Labrafac lipophile® WL 1349	846	1028	1209	846	1028	846	1028	282	343	282	343
Water	6056	6962	7143	6056	6962	6056	6962	2018	2320	2018	2320
DiO	-	-	-	12	15	-	-	4	5	-	-
DiD	-	-	-	-	-	12	15	-	-	4	5
CBD	-	-	-	-	-	-	-	15	15	15	15

Table 2.2.1: Detailed excipient weight (in mg) for each formulation of LNC in final suspension.

2.5. *In vitro* cytotoxicity

LNCs (formulations 1-3) were assessed for cytotoxicity against hCMEC/D3 cells using a MTT assay. Briefly, hCMEC/D3 cells were seeded into collagen-coated 96-well plates at a density of 2×10^4 cells/well. After cells had been confluent for 48 hours, they were treated with suspensions of LNCs (200 µL) for 1, 4 and 24 hours in three different experiments. Then, the medium was removed and 60 µL of MTT solution (1 mg/mL) in complete EBM-2 were added to each well and incubated for 4 hours. Afterwards, the media containing MTT was removed and 100 µL of DMSO was added to each well. The plates were agitated for 10 minutes and the absorbance was measured at 570 nm using a microplate reader (FLUOstar Omega, BMG Labtech). Experiments were

performed in triplicate at each time-point. hCMEC/D3 cells without treatment served as control. Cell viability of each group was expressed as a percentage relative to that of control.

2.6. *In vitro* cellular uptake

2.6.1 Uptake experiments evaluated by flow cytometry

To quantitatively evaluate the BBB targeting ability of LNCs *in vitro*, hCMEC/D3 cells were seeded into collagen-coated 6-well plates at a density of 3 x 10^5 cells/well. After cells had been confluent for 48 hours, the culture medium was replaced by DiO-labeled LNCs (F4, F5, F8 and F9 at an equivalent dye concentration of 1.65 µg DiO/mL of suspension) suspended in complete EBM-2 (2 mL) wherewith cells were incubated for 4 and 24 hours in two different experiments. Then, cells were rinsed with HBSS, trypsinized and finally resuspended in 0.3 mL HBSS. The fluorescence intensity of cells treated with fluorescent-LNCs was analyzed with a flow cytometer (FACScalibur, BD Biosciences). Experiments were performed in triplicate at each time-point. hCMEC/D3 cells treated with blank LNCs served as control. Cellular uptake of each group was expressed as fold-increase in fluorescence mean relative to that of control after correction for the different amount of dye per individual LNC in each formulation.

2.6.2. Uptake experiments evaluated by laser scanning confocal microscopy

To qualitatively illustrate the BBB targeting ability of LNCs *in vitro*, hCMEC/D3 cells were seeded into collagen- and fibronectin-coated chamber slides at a density of 3 x 10^4 cells/well. After cells had been confluent for 48 hours, the culture medium was replaced by DiO-labeled LNCs (F5 and F9 at an equivalent dye concentration of 1.65 µg DiO/mL of suspension) suspended in complete EBM-2 (0.3 mL) wherewith cells were incubated for 24 hours. Then, cells were rinsed with HBSS and mounted with Vectashield® with DAPI mounting medium. The cells were then observed with a laser scanning confocal microscope (Leica SP5, 405 nm for DAPI, 488 nm for DiO) using LEICA LAS AF software. hCMEC/D3 cells treated with blank LNCs served as control. 3D imaging reconstruction was performed by means of IMARIS software.

2.7. Monolayer integrity in the presence of lipid nanocapsules

An *in vitro* BBB model with the human cerebral endothelial cell line hCMEC/D3 was established. Succinctly, hCMEC/D3 cells were seeded into collagen- and fibronectin-coated 12-well hanging cell culture inserts at confluence and incubated for 72 hours in complete EBM-2. The monolayer integrity was assessed by determining the permeability coefficient across the hCMEC/D3 monolayer of the hydrophilic tracer tetramethyl-rhodamine-isothiocyanate–dextran (TRITC-dextran, MW 150 kDa) both in the presence and the absence of LNCs. Briefly, 400 µL of a TRITC-dextran solution (2 mg/mL) in DMEM without phenol red supplemented with 0.1% (v/v) FBS were added in the apical chamber of both cell-seeded and non-seeded inserts, whereas 1.2 mL of fresh DMEM without phenol red supplemented with 0.1% (v/v) FBS were added in the receptor chamber. At 2, 4, 6, 8, 12 and 24 hours, 200 µL from the basolateral compartment were sampled and replaced with fresh medium. At 24 hours, the apical compartment was likewise sampled (100 µL). The concentration of TRITC-dextran was determined using a microplate reader (FLUOstar Omega, BMG Labtech, excitation

wavelength: 544 nm, emission wavelength: 590 nm). The concentrations at the different time points were used to define a linear region within which the permeability coefficients can be calculated [28]. The apparent permeability coefficients were calculated using Equation 1:

$$P_{app}(^{cm}/_{S}) = -\frac{V_D * V_A}{A * t(V_D + V_A)} \ln\left(1 - \frac{(V_D + V_A)}{V_D} \frac{C_A(t)}{C_D(0)}\right)$$ (Equation 2.2.1)

where $C_D(0)$ is the TRITC-dextran concentration placed in the donor compartment at the beginning of the experiment; $C_D(t)$ and C_A (t) are the sample concentrations after the incubation time has elapsed in the donor and acceptor compartment, respectively; t is the time; A is the surface area of the filter insert, and V_D and V_A are the volume of buffer solution in the donor and acceptor compartment, respectively.

To calculate the effective TRITC-dextran permeability (P_{eff}), the contribution of the insert support to the overall resistance was included as detailed in Equation 2:

$$\frac{1}{A * P_{eff}^{hCMEC/D3\ monolayer}} = \frac{1}{A * P_{app}^{cell+filter}} - \frac{1}{A * P_{app}^{filter}}$$ (Equation 2.2.2)

where A is the surface area of the filter insert, $P_{eff}^{monolayer}$ stands for the effective permeability solely due to the hCMEC/D3 monolayer, $P_{app}^{cell+filter}$ is the apparent permeability calculated for the cell-seeded inserts and P_{app}^{filter} is the apparent permeability calculated for the filters with no cells. Experiments were done in triplicate.

2.8. Transport of LNCs across the hCMEC/D3 monolayer *in vitro*

After having established the *in vitro* BBB model with hCMEC/D3 cell line as described in 2.7, 400 µL of a suspension of DiO fluorescently-labeled LNCs (F4, F5, F8 and F9 at an equivalent dye concentration of 1.65 µg DiO/mL of suspension) in DMEM without phenol red supplemented with 0.1% (v/v) FBS were added in the apical chamber of both cell-seeded and non-seeded inserts, whereas 1.2 mL of fresh DMEM without phenol red supplemented with 0.1% (v/v) FBS were added in the receptor chamber. At 2, 4, 6, 8, 12 and 24 hours, 200 µL from the basolateral compartment were sampled and replaced with fresh medium. At 24 hours, the apical compartment was likewise sampled (100 µL). The concentration of DiO was determined using a microplate reader (FLUOstar Omega, BMG Labtech, excitation wavelength: 485 nm, emission wavelength: 520 nm). These concentrations were used to calculate the effective permeability coefficients (P_{eff}) as described in 2.7. Only in those cases wherein less than 90% of the DiO dose was recovered between both apical and basolateral chambers, was Equation 1 replaced by Equation 3 to take the retention factor (R) into account:

$$P_{app}(^{cm}/_{S}) = -\frac{V_D * V_A}{A * t(V_D + V_A)} \ln\left(1 - \frac{(V_D + V_A)}{V_D} \frac{C_A(t)}{(1-R) * C_D(0)}\right)$$ (Equation 2.2.3)

2.9. Biodistribution of LNCs in healthy mice

The tissue biodistribution of LNCs was investigated in healthy mice. The mice (n=4-5 per group) were injected via the tail vein with 150 µL of different DiD-fluorescently-labeled LNCs (F6, F7, F10, F11). Ninety minutes (for all formulations) and

four hours (for F6 and F10) after administration, mice were sacrificed and the brain, liver, spleen, kidneys, lungs, heart and blood were collected and homogenized in 3-fold volume of ethanol for dye extraction. The concentration of DiD was measured using a microplate reader (Varioskan Flash, Thermo Scientific, excitation wavelength: 644 nm, emission wavelength: 665 nm). Results were expressed as percentage of the injected dose per organ.

2.10. Statistical analysis

All experiments were done at least in triplicate and all data are expressed as mean ± SD. Unpaired Student's t test was used for two-group analysis. Statistical significance was fixed as *:p<0.05, **:p<0.01,***:p<0.001. All the data were analyzed using the GraphPad Prism 7 software.

3. Results

3.1. Preparation and characterization of lipid nanocapsules

Figure 2.2.1: Characterization of the size distribution of the eleven formulations of LNCs: blank (F1-F3), fluorescently-labeled (F4-F7) and CBD-decorated (F8-F11). (a) Average volume diameter (nm). (b) Polydispersity index (PdI).

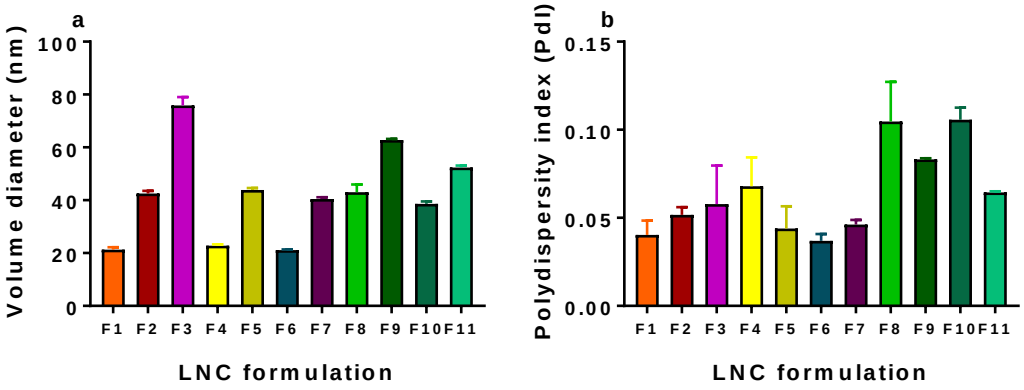

Eleven different formulations of LNCs were prepared by the PIT method by varying their relative proportions of excipients as detailed in Table 1. The size distribution of all LNC batches is thoroughly described in Figure 1, both in terms of mean volume diameter (Figure 1a) and polydispersity index (Figure 1b). In all cases, monodisperse nanocapsules were obtained within the size range 20-80 nm. In particular, we obtained monodisperse blank LNCs of 20 nm (F1), 40 nm (F2) and 80 nm (F3). Noticeably, the inclusion of fluorescent dyes did not significantly vary the size distribution of their blank counterparts: after loading F1 and F2 with fluorescent dyes, we obtained analogously-sized LNCs: 20 nm (F4 and F6 for DiO and DiD, respectively) and 40 nm (F5 and F7 for DiO and DiD, respectively). However, the modification of LNCs with CBD significantly altered their average volume diameter: the decoration of dye-loaded LNCs with CBD increased the particle size to 40 nm (F8 and F10) and 55 nm (F9 and F11), respectively. This increase in particle size was solely due to the presence of the cannabinoid, since the contribution of the solvent was ruled out

following incubation of LNCs with the pure solvent at the same ratio (Figure S1). Hence, on the one hand, the role played by particle size in the BBB targeting properties will be assessed separately in non-modified LNCs and in CBD-decorated LNCs, and on the other hand, the influence of CBD-decoration will be evaluated for equally-sized LNCs.

3.2. *In vitro* cytotoxicity

To determine the most suitable size of LNCs for conducting the *in vitro* experiments with the hCMEC/D3 monolayer, an MTT assay was used. Blank LNCs in three different sizes (20 nm –F1-, 40 nm –F2- and 80 nm –F3-) were tested. In a first experiment, we normalized the concentration of LNC according to the number of LNC per mL of suspension. The number of LNC in suspension was calculated using equation 4 (taken from [29] with minor modifications):

$$N = \frac{\frac{m_{Lab}}{d_{Lab}} + \frac{km_{Kol}}{d_{Kol}} + \frac{m_{Lip}}{d_{Lip}}}{\frac{4}{3}\pi r_V^3} \quad \text{(Equation 2.2.4)}$$

where m_{Lab}, m_{Kol} and m_{Lip} are the excipient weights of Labrafac lipophile® WL 1349, Kolliphor® HS15 and Lipoid® S75, respectively, as detailed in Table 1. Similarly, d_{Lab}, d_{Kol} and d_{Lip} represent the respective densities of each of the excipients and were obtained from suppliers (d_{Lab} = 1.048 g/mL, d_{Kol} = 0.945 g/mL and d_{Lip} = 1 g/mL). k refers to the percentage of poly glycol esters present in Kolliphor® HS15 and involved in the formulation procedure (k= 70% as declared by supplier).

Figure 2.2.2: In vitro cytotoxicity of LNCs against hCMEC/D3 cells at different time points. (a) 20 nm- (F1), 40 nm- (F2) and 80 nm-(F3) sized LNCs in suspension at a concentration of 10^{13} LNCs; (b) 20 nm- (F1) and 40 nm- (F2) sized LNCs in suspension at an equivalent DiO concentration of 1.65 µg DiO/mL (p>0.05).

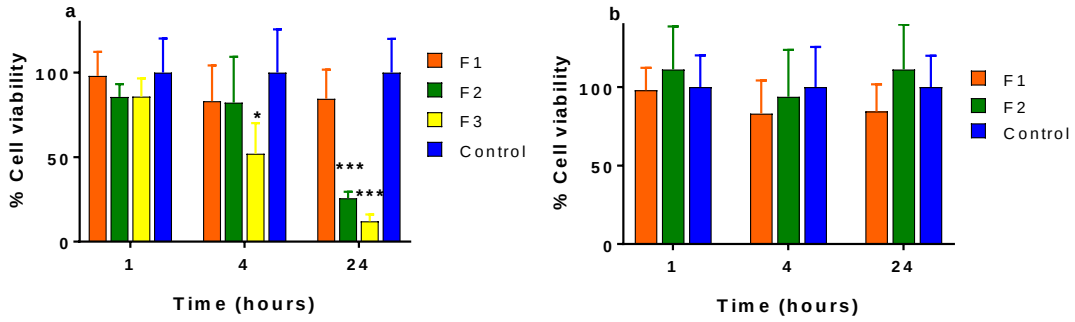

Consistently, hCMEC/D3 cells were incubated with a suspension of 10^{13} LNCs/mL for 1h, 4h and 24 hours. Whereas none of the formulations of LNCs showed significant cytotoxicity at the earliest time point (p>0.05), F2 exhibited substantial toxicity at 24 hours and F3 started causing significant toxicity already at 4 hours (Figure 2a). As particle size progressively increases from F1 to F3, we concluded that LNCs show a size-dependent toxicity pattern on hCMEC/D3 cells. Nevertheless, to be able to evaluate the role played by particle size on BBB-targeting in subsequent experiments, we only ruled out the biggest particles (F3). In a subsequent experiment, we evaluate

the cytotoxicity of F1 and F2-LNCs at an equivalent concentration of 110 µg of internal oily phase/mL of nanocapsule suspension to ultimately normalize the *in vitro* studies as a function of the different payloads (fluorescent dye) (Figure 2b). Remarkably, in this case no toxicity was observed for any of the LNCs at any time point ($p>0.05$). Therefore, these two formulations at these non-toxic concentrations (that correspond to an equivalent concentration of 1.65 µg of DiO/mL for the fluorescently-labeled LNCs) were used henceforth for all subsequent *in vitro* experiments.

3.3. *In vitro* cellular uptake

Figure 2.2.3: Evaluation of the *in vitro* cellular uptake of LNCs by flow cytometry expressed as folds increase in mean fluorescence intensity versus control. (a) Quantitative analysis of cellular uptake of DiO-fluorescently labeled LNCs (F4, F5, F8, and F9) after 4 and 24 hours incubation. (b) Evaluation of the role of particle size on the *in vitro* cellular uptake (non-modified LNCs) at 4 and 24 hours (***: $p<0.001$ and **: $p<0.01$, respectively). (c) Evaluation of the role of particle size on the *in vitro* cellular uptake (CBD-decorated LNCs) at 4 and 24 hours (***: $p<0.001$ and **: $p<0.01$, respectively). (d) Evaluation of the role of cannabinoids on the *in vitro* cellular uptake (equally-sized LNCs) at 4 and 24 hours (***: $p<0.001$ and *: $p<0.05$, respectively).

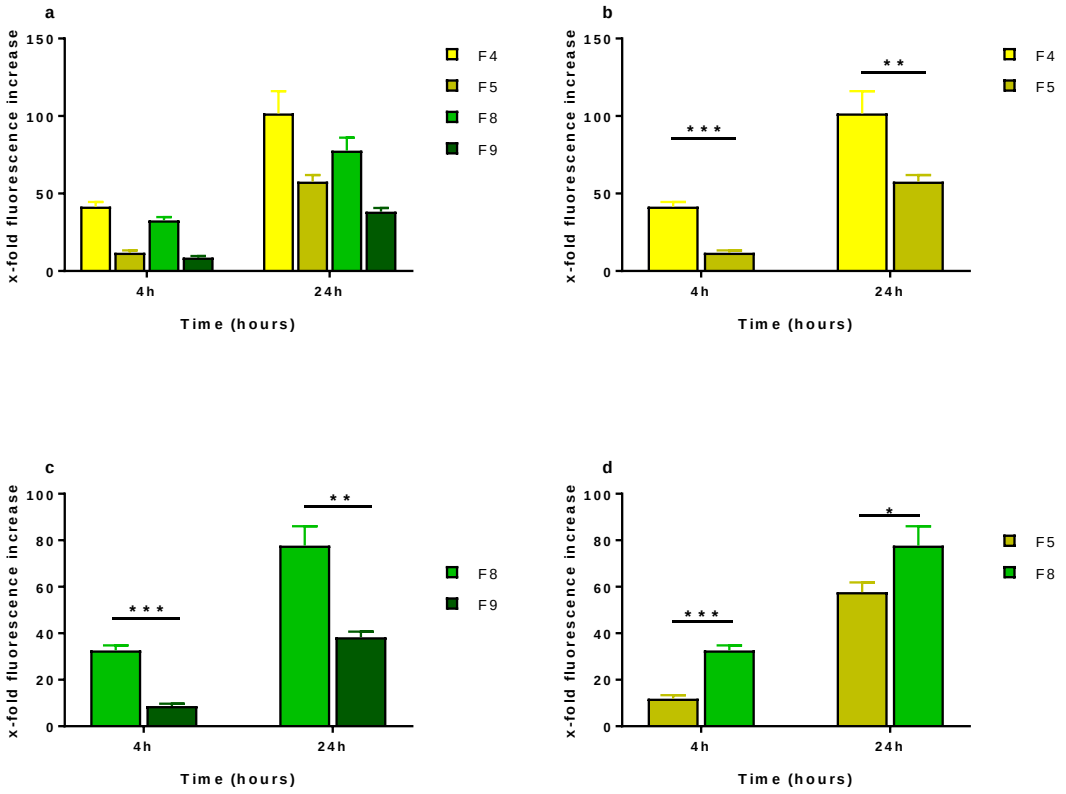

The BBB targeting ability of DiO-labeled LNCs (F4, F5, F8 and F9 at an equivalent dye concentration of 1.65 µg DiO/mL of suspension) was tested *in vitro*. Both the role played by particle size (F4 vs F5; F8 vs F9) and functionalization with cannabinoids (F5 vs F8) in the extent of *in vitro* cellular uptake was quantitatively evaluated. The quantitative analysis of the data obtained with the flow cytometer at 4

and 24 hours is shown in Figure 3a. All formulations tested exhibited a time-dependent cellular uptake with higher fluorescence intensities after incubating hCMEC/D3 cells with LNCs for 24 hours (**: $p<0.01$). Likewise, a consistent comparison of the role played by particle size can be drawn for non-modified LNCs (Figure 3b) and for CBD-decorated LNCs (Figure 3c). In both cases the smaller the particle size, the higher the cellular uptake and the ensuing BBB targeting ability (**: $p<0.01$). Interestingly, the modification with CBD also enhanced the *in vitro* BBB targeting properties of LNC, as it was concluded from a comparison of equally-sized non-modified and CBD-decorated LNCs (Figure 3d, *: $p<0.05$). The aforementioned results were obtained at 4 and 24 hours, demonstrating that the trends in cellular uptake were steady throughout the period evaluated.

Figure 2.2.4: Evaluation of the *in vitro* cellular uptake of LNCs by laser scanning confocal microscopy: DAPI (left), DiO (center), merged (right). (a) Blank LNCs (F2). (b) DiO-labeled LNCs (F5). (c) CBD-decorated DiO-labeled LNCs (F9). Scale bar = 25 μm. 3D video reconstructions from the Z-stack projections are available as Supplementary material.

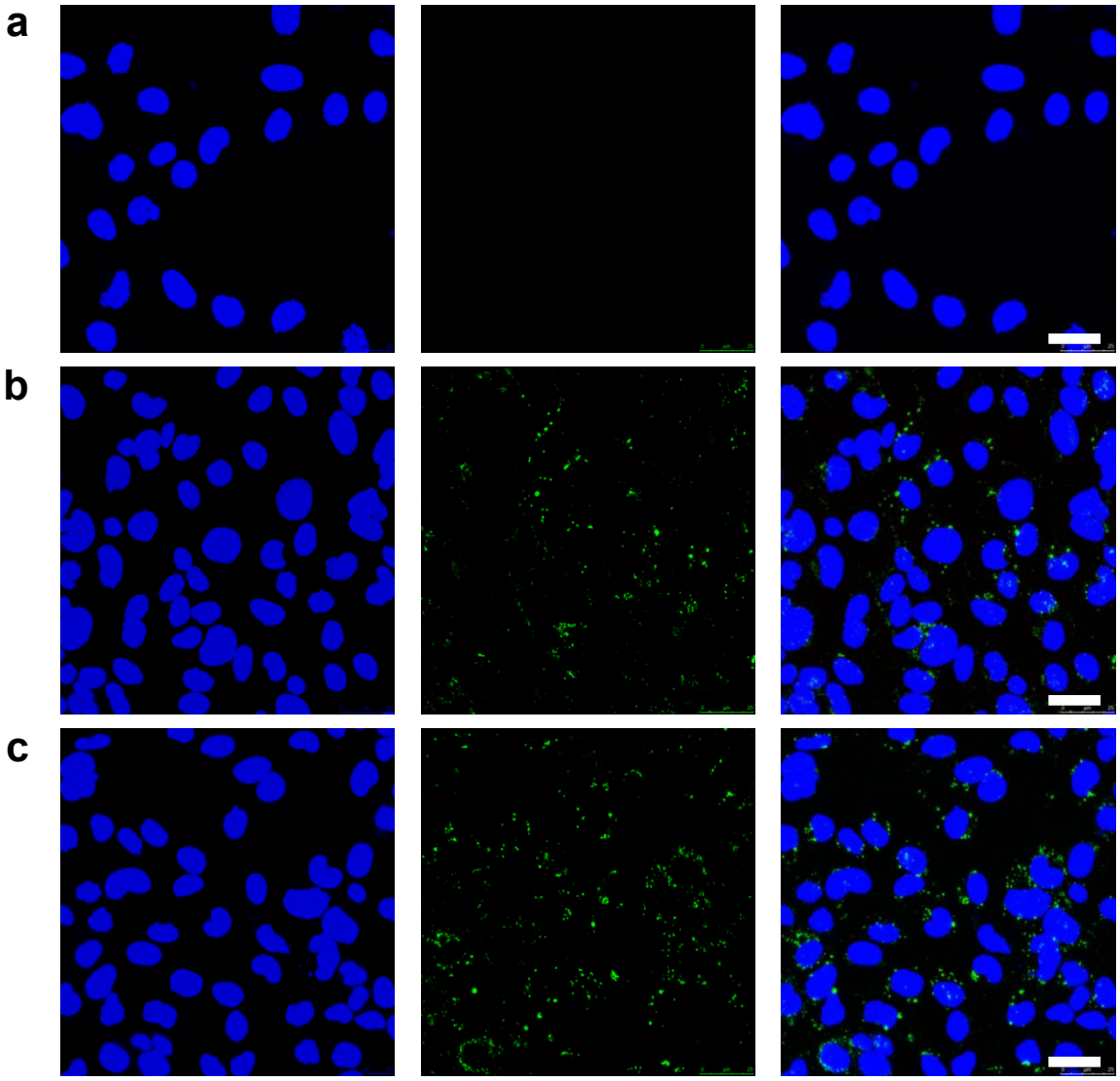

In the case of F5 and F9, the *in vitro* BBB targeting ability of LNCs was further evidenced qualitatively by laser scanning confocal microscopy. As shown in Figure 4,

both unmodified and CBD-decorated LNCs were internalized by hCMEC/D3 in accordance with the data obtained by flow cytometry. The 3D video reconstruction performed by means of the IMARIS software with the Z-stack projections helped evidence that the fluorescent signal from LNCs localized in the intracellular compartment of the cerebral endothelial cells, preferentially in the perinuclear region (Supplementary material).

3.4. Monolayer integrity of the in vitro BBB model in the presence of LNCs

The *in vitro* BBB model with a monolayer of hCMEC/D3 was established (Figure 5a). The effect of LNCs on the integrity of confluent cerebral endothelial cell monolayers was investigated by determining the permeability coefficient of fluorescent TRITC-dextran (Figure 5b). Importantly, there were no statistically significant differences between the calculated permeability coefficients of TRITC-dextran in the presence and the absence of LNCs ($p>0.05$). Consequently, it was concluded that, during the period evaluated, LNCs did not significantly alter the monolayer properties of hCMEC/D3 cells. These results ultimately enabled the paracellular contribution to the ensuing *in vitro* transport experiments of LNCs across the monolayer to be ruled out during at least 24 hours.

Figure 2.2.5: Evaluation of the monolayer integrity of the *in vitro* BBB model upon exposure to LNCs. (a) Scheme of the *in vitro* BBB model with the monolayer of hCMEC/D3 cells. (b) Permeability coefficients of TRITC-dextran across the *in vitro* BBB model calculated after 24 hours both in the presence and the absence of LNCs ($p>0.05$).

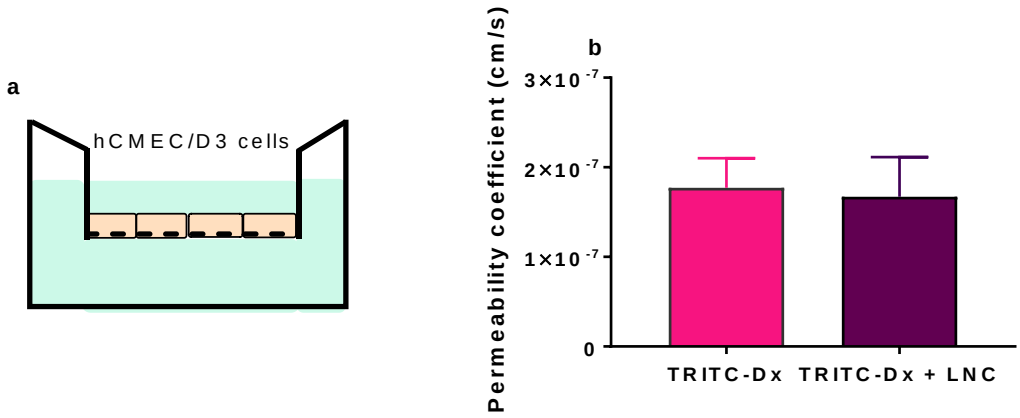

3.5. Transport of LNCs across the hCMEC/D3 monolayer *in vitro*

The BBB transcytosis ability of DiO-labeled LNCs (F4, F5, F8 and F9 at an equivalent dye concentration of 1.65 µg DiO/mL of suspension) was tested *in vitro*. Similarly to the experimental design followed to evidence the cellular uptake, both the role played by particle size (F4 vs F5; F8 vs F9) and functionalization with cannabinoids (F5 vs F8) in the permeability coefficient of LNCs across the hCMEC/D3 monolayer were quantitatively analyzed. In line with the results obtained for cellular uptake, a consistent comparison of the role played by particle size can be drawn for non-modified LNCs (Figure 6a) and for CBD-decorated LNCs (Figure 6b). In both

cases the smaller the particle size, the higher the permeability coefficient across the hCMEC/D3 monolayer and the ensuing BBB transcytosis ability (**: p<0.01). Likewise, as expected from the cellular uptake results, the comparison of equally-sized non-modified and CBD-decorated LNCs revealed that the modification with CBD also enhanced the permeability coefficients of LNCs (Figure 6c, ***: p<0.001).

Figure 2.2.6: Evaluation of the influence of different factors on the *in vitro* permeability of LNCs across the hCMEC/D3 monolayer. (a) Influence of particle size on permeability coefficients (non-modified LNCs) (**: p<0.01). (b) Influence of particle size on permeability coefficients (CBD-decorated LNCs) (***: p<0.001). (c) Influence of the modification with CBD on permeability coefficients (equally-sized LNCs) (***: p<0.001).

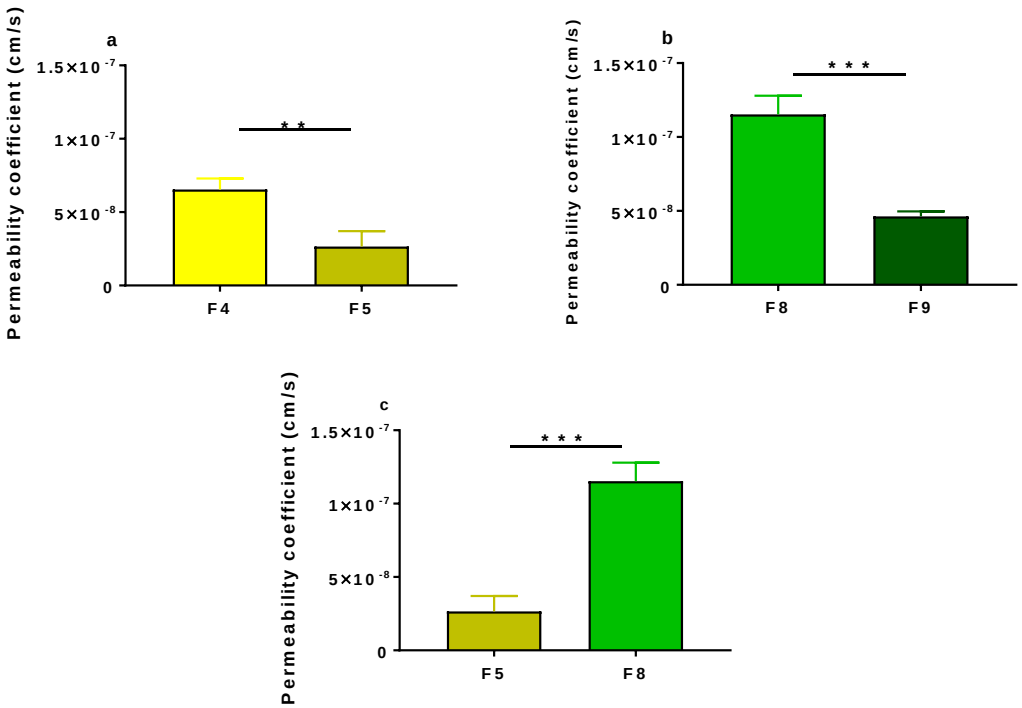

3.6. Biodistribution of LNCs in healthy mice

The BBB targeting properties of DiD-labeled LNCs (F6, F7, F10, F11) were tested *in vivo*. We determined the percentage of the injected dose of the different DiD-labeled LNCs located in each organ (namely, blood, brain, lungs, kidneys, heart, spleen and liver) following intravenous injection. The blood was estimated to represent 6% of the mice weight to calculate the total percentage of the LNC dose existing in this compartment. As occurred with cellular uptake and transport across the *in vitro* BBB model, both the role played by particle size (F6 vs F7; F10 vs F11) and functionalization with CBD (F7 vs F10) in the extent of *in vivo* brain targeting was quantitatively evaluated. The percentages of injected dose in all organs but for the brain are shown in Figure 7. Particle size certainly influences the *in vivo* biodistribution of LNCs: smaller nanocapsules achieved significantly higher plasma levels; whereas bigger LNCs were recognized to a higher extent by the reticuloendothelial organs (liver and spleen). These size-dependent results were consistently obtained both with non-modified LNCs (Figure 7a) and with CBD-decorated LNCs (Figure 7b). Alternatively,

the modification of LNCs with CBD helped extend their plasma levels and concomitantly reduced the extent of removal by the liver (Figure 7c).

Figure 2.2.7: *In vivo* biodistribution of DiD-labeled LNCs in healthy mice 90 minutes after their intravenous injection (expressed as percentage of the injected dose per organ; namely, blood, lungs, kidneys, heart, spleen and liver). (a) Influence of particle size on biodistribution (non-modified LNCs). (b) Influence of particle size on biodistribution (CBD-decorated LNCs). (c) Influence of the modification with CBD on biodistribution (equally-sized LNCs).

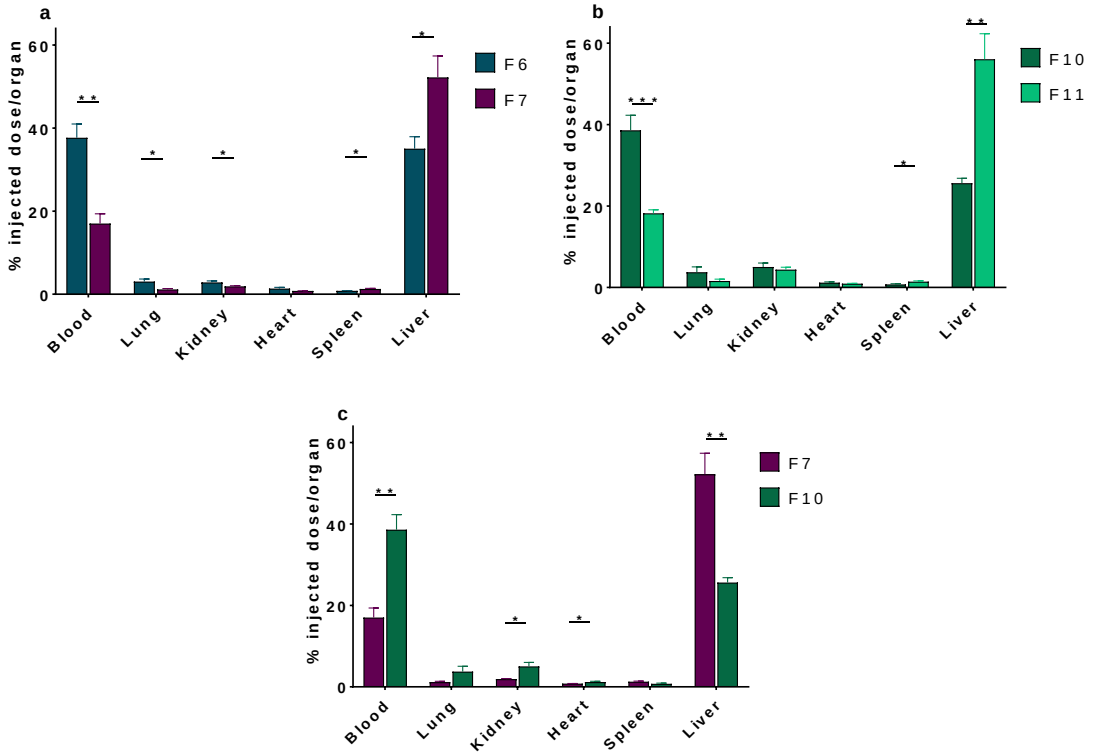

The percentage of the injected dose distributed into the brain in each case is shown in Figure 8. In accordance with the results obtained *in vitro*, both particle size and modification with CBD played a pivotal role in *in vivo* brain targeting. On the one hand, smaller LNCs showed significantly higher brain targeting properties. This trend was steadily observed both for non-modified LNCs (Figure 8a, *: $p<0.05$) and for CBD-decorated LNCs (Figure 8b, **: $p<0.01$). On the other hand, the modification of LNCs with CBD significantly contributed to enhance the BBB targeting properties of equally-sized LNCs (Figure 8c, *: $p<0.05$).

The biodistribution of LNCs on a longer term (4 hours after administration) was assessed for F6 and F10 (namely, those formulations with the highest levels in plasma 90 minutes after administration). Similarly, Figures 9 and 10 represent the time-course of the percentage of the injected dose in the major organs and in the brain, respectively. In comparison their biodistribution at an earlier time point, the percentage of the injected dose in blood and brain decreased with time, whereas the levels in the reticuloendothelial organs progressively augmented. Similar trends were observed for F6 (Figures 9a and 10a) and for F10 (Figures 9b and 10b).

Figure 2.2.8: *In vivo* biodistribution of DiD-labeled LNCs in the brain of healthy mice 90 minutes after their intravenous injection (expressed as percentage of the injected dose). (a) Influence of particle size on biodistribution (non-modified LNCs) (*: $p<0.05$). (b) Influence of particle size on biodistribution (CBD-decorated LNCs) (**: $p<0.01$). (c) Influence of the modification with CBD on biodistribution (equally-sized LNCs) (*: $p<0.05$).

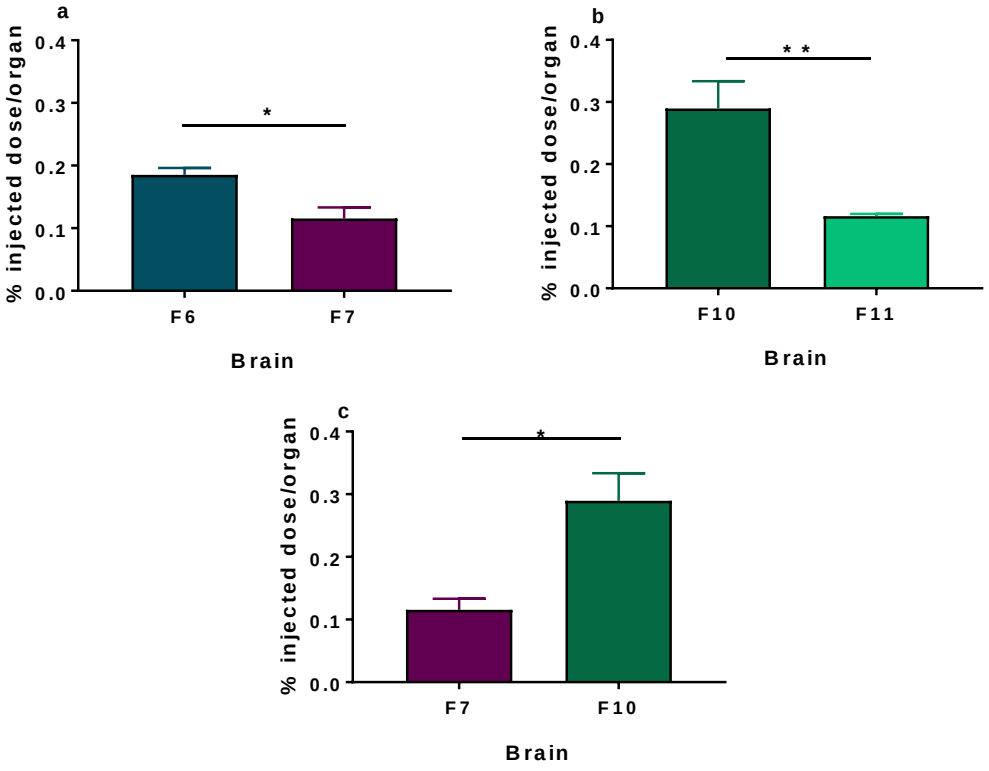

Figure 2.2.9: *In vivo* biodistribution of DiD-labeled LNCs in healthy mice (expressed as percentage of the injected dose per organ; namely, blood, lungs, kidneys, heart, spleen and liver). Time-course biodistribution of (a) DiD-labeled LNCs (F6) and (b) CBD-decorated DiD-labeled LNCs (F10).

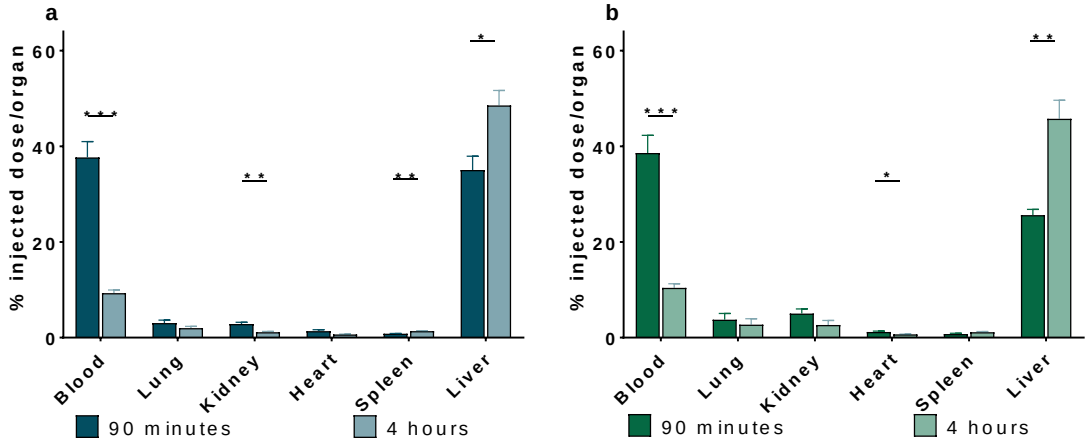

4. Discussion

Diseases affecting the central nervous system (CNS) should be regarded as a major health challenge of the twenty-first century due to their steadily rising incidences and to the current lack of effective treatments in most cases, since brain drug delivery is truly hindered by the presence of the blood-brain barrier (BBB) [30]. As intravenous administration represents a minimally-invasive therapeutic alternative, nanomedicine holds the greatest promise among the strategies available to enhance the passage across the BBB.

Figure 2.2.10: *In vivo* biodistribution of DiD-labeled LNCs in the brain of healthy mice (expressed as percentage of the injected dose). Time-course biodistribution of (a) DiD-labeled LNCs (F6) and (b) CBD-decorated DiD-labeled LNCs (F10).

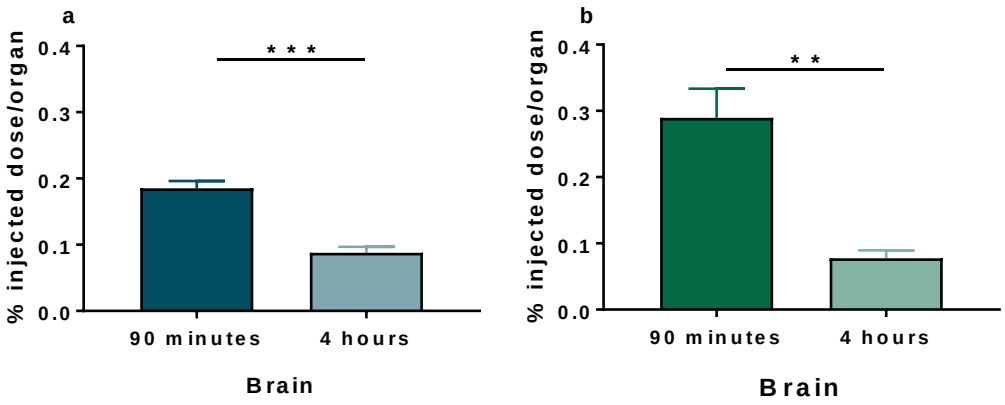

Accordingly, intravenously-administered nanomedicines have already reached clinical trials for the treatment of different CNS diseases (with a focus on brain tumors, but also including neurodegenerative diseases such as multiple sclerosis). Noticeably, given their non-toxic, biocompatible and biodegradable nature, most of the launched clinical trials evaluate lipid-based carriers and, particularly, liposomes (ClinicalTrials.gov Identifiers: NCT00734682, NCT02861222, NCT00019630, NCT00944801, NCT01222780, NCT01386580, NCT02048358 and NCT02340156). Although some of these trials evaluated passively-targeted nanomedicines, it has been evidenced that the hypothesized BBB disruption in most CNS diseases only occurs substantially in advances stages and in the most affected areas. Hence, efficient brain targeting of nanomedicines should not solely rely on passive targeting [31]. Therefore, brain active targeting of nanomedicines to trigger transcytosis into the CNS through specific binding with transporters overexpressed on the brain endothelium is being widely explored [32]. Nonetheless, for brain active targeting to achieve high translational impact some criteria in the selection of targeting moieties must be met: on the one hand, the use of physiological substances develops competitive phenomena with endogenous substrates, whereas on the other hand, the use of peptide ligands must ensure non-immunogenicity [12]. As a result, research on novel exogenous non-immunogenic ligands has become a research hotspot.

On account of the aforementioned context, in the present study we have prepared cannabidiol (CBD)-decorated lipid nanocapsules (LNCs) as innovative candidates to achieve brain targeting. Their brain targeting ability was evaluated both *in vitro* and *in vivo*. LNCs were chosen according both to their high drug loading potential within their oily core (unlike liposomes) and to their high kinetic stability provided by their solid surfactant shell. These carriers were prepared by the energetically-efficient phase inversion temperature (PIT) method. In order to evaluate the influence of particle size on the transcytosis mechanisms that mediate brain targeting, monodisperse LNCs in different sizes were prepared by varying the relative proportions of their excipients (Table 1). Alternatively, we hypothesized that given the plethora of receptors of the CNS to which cannabinoids have been reported to bind, cannabinoids hold great promise to enhance the brain targeting properties of nanocarriers. In particular, cannabidiol (CBD), the main cannabinoid devoid of psychotropic effects, seems the appropriate lead candidate to test the possibilities of this hypothesis [21]. Hence, preformed LNCs were later decorated with CBD to evaluate its role as brain targeting molecule.

The different LNCs were firstly evaluated *in vitro* with cell viability, uptake and permeability experiments conducted on the human brain endothelial cell line hCMEC/D3. This cell line was used as the *in vitro* BBB model given both their human origin and their better barrier properties in comparison with other commonly used cell lines [33]. Cell viability experiments evidenced a size-dependent toxicity pattern on hCMEC/D3 cells. This correlation between particle size and cytotoxic effect on cerebral endothelial cells had not been studied previously. Hence, we ruled out the most cytotoxic particle size against the hCMEC/D3 cells and, for the remaining sizes, we determined non-toxic concentrations to perform both the uptake and the permeability experiments at equivalent concentrations of the dye-labeled LNCs.

The BBB targeting efficiency of dye-labeled LNCs was measured by their cellular uptake through flow cytometry. The internalization of LNCs by hCMEC/D3 followed a time-dependent pattern. Results consistently demonstrated a significantly higher BBB-targeting effect for smaller LNCs (for both unmodified-LNCs and CBD-decorated LNCs) and for CBD-decorated LNCs (for equally-sized LNCs). The images taken by confocal microscopy further evidenced qualitatively the efficient internalization of LNCs. A 3D video reconstruction of the Z-stacks of these images seems to support a perinuclear localization of the LNCs within the hCMEC/D3 cells.

The BBB transcytosis efficiency of dye-labeled LNCs was measured through permeability experiments across the *in vitro* BBB model. The integrity of the BBB model throughout the 24 hours that lasted the permeability experiments was previously demonstrated with TRITC-dextran as hydrophilic tracer: a comparison of the permeability coefficients of TRITC-dextran across the endothelium cell monolayer *in vitro* was not altered by the presence of LNCs ($p>0.05$). As a result, the *in vitro* BBB model was suitable for evaluating the transport ability of the different LNCs. We calculated herein the permeability coefficient as a robust parameter that enables the comparison of the different transport efficiencies. Importantly, permeability coefficient remains constant throughout the experiment, which is not the case for the transport

ratio expressed as percentage of passage across the endothelial monolayer. Although this ratio is being broadly utilized to express transport efficiencies [13, 15, 16, 19, 34-37], it varies with the different time points and does not take into account important experimental parameters such as the insert surface area or the volumes of the acceptor and the donor chambers to normalize the data (which is precisely one of the main advantages of *in vitro* studies in comparison with the higher unquantifiable variability of *in vivo* experiments). For this reason, the efficiency of different brain active targeting strategies cannot be readily compared with transport ratios calculated as percentage. In order to attempt a comparison between various BBB-targeting peptides, Chen et al recently evaluated all these ligands in the same nanocarrier [17]. Nevertheless, this strategy will no longer be plausible with the widening in the brain targeting armamentarium. Noticeably, the cellular uptake results were consistent with the permeability experiments: the permeability coefficients across the endothelial monolayer were significantly higher for smaller LNCs (for both unmodified-LNCs and CBD-decorated LNCs) and for CBD-decorated LNCs (for equally-sized LNCs). Taken together, the *in vitro* results highlighted that CBD modification on LNCs plays a major role in the transport enhancement across the BBB model and so does a reduction in particle size (within the tested size-range: 20-60 nm).

The *in vitro* BBB-targeting and penetrating properties across the hCMEC/D3 monolayers were validated with biodistribution studies in mice following intravenous administration of dye-loaded LNCs. For *in vivo* experiments, we switched to the near-infrared dye DiD as it is excited and emits within the wavelength window of 640−800 nm (namely, the wavelength range with the lowest absorption in tissue). Although brain targeting efficiency has often been evaluated in pathophysiological models, given that BBB dysfunction only occurs in the most damaged brain regions, we aimed at evidencing targeting properties at earlier stages of the CNS diseases with biodistribution studies in healthy mice. Accordingly, we were forced to test smaller-sized nanocapsules (20-55 nm) than the 100 nm-sized (or even above) carriers that have been developed for their evaluation in rodent models of CNS diseases [13, 15, 17, 35, 38, 39].

The *in vivo* results strongly confirmed the auspicious results obtained with the *in vitro* BBB model as, on the one hand, a decrease in particle size yielded a higher transcytosis rate to brain (1.6-fold increase for unmodified LNCs and 2.5-fold increase for CBD-decorated LNCs) and, on the other hand, the modification of LNCs with CBD showed higher brain targeting properties *in vivo* (2.5-fold increase for equally sized LNCs). The increase in brain levels highly correlated with the higher available plasma concentration and lower recognition by the reticuloendothelial organs observed for these formulations. As also occurred with *in vitro* results, it is often difficult to draw comparisons between *in vivo* results reported by different authors, especially in those studies that only specify the amount of fluorescent tracer distributed into the brain tissue, since this amount depends on the dye dose administered [40-42]. A comparison with those scarce studies that explored the brain targeting properties of carriers within the here tested size range (namely, 20-60 nm) and expressed their results as percentage of the injected dose per gram of brain overall revealed brain levels in the

same order as those obtained herein [43, 44]. In particular, in [43] the maximal percentage of injected dose per gram of brain tissue (slightly below 0.3% for the targeted nanocarrier) was accomplished at a much later time point (t_{max} around 24h) than the reported herein (0.6% of injected dose per gram of brain tissue at only 90 minutes following intravenous injection). However, it is worth mentioning that all these studies evaluated the biodistribution in glioma-bearing rodent models. Hence, whereas in our study only transcellular routes can be exploited for brain targeting, in the glioma-bearing models the transcellular routes can be significantly supplemented with paracellular pathways across the blood-brain barrier to enhance the targeting properties (the extent of this contribution will highly depend on the disease stage). As a result, the evaluation of our nanocarrier system in an animal model of disease is expected to exhibit values even higher than those reported herein. Apart from that, Luo et al. had to utilize a double targeting strategy to achieve higher percentage of injected dose per gram of brain tumor [44]. More importantly, enhancement in brain targeting achieved with the conjugation of CBD to LNCs with regards to nude nanocapsules outperformed the enhancement observed for the gluthatione functionalization strategy (not statistically significant) tested in a seminal study with healthy mice that laid the foundations for the G-Technology® (the main brain active strategy that have already entered clinical trials for the treatment of CNS diseases) [45].

Altogether, the enhancement in the brain targeting properties of LNCs achieved with CBD as targeting moiety and the correlation between reduction in particle size (within the size range 20-55 nm) and increase in transcytosis across brain capillaries have been consistently evidenced both *in vitro* through cellular uptake experiments by flow cytometry and confocal microscopy and through transport experiments across a endothelial monolayer and *in vivo* through biodistribution studies in healthy mice. The most likely mechanism of brain targeting of CBD is receptor-mediated transcytosis across the brain endothelium. CBD binds to many receptors preferentially located at the CNS level [21, 22, 27], and among those, dopamine receptor has been postulated to specifically locate at the BBB and has recently started being tested as a potential receptor to mediate brain targeting of nanomedicines with exogenous ligands [35].

5. Conclusion

We have developed and evaluated pre-clinically both *in vitro* and *in vivo* an innovative BBB-targeted lipid nanocarrier aimed at brain active targeting following intravenous administration. In particular, we obtained monodisperse lipid nanocapsules by the phase inversion method and decorated them with non-psychotropic cannabinoids as pioneering brain targeting molecules. Both the permeability experiments across an *in vitro* BBB model and the biodistribution experiments demonstrated that the highest brain transcytosis rate was achieved with the smallest cannabinoid-decorated LNCs. Since the transport efficiency across the BBB certainly determines the efficacy of the treatments for brain disorders, our results indicate that small cannabinoid-decorated lipid nanocapsules represent an auspicious platform for the design and development of novel therapies for CNS diseases. Moreover, our study serves to widen with cannabinoids the yet scarce armamentarium of exogenous and non-immunogenic ligands available for brain targeting. Lastly, the consistency between

the *in vitro* and *in vivo* results served to validate our *in vitro* BBB model with the human brain endothelial cell line hCMEC/D3 as a versatile screening method to evaluate the passage of nanocarriers across the BBB that meets the high-throughput demands in the early stages of drug discovery and lacks ethical constraints.

Acknowledgements

This work was supported by the Complutense Research Fund (Ref. 16/83) and by the Research Group GR35/10 Santander-UCM: Parenteral Administration of Drugs. J. A.-B.would like to thank the Spanish Ministry of Education for his contract within the Professor Training Program FPU (Ref. FPU13/02325) and for funding two research stays at the School of Life, Health and Chemical Sciences, The Open University (United Kingdom) (Refs. EST15/00534 and EST16/00556). The authors would like to thank to Shereen Nizari for the help provided with the IMARIS software and to Rubén Fernández-de-la-Rosa for the help provided with the intravenous administration to mice.

References

[1] Silberberg D, Anand NP, Michels K, Kalaria RN. Brain and other nervous system disorders across the lifespan - global challenges and opportunities. Nature. 2015;527:S151-S4.

[2] Saraiva C, Praca C, Ferreira R, Santos T, Ferreira L, Bernardino L. Nanoparticle-mediated brain drug delivery: Overcoming blood-brain barrier to treat neurodegenerative diseases. J Control Release. 2016;235:34-47.

[3] Oberoi RK, Parrish KE, Sio TT, Mittapalli RK, Elmquist WF, Sarkaria JN. Strategies to improve delivery of anticancer drugs across the blood-brain barrier to treat glioblastoma. Neuro-Oncology. 2016;18:27-36.

[4] Aparicio-Blanco J, Torres-Suarez A-I. Towards tailored management of malignant brain tumors with nanotheranostics. Acta biomaterialia. 2018.

[5] Abbott NJ. Blood-brain barrier structure and function and the challenges for CNS drug delivery. J Inherit Metab Dis. 2013;36:437-49.

[6] Mitragotri S, Burke PA, Langer R. Overcoming the challenges in administering biopharmaceuticals: formulation and delivery strategies. Nat Rev Drug Discov. 2014;13:655-72.

[7] Obermeier B, Daneman R, Ransohoff RM. Development, maintenance and disruption of the blood-brain barrier. Nat Med. 2013;19:1584-96.

[8] Tsou YH, Zhang XQ, Zhu H, Syed S, Xu XY. Drug Delivery to the Brain across the Blood-Brain Barrier Using Nanomaterials. Small. 2017;13:17.

[9] Miranda A, Blanco-Prieto MJ, Sousa J, Pais A, Vitorino C. Breaching barriers in glioblastoma. Part II: Targeted drug delivery and lipid nanoparticles. Int J Pharm. 2017;531:389-410.

[10] Sweeney MD, Sagare AP, Zlokovic BV. Blood-brain barrier breakdown in Alzheimer disease and other neurodegenerative disorders. Nat Rev Neurol. 2018;14:133-50.

[11] van Tellingen O, Yetkin-Arik B, de Gooijer MC, Wesseling P, Wurdinger T, de Vries HE. Overcoming the blood-brain tumor barrier for effective glioblastoma treatment. Drug Resist Update. 2015;19:1-12.

[12] Oller-Salvia B, Sanchez-Navarro M, Giralt E, Teixido M. Blood-brain barrier shuttle peptides: an emerging paradigm for brain delivery. Chem Soc Rev. 2016;45:4690-707.

[13] Cui Y, Zhang M, Zeng F, Jin HY, Xu Q, Huang YZ. Dual-Targeting Magnetic PLGA Nanoparticles for Codelivery of Paclitaxel and Curcumin for Brain Tumor Therapy. ACS Appl Mater Interfaces. 2016;8:32159-69.

[14] Johnsen KB, Burkhart A, Melander F, Kempen PJ, Vejlebo JB, Siupka P, et al. Targeting transferrin receptors at the blood-brain barrier improves the uptake of immunoliposomes and subsequent cargo transport into the brain parenchyma. Sci Rep. 2017;7:13.

[15] Wei XL, Gao J, Zhan CY, Xie C, Chai ZL, Ran D, et al. Liposome-based glioma targeted drug delivery enabled by stable peptide ligands. J Control Release. 2015;218:13-21.

[16] Wei XL, Zhan CY, Shen Q, Fu W, Xie C, Gao J, et al. A D-Peptide Ligand of Nicotine Acetylcholine Receptors for Brain-Targeted Drug Delivery. Angew Chem-Int Edit. 2015;54:3023-7.

[17] Chen CT, Duan ZQ, Yuan Y, Li RX, Pang L, Liang JM, et al. Peptide-22 and Cyclic RGD Functionalized Liposomes for Glioma Targeting Drug Delivery Overcoming BBB and BBTB. ACS Appl Mater Interfaces. 2017;9:5864-73.

[18] Kim JS, Shin DH, Kim JS. Dual-targeting immunoliposomes using angiopep-2 and CD133 antibody for glioblastoma stem cells. J Control Release. 2018;269:245-57.

[19] Byeon HJ, Thao LQ, Lee S, Min SY, Lee ES, Shin BS, et al. Doxorubicin-loaded nanoparticles consisted of cationic- and mannose-modified-albumins for dual-targeting in brain tumors. J Control Release. 2016;225:301-13.

[20] Du D, Chang ND, Sun SL, Li MH, Yu H, Liu MF, et al. The role of glucose transporters in the distribution of p-aminophenyl-alpha-D-mannopyranoside modified liposomes within mice brain. J Control Release. 2014;182:99-110.

[21] Pisanti S, Malfitano AM, Ciaglia E, Lamberti A, Ranieri R, Cuomo G, et al. Cannabidiol: State of the art and new challenges for therapeutic applications. Pharmacol Ther. 2017;175:133-50.

[22] Laprairie RB, Bagher AM, Kelly MEM, Denovan-Wright EM. Cannabidiol is a negative allosteric modulator of the cannabinoid CB1 receptor. Br J Pharmacol. 2015;172:4790-805.

[23] Espejo-Porras F, Fernandez-Ruiz J, Pertwee RG, Mechoulam R, Garcia C. Motor effects of the non-psychotropic phytocannabinoid cannabidiol that are mediated by 5-HT1A receptors. Neuropharmacology. 2013;75:155-63.

[24] De Petrocellis L, Ligresti A, Moriello AS, Allara M, Bisogno T, Petrosino S, et al. Effects of cannabinoids and cannabinoid-enriched Cannabis extracts on TRP channels and endocannabinoid metabolic enzymes. Br J Pharmacol. 2011;163:1479-94.

[25] Sylantyev S, Jensen TP, Ross RA, Rusakov DA. Cannabinoid- and lysophosphatidylinositol-sensitive receptor GPR55 boosts neurotransmitter release at central synapses. Proc Natl Acad Sci U S A. 2013;110:5193-8.

[26] Mecha M, Feliu A, Inigo PM, Mestre L, Carrillo-Salinas FJ, Guaza C. Cannabidiol provides long-lasting protection against the deleterious effects of inflammation in a viral model of multiple sclerosis: A role for A(2A) receptors. Neurobiol Dis. 2013;59:141-50.

[27] Seeman P. Cannabidiol is a partial agonist at dopamine D2High receptors, predicting its antipsychotic clinical dose. Transl Psychiatr. 2016;6:4.

[28] Aparicio-Blanco J, Martin-Sabroso C, Torres-Suarez AI. In vitro screening of nanomedicines through the blood brain barrier: A critical review. Biomaterials. 2016;103:229-55.

[29] Bastiat G, Pritz CO, Roider C, Fouchet F, Lignieres E, Jesacher A, et al. A new tool to ensure the fluorescent dye labeling stability of nanocarriers: A real challenge for fluorescence imaging. J Control Release. 2013;170:334-42.

[30] Banks WA. From blood-brain barrier to blood-brain interface: new opportunities for CNS drug delivery. Nat Rev Drug Discov. 2016;15:275-92.

[31] Gao HL, Qian J, Cao SJ, Yang Z, Pang ZQ, Pan SQ, et al. Precise glioma targeting of and penetration by aptamer and peptide dual-functioned nanoparticles. Biomaterials. 2012;33:5115-23.

[32] Aparicio-Blanco J, Torres-Suárez AI. Managing CNS Tumors: The Nanomedicine Approach. In: Morgan LR, editor. New Approaches to the Management of Primary and Secondary CNS Tumors: InTech; 2017.

[33] Toman P, Lien CF, Ahmad Z, Dietrich S, Smith JR, An Q, et al. Nanoparticles of alkylglyceryl-dextran-graft-poly(lactic acid) for drug delivery to the brain: Preparation and in vitro investigation. Acta Biomaterialia. 2015;23:250-62.

[34] Jiang XY, Xin HL, Ren QY, Gu JJ, Zhu LJ, Du FY, et al. Nanoparticles of 2-deoxy-D-glucose functionalized poly(ethylene glycol)-co-poly(trimethylene carbonate) for dual-targeted drug delivery in glioma treatment. Biomaterials. 2014;35:518-29.

[35] Belhadj Z, Ying M, Cao X, Hu XF, Zhan CY, Wei XL, et al. Design of Y-shaped targeting material for liposome-based multifunctional glioblastoma-targeted drug delivery. J Control Release. 2017;255:132-41.

[36] Su CH, Tsai CY, Tomanek B, Chen WY, Cheng FY. Evaluation of blood-brain barrier-stealth nanocomposites for in situ glioblastoma theranostics applications. Nanoscale. 2016;8:7866-70.

[37] Huang YK, Liu WC, Gao F, Fang XL, Chen YZ. c(RGDyK)-decorated Pluronic micelles for enhanced doxorubicin and paclitaxel delivery to brain glioma. Int J Nanomed. 2016;11:1629-41.

[38] Gao JQ, Lv Q, Li LM, Tang XJ, Li FZ, Hu YL, et al. Glioma targeting and blood-brain barrier penetration by dual-targeting doxorubincin liposomes. Biomaterials. 2013;34:5628-39.

[39] Wei L, Guo XY, Yang T, Yu MZ, Chen DW, Wang JC. Brain tumor-targeted therapy by systemic delivery of siRNA with Transferrin receptor-mediated core-shell nanoparticles. Int J Pharm. 2016;510:394-405.

[40] Cook RL, Householder KT, Chung EP, Prakapenka AV, DiPerna DM, Sirianni RW. A critical evaluation of drug delivery fromligandmodified nanoparticles: Confounding small molecule distribution and efficacy in the central nervous system. J Control Release. 2015;220:89-97.

[41] Wang BY, Lv LY, Wang ZY, Zhao Y, Wu L, Fang XL, et al. Nanoparticles functionalized with Pep-1 as potential glioma targeting delivery system via interleukin 13 receptor alpha 2-mediated endocytosis. Biomaterials. 2014;35:5897-907.

[42] Chen YC, Chiang CF, Chen LF, Liang PC, Hsieh WY, Lin WL. Polymersomes conjugated with des-octanoyl ghrelin and folate as a BBB-penetrating cancer cell-targeting delivery system. Biomaterials. 2014;35:4066-81.

[43] Luo ZM, Yan ZQ, Jin K, Pang Q, Jiang T, Lu H, et al. Precise glioblastoma targeting by AS1411 aptamer-functionalized poly (L-gamma-glutamylglutamine)-paclitaxel nanoconjugates. J Colloid Interface Sci. 2017;490:783-96.

[44] Luo ZM, Jin K, Pang Q, Shen S, Yan ZQ, Jiang T, et al. On-Demand Drug Release from Dual-Targeting Small Nanoparticles Triggered by High-Intensity Focused Ultrasound Enhanced Glioblastoma-Targeting Therapy. ACS Appl Mater Interfaces. 2017;9:31612-25.

[45] Gaillard PJ, Appeldoorn CCM, Dorland R, van Kregten J, Manca F, Vugts DJ, et al. Pharmacokinetics, Brain Delivery, and Efficacy in Brain Tumor-Bearing Mice of Glutathione Pegylated Liposomal Doxorubicin (2B3-101). PLoS One. 2014;9:10.

Supporting Information

Cannabidiol-targeted lipid nanocapsules across the blood-brain barrier: in vitro and in vivo evaluation

Juan Aparicio-Blanco [a,b,] Ignacio A. Romero [b], David K. Male [b], Karla Slowing [c], Luis García [c], Ana I. Torres-Suárez [a, d]

[a] Department of Pharmaceutics and Food Technology, Complutense University, Madrid, Spain

[b] School of Life, Health and Chemical Sciences, Faculty of Science, The Open University, Milton Keynes, United Kingdom

[c] Department of Pharmacology, Pharmacognosy and Botany, Complutense University, Madrid, Spain

[d] University Institute of Industrial Pharmacy, Complutense University, Madrid, Spain

Figure 2.2.S1: Influence of methanol addition on particle size of LNCs ($p>0.05$).

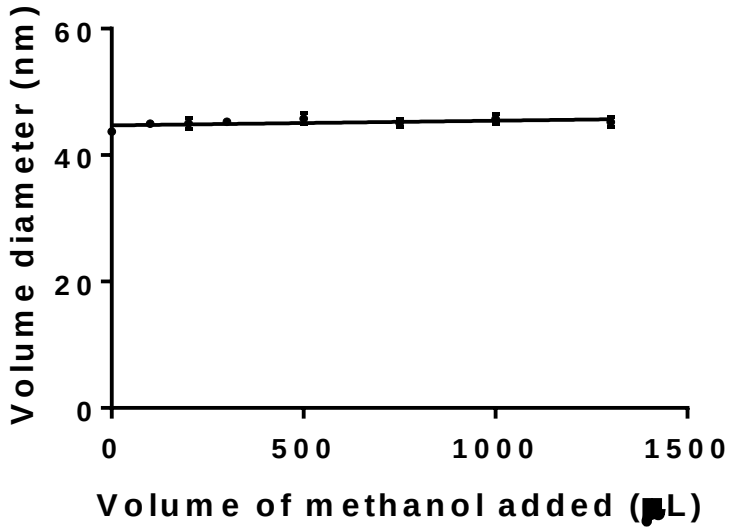

Chapter 3: Lipid nanocapsules loaded and decorated with cannabidiol for glioma therapy

The therapeutic potential of several cannabinoids has become a research hotspot. In this regard, precisely due to the lack of psychoactive effects, CBD is doubtless the most auspicious phytocannabinoid for the treatment of various pathologies, namely inflammatory and neurodegenerative diseases, mental disorders, neuropathic pain, epilepsy and cancer [1]. In the latter case, apart from palliating cancer-related symptoms (such as nausea, pain or anorexia), CBD has been reported to promote apoptotic cancer cell death through the production of reactive oxygen species, to impair tumor angiogenesis and to reduce cell migration that ultimately accounts for metastasis [2]. In the case of gliomas, the expression of different receptors to which cannabinoids bind is increased (cannabinoid receptors 1 and 2 (CB_1 and CB_2) [3] and transient potential vanilloid receptor type 2 (TRPV2) [4]). Accordingly, activation of these receptors by CBD induced apoptosis of glioma cells, while no effects were observed in normal human astrocytes [4, 5]. Therefore, we hypothesized on the one hand, that CBD can serve to widen the therapeutic armamentarium against malignant brain tumors thanks to its synergistic effects with the currently available drugs and radiotherapy [6], and, on the other hand, that CBD can act as a glioma-targeting molecule for nanocarriers. If existing, this glioma-targeting effect, added to the results from the previous chapter, where we have introduced CBD as a pioneering brain active targeting moiety across the blood-brain barrier (BBB), would ultimately enable a dual-targeting strategy for intravenous treatment of glioma to be designed.

Nonetheless, the high lipophilicity of cannabinoids, including CBD, has truly constrained their therapeutic potential due to formulation problems. In this context, these substances can take great advantage of nanomedicine-based formulation strategies. Consistently, several studies on nanocarriers encapsulating different kinds of cannabinoids have started being published recently for distinct therapeutic purposes (Table 1). Notwithstanding that for cannabinoids to achieve high translational impact these should be devoid of psychoactive effects, the focus so far has been mainly put on the encapsulation of Δ^9-THC and Δ^9-THC analogues.

Therefore, this chapter is devoted to evaluating the potential of the lipid LNCs as carriers for CBD for glioma therapy. To this end, we develop two distinct strategies to incorporate CBD in the LNCs depending on the ultimate therapeutic purpose.

Cannabinoid	Type of cannabinoid	Carrier	Therapeutic potential	Ref
$^{9}\Delta$-THC	Phytocannabinoid	Mesoporous silica nanoparticles	*In vivo* neuropathic pain relief	[7]
$^{9}\Delta$-THC	Phytocannabinoid	PLGA nanoparticles	*In vitro* and *in vivo* chemotherapy for lung cancer	[8]
$^{9}\Delta$-THC	Phytocannabinoid	PLGA nanoparticles	*In vitro* chemotherapy for colon adenocarcinoma	[9]
$^{9}\Delta$-THC and CBD	Phytocannabinoid	Nanolipospheres	-	[10]
AEA	Endocannabinoid	Poly-ε-caprolactone nanoparticles	-	[11]
Rimonabant	Synthetic cannabidomimetic	Nanostructured lipid carriers	-	[12]
Rimonabant, URB597 and AM251	Synthetic cannabidomimetic	Nanostructured lipid carriers	-	[13]
WIN55,212-2	Synthetic cannabidomimetic	Styrene maleic acid micelles	*In vivo* neuropathic pain relief	[14]
Dexanabinol	Synthetic cannabidomimetic	Solid lipid nanoparticles	*In vivo* antidepressant effect	[15]
CB13	Synthetic cannabidomimetic	PLGA nanoparticles	*In vivo* neuropathic pain relief	[16]
CB13	Synthetic cannabidomimetic	PLGA nanoparticles	-	[17, 18]
CB13	Synthetic cannabidomimetic	Lipid nanoparticles	-	[17, 19]

Table 3.0.1: Published articles on the encapsulation of different kinds of cannabinoids within nanocarriers. $^{9}\Delta$-THC: 9-delta-tetrahydrocannabinol, AEA: anandamide.

On the one hand, LNCs can overcome the dosing problems traditionally associated with cannabinoids. So as to evaluate the *in vitro* the efficacy of LNCs as extended-release carriers against the human glioblastoma cell line U373MG, we have encapsulated CBD at high drug loading into the oily core of LNCs. The role played by the size of LNCs in drug release and cytotoxicity is likewise thoroughly explored. On the other hand, to explore the potential of this phytocannabinoid to target any of the cannabinoid receptors overexpressed in glioma cells as aforementioned, we have developed a functionalization strategy of LNCs with CBD. It should be stated that this strategy was already utilized in the previous chapter as a brain active targeting strategy, but it is technologically described and characterized in detail in this third chapter due to formatting reasons, since this dissertation is organized as a compendium of research articles that must exhibit stand-alone entity for publication. The combination of both strategies would hold great promise for glioma therapy.

This third chapter encompasses the scientific publications “Glioblastoma multiforme and lipid nanocapsules: a review” and “The potential of lipid nanocapsules decorated and loaded with cannabidiol for the treatment of malignant gliomas: *in vitro* evaluation”. In the review article we first provide an in-depth analysis of the possibilities of LNCs for treating malignant gliomas. Subsequently, in the original research article, we design and characterize the aforementioned two distinct strategies to incorporate CBD depending on the ultimate therapeutic purpose. To evaluate the *in vitro* glioma-targeting efficiency of the functionalization strategy of LNCs with CBD, we conduct uptake experiments on the human glioblastoma cell line U373MG. To test the *in vitro* efficacy of CBD-encapsulating LNCs as extended-release carriers we conduct cell viability experiments with the same human glioblastoma cell line. The role played by the particle size of LNCs is evaluated in both experiments.

References

[1] Pisanti S, Malfitano AM, Ciaglia E, Lamberti A, Ranieri R, Cuomo G, et al. Cannabidiol: State of the art and new challenges for therapeutic applications. Pharmacology & therapeutics. 2017;175:133-50.

[2] Velasco G, Hernandez-Tiedra S, Davila D, Lorente M. The use of cannabinoids as anticancer agents. Prog Neuro-Psychopharmacol Biol Psychiatry. 2016;64:259-66.

[3] Wu XY, Han LJ, Zhang XL, Li L, Jiang CZ, Qiu Y, et al. Alteration of endocannabinoid system in human gliomas. J Neurochem. 2012;120:842-9.

[4] Nabissi M, Morelli MB, Amantini C, Liberati S, Santoni M, Ricci-Vitiani L, et al. Cannabidiol stimulates Aml-1a-dependent glial differentiation and inhibits glioma stem-like cells proliferation by inducing autophagy in a TRPV2-dependent manner. Int J Cancer. 2015;137:1855-69.

[5] Sanchez C, de Ceballos ML, del Pulgar TG, Rueda D, Corbacho C, Velasco G, et al. Inhibition of glioma growth in vivo by selective activation of the CB2 cannabinoid receptor. Cancer Res. 2001;61:5784-9.

[6] Fowler CJ. Delta(9)-Tetrahydrocannabinol and Cannabidiol as Potential Curative Agents for Cancer: A Critical Examination of the Preclinical Literature. Clin Pharmacol Ther. 2015;97:587-96.

[7] Xie JR, Xiao DJ, Zhao JN, Hu NQ, Bao Q, Jiang L, et al. Mesoporous Silica Particles as a Multifunctional Delivery System for Pain Relief in Experimental Neuropathy. Adv Healthc Mater. 2016;5:1213-21.

[8] Martin-Banderas L, Munoz-Rubio I, Prados J, Alvarez-Fuentes J, Calderon-Montano JM, Lopez-Lazaro M, et al. In vitro and in vivo evaluation of Delta(9)-tetrahidrocannabinol/PLGA nanoparticles for cancer chemotherapy. Int J Pharm. 2015;487:205-12.

[9] Martin-Banderas L, Munoz-Rubio I, Alvarez-Fuentes J, Duran-Lobato M, Arias JL, Holgado MA, et al. Engineering of Delta(9)-tetrahydrocannabinol delivery systems based on surface modified-PLGA nanoplatforms. Colloid Surf B-Biointerfaces. 2014;123:114-22.

[10] Cherniakov I, Izgelov D, Barasch D, Davidson E, Domb AJ, Hoffman A. Piperine-pro-nanolipospheres as a novel oral delivery system of cannabinoids: Pharmacokinetic evaluation in healthy volunteers in comparison to buccal spray administration. J Control Release. 2017;266:1-7.

[11] Ligresti A, De Petrocellis L, de la Ossa DHP, Aberturas R, Cristino L, Moriello AS, et al. Exploiting Nanotechnologies and TRPV1 Channels to Investigate the Putative Anandamide Membrane Transporter. PLoS One. 2010;5:12.

[12] Esposito E, Ravani L, Drechsler M, Mariani P, Contado C, Ruokolainen J, et al. Cannabinoid antagonist in nanostructured lipid carriers (NLCs): design, characterization and in vivo study. Mater Sci Eng C-Mater Biol Appl. 2015;48:328-36.

[13] Esposito E, Drechsler M, Cortesi R, Nastruzzi C. Encapsulation of cannabinoid drugs in nanostructured lipid carriers. Eur J Pharm Biopharm. 2016;102:87-91.

[14] Linsell O, Brownjohn PW, Nehoff H, Greish K, Ashton JC. Effect of styrene maleic acid WIN55,212-2 micelles on neuropathic pain in a rat model. J Drug Target. 2015;23:353-9.

[15] He XL, Yang L, Wang M, Zhuang XZ, Huang RQ, Zhu RR, et al. Targeting the Endocannabinoid/CB1 Receptor System For Treating Major Depression Through Antidepressant Activities of Curcumin and Dexanabinol-Loaded Solid Lipid Nanoparticles. Cell Physiol Biochem. 2017;42:2281-94.

[16] Berrocoso E, Rey-Brea R, Fernandez-Arevalo M, Mico JA, Martin-Banderas L. Single oral dose of cannabinoid derivate loaded PLGA nanocarriers relieves neuropathic pain for eleven days. Nanomed-Nanotechnol Biol Med. 2017;13:2623-32.

[17] Duran-Lobato M, Martin-Banderas L, Goncalves LMD, Fernandez-Arevalo M, Almeida AJ. Comparative study of chitosan- and PEG-coated lipid and PLGA nanoparticles as oral delivery systems for cannabinoids. J Nanopart Res. 2015;17:17.

[18] Martin-Banderas L, Alvarez-Fuentes J, Duran-Lobato M, Prados J, Melguizo C, Fernandez-Arevalo M, et al. Cannabinoid derivate-loaded PLGA nanocarriers for oral administration: formulation, characterization, and cytotoxicity studies. Int J Nanomed. 2012;7:5793-806.

[19] Duran-Lobato M, Martin-Banderas L, Lopes R, Goncalves LMD, Fernandez-Arevalo M, Almeida AJ. Lipid nanoparticles as an emerging platform for cannabinoid delivery: physicochemical optimization and biocompatibility. Drug Dev Ind Pharm. 2016;42:190-8.

Review

Journal of
Biomedical Nanotechnology
Vol. 11, 1283–1311, 2015
www.aspbs.com/jbn

Glioblastoma Multiforme and Lipid Nanocapsules: A Review

Juan Aparicio-Blanco[1] and Ana-Isabel Torres-Suárez[1,2,*]

[1] *Department of Pharmaceutical Technology, Faculty of Pharmacy, Complutense University, Madrid, 28040, Spain*
[2] *University Institute of Industrial Pharmacy, Complutense University, Madrid, 28040, Spain*

Epidemiological data on central nervous system disorders call for a focus on the major hindrance to brain drug delivery, blood-central nervous system barriers. Otherwise, there is little chance of improving the short-term survival of patients with diseases such as glioblastoma multiforme, which is one of the brain disorders associated with many years of life lost. Targetable nanocarriers for treating malignant gliomas are a unique way to overcome low chemotherapeutic levels at target sites devoid of systemic toxicity. This review describes the currently available targetable nanocarriers, focusing particularly on one of the newest nanocarriers, lipid nanocapsules. All of the strategies that are likely to be exploited by lipid nanocapsules to bypass blood-central nervous system barriers, including the most recent targeting approaches (mesenchymal cells), and novel administration routes (convection enhanced delivery) are discussed, together with their most remarkable achievements in glioma-implanted animal models. Although these systems are promising, much research remains to be done in this field.

KEYWORDS: *Central Nervous System, Brain Tumors, Brain Drug Delivery, Blood–Brain Barrier, Blood-Cerebrospinal Barrier, Nanocarrier, Active Targeting, Passive Targeting.*

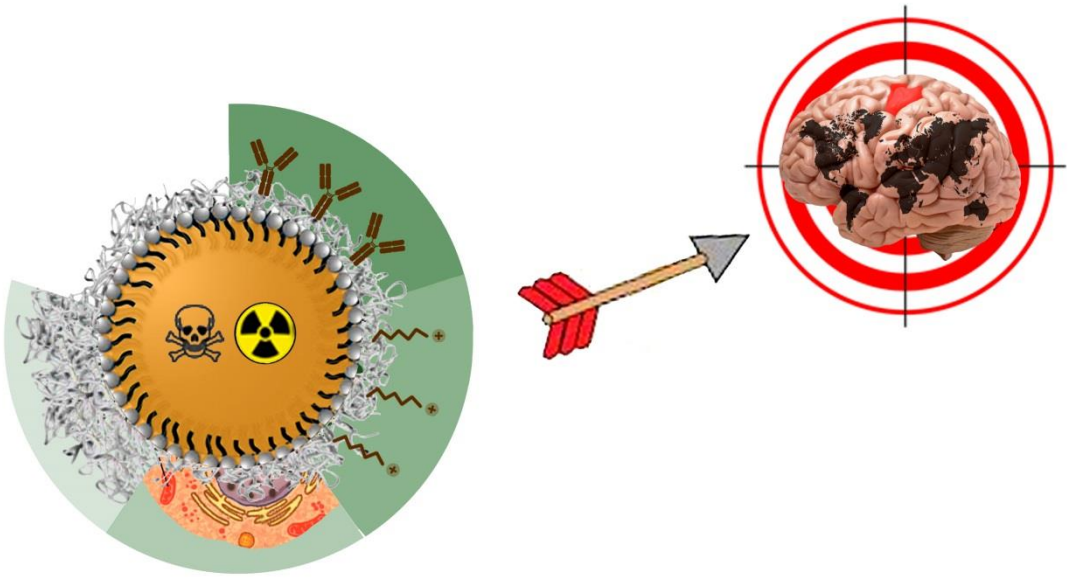

Glioblastoma Multiforme and Lipid Nanocapsules: A Review

Juan Aparicio-Blanco [a], Ana I. Torres-Suárez [a,b]

[a] Department of Pharmaceutical Technology and Food Engineering, Complutense University, 28040, Madrid, Spain

[b] University Institute of Industrial Pharmacy, Complutense University, Madrid, Spain

Abstract

Epidemiological data on central nervous system disorders call for a focus on the major hindrance to brain drug delivery, blood-central nervous system barriers. Otherwise, there is little chance of improving the short-term survival of patients with diseases such as glioblastoma multiforme, which is one of the brain disorders associated with many years of life lost. Targetable nanocarriers for treating malignant gliomas are a unique way to overcome low chemotherapeutic levels at target sites devoid of systemic toxicity. This review describes the currently available targetable nanocarriers, focusing particularly on one of the newest nanocarriers, lipid nanocapsules. All of the strategies that are likely to be exploited by lipid nanocapsules to bypass blood-central nervous system barriers, including the most recent targeting approaches (mesenchymal cells), and novel administration routes (convection enhanced delivery) are discussed, together with their most remarkable achievements in glioma-implanted animal models. Although these systems are promising, much research remains to be done in this field.

Keywords

Central nervous system, brain tumors, brain drug delivery, blood–brain barrier, blood-cerebrospinal barrier, nanocarrier, active targeting, passive targeting

The potential of lipid nanocapsules decorated and loaded with cannabidiol for the treatment of malignant gliomas: in vitro evaluation

Juan Aparicio-Blanco [a], Víctor Sebastián [b,c], Jean P. Benoit [d], Ana I. Torres-Suárez [a, e]

[a] Department of Pharmaceutics and Food Technology, Complutense University, Madrid, Spain

[b] Department of Chemical Engineering, Aragon Institute of Nanoscience (INA), University of Zaragoza, Zaragoza, Spain

[c] Networking Research Center on Bioengineering, Biomaterials and Nanomedicine (CIBER-BBN), Madrid, Spain

[d] MINT, UNIV Angers, INSERM 1066, CNRS 6021, Université Bretagne Loire, Angers, France

[e] University Institute of Industrial Pharmacy, Complutense University, Madrid, Spain

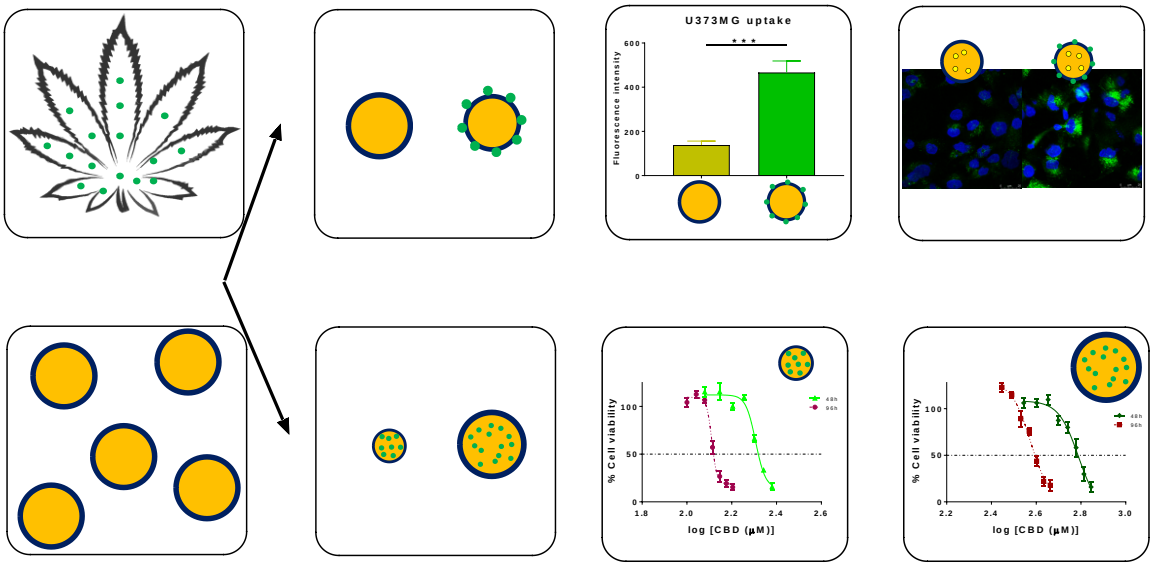

The potential of lipid nanocapsules decorated and loaded with cannabidiol for the treatment of malignant gliomas: *in vitro* evaluation

Juan Aparicio-Blanco [a], Víctor Sebastián [b, c], Jean P. Benoit [d], Ana I. Torres-Suárez [a, e]

[a] Department of Pharmaceutics and Food Technology, Complutense University

[b] Department of Chemical Engineering, Aragon Institute of Nanoscience (INA), University of Zaragoza, Zaragoza, Spain

[c] Networking Research Center on Bioengineering, Biomaterials and Nanomedicine (CIBER-BBN), Madrid, Spain

[d] MINT, UNIV Angers, INSERM 1066, CNRS 6021, Université Bretagne Loire, Angers, France

[e] University Institute of Industrial Pharmacy, Complutense University

Abstract

The therapeutic potential of cannabinoids has been truly constrained heretofore due to two main issues: their strong psychoactive effects and their high lipophilicity. In this context, precisely due to the lack of psychoactive properties, cannabidiol, the second major component of *Cannabis sativa*, arises as the phytocannabinoid with the most auspicious therapeutic potential. Hence, the incorporation of CBD in lipid nanocapsules will contribute to overcome the dosing problems associated with cannabinoids.

Herein, we have encapsulated CBD into the oily core of LNCs to test their *in vitro* efficacy as extended-release carriers against the human glioblastoma cell line U373MG. The *in vitro* antitumor effect of CBD against human glioblastoma was demonstrated and the size of LNCs played a pivotal role in the extent of CBD release: 20 nm-sized LNCs reduced by 3.0-fold the IC_{50} value of 50-nm sized LNCs. Moreover, to explore the potential of this phytocannabinoid to target any of the cannabinoid receptors overexpressed in glioma cells, we have developed a functionalization strategy of LNCs with CBD that enhanced the *in vitro* glioma targeting properties by 3.4-fold in comparison with their equally-sized unmodified counterparts. Lastly, the combination of CBD-loading with CBD-functionalization further reduced the IC_{50} values. Hence, the potential of these two strategies of CBD incorporation into LNCs deserves subsequent *in vivo* evaluation.

Keywords

Cannabinoids, lipid nanocarriers, glioma targeting, extended-release, phase inversion temperature

1. Introduction

Cannabis sativa is an herbaceous plant that contains over one hundred distinct pharmacologically-active terpenophenols that are produced in its glandular trichomes [1]. These compounds are known as phytocannabinoids since they chiefly exert their pharmacological effect on cannabinoid receptors. Other two types of cannabinoids are currently acknowledged: endocannabinoids, produced naturally by animals and humans, and synthetic cannabidomimetics.

Various cannabinoids produce strong psychoactive effects, which have truly constrained their therapeutic potential. As a proof of it, the marketing authorization of rimonabant, a synthetic cannabidomimetic that had been approved as anorectic for obese patients, was withdrawn in 2009 due to its severe psychiatric side effects. Fortunately, cannabidiol (CBD), the second major component of *Cannabis sativa*, with the tetrahydrofuran ring cleaved, is devoid of psychoactive properties. Precisely due to this lack of psychoactive effects, CBD is doubtless the most auspicious phytocannabinoid for the treatment of various pathologies, namely inflammatory and neurodegenerative diseases, mental disorders, neuropathic pain, epilepsy and cancer [2]. In the latter case, apart from palliating cancer-related symptoms (such as nausea, pain or anorexia), CBD has been reported to promote apoptotic cancer cell death through the production of reactive oxygen species, to impair tumor angiogenesis and to reduce cell migration that ultimately accounts for metastasis [3-5]. Particularly, the expression of different receptors to which the phytocannabinoids bind is increased in glioma (cannabinoid receptors 1 and 2 (CB1 and CB2) [6] and transient potential vanilloid receptor type 2 (TRPV2) [7]). Accordingly, activation of these receptors by CBD induced apoptosis of glioma cells, while no effects were observed in normal human astrocytes [7, 8].

Glioblastomas are the most prevalent and aggressive type of glioma (classified as the highest malignancy grade of gliomas by the World Health Organisation due to their high proliferative potential and invasiveness) [9]. Since the current standard of care of glioblastoma remains questionable, with a poor median survival of 14.6 months and a 2-year survival rate of 26.5% [10], CBD can serve to widen the therapeutic armamentarium for the treatment of malignant brain tumors thanks to its synergistic effects with the currently available drugs and radiotherapy [11]. As a proof of it, CBD has already reached the clinical trials stage in combination with chemo and/or radiotherapy for patients with glioblastoma (NCT01812616, NCT01812603, NCT03246113 and NCT03529448).

Nonetheless, the high lipophilicity of cannabinoids, including CBD, has also hampered their therapeutic potential. In this context, these substances can take great advantage of nanomedicine-based formulation strategies. Consistently, several studies on nanocarriers encapsulating the different kinds of cannabinoids (phytocannabinoids [12-14], cannabidomimetics [15-18], and endocannabinoids [19] have started being published recently with distinct therapeutic purposes. Notwithstanding that for cannabinoids to achieve high translational impact these should be devoid of

psychoactive effects, the focus so far has been mainly put on the encapsulation of Δ^9-THC and Δ^9-THC analogues.

Herein, we develop monodisperse lipid nanocapsules (LNCs) as biocompatible and biodegradable carriers for CBD, the major non-psychotropic phytocannabinoid. LNCs are prepared by the energetically efficient phase inversion temperature method. We encapsulate CBD into the oily core of LNCs at high drug loading, under the assumption that it would help overcome classical formulation issues linked to cannabinoids and attain a platform for its prolonged release after administration. Their *in vitro* efficacy against the human glioblastoma cell line U373MG is evaluated by means of cell viability experiments. The role played by the size of LNCs in CBD release and cytotoxicity is likewise thoroughly explored. Moreover, we evaluate the possibilities of this cannabinoid to target any of the cannabinoid receptors overexpressed in glioma cells as aforementioned. To this end, we develop a functionalization strategy of LNCs with CBD wherewith subsequently conduct uptake experiments on the same human glioblastoma cell line to evidence the potential targeting efficiency of this strategy.

2. Materials and methods

2.1. Materials

Labrafac lipophile® WL 1349 (caprylic-capric acid triglycerides) was kindly supplied by Gattefossé. Kolliphor® HS15 ($C_{18}E_{15}$ polyethylene glycol (15) 12-hydroxystearate) was a gift from BASF. Lipoid® S75 (soybean lecithin with 70% of phosphatidylcholine) was supplied by Lipoid-Gmbh. NaCl was purchased from Panreac. De-ionized water was obtained from a MilliQ® Purification System. The fluorescent dye 3,3'-dioctadecyloxacarbocyanine perchlorate (DiO) was purchased from Invitrogen Molecular Probes. Cannabidiol (CBD) was provided by THC-Pharma. Methanol, acetonitrile and tetrahydrofuran HPLC grade were purchased from Fisher Scientific. Amicon® Ultra 15 mL Centrifugal Filters (MWCO: 10 kDa) were supplied by Merck Millipore. Dulbecco's Modified Eagle Medium (DMEM) and Penicillin-Streptomycin (10,000 U/mL) were provided by Gibco. Fetal bovine serum was supplied by Biowest. Hank's Balanced Salt Solution (HBSS), 3-(4,5-dimethyl-2-thiazolyl)-2,5-diphenyl-2H-tetrazolium bromide (MTT), dimethyl-sulfoxide (DMSO) and sterile Nunc Lab-Tek® chamber slides (8 wells, Permanox® slide, 0.8 cm^2/well) were purchased from Sigma-Aldrich. Vectashield® mounting medium with DAPI (H-1200) was provided by Vector Laboratories.

2.2. Cell line

The human glioblastoma U373MG cells were cultured in DMEM medium supplemented with 10% fetal bovine serum (FBS), 100 U/mL penicillin and 100 µg/mL streptomycin at 37ºC in an humidified atmosphere containing 5% CO_2. For all experiments, cells between passage 15 and 25 were used.

2.3. Preparation of lipid nanocapsules

2.3.1. Blank lipid nanocapsules

Lipid nanocapsules (LNCs) were prepared by the phase inversion temperature (PIT) method. Succinctly, Labrafac lipophile® WL 1349,Koliphor® HS15, Lipoid® S75, NaCl and water were mixed under magnetic stirring and progressively heated over the phase inversion temperature of the system. Subsequently, the mixture was gradually cooled down until the phase inversion temperature was reached. Then, a sudden quench with cold water (5 mL) was performed to obtain the final suspension of LNCs. By varying the relative proportions of the excipients, formulations of blank LNCs in different sizes were prepared.

2.3.2. Cannabidiol-loaded LNCs

Cannabidiol (CBD) was encapsulated in LNCs for *in vitro* efficacy experiments. To prepare the CBD-loaded LNCs, the cannabinoid was firstly dissolved in the oily phase that constitute the core of the LNCs at a concentration of 15 % CBD/ Labrafac lipophile® WL1349 (w/w). Then, the remaining excipients were added and progressively heated and cooled down around the phase inversion temperature as indicated in 2.3.1.

2.3.3. Fluorescently-labeled LNCs

The fluorescent dye DiO was encapsulated in LNCs for particle tracking purposes in *in vitro* experiments. To prepare the dye-loaded LNCs, the fluorescent dye was firstly dissolved in the oily phase that constitute the core of the LNCs at a weight ratio of 15 mg of dye/ g of Labrafac lipophile® WL1349. Then, the remaining excipients were added and progressively heated and cooled down around the phase inversion temperature as indicated in 2.3.1.

2.3.4. Functionalization of LNCs with CBD

Pre-formed blank LNCs were incubated with a CBD solution to ultimately obtain functionalized LNCs at two different concentrations of CBD (10 mg/mL in a 1:4 (v/v) ratio for a final CBD concentration of 2.5 mg/mL and 15 mg/mL in a 1:3 (v/v) ratio for a final CBD concentration of 5 mg/mL, respectively). The mixture was gently stirred overnight until complete solvent evaporation. The contribution of the solvent itself to the size distribution of LNCs was ruled out by incubating LNCs with pure solvent. Similarly, fluorescently-labeled and CBD-loaded LNCs were also functionalized with CBD at the higher concentration (5 mg/mL).

The detailed excipient weight for each group of LNCs is shown in Table 1: blank LNCs (F1-F3), CBD-loaded LNCs (F4-F6), CBD-functionalized LNCs (2.5 mg/mL –F7-F9- and 5 mg/mL –F10-F12), fluorescently-labeled LNCs (F13-F16) and CBD-functionalized-CBD-loaded LNCs (F17 and F18).

Table 3.2.1: Detailed excipient weight (in mg) for each formulation of LNC in final suspension.

Excipient	F1	F2	F3	F4	F5	F6	F7	F8	F9	F10	F11	F12	F13	F14	F15	F16	F17	F18
Kolliphor ® HS15	1934	846	484	1934	846	484	860	376	215	645	282	161	1934	846	645	282	645	282
Lipoid® S75	75	75	75	75	75	75	33	33	33	25	25	25	75	75	25	25	25	25
NaCl	89	89	89	89	89	89	40	40	40	30	30	30	89	89	30	30	30	30
Labrafac lipophile® WL 1349	846	1028	1209	846	1028	1209	376	457	537	282	343	403	846	1028	282	343	282	343
Water	6056	6962	7143	6056	6962	7143	2691	3094	3175	2018	2320	2381	6056	6962	2018	2320	2018	2320
CBD	-	-	-	127	154	181	10	10	10	15	15	15	-	-	15	15	57	66
DiO	-	-	-	-	-	-	-	-	-	-	-	-	12	15	4	5	-	-

2.4. Characterization of LNCs

2.4.1. Size distribution and zeta potential

The mean volume diameter and polydispersity index (PdI) of each formulation were measured by dynamic light scattering (DLS) using a Microtrac® Zetatrac™ Analyzer (Microtrac Inc., USA). Measurements were done in triplicate. The zeta potential of the different formulations of LNCs was measured by means of a Zetasizer Nano ZS (Malvern Instruments).

2.4.2. Morphological examination of LNCs

The morphological examination of LNCs was performed by transmission electron microscopy (TEM). TEM images were taken on a T20-FEI Tecnai thermoionic microscope at the Advanced Microscopy Laboratory, LMA, (Zaragoza, Spain). To prepare the samples for TEM, 20 µl of lipid nanocapsule suspension was dropped on a carbon copper grid (200 mesh), negatively stained with phosphotungstic acid and dried at room temperature. The microscope was operated at an acceleration voltage of 200 kV.

2.4.3. Incorporation efficiency and drug content

The incorporation efficiency (IE) and drug content (DC) of CBD in the different formulations of LNCs were determined by high performance liquid chromatography (HPLC). The HPLC method was adapted from [20]. An Agilent 1200 Infinity HPLC system was utilized. A mixture of methanol: acetonitrile: water (52:30:18 v/v) at a flow rate of 1.8 mL/min was used as mobile phase. The analytical column was a reversed-phase Mediterranea Sea® C18 (5µm 15 x 0,46 cm) (Teknokroma®). The retention time of CBD was 5 minutes.

The incorporation efficiency was calculated using Equation 1, whereas the drug content was calculated using Equation 2:

$$IE(\%) = \frac{Amount\ of\ CBD\ associated\ with\ LNCs}{Amount\ of\ CBD\ initally\ added} x100 \quad \text{(Equation 1)}$$

$$DC(\%) = \frac{Amount\ of\ CBD\ associated\ with\ LNCs}{Nanocapsule\ excipients' weight} x100 \quad \text{(Equation 2)}$$

where the amount of CBD associated with LNCs in each case was determined as the difference between the unassociated CBD filtered with 10 kDa Amicon® Centrifugal Filters (6000 rpm, 60 min) and the total amount of CBD in suspension derived from the lysis of LNCs with tetrahydrofuran (1:5 (v/v)).

2.5. *In vitro* cytotoxicity

Free CBD, CBD-loaded LNCs (F10 and F11) and CBD-functionalized CBD-loaded LNCs (F17 and F18) were assessed for cytotoxicity against human glioblastoma U373MG cells using a MTT assay. Briefly, U373MG cells were seeded into 96-well plates at a density of 2 x 10^4 cells/well. After cells had been confluent for 48 hours, they were treated with free CBD for 48 hours and with suspensions of LNCs

(200 µL) for 48 and 96 hours. Then, the medium was removed and 60 µL of MTT solution (1 mg/mL) in complete DMEM were added to each well and incubated for 4 hours. Afterwards, the media containing MTT was removed and 100 µL of DMSO was added to each well. The plates were agitated for 10 minutes and the absorbance was measured at 570 nm using a microplate reader (Varioskan Flash, Thermo Scientific). Experiments were performed in triplicate at each time-point. For each formulation of CBD-loaded LNCs, U373MG cells treated with their blank counterparts served as control. Cell viability of each group was expressed as a percentage relative to that of control. Inhibitory concentration (IC_{50}) was calculated in each case for comparison purposes.

2.6. *In vitro* cellular uptake

2.6.1 Uptake experiments evaluated by flow cytometry

To quantitatively evaluate the glioma targeting ability of LNCs *in vitro*, U373MG cells were seeded into 6-well plates at a density of 2.5 x 10^5 cells/well. After cells had been confluent for 48 hours, the culture medium was replaced by DiO-labeled LNCs (F13-F16 at an equivalent dye concentration of 1.65 µg DiO/mL of suspension) suspended in complete DMEM (2 mL) wherewith cells were incubated for 24 hours. Then, cells were rinsed with HBSS, trypsinized and finally resuspended in 0.3 mL HBSS. The fluorescence intensity of cells treated with fluorescent-LNCs was analyzed with a flow cytometer (Beckman Coulter Epics XL). Experiments were performed in triplicate. U373MG cells treated with blank LNCs served as control. Cellular uptake of each group was expressed as fold-increase in fluorescence mean relative to that of control after correction for the different amount of dye per individual LNC in each formulation.

2.6.2. Uptake experiments evaluated by laser scanning confocal microscopy

To qualitatively illustrate the glioma targeting ability of LNCs *in vitro*, U373MG cells were seeded into chamber slides at a density of 2 x 10^4 cells/well. After cells had been confluent for 48 hours, the culture medium was replaced by unmodified or CBD-functionalized DiO-labeled LNCs at an equivalent dye concentration of 1.65 µg DiO/mL suspended in complete DMEM (0.35 mL) wherewith cells were incubated for 24 hours. Then, cells were rinsed with HBSS and mounted with Vectashield® with DAPI mounting medium. The cells were then observed with a confocal microscope (Leica TCS SP5, 405 nm for DAPI, 488 nm for DiO). U373MG cells treated with blank LNCs served as control.

2.7. Statistical analysis

All experiments were done in triplicate and all data are expressed as mean ± SEM. Unpaired Student's t test was used for two-group analysis. Statistical significance was fixed as *:$p<0.05$, **:$p<0.1$,***:$p<0.001$. All the data were analyzed using the GraphPad Prism 7 software.

3. Results and discussion

Blank monodisperse LNCs were obtained by the PIT method in different sizes by varying the relative proportion of excipients as detailed in Table 1 (F1-F3). In formulations F4-F6, CBD was included in the formulation procedure as drug payload dissolved in the oily phase of the core of the capsules at a concentration of 15 % CBD/Labrafac lipophile® WL1349 (w/w). The choice of the oily phase was based on the solubility of CBD to easily achieve both high encapsulation efficiencies and drug loading. In this regard, whereas the authors that tried to encapsulate distinct cannabinoids in polymer nanoparticles only achieved encapsulation efficiencies around 70% [15, 16, 21], those studies that utilized lipid-based carriers exhibited values above 90% [17, 22]. This comparison has been corroborated by Durán-Lobato et al. [23]. Unlike these authors, we utilized a low-energy method to prepare monodisperse lipid carriers in smaller sizes. The high incorporation efficiencies reported herein (Table 2) are in agreement with those values achieved for the incorporation of drug substances with similar log P values into analogous carriers [24, 25] and significantly higher than those obtained with less lipophilic drug substances, as etoposide with a log P= 1.1 only achieved a 56% of incorporation efficiency [26]. However, whereas these authors achieved at best a drug loading of 1.5% [25], we have utilized herein much higher percentages of CBD content (Table 2, F4-F6). According to our size distribution measurements, for all these CBD-loaded formulations (F4-F6) there was a statistically significant increase in particle size that progressively augmented with the initial size of blank LNCs (Fig. 1a, $p<0.05$). These results are positively correlated with the respective percentage of drug loading that represented CBD in each case, which was the highest for the biggest LNCs (9.78%) and the lowest for the smallest ones (4.30%). Interestingly, the CBD loading in the oily core did not significantly alter the polydispersity index (PdI) in comparison with blank LNCs (Fig 1b, $p>0.05$). Moreover, in agreement with the hypothesized encapsulation within the oily core, no changes in the zeta potential profiles were evidenced (Fig. 1c-h). Indeed, values close to neutrality with high profile width were obtained in all cases, as it might be expected from a shell made of a complex mixture of poly (ethoxylated) surfactants (Kolliphor HS15®). Consistently, the width of the zeta potential distribution was progressively reduced with a decrease in the surfactant percentage (from the smallest (Fig. 1 c-d) to the biggest LNCs (Fig. 1 g-h)).

Table 3.2.2: Incorporation efficiencies (IE) and drug content (DC) of the different LNCs following the distinct strategies to incorporate CBD discussed in the text.

LNC formulation	IE (%)	DC (%)
F4	96.75 ± 1.45	4.30 ± 0.07
F5	96.43 ± 3.25	7.66 ± 0.30
F6	95.38 ± 1.25	9.78 ± 0.13
F7	94.17 ± 1.54	0.76 ± 0.02
F8	98.91 ± 2.75	1.16 ± 0.02
F9	95.22 ± 0.78	1.21 ± 0.01
F10	96.99 ± 2.58	1.55 ± 0.07
F11	95.97 ± 4.72	2.17 ± 0.06
F12	98.61 ± 2.02	2.51 ± 0.06

Figure 3.2.1: Characterization of the encapsulation strategy of CBD within the oily core of LNCs: blank (F1-F3) and CBD-loaded (F4-F6) LNCs. (a) Average volume diameter (nm). (b) Polydispersity index (PdI). (c-h) Zeta potential profiles of F1 (c), F4 (d), F2 (e), F5 (f), F3 (g) and F6 (h).

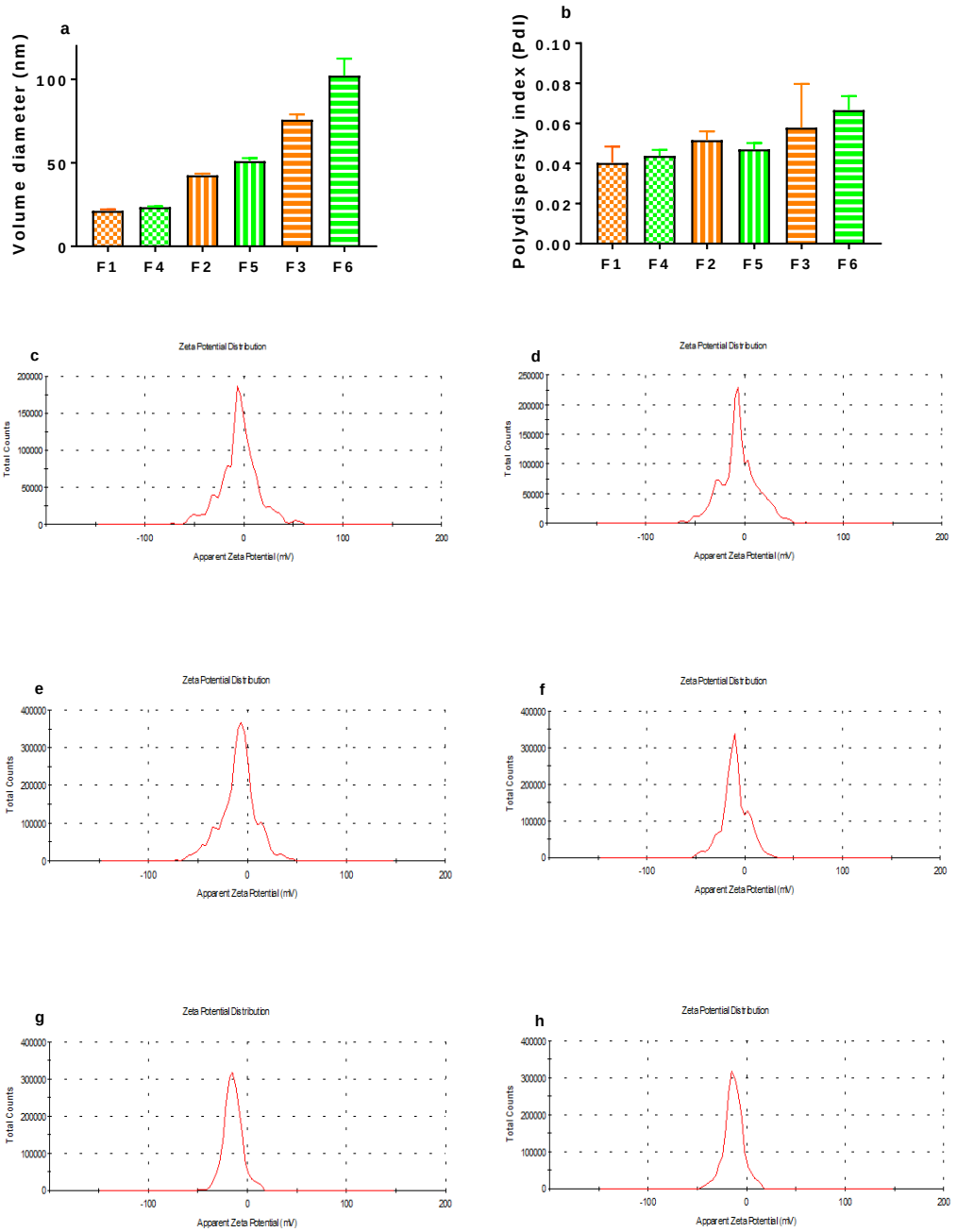

Moreover, to explore the potential of this phytocannabinoid to target any of the cannabinoid receptors overexpressed in glioma cells, we have developed a functionalization strategy of LNCs with CBD on their surface. This strategy consisted in the incubation of pre-formed LNCs with a CBD solution to obtain functionalized LNCs at two different concentrations of CBD (2.5 and 5 mg/mL, respectively). The incubation of LNCs with pure solvent did not contribute to any increase in particle size (data not

shown). Hence, all changes observed in the characterization of LNCs were attributed to the cannabinoid itself. We followed an analogous procedure to the one utilized by other authors to incorporate novel targeting peptides on the surface of LNCs [27, 28]. However, whereas these authors only achieved 48.3% adsorption efficiency, we report herein higher incorporation efficiencies for CBD-functionalization (Table 2). These results could be explained by the lower aqueous solubility of CBD than peptides, which ultimately favors its adsorption at the amphiphilic surfactant interface. According to the size distribution measurements, the functionalization with CBD significantly increased the particle size of blank LNCs (Fig. 2a, $p<0.05$). This increase in average volume diameter is noticeably higher than the increase observed for CBD-loaded LNCs (F4-F6), even if the percentage of drug content is much lower in the case of CBD-functionalized LNCs (Table 2). These results supported that CBD should be placed in a distinct location than the capsule core. Indeed, the increase in volume diameter followed an inverse size-related pattern: the greatest percentage of size increase was observed with the smallest LNCs (75%) and vice versa (33% increase for medium-sized LNCs and 16% increase for the biggest LNCs). The higher specific surface area and the higher surfactant density at the particle interface of the smallest LNCs could account for this trend observed upon CBD functionalization. Noticeably, the polydispersity index in the smallest and medium-sized LNCs was significantly increased in comparison with their blank counterparts (Fig. 2b, $p<0.01$), which did not occur when the CBD was incorporated dissolved in the oily core. Furthermore, in agreement with the hypothesized superficial location of CBD, the zeta potential profiles were remarkably smoothed in comparison to the ones previously obtained both for blank and CBD-loaded LNCs (Fig. 2 c-h). These profiles are consistent with a shell dominated by a single entity instead of the former mixture of poly (ethoxylated) surfactants and, accordingly, were steadily sharpened with an increase in CBD content in the final formulation from 2.5 mg/mL (Fig. 2 c, e, g) to 5 mg/mL (Fig. 2 d, f, h).

The different formulations of LNCs were visualized through transmission electron microscopy (TEM). Interestingly, TEM images served to evidence the spherical morphology of LNCs (Fig. 3). In no case did this geometry significantly vary upon incorporation of CBD. Moreover, the previous analysis of size distribution of the different formulations based on DLS data was highly corroborated with particle sizes observed through TEM (Fig. 3).

Altogether, our results highlight that LNCs arise as biocompatible and biodegradable carriers for CBD, the main non-psychotropic phytocannabinoid, which will doubtless contribute to palliate the technological constraints traditionally associated with cannabinoids due to their high lipophilicity [29]. In particular, we have encapsulated CBD into the oily core of LNCs at high drug loading to attain a prolonged-release platform for this cannabinoid wherewith we will test heir *in vitro* efficacy against the human glioblastoma U373MG cell line. Moreover, we have decorated the surface of LNCs with CBD wherewith subsequently conduct uptake experiments on the same human glioblastoma cell line to explore the possibilities of this cannabinoid to target *in vitro* any of the cannabinoid receptors overexpressed in glioma cells.

Figure 3.2.2: Characterization of the functionalization strategy of LNCs with CBD: blank (F1-F3), CBD-functionalized (2.5 mg CBD/mL of suspension) (F7-F9) and CBD-functionalized (5 mg/mL CBD/mL of suspension) (F10-F12) LNCs. (a) Average volume diameter (nm). (b) Polydispersity index (PdI). (c-h) Zeta potential profiles of F7 (c), F10 (d), F8 (e), F11 (f), F9 (g) and F12 (h).

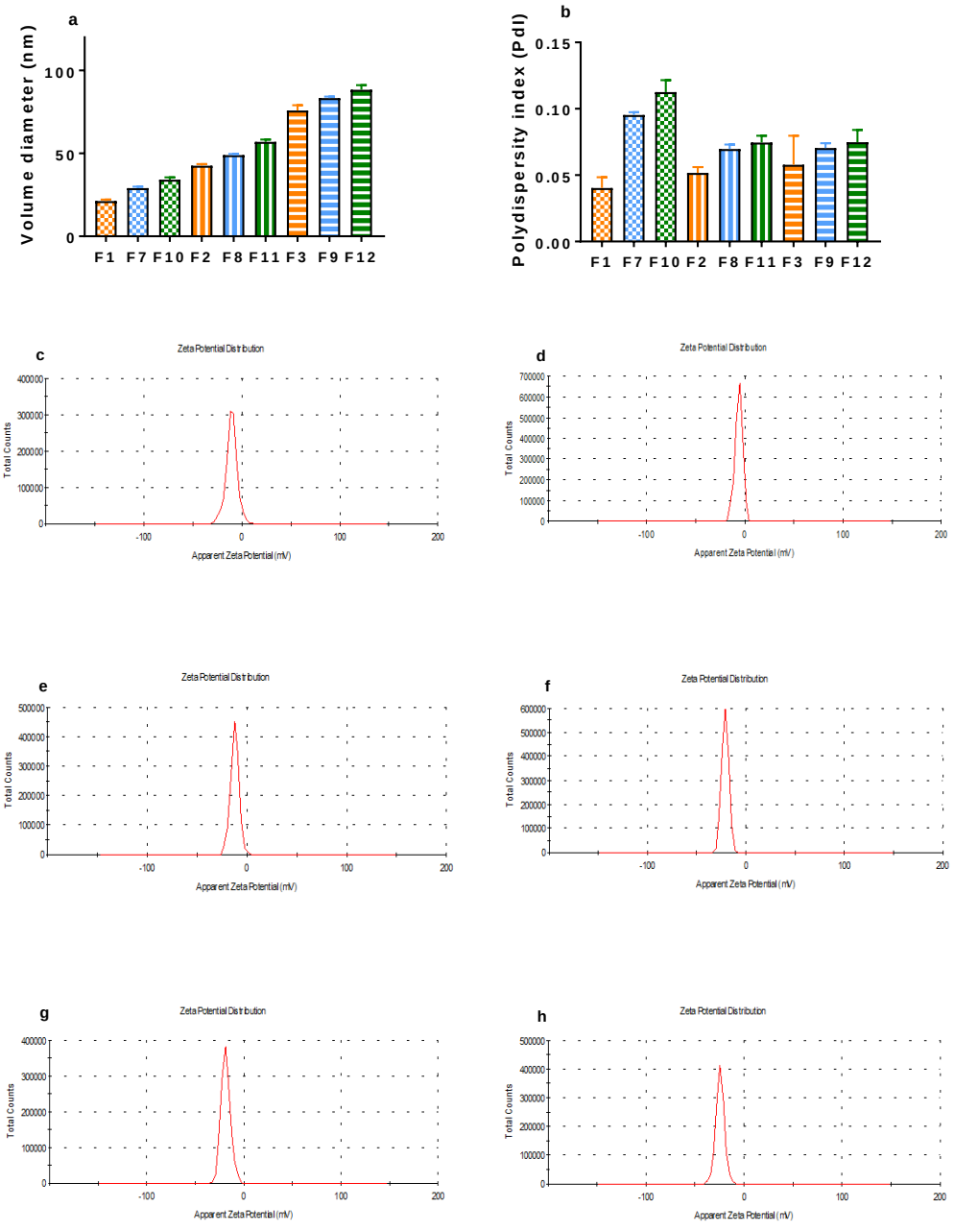

The fact of having obtained two distinct delivery systems with the CBD located either in the oily core or on the surface of the LNCs by varying the formulation procedure seems to refute the drop tensiometry experiments performed by some authors to elicit the disposition of a particular cargo within a core-shell carrier on the grounds of the monitored surface tension between the aqueous and oily phases upon addition of the cargo [27, 30]. These studies focus on the interactions with the aqueous

and oily phases but overlook the role played by the surfactant shell in the cargo incorporation. Moreover, they underestimate the potential influence of the technological incorporation procedure on the final disposition of the drug substance within the carrier.

Figure 3.2.3: TEM images of the different formulations of LNCs. (a) F1. (b) F4. (c) F10. (d) F2. (e) F5. (f) F11. (g) F3. (h) F6. (i) F12.

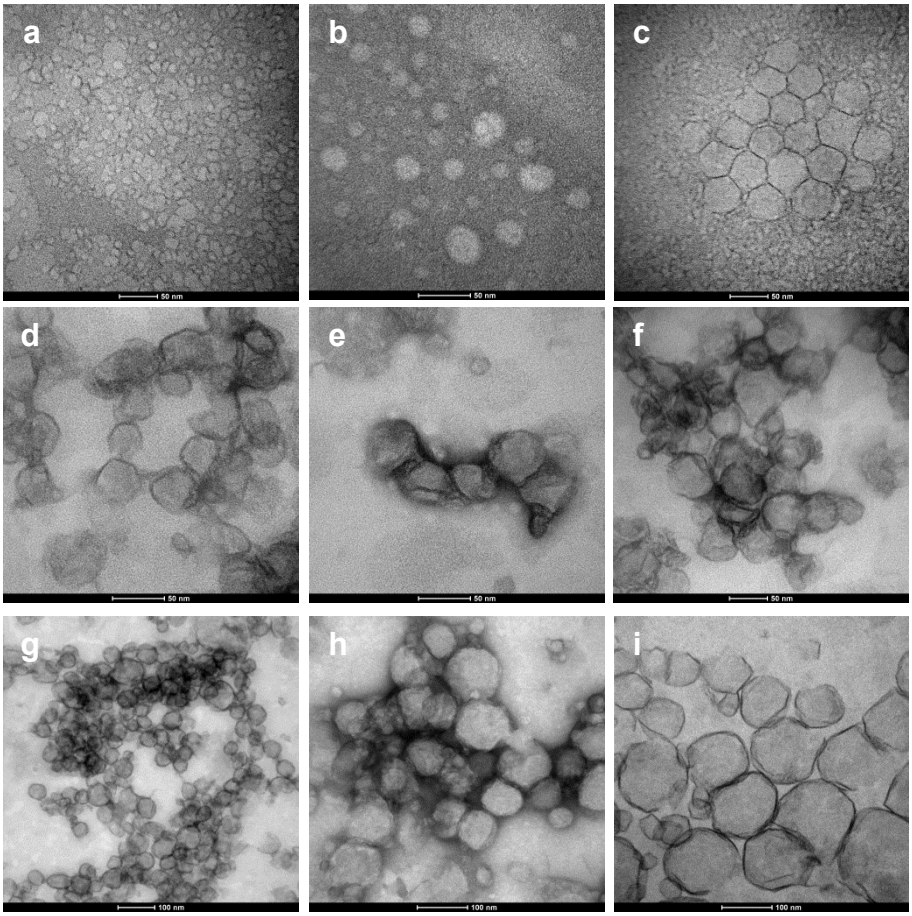

Furthermore, both unmodified and CBD-decorated fluorescently-labeled LNCs were developed for *in vitro* particle tracking purposes (F13-F16) and CBD-decorated-CBD-loaded LNCs were obtained to evidence if the CBD-decoration could enhance the *in vitro* cytoxicity of CBD-loaded LNCs. As shown in Figure 4a, after loading F1 and F2 with fluorescent dyes, we obtained analogously-sized LNCs: 20 nm (F13) and 40 nm (F14). However, the decoration of dye-loaded LNCs with CBD increased the particle size to 40 nm (F15) and 60 nm (F16), respectively. Similarly, the functionalization with CBD of CBD-loaded LNCs (F4 and F5) significantly increased the average volume diameter to 40 nm (F17) and 60 nm (F18), respectively (Figure 4a). As observed with unloaded LNCs, the polydispersity index invariably increased after CBD decoration in comparison with their untargeted counterparts (Figure 4b).

In cytotoxicity experiments, the role played by particle size in the efficacy as extended-release carriers for CBD will be evaluated with 20 nm and 50 nm-sized CBD-loaded LNCs (namely, F4 and F5).

Figure 3.2.4: Characterization of the size distribution of the fluorescently-labeled LNCs and CBD-functionalized-CBD-loaded LNCs: blank (F1-F2), non-functionalized fluorescently-labeled (F13-F14), CBD-functionalized fluorescently-labeled (F15-F16) and CBD-decorated-and-CBD-loaded (F17-F18) LNCs. (a) Average volume diameter (nm). (b) Polydispersity index (PdI).

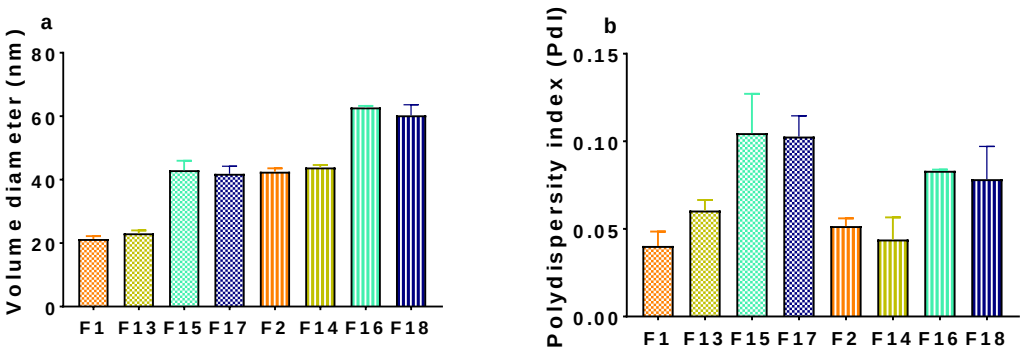

Free CBD and the LNCs loaded with CBD within their oily core were tested for *in vitro* efficacy against the human glioblastoma U373 MG cell line by the MTT assay. Blank LNCs were used as controls for their CBD-loaded counterparts. Remarkably, blank LNCs did not show any significant cytotoxicity against the U373MG cell line within the concentration range tested (cell viability above 70% versus untreated cells according to the ISO 10993-5 Biological evaluation of medical devices, Part 5: Tests for in vitro cytotoxicity). Hence, all changes observed in the percentage of cell viability were attributed to the extent of CBD released from the LNCs at each time point.

Both free CBD and CBD-loaded LNCs reduced the viability of U373MG cells in a concentration-dependent manner, demonstrating thereby the *in vitro* antitumor effect of CBD against human glioblastoma. As shown in Table 3, free CBD (IC_{50} = 29.1 μM) exhibited an evident anti-proliferative effect against the U373MG cells, with an IC_{50} value in agreement with those values reported in [31]. In all cases, the inclusion of CBD within the core of the LNCs considerably increases the IC_{50} value achieved with free CBD. These results are explained by the fact that free CBD is readily available to exert its cytotoxic effect on by glioma cells, whereas encapsulated CBD must be released from the oily core of LNCs firstly, a process that can be prolonged over longer periods. Other authors have recently observed analogous trends for other combinations of drug substances and carriers [32-34].

In particular, we report herein that the size of LNCs plays a pivotal role in the extent of CBD release. In this regard, based on a 48 h treatment period, 20 nm-sized LNCs (F4) outperformed the IC_{50} value of 50-nm sized LNCs (F5): 202.6 μM vs 615.4 μM, respectively (Figure 5, Table 3). This finding highlights the distinct release patterns according to particle size. Moreover, we further evaluated the cytotoxic effect of these formulations over 96 hours to demonstrate if LNCs could serve as efficient prolonged-release carriers. Effectively, both formulations continued to release CBD from their oily cores and the IC_{50} values were consequently reduced with a longer treatment period (129.1 μM vs 202.6 μM for F4 and 375.4 μM vs 615.4 μM for F5). As occurred on the 48 h treatment period, the IC_{50} values were lower for the smaller LNCs (129.1 μM vs

375.4 µM). Noticeably, regardless the incubation period, 20 nm-sized CBD-loaded LNCs (F4) achieved a 3-fold reduction in IC_{50} in comparison with 50-nm sized CBD-loaded LNCs (F5) (Table 3).

Table 3.2.3: IC_{50} values of free CBD and the different CBD-loaded LNCs against the U373MG cell line.

Formulation and time	IC_{50} (µM)
Free CBD 48h	29.1
F4 48h	202.6
F4 96h	129.1
F5 48h	615.4
F5 96h	375.4
F17 48h	158.6
F18 48h	513.2

Figure 3.2.5: Cytotoxicity of free CBD and undecorated CBD-loaded LNCs against the U373MG cell line.

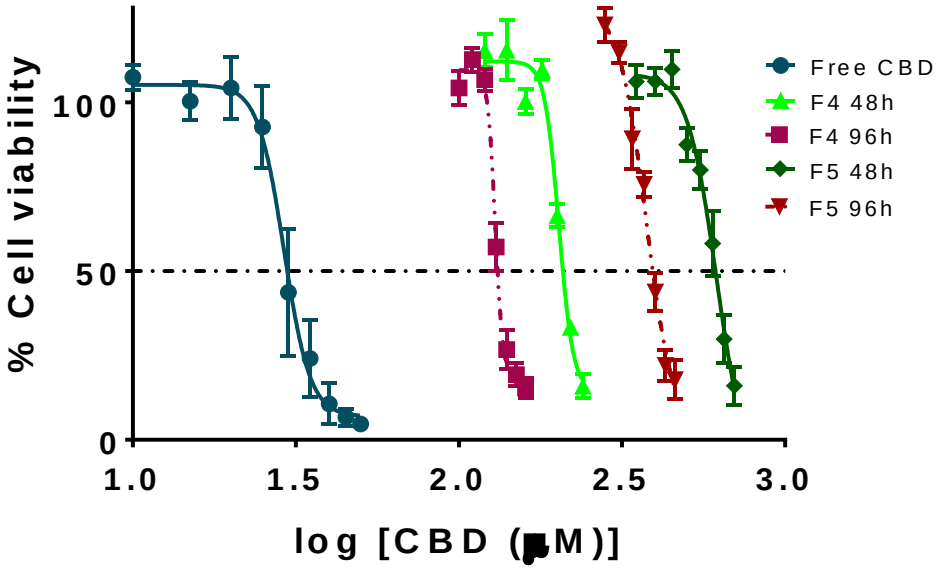

So as to determine their *in vitro* glioma targeting ability, different formulations of fluorescently-labeled LNCs at an equivalent dye concentration of 1.65 µg DiO/mL of suspension were tested on the human glioblastoma U373MG cell line by flow cytometry (Figure 6). In uptake experiments, the role played by particle size in the glioma targeting properties will be assessed separately in non-modified and in CBD-decorated dye-loaded LNCs (namely, F13 vs F14 and F15 vs F16) and, on the other hand, the influence of CBD-decoration in glioma targeting will be evaluated for equally-sized LNCs (namely, F14 vs F15).

Overall, all tested formulations were efficiently internalized by the human malignant glioma cells with more than 99% of positive cells in all cases. On the one hand, the influence of particle size on the extent of cellular uptake by the human glioblastoma cell line was evaluated with the purpose of determining the most

auspicious features that the ideal carrier should accomplish to move forward to *in vivo* studies. This influence was evaluated both in the absence (F13 vs F14) and in the presence of the cannabinoid on the surface of the LNCs (F15 vs F16). In this regard, the measured fluorescence intensities allowed us to draw a consistent comparison of the role played by particle size for both unmodified LNCs (Figure 6a, $p<0.05$) and CBD-functionalized LNCs (Figure 6b, $p<0.001$): a decrease in volume diameter yielded an increase in *in vitro* uptake by malignant glioma cells.

On the other hand, the role played by the functionalization with CBD in the extent of in vitro cellular uptake was also quantitatively evaluated. The modification with CBD significantly enhanced the *in vitro* glioma targeting properties of LNCs, as it was concluded from a comparison of equally sized unmodified and CBD-functionalized LNCs (F14 vs F15, Figure 6c, $p<0.001$). Altogether, the highest glioma targeting ability was achieved with the smallest cannabinoid-modified LNC formulation (F15 in Table 1).

Figure 3.2.6: Evaluation of the *in vitro* cellular uptake of LNCs into the human glioblastoma U373MG cell line by flow cytometry expressed as folds increase in mean fluorescence intensity versus control. (a) Evaluation of the role played by particle size on the *in vitro* cellular uptake of unmodified LNCs ($p<0.05$). (b) Evaluation of the role played by particle size on the *in vitro* cellular uptake of CBD-functionalized LNCs ($p<0.001$). (c) Evaluation of the influence of CBD-functionalization on the *in vitro* glioma targeting efficiency for equally-sized LNCs ($p<0.001$).

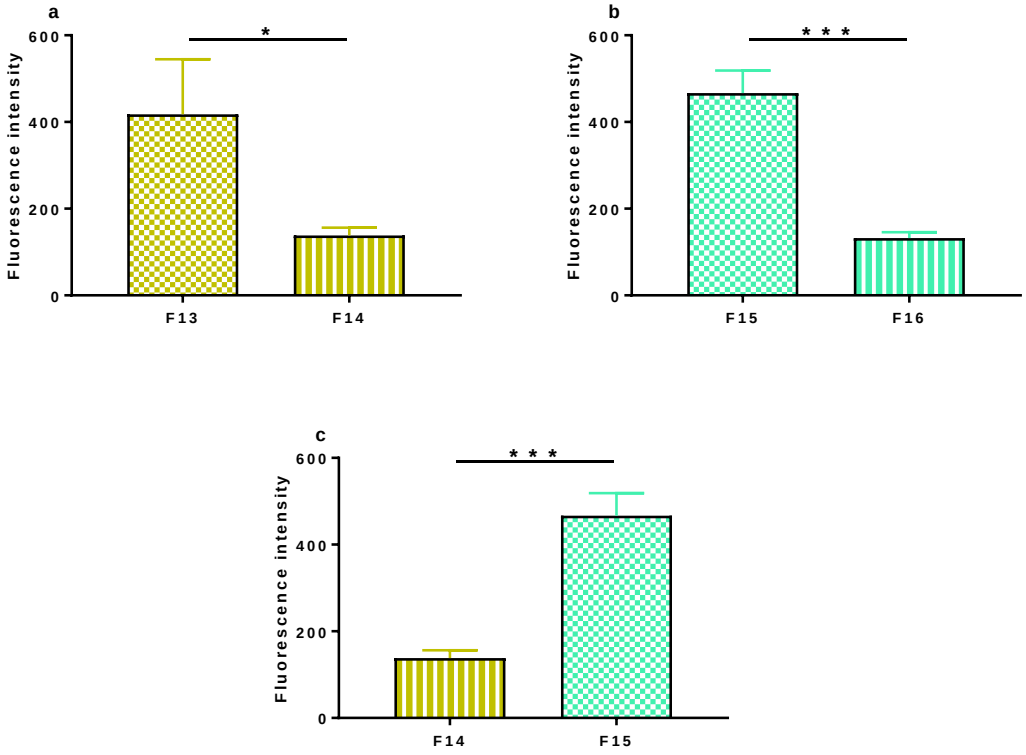

We have reported herein that the modification of LNCs with CBD enhanced the *in vitro* glioma targeting properties by 3.4-fold in comparison with their equally-sized unmodified counterparts. These auspicious *in vitro* glioma-targeting properties

demonstrated for the CBD-functionalization strategy are in the same order of magnitude than those observed with other glioma targeting moieties [35, 36]. For instance, the aptamer AS1411 that binds to nucleolin, a protein overexpressed in highly proliferative cells yielded a 3-fold increase in *in vitro* glioma-targeting properties of poly glutamylglutamine nanoconjugates when tested in the human glioblastoma U87MG cell line [35]. With this same cell line, angiopep-2 (a targeting moiety currently in clinical trials for different brain tumor conditions that promotes receptor-mediated transcytosis across the low density lipoprotein receptor LRP1) enhanced the cellular uptake of poly (lactic-*co*-glycolic) acid nanoparticles by 3.6-fold [36]. Unlike angiopep-2, the non-peptide nature of CBD makes it less prone to cause immunogenicity.

Interestingly, CBD performed better than other tested glioma-targeting moieties. In this regard, two different ligands of the transferrin receptor highly expressed in glioma cells yielded a 1.73-fold and 2.28-fold increase (for transferrin [37] and T7 peptide [38], respectively) in cellular uptake of liposomes and core-shell nanoparticles into the C6 and U87MG cell lines. Analogously, mannose as ligand targeting the glucose transporter only achieved a 1.18-fold increase in cellular uptake of liposomes into the rat glioma C6 cell line [37].

Concomitantly, we have reported herein that a reduction in particle size of LNCs enhanced the cellular uptake by 3.0-fold for unmodified LNCs and 3.5-fold for CBD-modified LNCs. In this regard, it is worth mentioning that none of the aforementioned studies evaluated the role played by particle size on the internalization extent of nanocarriers by glioma cells.

Moreover, the *in vitro* glioma targeting ability of LNCs was further analyzed qualitatively by confocal microscopy. As shown in Figure 7, both unmodified and CBD-functionalized LNCs were efficiently internalized by U373MG cells. The images taken by confocal microscopy consistently demonstrated a significantly higher glioma targeting effect for CBD-functionalized LNCs. Furthermore, intracellularly LNCs seem to exhibit a perinuclear location, as the images from the DiO channel perfectly serves to delimit the nuclear region.

Given the enhancement in *in vitro* glioma targeting properties of the CBD-decorated LNCs evidenced by flow cytometry and confocal microscopy, we tested if the functionalization of CBD-loaded LNCs with CBD, with the ensuing enhanced internalization extent, could further reduce the IC_{50} values achieved for their undecorated counterparts. As shown in Figure 8, CBD-functionalized CBD-loaded LNCs outperformed the cytotoxicity of CBD-loaded LNCs following 48 hours treatment (namely, 158.6 μM vs 202.6 μM for F17 and F4; and 513.2 μM vs 615.4 μM for F18 and F5, respectively, Table 3). These results can be accounted for by the differences in the drug release rate as a function of the distinct location of the CBD in each formulation. Whereas CBD-decorated LNCs exhibit part of the cannabinoid on their surface, and hence more prone to faster release within glioma cells, undecorated CBD-loaded LNCs have the totality of the drug encapsulated within the oily core, wherein CBD has higher solubility and calls for a longer distance for diffusion.

Figure 3.2.7: Evaluation of the *in vitro* cellular uptake of LNCs into the human glioblastoma U373MG cell line by confocal microscopy: DAPI (left), DiO (center), merged (right). (a) Blank LNCs. (b) unmodified fluorescently-labeled LNCs. (c) CBD-decorated fluorescently-labeled LNCs. Scale bar = 25 µm.

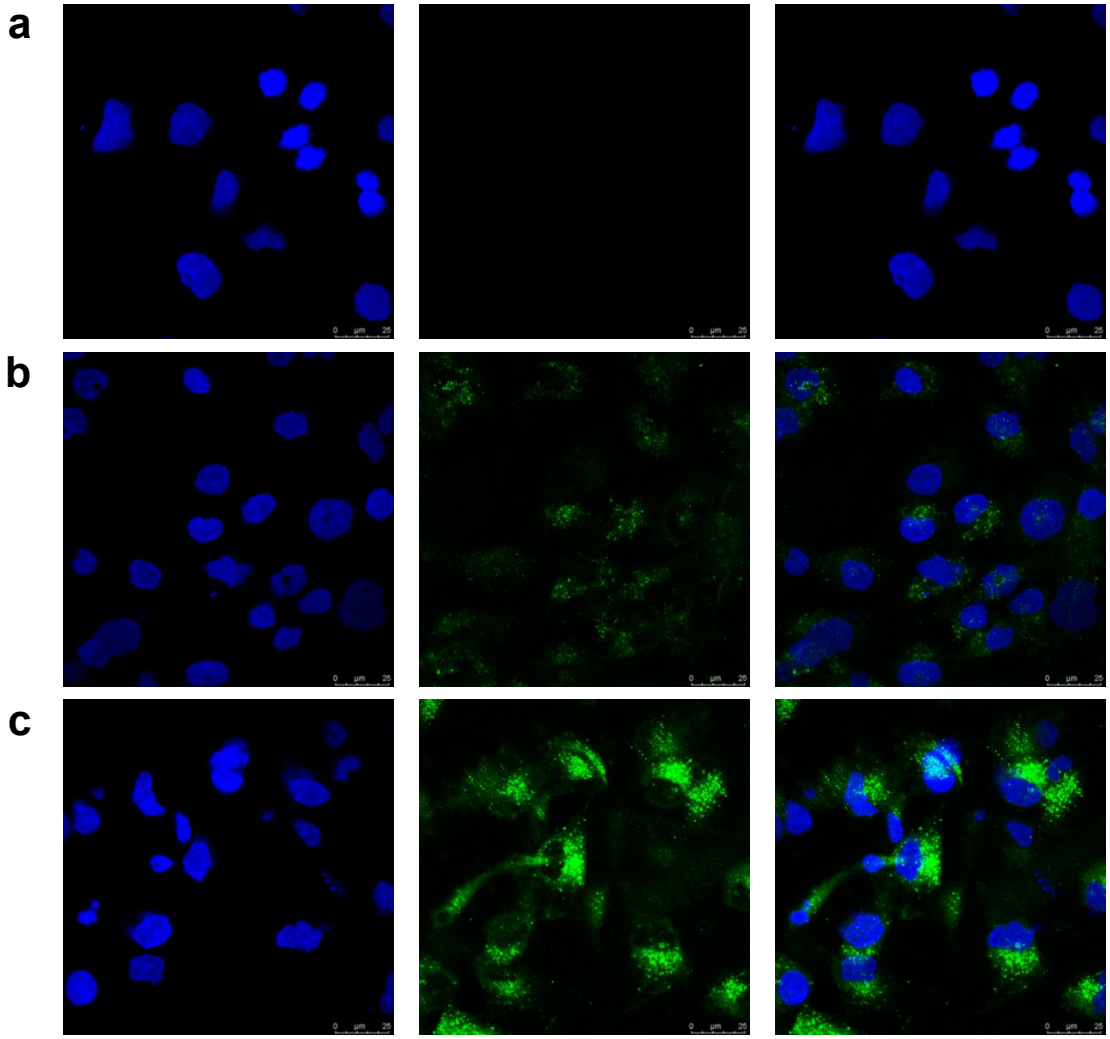

Altogether, results from cytotoxicity and uptake experiments are highly interrelated. On the one hand, a decrease in volume diameter yields a reduction in the IC_{50} values in cytotoxicity experiments due to the faster CBD release and an increase in the *in vitro* uptake by glioblastoma cells. Hence, the cellular uptake and the drug release rate that ultimately leads to greater cytotoxicity against glioma cells can be tailored by varying the particle size of LNCs. On the other hand, the functionalization of with CBD further reduced the IC_{50} values of CBD-loaded LNCs and enhanced the *in vitro* glioma targeting properties of LNCs.

4. Conclusions

Although cannabinoids show auspicious pharmacological properties, their therapeutic potential has not yet been widely explored due to two main issues: their strong psychoactive effects and their high lipophilicity. Hence, precisely due to their lack of psychoactive properties, cannabidiol (CBD) can take great advantage of

nanomedicine-based formulation strategies for the treatment of various pathologies. In particular, CBD has been reported to not only palliate cancer-related symptoms (such as nausea, pain or anorexia) but also promote apoptotic cancer cell death through the production of reactive oxygen species, impair tumor angiogenesis and reduce cell migration. Therefore, CBD could serve to widen the therapeutic armamentarium for the treatment of malignant brain tumors thanks to its synergistic effects with the currently available treatments and to this end, we have encapsulated CBD into the oily core of LNCs at high drug loading and evaluated their *in vitro* efficacy as prolonged-release carriers against the human glioblastoma cell line U373MG. The *in vitro* antitumor effect of CBD against human glioblastoma has been confirmed and the size of LNCs has been evidenced to play a pivotal role in the extent of CBD release: 20 nm-sized LNCs reduced by 3.0-fold the IC_{50} value of 50-nm sized LNCs.

Figure 3.2.8: Comparison of the cytotoxicity of undecorated CBD-loaded LNCs (F4 and F5) with CBD-functionalized CBD-loaded LNCs (F17 and F18) against the U373MG cell line following 48 hours treatment.

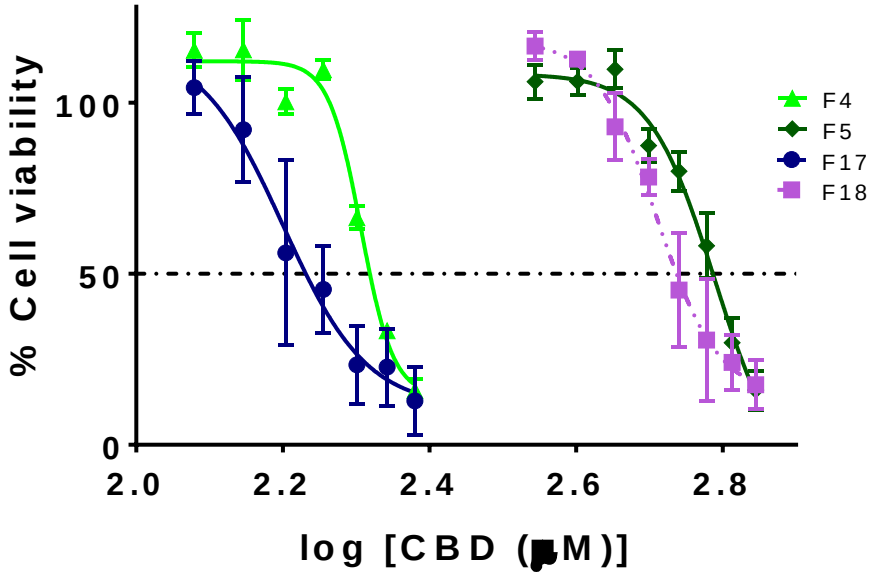

Moreover, since the expression of different receptors to which the cannabinoids bind is increased in glioma, CBD could actively target glioma cells. Therefore, we have functionalized LNCs with CBD and evaluated their *in vitro* glioma targeting ability with the same human glioblastoma cell line. The functionalization of LNCs with CBD enhanced the *in vitro* glioma targeting properties by 3.4-fold in comparison with their equally-sized unmodified counterparts. These glioma-targeting properties equal the enhancements obtained with some other targeting moieties such as the AS1411 and angiopep-2 (the latter has already reached the clinical trials stage) and even outperform those achieved with transferrin and mannose.

Lastly, provided that the functionalization with CBD enhances the *in vitro* glioma targeting, we further evaluated if the functionalization of CBD-loaded LNCs with CBD could further reduced the IC_{50} values achieved for their undecorated counterparts. In all

cases, CBD-functionalized CBD-loaded LNCs outperformed the cytotoxicity of CBD-loaded LNCs following 48 hours treatment.

Taken together, our results offer great promise for subsequent *in vivo* evaluation of LNCs loaded and decorated with CBD.

Acknowledgements

This work was supported by the Complutense Research Fund (Ref. 16/83) and by the Research Group GR35/10 Santander-UCM: Parenteral Administration of Drugs. J. A.-B. would like to thank the Spanish Ministry of Education for his contract within the Professor Training Program FPU (Ref. FPU13/02325) and for funding a research stay at L'unité Micro et Nanomédecines Biomimétiques (MINT) INSERM 1066 CNRS 6021, Angers University (France) (Ref. EST14/00229). J. A.-B. and A. T.-S. would like to thank to Carmen Doñoro, Pedro Lastres, Maite Seisdedos and Gema Elvira from the Biological Research Center (CIB, Spanish National Research Council CSIC) for the help provided with the cell culture facilities, flow cytometry analysis and confocal microscopy, respectively. V.S. would like to thank CIBER-BBN for support. CIBER-BBN is an initiative funded by the VI National R&D&i Plan 2008–2011 financed by the Instituto de Salud Carlos III with the assistance of the European Regional Development Fund.

References

[1] Andre CM, Hausman JF, Guerriero G. Cannabis sativa: The Plant of the thousand and one Molecules. Front Plant Sci. 2016;7:17.

[2] Pisanti S, Malfitano AM, Ciaglia E, Lamberti A, Ranieri R, Cuomo G, et al. Cannabidiol: State of the art and new challenges for therapeutic applications. Pharmacol Ther. 2017;175:133-50.

[3] Velasco G, Hernandez-Tiedra S, Davila D, Lorente M. The use of cannabinoids as anticancer agents. Prog Neuro-Psychopharmacol Biol Psychiatry. 2016;64:259-66.

[4] Velasco G, Sanchez C, Guzman M. Towards the use of cannabinoids as antitumour agents. Nat Rev Cancer. 2012;12:436-44.

[5] de la Ossa DHP, Lorente M, Gil-Alegre ME, Torres S, Garcia-Taboada E, Aberturas MD, et al. Local Delivery of Cannabinoid-Loaded Microparticles Inhibits Tumor Growth in a Murine Xenograft Model of Glioblastoma Multiforme. PLoS One. 2013;8:8.

[6] Wu XY, Han LJ, Zhang XL, Li L, Jiang CZ, Qiu Y, et al. Alteration of endocannabinoid system in human gliomas. J Neurochem. 2012;120:842-9.

[7] Nabissi M, Morelli MB, Amantini C, Liberati S, Santoni M, Ricci-Vitiani L, et al. Cannabidiol stimulates Aml-1a-dependent glial differentiation and inhibits glioma stem-like cells proliferation by inducing autophagy in a TRPV2-dependent manner. Int J Cancer. 2015;137:1855-69.

[8] Sanchez C, de Ceballos ML, del Pulgar TG, Rueda D, Corbacho C, Velasco G, et al. Inhibition of glioma growth in vivo by selective activation of the CB2 cannabinoid receptor. Cancer Res. 2001;61:5784-9.

[9] Louis DN, Perry A, Reifenberger G, von Deimling A, Figarella-Branger D, Cavenee WK, et al. The 2016 World Health Organization Classification of Tumors of the Central Nervous System: a summary. Acta Neuropathol. 2016;131:803-20.

[10] Aparicio-Blanco J, Torres-Suárez AI. Managing CNS Tumors: The Nanomedicine Approach. In: Morgan LR, editor. New Approaches to the Management of Primary and Secondary CNS Tumors: InTech; 2017.

[11] Fowler CJ. Delta(9)-Tetrahydrocannabinol and Cannabidiol as Potential Curative Agents for Cancer: A Critical Examination of the Preclinical Literature. Clin Pharmacol Ther. 2015;97:587-96.

[12] Cherniakov I, Izgelov D, Barasch D, Davidson E, Domb AJ, Hoffman A. Piperine-pro-nanolipospheres as a novel oral delivery system of cannabinoids: Pharmacokinetic evaluation in healthy volunteers in comparison to buccal spray administration. J Control Release. 2017;266:1-7.

[13] Xie JR, Xiao DJ, Zhao JN, Hu NQ, Bao Q, Jiang L, et al. Mesoporous Silica Particles as a Multifunctional Delivery System for Pain Relief in Experimental Neuropathy. Adv Healthc Mater. 2016;5:1213-21.

[14] Martin-Banderas L, Munoz-Rubio I, Prados J, Alvarez-Fuentes J, Calderon-Montano JM, Lopez-Lazaro M, et al. In vitro and in vivo evaluation of Delta(9)-tetrahidrocannabinol/PLGA nanoparticles for cancer chemotherapy. Int J Pharm. 2015;487:205-12.

[15] Berrocoso E, Rey-Brea R, Fernandez-Arevalo M, Mico JA, Martin-Banderas L. Single oral dose of cannabinoid derivate loaded PLGA nanocarriers relieves neuropathic pain for eleven days. Nanomed-Nanotechnol Biol Med. 2017;13:2623-32.

[16] Martin-Banderas L, Alvarez-Fuentes J, Duran-Lobato M, Prados J, Melguizo C, Fernandez-Arevalo M, et al. Cannabinoid derivate-loaded PLGA nanocarriers for oral administration: formulation, characterization, and cytotoxicity studies. Int J Nanomed. 2012;7:5793-806.

[17] Esposito E, Ravani L, Drechsler M, Mariani P, Contado C, Ruokolainen J, et al. Cannabinoid antagonist in nanostructured lipid carriers (NLCs): design, characterization and in vivo study. Mater Sci Eng C-Mater Biol Appl. 2015;48:328-36.

[18] He XL, Yang L, Wang M, Zhuang XZ, Huang RQ, Zhu RR, et al. Targeting the Endocannabinoid/CB1 Receptor System For Treating Major Depression Through Antidepressant Activities of Curcumin and Dexanabinol-Loaded Solid Lipid Nanoparticles. Cell Physiol Biochem. 2017;42:2281-94.

[19] Ligresti A, De Petrocellis L, de la Ossa DHP, Aberturas R, Cristino L, Moriello AS, et al. Exploiting Nanotechnologies and TRPV1 Channels to Investigate the Putative Anandamide Membrane Transporter. PLoS One. 2010;5:12.

[20] de la Ossa DHP, Ligresti A, Gil-Alegre ME, Aberturas MR, Molpeceres J, Di Marzo V, et al. Poly-epsilon-caprolactone microspheres as a drug delivery system for cannabinoid administration: Development, characterization and in vitro evaluation of their antitumoral efficacy. J Control Release. 2012;161:927-32.

[21] Martin-Banderas L, Munoz-Rubio I, Alvarez-Fuentes J, Duran-Lobato M, Arias JL, Holgado MA, et al. Engineering of Delta(9)-tetrahydrocannabinol delivery systems based on surface modified-PLGA nanoplatforms. Colloid Surf B-Biointerfaces. 2014;123:114-22.

[22] Esposito E, Drechsler M, Cortesi R, Nastruzzi C. Encapsulation of cannabinoid drugs in nanostructured lipid carriers. Eur J Pharm Biopharm. 2016;102:87-91.

[23] Duran-Lobato M, Martin-Banderas L, Goncalves LMD, Fernandez-Arevalo M, Almeida AJ. Comparative study of chitosan- and PEG-coated lipid and PLGA nanoparticles as oral delivery systems for cannabinoids. J Nanopart Res. 2015;17:17.

[24] Gamboa GVU, Palma SD, Lifschitz A, Ballent M, Lanusse C, Passirani C, et al. Ivermectin-loaded lipid nanocapsules: toward the development of a new antiparasitic delivery system for veterinary applications. Parasitol Res. 2016;115:1945-53.

[25] Groo AC, Saulnier P, Gimel JC, Gravier J, Ailhas C, Benoit JP, et al. Fate of paclitaxel lipid nanocapsules in intestinal mucus in view of their oral delivery. International Journal of Nanomedicine. 2013;8:4291-302.

[26] Saliou B, Thomas O, Lautram N, Clavreul A, Hureaux J, Urban T, et al. Development and in vitro evaluation of a novel lipid nanocapsule formulation of etoposide. Eur J Pharm Sci. 2013;50:172-80.

[27] Balzeau J, Pinier M, Berges R, Saulnier P, Benoit JP, Eyer J. The effect of functionalizing lipid nanocapsules with NFL-TBS.40-63 peptide on their uptake by glioblastoma cells. Biomaterials. 2013;34:3381-9.

[28] Carradori D, Saulnier P, Preat V, des Rieux A, Eyer J. NFL-lipid nanocapsules for brain neural stem cell targeting in vitro and in vivo. J Control Release. 2016;238:253-62.

[29] Holgado MA, Martin-Banderas L, Alvarez-Fuentes J, Fernandez-Arevalo M. Neuroprotective effect of cannabinoids nanoplatforms in neurodegenerative diseases. J Drug Deliv Sci Technol. 2017;42:84-93.

[30] Bastiat G, Pritz CO, Roider C, Fouchet F, Lignieres E, Jesacher A, et al. A new tool to ensure the fluorescent dye labeling stability of nanocarriers: A real challenge for fluorescence imaging. J Control Release. 2013;170:334-42.

[31] Massi P, Vaccani A, Ceruti S, Colombo A, Abbracchio MP, Parolaro D. Antitumor effects of cannabidiol, a nonpsychoactive cannabinoid, on human glioma cell lines. J Pharmacol Exp Ther. 2004;308:838-45.

[32] Chen CT, Duan ZQ, Yuan Y, Li RX, Pang L, Liang JM, et al. Peptide-22 and Cyclic RGD Functionalized Liposomes for Glioma Targeting Drug Delivery Overcoming BBB and BBTB. ACS Appl Mater Interfaces. 2017;9:5864-73.

[33] Belhadj Z, Ying M, Cao X, Hu XF, Zhan CY, Wei XL, et al. Design of Y-shaped targeting material for liposome-based multifunctional glioblastoma-targeted drug delivery. J Control Release. 2017;255:132-41.

[34] Wei XL, Gao J, Zhan CY, Xie C, Chai ZL, Ran D, et al. Liposome-based glioma targeted drug delivery enabled by stable peptide ligands. J Control Release. 2015;218:13-21.

[35] Luo ZM, Yan ZQ, Jin K, Pang Q, Jiang T, Lu H, et al. Precise glioblastoma targeting by AS1411 aptamer-functionalized poly (L-gamma-glutamylglutamine)-paclitaxel nanoconjugates. J Colloid Interface Sci. 2017;490:783-96.

[36] Luo ZM, Jin K, Pang Q, Shen S, Yan ZQ, Jiang T, et al. On-Demand Drug Release from Dual-Targeting Small Nanoparticles Triggered by High-Intensity Focused Ultrasound Enhanced Glioblastoma-Targeting Therapy. ACS Appl Mater Interfaces. 2017;9:31612-25.

[37] Ying X, Wen H, Lu WL, Du J, Guo J, Tian W, et al. Dual-targeting daunorubicin liposomes improve the therapeutic efficacy of brain glioma in animals. J Control Release. 2010;141:183-92.

[38] Wei L, Guo XY, Yang T, Yu MZ, Chen DW, Wang JC. Brain tumor-targeted therapy by systemic delivery of siRNA with Transferrin receptor-mediated core-shell nanoparticles. Int J Pharm. 2016;510:394-405.

Chapter 4: Perspectives on nanomedicine and malignant brain tumors: the advent of theranostics

Given the extremely heterogeneous nature of malignant brain tumors, the assumption that a single therapy could be beneficial for all patients is no longer plausible. At best, each treatment would only be effective for certain target populations at certain stages of disease. In this context, the advent of theranostics, defined as the combination of imaging and therapeutic agents for their simultaneous delivery, holds tremendous promise for the individualized management of malignant brain tumors at distinct levels [1].

Firstly, simultaneous imaging and therapy could provide non-invasive monitoring of drug distribution and accumulation at the tumor site together with early feedback on disease progression to speed up triage of those patients most likely to respond to the treatment and to avoid overdosing non-responders [2]. In particular, theranostics can serve to evaluate the extent of vasculature disruption and eventually predict the outcome of the EPR effect. Similarly, theranostics can evidence the effectiveness of a particular active targeting strategy in a given patient and ultimately predict its failure or success [3].

Secondly, theranostics can provide a valuable platform for image-guided cancer therapy with unprecedented spatiotemporal control. In novel physical stimulus-responsive therapies, an external stimulus must be applied locally to selectively activate the therapeutic agents in the tumorigenic area, thereby greatly reducing toxicity in healthy tissues [4, 5]. Hence, precise monitoring of the delivery of the therapeutic agent would accurately locate the target site and determine when the physical stimulus should be applied, namely, when maximum levels of stimulus-responsive agent are achieved at the tumor site [6, 7].

Thirdly, theranostics could also be beneficial in the intraoperative setting [8]. The imaging function of theranostics could help identify the boundaries between neoplastic and healthy tissue to improve the intraoperative delineation of tumor margins for complete surgical resection [9]. The therapeutic function of theranostics would serve to eradicate inoperable tumor margins.

Nanomedicines are promising platforms for brain theranostics [3, 10]. Nanotheranostics would prevent the differences in biodistribution that occur when imaging and therapeutic agents are administered separately [11]. Hence, this fourth chapter is devoted to the possibilities that nanocarriers offer to achieve a personalized follow-up of brain tumors by means of theranostics.

This chapter consists of a review article entitled “Towards tailored management of malignant brain tumors with nanotheranostics” (Acta Biomaterialia 73 (2018) 52-63), where the barriers to the clinical implementation of theranostic nanomedicine for tracking tumor responses to treatment and for guiding stimulus-activated therapies and surgical resection of malignant brain tumors are discussed. Likewise, the criteria that nanotheranostic systems need to fulfil to become clinically relevant formulations are analyzed in depth, focusing on theranostic agents already tested *in vivo*.

[1] Jo SD, Ku SH, Won YY, Kim SH, Kwon IC. Targeted Nanotheranostics for Future Personalized Medicine: Recent Progress in Cancer Therapy. Theranostics. 2016;6:1362-77.

[2] Mura S, Couvreur P. Nanotheranostics for personalized medicine. Adv Drug Deliv Rev. 2012;64:1394-416.

[3] Muthu MS, Leong DT, Mei L, Feng SS. Nanotheranostics - Application and Further Development of Nanomedicine Strategies for Advanced Theranostics. Theranostics. 2014;4:660-77.

[4] Chen Q, Ke HT, Dai ZF, Liu Z. Nanoscale theranostics for physical stimulus-responsive cancer therapies. Biomaterials. 2015;73:214-30.

[5] Terreno E, Uggeri F, Aime S. Image guided therapy: The advent of theranostic agents. J Control Release. 2012;161:328-37.

[6] Chen QW, Wen J, Li HJ, Xu YQ, Liu FY, Sun SG. Recent advances in different modal imaging-guided photothermal therapy. Biomaterials. 2016;106:144-66.

[7] Ding Q, Liu DF, Guo DW, Yang F, Pang XY, Che BRE, et al. Shape-controlled fabrication of magnetite silver hybrid nanoparticles with high performance magnetic hyperthermia. Biomaterials. 2017;124:35-46.

[8] Rutka JT, Kim B, Etame A, Diaz RJ. Nanosurgical Resection of Malignant Brain Tumors: Beyond the Cutting Edge. ACS Nano. 2014;8:9716-22.

[9] Su XH, Cheng K, Wang C, Xing L, Wu H, Cheng Z. Image-guided resection of malignant gliomas using fluorescent nanoparticles. Wiley Interdiscip Rev-Nanomed Nanobiotechnol. 2013;5:219-32.

[10] Overchuk M, Zheng G. Overcoming obstacles in the tumor microenvironment: Recent advancements in nanoparticle delivery for cancer theranostics. Biomaterials. 2018;156:217-37.

[11] Choi KY, Liu G, Lee S, Chen XY. Theranostic nanoplatforms for simultaneous cancer imaging and therapy: current approaches and future perspectives. Nanoscale. 2012;4:330-42.

Acta Biomaterialia 73 (2018) 52–63

Contents lists available at ScienceDirect

Acta Biomaterialia

journal homepage: www.elsevier.com/locate/actabiomat

Review article

Towards tailored management of malignant brain tumors with nanotheranostics

Juan Aparicio-Blanco [a], Ana-Isabel Torres-Suárez [a,b,*]

[a] Department of Pharmaceutical Technology and Food Engineering, Complutense University, 28040 Madrid, Spain
[b] University Institute of Industrial Pharmacy, Complutense University, Madrid, Spain

ARTICLE INFO

Article history:
Received 21 December 2017
Received in revised form 16 April 2018
Accepted 16 April 2018
Available online 17 April 2018

Keywords:
Brain theranostics
Brain targeting
Blood-brain barrier
Nanoimaging
Nanomedicine

ABSTRACT

Malignant brain tumors still represent an unmet medical need given their rapid progression and often fatal outcome within months of diagnosis. Given their extremely heterogeneous nature, the assumption that a single therapy could be beneficial for all patients is no longer plausible. Hence, early feedback on drug accumulation at the tumor site and on tumor response to treatment would help tailor therapies to each patient's individual needs for personalized medicine. In this context, at the intersection between imaging and therapy, theranostic nanomedicine is a promising new technique for individualized management of malignant brain tumors. Although brain nanotheranostics has yet to be translated into clinical practice, this field is now a research hotspot due to the growing demand for personalized therapies. In this review, the barriers to the clinical implementation of theranostic nanomedicine for tracking tumor responses to treatment and for guiding stimulus-activated therapies and surgical resection of malignant brain tumors are discussed. Likewise, the criteria that nanotheranostic systems need to fulfil to become clinically relevant formulations are analyzed in depth, focusing on theranostic agents already tested *in vivo*. Currently, magnetic nanoparticles exploiting brain targeting strategies represent the first generation of preclinical theranostic nanomedicines for the management of malignant brain tumors.

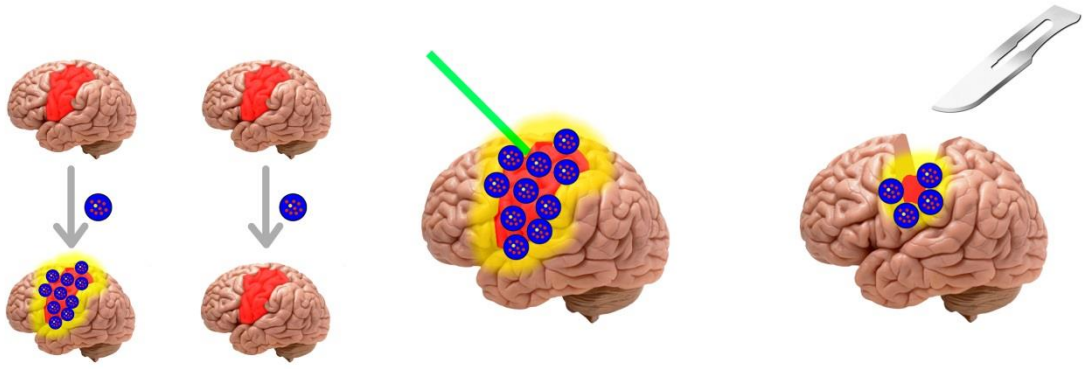

Towards tailored management of malignant brain tumors with nanotheranostics

Juan Aparicio-Blanco [a], Ana-Isabel Torres-Suárez [a, b,*]

[a] Department of Pharmaceutical Technology and Food Engineering, Complutense University, 28040, Madrid, Spain

[b] University Institute of Industrial Pharmacy, Complutense University, Madrid, Spain

Abstract

Malignant brain tumors still represent an unmet medical need given their rapid progression and often fatal outcome within months of diagnosis. Given their extremely heterogeneous nature, the assumption that a single therapy could be beneficial for all patients is no longer plausible. Hence, early feedback on drug accumulation at the tumor site and on tumor response to treatment would help tailor therapies to each patient's individual needs for personalized medicine. In this context, at the intersection between imaging and therapy, theranostic nanomedicine is a promising new technique for individualized management of malignant brain tumors. Although brain nanotheranostics has yet to be translated into clinical practice, this field is now a research hotspot due to the growing demand for personalized therapies. In this review, the barriers to the clinical implementation of theranostic nanomedicine for tracking tumor responses to treatment and for guiding stimulus-activated therapies and surgical resection of malignant brain tumors are discussed. Likewise, the criteria that nanotheranostic systems need to fulfil to become clinically relevant formulations are analyzed in depth, focusing on theranostic agents already tested *in vivo*. Currently, magnetic nanoparticles exploiting brain targeting strategies represent the first generation of preclinical theranostic nanomedicines for the management of malignant brain tumors.

Statement of significance

The development of nanocarriers that can be used both in imaging studies and the treatment of brain tumors could help identify which patients are most and least likely to respond to a given treatment. This will enable clinicians to adapt the therapy to the needs of the patient and avoid overdosing non-responders. Given the many different approaches to non-invasive techniques for imaging and treating brain tumors, it is important to focus on the strategies most likely to be implemented and to design the most feasible theranostic biomaterials that will bring nanotheranostics one step closer to clinical practice.

Keywords

Brain theranostics, brain targeting, blood-brain barrier, nanoimaging, nanomedicine

1. Introduction

Central nervous system (CNS) tumors are stratified by the World Health Organization according to their proliferative potential, to their likelihood of dissemination and to their overall clinical prognosis [1]. Since around 95% of malignant CNS tumors occur in the brain, the focus henceforth will be on malignant brain tumors. In particular, malignant primary brain tumors account for 2% of all cancers and typically originate from glial cells (being thus referred to as gliomas) [2]. Brain metastases occur in 10%-30% of all cancer patients, of whom 70%-80% develop multiple lesions. The high incidence of intracranial metastases is primarily due to the fact that whereas new chemotherapeutic agents have improved prognosis for many cancers, they have failed to prevent the spread of neoplasms into the brain due to their low blood–brain barrier (BBB) penetration. This is a major obstacle to brain delivery [3].

The standard of care in malignant brain tumors consists of maximal surgical resection (if eligible) combined with radiotherapy, chemotherapy and symptomatic treatment [4]. Even so, malignant brain tumors (with a median survival of 8 months for brain metastases and 14.2 months for malignant primary brain tumors) still constitute an unmet clinical challenge, since recurrence within a few months is common [3, 5].

In fact, given the extremely heterogeneous nature of malignant brain tumors, it is no longer plausible to assume that a single therapy could be effective in all patients. At best, each treatment would only be effective for certain target populations at certain stages of disease. In this context, the advent of theranostics, defined as the combination of imaging and therapeutic agents for their simultaneous delivery [6], holds tremendous promise for the management of malignant brain tumors at various levels.

Firstly, simultaneous imaging and therapy could provide non-invasive monitoring of drug distribution and accumulation at the tumor site together with early feedback on disease progression to speed up triage of those patients most likely to respond to the treatment. This will ultimately validate or rule out the therapeutic approaches to tailored clinical management of malignant brain tumors with maximal therapeutic indexes [7-9]. In addition, non-invasive imaging may serve to identify potential recurrences, which could prompt further changes in therapy [10]. Alternative protocols should be evaluated for potential non-responders [7, 8]: if the lack of response is due to the fact that one of the targets has become unavailable, theranostics could devise alternate targets [11].

Secondly, theranostics can provide a valuable platform for image-guided cancer therapy with unprecedented spatiotemporal control [12], because in novel physical stimulus-responsive therapies, an external stimulus must be applied locally to selectively activate the therapeutic agents in the tumorigenic area, thereby greatly reducing toxicity in healthy tissues [13]. Hence, precise monitoring of the delivery of the therapeutic agent would accurately locate the target site and determine when the physical stimulus should be applied, namely, when maximum levels of stimulus-responsive agent are achieved at the tumor site [14].

Thirdly, theranostics could also be beneficial in the intraoperative setting [15]. The imaging function of theranostics could help identify the boundaries between neoplastic and healthy tissue and thus improve the intraoperative delineation of tumor margins for surgical resection [16]. The therapeutic function of theranostics would serve to eradicate inoperable tumor margins. Therefore, theranostics would not only improve intraoperative brain tumor boundary delineation to increase the chances of complete surgical resection but could also help in the resection of marginal tumor cells [17].

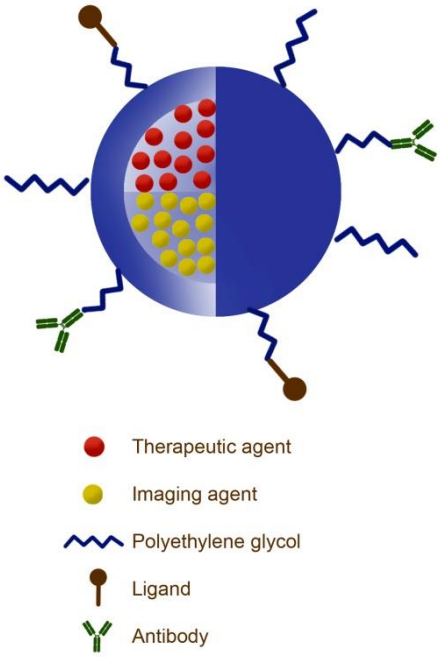

Figure 4.1.2. Scheme of a targeted theranostic nanocarrier.

In this regard, nanomedicines are promising platforms for brain theranostics (Figure 1). Theranostic nanomedicine consists of colloid carriers in which imaging and therapeutic agents are adsorbed, conjugated, entrapped or encapsulated [18-20]. Interestingly, nanocarriers could be targeted to enhance the availability of both contrast and therapeutic agents in the entire diseased brain area [21, 22]. On the one hand, the use of targeted nanoimaging could improve contrast by increasing the amount of imaging agent at the tumor site and minimizing imaging background signals with less systemic exposure. This improved resolution would enable disease progression to be monitored in real time, and also identify previously undetectable lesions for complete surgical resection [23-25]. On the other hand, the use of targeted nanotherapy could improve therapeutic outcomes by enhancing the amount of therapeutic agent delivered to the tumor site and reduce toxicity by preventing distribution to peripheral tissues [26-28]. The therapeutic field that could most benefit from nanotheranostics is chemotherapy, where dose availability at the target site cannot be counterbalanced with higher doses for fear of severe side effects. Nanotheranostics would prevent the differences in biodistribution that occur when imaging and therapeutic agents are administered separately [29].

Nanotheranostics for the management of brain tumors is compatible with localized and systemic administration. Localized delivery can be used to bypass the BBB [30-32]. However, the mechanical breach of this barrier might also allow neurotoxic compounds to enter the brain or, in the case of gliomas, even promote tumor dissemination. Moreover, localized delivery involves neurosurgical procedures, and is therefore incompatible with multiple dose regimens.

Intravenous administration, in contrast, is a less invasive and more suitable for multiple dosing regimens. However, the development of nanocarriers that can effectively cross the brain endothelium and accurately target brain cancer cells remains a major challenge [11, 24]. With nanotheranostics, malignant brain tumor targeting can be accomplished by passive, active or external physical stimuli-responsive targeting (Figure 2) [33-35].

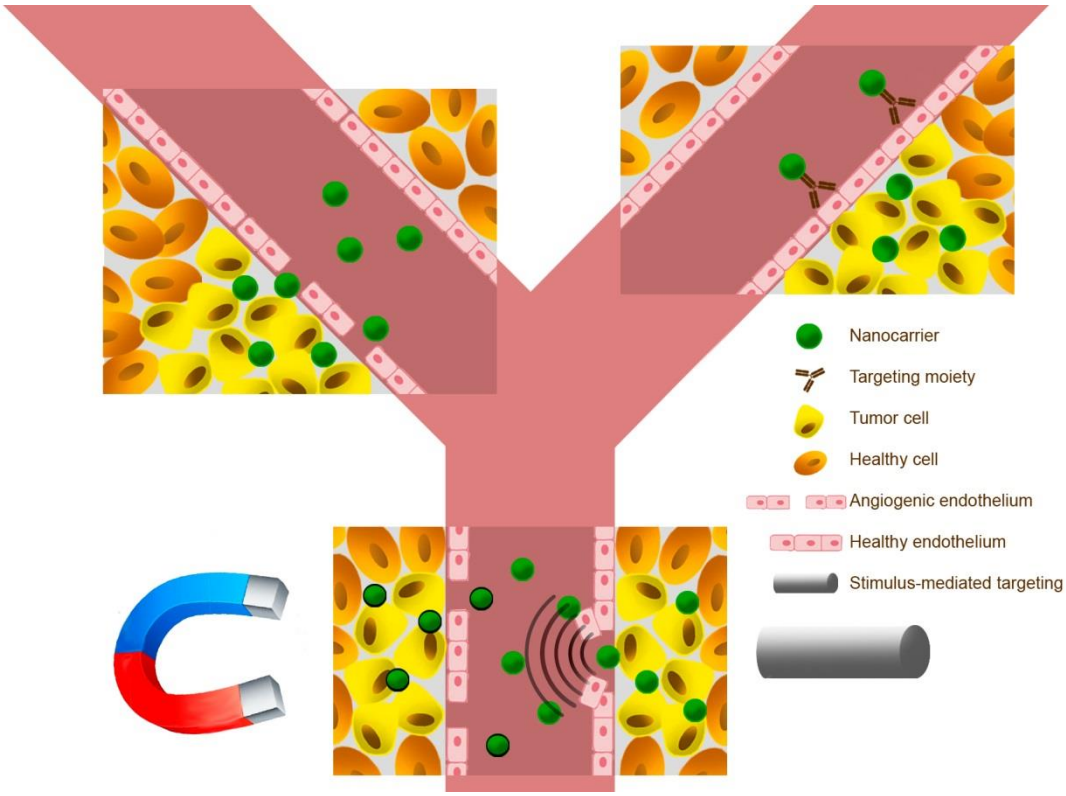

Figure 4.1.2. Potential targeting strategies for malignant brain tumor theranostics following intravascular administration: passive targeting (upper left), active targeting (upper right) and external physical stimuli-responsive targeting (bottom).

In the case of malignant brain tumors, the rationale for passive targeting is based on the diffusion of intravascularly administered nanotheranostics through the interendothelial gaps of the tumor's "leaky" neovasculature (the blood-brain tumor barrier [BBTB]), a singularity termed the enhanced permeability and retention (EPR) effect [36]. For optimal passive targeting of malignant gliomas, the nanocarriers should fulfil two criteria: they should be less than 100 nm and "stealth" (namely, provided with hydrophilic coating [37]) to prevent removal by the reticuloendothelial system and ensure enough circulation time to enable extravasation; and, they should remain above the endothelial pore threshold of healthy tissue (typically 10 nm) to achieve selective

extravasation at the tumor site [38]. The efficiency of the EPR effect relies on the stage of the disease, since the BBTB closely resembles the non-fenestrated endothelium of healthy brain capillaries in the infiltrative areas of malignant brain tumors [39]. Therefore, theranostics can evaluate the extent of vasculature disruption and eventually predict the outcome of this targeting strategy.

Active targeting with ligands that bind to receptors overexpressed on the brain endothelium and/or tumor cell membranes could further improve the selective distribution of the therapy across the BBB/BBTB and eventually to the tumor cells [40, 41]. Different receptors in the brain could be used for this purpose (Table 1).

Receptor localization	Receptor name	Targeting moiety	Ref.
Receptors overexpressed on the fully functional endothelium of infiltrative areas	Transferrin receptor	Physiological ligands (lactoferrin, transferrin)	[42, 43]
		Monoclonal antibodies (8D3; OX26)	[44, 45]
	Nicotinic receptor	Peptides derived from neurotoxins	[46, 47]
	Low-density lipoprotein receptor	Angiopep-2	[48, 49]
	GLUT1 transporter	Monosaccharides (mannose, glucose)	[50, 51]
	GM1 ganglioside	G23 peptide	[52]
Receptors expressed on endothelial cells of neovasculature	$\alpha_V\beta_3$ integrin	RGD peptide	[47, 53, 54]
	Aminopeptidase N	NGR peptide	[55]
	Nucleolin	F3 peptide	[56, 57]
		AS1411 aptamer	[58, 59]
	Neuropilin-1	Tumor vasculature-homing peptide	[60]
Receptors overexpressed on tumor cells	Low-density lipoprotein receptor	Angiopep-2	[48, 49]
	$\alpha_V\beta_3$ integrin	RGD peptide	[47, 53, 54]
	EGFRvIII	Monoclonal antibody against EGFRvIII	[31]
	IL-13 receptor α2	PEP-1 peptide	[61]
	IL-4 receptor	AP-1 peptide	[62]
	Insulin receptor	Monoclonal antibody (83-14)	[44]
	MMP-2	Chlorotoxin	[45, 63]

Table 4.1.1: Different receptors exploited for active targeting of brain tumors, classified by location. EGFRvIII: malignant isoform of the epidermal growth factor (EGFR), IL-13, Il-4: interleukins 13 and 4; MMP-2: membrane-bound matrix metalloproteinase-2.

However, active targeting depends on the type of receptors expressed in each case [64]. The assessment of the nanotheranostic accumulation at the tumor site could

show the tumor targeting effectiveness and ultimately predict the failure or success of a particular active targeting strategy in a given patient [18].

Finally, nanocarriers can also be guided to the malignant brain tumor site by external stimuli-responsive targeting. Being a physical phenomenon, this targeting does not rely on the idiosyncrasy of the tumor but can be controlled on-demand in a spatial and temporal manner [13]. Magnetic targeting is a noninvasive strategy that has been used to deliver magnetic nanotheranostics to the tumor area via a locally applied external magnetic field [65, 66]. Alternatively, low-frequency focused ultrasound can be used to cause a local, reversible disruption of the tumor vasculature and thus facilitate broader distribution of nanocarriers to the brain tumor site [67]. However, the transient disruption of the BBTB might also lead to tumor dissemination.

Several combinations of therapy and imaging techniques can be envisaged in malignant brain tumor theranostics (Table 2).

		Advantages		Disadvantages	Potential for clinical translation as glioma theranostics	Ref.
Imaging techniques	MRI	Unlimited tissue penetration	High resolution	Relatively low sensitivity	Gold standard method for clinical diagnosis of malignant brain tumors	[68, 69]
	Radionuclide-based imaging	Unlimited tissue penetration	High resolution	Exposure to radioactive agents	High for functional imaging	[70, 71]
	CT	Unlimited tissue penetration		Limited soft-tissue resolution	High for anatomical imaging	[72]
	Optical imaging	High sensitivity	Multicolor imaging	Poor tissue penetration	Limited to the intraoperative setting	[69]
Therapeutic approaches	Chemotherapy	High potency		Severe side effects	Currently included in the standard of care of malignant gliomas	[73, 74]
	Internal radiotherapy	High potency		Severe side effects	Moderate	[75]
	External stimulus-responsive therapy	Reduced toxicity until activation by external stimuli		Moderate potency	Currently limited to the intraoperative setting	[76]

Table 4.1.2. An overview of imaging and therapeutic possibilities for theranostic nanomedicine of malignant gliomas. MRI: magnetic resonance imaging; CT: computed tomography.

Magnetic resonance imaging (MRI), computed tomography (CT), and positron-emission tomography (PET) are widely used non-invasive anatomical and functional imaging techniques for brain tumor diagnosis [77]. Specifically, MRI is the gold standard for brain tumor diagnosis. MRI uses non-ionizing radiation to provide high spatial resolution with no tissue-penetrating limitations. The main drawback of this technique is its relatively low sensitivity. This, however, be overcome by using targeted nanotheranostics to enhance image contrast by depositing a greater amount of contrast agent at the tumor site. Furthermore, since MRI scanners are widely available in hospitals, they could be used in clinical practice to monitor the biodistribution and therapeutic efficacy of nanotheranostics in brain tumor patients [78].

In contrast, optical imaging techniques have poor spatial resolution and tissue penetration due to light scattering by soft tissues and the physical barrier created by the skull. This would limit the clinical usefulness of optical imaging to delineate tumor margins for intraoperative-guidance during tumor resection [69, 79].

Likewise, the therapeutic uses of nanotheranostics are not limited to chemotherapy: adjuvant therapies, including stimulus-responsive therapies driven by external physical stimuli, are another tool in the therapeutic armamentarium for malignant brain tumors.

Photothermal therapy (PTT) and photodynamic therapy (PDT) are the most promising light-activated techniques for brain nanotheranostics. PTT is a phototherapy method in which near infrared (NIR) absorbing agents under light exposure effectively transform the energy of incident light into heat for the ablation of adjacent cancerous cells [80], which are more sensitive to hyperthermia than healthy tissue. PDT, meanwhile, is a phototherapy strategy in which photosensitizers under light exposure transfer the energy from the incident light to surrounding oxygen molecules to generate reactive oxygen species that ultimately induce local tissue apoptosis and necrosis [81]. Most widely utilized photosensitizers are triggered by visible light. Nevertheless, given the poor NIR-visible light penetration depth in tissues and through the skull, the realistic clinical value of phototherapies may be limited to intraoperative treatment of inoperable tumor margins, after bulk resection of the malignant brain tumor. Indeed, PDT is already being clinically tested as an intraoperative adjuvant therapy for brain tumors (clinicaltrials.gov identifiers: NCT01682746, NCT01966809, NCT01148966).

Magnetic hyperthermia, a magnetic field-responsive therapy, is based on selective ablation of tumor tissue by the heat generated from the displacement of magnetic nanocarriers under the action of a magnetic field [82]. Magnetic hyperthermia offers greater tissue penetration than light-activated therapies. Because high levels of magnetic nanocarriers at the tumor site are required to generate heat, magnetic agents are mostly administered intratumorally beforehand. Nanotherm® is a commercially available system for treating malignant gliomas intracranially using magnetic hyperthermia [83]. However, for systemic administration nanocarriers should exhibit higher magnetic heating susceptibility and tumor targeting properties.

In view of the many different approaches available, we have determined the features that nanotheranostics should fulfil to improve management of malignant brain tumors in the clinical setting. We describe in detail the most suitable brain nanotheranostics for clinical use, focusing on those candidates already tested *in vivo*. Although many studies in theranostics deal exclusively with imaging properties (leaving the therapeutic effect unexplored), we will only discuss those studies that evaluate both the imaging and therapeutic functions of nanocarriers on orthotopic malignant brain tumor models.

2. Brain tumor nanotheranostics

2.1. MRI

2.1.1. T1-weighted MRI for image-guided therapy of malignant brain tumors

Gadolinium chelates are typically used for imaging malignant brain tumors by contrast-enhanced T1-weighted MRI to distinguish between white and gray matter. However, these contrast agents do not leak into healthy regions of the brain and accurate delineation of tumor boundaries greatly relies on the extent of BBB disruption in the entire tumor area. Targeted gadolinium-loaded nanocarriers are being developed to potentially enhance the sensitivity and effectiveness of this contrast agent [84, 85]. As a result, brain nanotheranostics that include paramagnetic gadolinium in chelated form in amphiphilic complexes as a T1-weighted MRI contrast agent have been developed.

Since the current standard of care in malignant brain tumors entails radiotherapy, this therapeutic approach has been combined with the T1-weighted MRI imaging function for theranostic purposes [86, 87]. Miladi et al. [88] used 2-2.5 nm-sized gold nanoparticles coated with gadolinium chelates (zeta potential: -30 mV) for image-guided radiotherapy in rats orthotopically implanted with a 9L gliosarcoma, under the assumption that gold is able to absorb high-energy ionizing radiation to cause thermal ablation of tumors, thereby acting as a radio-sensitizing agent. The inclusion of gadolinium allowed the distribution of gold nanoparticles to be monitored by T1-weighted MRI following intravenous injection and this determined the optimal timing of x-ray irradiation. As a result, survival increased 473% with the nanotheranostics radiosensitizing therapy plus concomitant micro beam radiation therapy (median survival time: 129 days after tumor implantation) in comparison with non-treated rats (median survival time: 22.5 days after tumor implantation). Importantly, this thermal therapy shows realistic clinical potential for brain tumor theranostics due to the deeper tissue penetration of x-rays compared with visible light. Subsequently, these authors exploited the potential of gadolinium itself as a radiosensitizer in the same orthotopic model with polysiloxane nanoparticles doped with gadolinium chelates (particle size: 2 nm) [89]. They applied the MRI-guided microbeam radiotherapy when gadolinium content was simultaneously high in the tumor bed and negligible in the surrounding healthy tissue to achieve an impressive increase in survival of gliosarcoma-bearing rats: the median survival time was 5-fold extended in comparison with the group

radiated at the non-optimal time and half of the rats were still alive 100 days after tumor implantation.

Since functionalization with active targeting moieties could further enhance the distribution of gadolinium-containing nanotheranostics to malignant brain tumors, Bechet et al. [60] developed 3 nm-sized silica-based nanoparticles (zeta potential: 22 mV) functionalized with a tumor-homing heptapeptide (ATWLPPR) that targets neuropilin-1, a receptor specifically located on angiogenic endothelial cells. These particles encapsulated both gadolinium oxide as MRI contrast agent along with chlorin as photosensitizer for PDT of brain tumors guided by interventional MRI. Following intravenous injection of neovasculature-targeted nanocarriers in rats bearing the orthotopic glioblastoma model U87, the MRI function of the system guided the stereotactic implantation of the optical fiber to perform the PDT. Notably, an 80% reduction in intratumoral blood perfusion was observed in those rats treated with the targeted nanotheranostics. Moreover, histological examination of brain sections indicated vascular disruption and edema following MRI-guided PDT with targeted carriers.

2.1.2. T2-weighted MRI

Superparamagnetic iron oxide nanoparticles are also widely used as T2 agents to provide contrast enhancement to identify watery tissue thanks to their high magnetic susceptibility [90]. As with T1-agents, the extent of tissue contrast enhancement relies on vascular extravasation. Consequently, brain-targeted iron oxide nanoparticles have been developed for glioma theranostic purposes.

Superparamagnetic iron oxide nanoparticles show great potential for clinical translation of brain theranostics since they are already used as MRI contrast agents and can be easily upgraded to nanotheranostics by encapsulating different therapeutic agents. Different anticancer agents (drug substances, genes, antibodies) or photosensitizers can be loaded into iron oxide nanoparticles for theranostic purposes, namely a combination of MRI with chemotherapy [66, 91, 92] or with photodynamic therapy [56, 60, 93] for localized treatment. Moreover, iron oxide nanoparticles themselves simultaneously exhibit therapeutic properties, since they generate heat under alternating magnetic fields for thermal ablation of tumors; hence they can function as brain nanotheranostics on their own.

Iron oxide nanoparticles usually consist of a magnetite (Fe_3O_4) or maghemite (γ-Fe_2O_3) core with a polymer coating to improve biocompatibility and water solubility and further surface modification for targeted delivery [94]. Besides acting as theranostic agents by themselves, iron oxide nanoparticles can be loaded into other nanoplatforms along with different anticancer drugs.

As a result of such versatility, numerous iron-oxide-based nanocarriers have been tested in rodent models for brain theranostics following both systemic administration (summarized in Table 3) and localized delivery (summarized in Table 4).

Therapeutic agent	Targeting strategy	Tumor model	Imaging evaluation	Therapeutic evaluation	Nanocarrier	Ref.
Carmustine	Magnetic field [e]	C6-bearing rats	Measurement of tumor size by MRI		Polyaniline-coated Fe_3O_4 cores	[66]
Carmustine	Magnetic field + Ultrasound [e]	C6-bearing rats	Measurement of tumor size by MRI		Polyaniline-coated Fe_3O_4 cores	[95]
				Survival monitoring		
Epirubicin	Magnetic field + Ultrasound [e]	C6-bearing rats	Measurement of tumor size by MRI		Polyaniline-coated Fe_3O_4 cores	[91]
Doxorubicin	[p] + Magnetic field [e]	C6-bearing rats	Measurement of tumor size by MRI		PEG-coated Fe_3O_4 cores	[96]
				Survival monitoring		
Doxorubicin	Magnetic field + Ultrasound [e]	C6-bearing rats	MRI	-	Microbubbles	[92, 97]
Doxorubicin	G23 peptide [a]	U87-*luc2*-bearing mice	MRI	Measurement of tumor size by endogenous fluorescence imaging	Alginate-coated iron oxide core	[52]
$D[KLAKLAK]_2$	CGKRK [a*]	005, U87-bearing mice	MRI	Survival monitoring	Iron oxide nanoworms	[98]
Photophrin (PDT)	[p]	9L-bearing rats	Measurement of tumor size by diffusion MRI		Polymeric nanoparticles	[93]
Photophrin (PDT)	F3 peptide [a]	9L-bearing rats	Measurement of tumor size by diffusion MRI		Polymeric nanoparticles	[56]
				Survival monitoring		

Table 4.1.3. Intravenously-administered iron-oxide-based nanocarriers for malignant brain tumor nanotheranostics in tumor-bearing rodent models. [p]: passive targeting; [a]: active targeting; [e]:external physical stimuli-responsive targeting. [*]: active targeting with tumor vasculature homing peptides; PDT: photodynamic therapy.

2.1.2.1. *T2-weighted MRI for evaluation of malignant brain tumor response to chemotherapy*

- Intravenously administered

Many studies that simultaneously evaluate MRI contrast enhancement with the efficacy of chemotherapeutics in brain tumors use an external magnetic field to improve the delivery of magnetic nanoparticles across the BBB [66, 96]. Some further potentiate this external physical stimulus-responsive targeting with focused ultrasound for local disruption of the BBB at the tumor site [91, 92, 95, 97].

Hua et al. [66, 95] loaded polyaniline-coated magnetite nanoparticles with carmustine (particle size: 80 nm, zeta potential: -30 mV). This nanotheranostic system was administered intravenously in rats with brain tumors induced by intracranial

injection of C6 glioma cells. The aim was to monitor the therapeutic effect of carmustine by measuring the tumor size by MRI. As shown in Figure 3, prominent glioma shrinkage was evidenced by MRI after 1 week of treatment with carmustine-loaded carriers at the highest dose tested (5mg/kg) [66]. Notably, the carmustine dose required for effective tumor suppression was significantly reduced when synergistically combining magnetic targeting with focused ultrasound-transient BBB disruption (1 mg/kg) [95]. As shown in Figure 4, an effective dose of 1 mg of carmustine/kg significantly suppressed tumor growth when magnetic/ultrasound focusing was applied, but was unable to induce tumor shrinkage in the absence of external targeting.

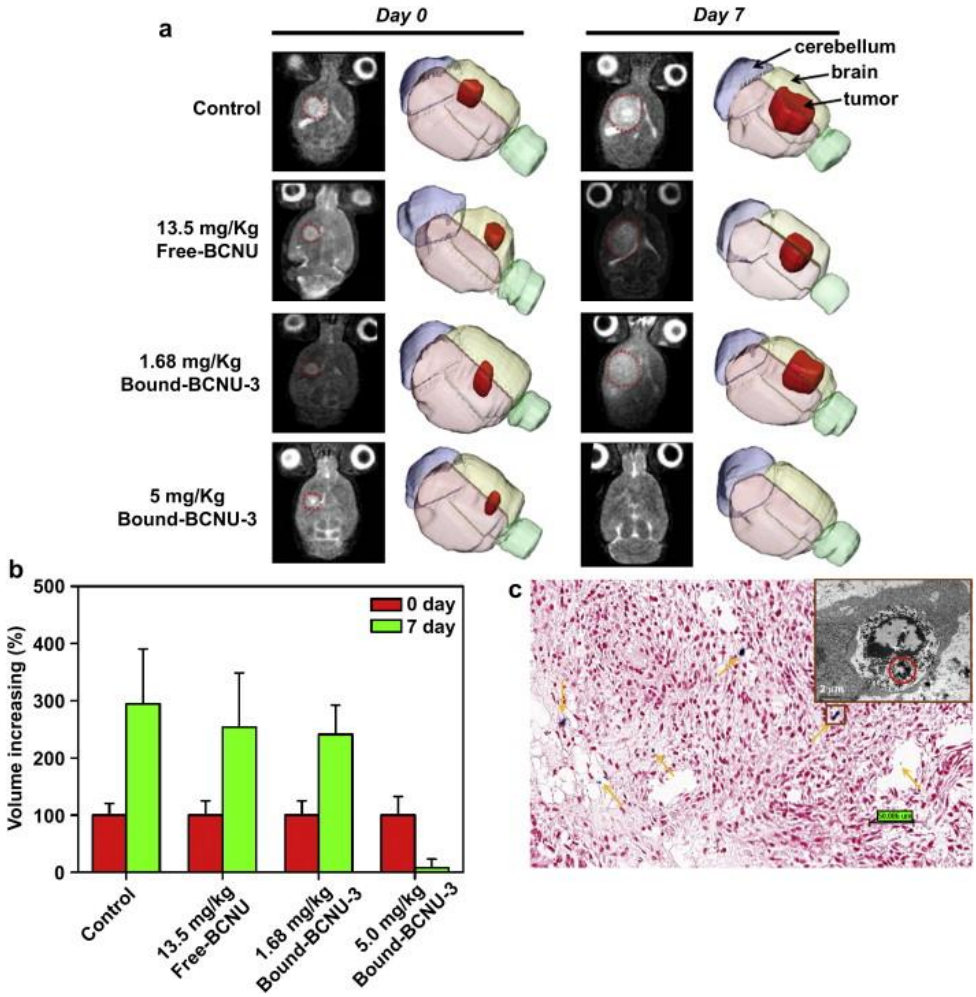

Figure 4.1.3. (a) MR images and corresponding 3-D reconstructions of rat brains with tumors induced by intracranial injection of C6 cells. Animals were treated with intravenous free-BCNU, or two different doses of bound-BCNU-3 and application of an external magnetic field. Images were taken on the day of treatment (Day 0) and 1 week later (Day 7). (b) Quantitative analysis of the effect of the various treatments on tumor size. Values are the means ± S.D. (n = 6). (c) Section stained with Prussian Blue (100x) shows uptake of iron in brain tumor tissue (arrows); (inset) TEM image of a tumor cell in the brain tissue. Reprinted from Biomaterials, 32, Hua; Liu; Yang; Chen; Tsai; Huang; Tseng; Lyu; Mab; Tang; Yen; Wei, The effectiveness of a magnetic nanoparticle-based delivery system for BCNU in the treatment of gliomas, 516-527, Copyright (2011), with permission from Elsevier.

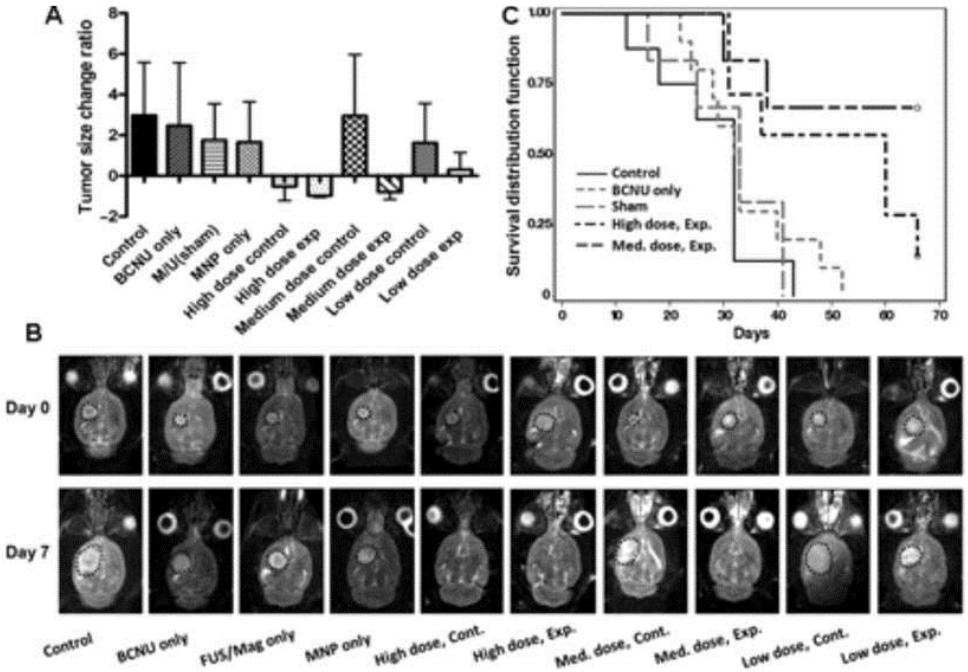

Figure 4.1.4. (A) Ratios of average tumor volume changes in the first week after treatment. M/U, magnetic/ultrasound focusing treatment only; high dose, 5 mg immobilized BCNU/kg; medium dose, 1 mg immobilized BCNU/kg; low dose, 0.5 mg immobilized BCNU/kg; dose controls, without M/U treatment; dose exp, with M/U treatment. (B) Representative examples of longitudinal brain tumor monitoring using T2-weighted MRI of each group (Days 0 and 7 posttreatment). (C) Kaplan–Meier survival curves. Survival improvement at high and medium doses is statistically significant. Reprinted from Novel magnetic/ultrasound focusing system enhances nanoparticle drug delivery for glioma treatment, Chen; Liu; Hua; Yang; Huang; Chu; Lyu; Tseng; Feng; Tsai; Chen; Lu; Wang; Yen; Ma; Wu, , Neuro-Oncology, 2010, 12 (10), 1050-1060 with permission from Oxford University Press.

The same authors tested iron oxide nanoparticles conjugated with epirubicin (particle size: 75 nm) in the same rodent model of glioma following focused ultrasound and magnetic targeting [91]. MRI monitoring of the therapeutic response revealed a 2.6-fold increase in relaxation rate after focused ultrasound/magnetic targeted treatment in comparison with non-treated controls. Moreover, epirubicin-loaded iron oxide nanoparticles in combination with focused ultrasound and magnetic targeting provided the most effective control of tumor progression in the murine glioma model, with a 66% improvement in median survival times relative to untreated controls [91].

Xu et al. [96] also potentiated passive targeting of doxorubicin-loaded polyethylene glycol-coated iron oxide nanoparticles (particle size: 58 nm, zeta potential:

28 mV) with magnetic targeting to overcome to a greater extent the BBB. They tested therapeutic efficacy following intravenous administration in rats implanted orthotopically with C6 glioma cells by measuring the tumor size using real-time MRI monitoring and recording median survival times. As shown in Figure 5, brain MRI studies of glioma-bearing rats at different monitoring times and glioma animal survival rates were highly correlated: magnetically-targeted doxorubicin-loaded iron oxide nanoparticles achieved complete suppression of tumor growth at day 28 after treatment and significantly prolonged median survival in comparison with the control group, the free doxorubicin solution group, and the magnetically untargeted doxorubicin-loaded iron oxide nanoparticles group.

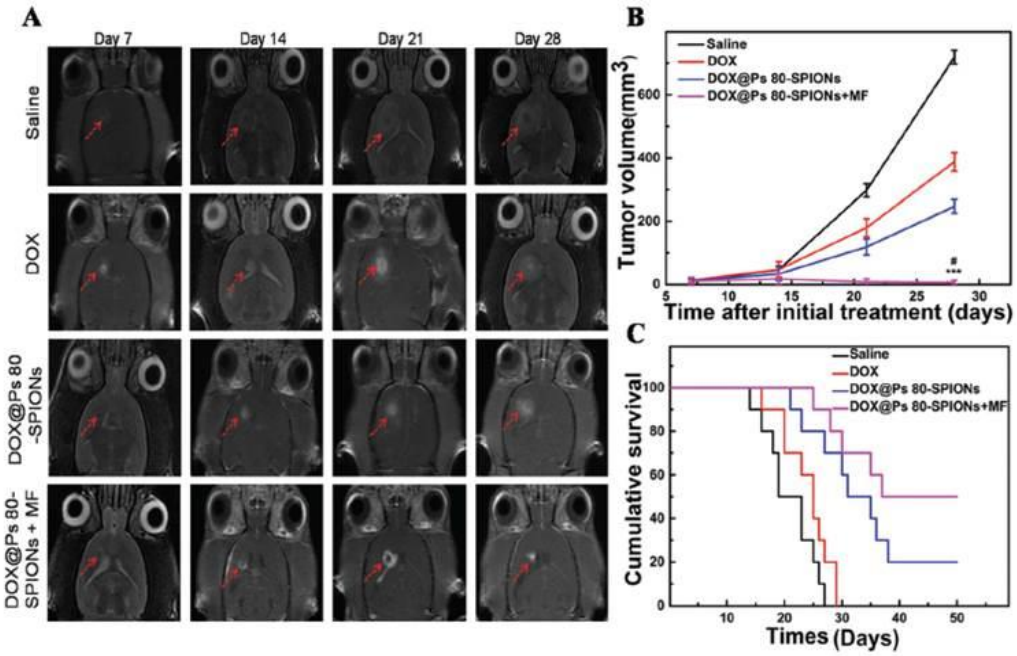

Figure 4.1.5. Tumor volumes monitored by MRI (A) and glioma animal survival were analyzed by the median survival days (B). DOX@Ps 80-SPIONs + MF treatment completely suppressed the growth of brain tumor and significantly prolonged animal survival (C) ($^{\#}p < 0.01$ vs. DOX@Ps 80-SPIONs; ***$p < 0.001$ vs. other groups). Reproduced from Nanoscale, 8 (2016), Xu; Mao; Yang; Huang; Yang; Lyu; Xu; Chen; Fan; Zou; Gao; Yin; Xiao; Lu; Zhang; Zhao, Glioma-targeted superparamagnetic iron oxide nanoparticles as drug-carrying vehicles for theranostic effects, 14222-14236, with permission of The Royal Society of Chemistry

Fan et al. [92] developed an alternative nanotheranostic system by loading doxorubicin and iron oxide nanoparticles into microbubbles (1-3 μm) to open the BBB of rats bearing the C6 glioma model by cavitation on focused ultrasound exposure. External magnetic guidance was also performed to significantly increase the accumulation of iron oxide nanoparticles at the tumor site. As evidenced by MRI, external magnetic guidance increased iron oxide nanoparticles accumulation in the glioma area by 22.4% in comparison with 12% achieved without magnetic targeting. In a subsequent study, these authors validated the high correlation between changes in the relaxation rates within tumors caused by iron oxide nanoparticles and doxorubicin

levels (quantified by inductively coupled plasma-atomic emission spectroscopy and high performance liquid chromatography, respectively) [97]. Significantly, these results confirm the non-invasive traceability of brain nanotheranostics by MRI.

Various active targeting strategies towards receptors overexpressed on endothelial cells within tumor vasculature have also been used for brain nanotheranostics combining MRI contrast enhancement and chemotherapy. For instance, Su et al. [52] loaded doxorubicin into alginate-coated magnetite nanoparticles and tagged them with G23 peptides on their surface (particle size: 140 nm, zeta potential: -15 mV) to preferentially target ganglioside GM1. When intravenously administered to mice bearing the U87MG-luc2 (human glioblastoma cell line) tumor, contrast-enhanced T_2-weighted MRI images of the brain confirmed that the nanotheranostic system had crossed the BBTB. Moreover, the monitoring of the tumor size evidenced a significant shrinkage of the tumors 7 days after treatment with the targeted doxorubicin-loaded carrier.

Agemy et al. [98] developed a nanotheranostic system targeted to tumor endothelium by incorporating a peptide that binds to tumor endothelial cells (CGKRK). Another peptide with proapoptotic activity ($_D$[KLAKLAK]$_2$) was loaded as the therapeutic agent on iron oxide nanoworms (length: 80–100 nm, width: 30 nm). Systemic treatment of glioblastoma-bearing mice with this system revealed predilection of the nanocarriers for tumor vasculature as evidenced by MRI. Furthermore, this carrier showed impressive efficacy in three glioblastoma mice models (one model induced by injection of a lentiviral vector expressing both an oncogene and a p53 silencing RNA, and two transplanted glioblastoma models: 005 and U87): in the first glioblastoma model, targeted nanoworms cured all but 1 of 10 mice; and in the transplanted ones, they increased median survival from 32 to 52 and 60 days, respectively.

- Local delivery

These iron-oxide-based nanoplatforms have not only been evaluated following systemic administration. Localized delivery of brain nanotheranostics has also been assayed in various rodent models (as outlined in Table 4).

Bernal et al. [30] developed polymeric nanoparticles loaded with both iron oxide particles and temozolomide (particle size: 80 nm; zeta potential: -8 mV) and administered them to mice bearing the glioblastoma U87MG model by convection-enhanced delivery (CED). The distribution of the nanoparticles within the brain was evidenced by MRI. The CED delivery of nanocarriers significantly prolonged median survival of the mice implanted with the intracranial glioblastoma model in comparison with the treatment with their blank counterparts.

Additionally, some locally administered nanotheranostic agents have been actively targeted against receptors overexpressed on glioma cells [31, 63, 99]. Hadjipanayis et al. [31] developed iron oxide nanoparticles (particle size: 10 nm) conjugated to the anti-EGFRvIII antibody that selectively binds to the epidermal growth factor receptor constitutively expressed by human glioblastoma tumors (EGFRvIII). The administration of these nanocarriers by CED to mice implanted with EGFRvIII-

expressing glioblastoma xenografts revealed MRI contrast enhancement within the tumor tissue and a significant increase in median survival times, with one long-term survivor (120 days after treatment). Similarly, chlorotoxin has also been explored as a glioma-targeting moiety for nanotheranostics aimed at overcoming the acquired resistance mechanism to glioma chemotherapy related to the expression of O^6 methylguanine‐DNA methyltransferase (MGMT), a repair gene that counteracts the mechanism of action of alkylating agents such as temozolomide [100]. Yoo et al. [63] stereotactically injected chlorotoxin-targeted theranostic nanoparticles (particle size: 35 nm) containing both dextran-coated iron oxide nanoparticles and small interference RNA (siRNA) to silence O^6 methylguanine-methyltransferase (MGMT), thereby sensitizing glioblastoma rodent models to temozolomide. Importantly, the combined treatment of mice exhibiting the orthotopic human glioblastoma xenograft T98G with locally administered nanotheranostics and intraperitoneal temozolomide led to significant delay in tumor growth monitored on T2-weighted MRI. Stephen et al. [99], loaded the MGMT inhibitor O^6-benzylguanine into iron oxide nanoparticles provided with a chitosan-polyethylene glycol coating and actively targeted by chlorotoxin (particle size: 75 nm; zeta potential: 4 mV). The concurrent CED administration of these nanoparticles with oral temozolomide in mice implanted with a glioblastoma xenograft (GBM6) doubled survival times compared to mice treated without the MGMT inhibitor. Importantly, these particles significantly reduced the severe myelosuppression caused by systemic administration of free O^6-benzylguanine. This could be explained by their confinement to the tumor region, as evidenced on simultaneous T2-weighted MRI.

Therapeutic agent	Targeting strategy	Tumor model	Imaging evaluation	Therapeutic evaluation	Nanocarrier	Ref.
Temozolomide	[p]	U87-bearing mice	MRI	Survival monitoring	Polymeric nanoparticles	[30]
EGFRvIII	EGFRvIII [a]	U87ΔEFGRv$_{III}$-bearing mice	MRI	Survival monitoring	Fe_3O_4 nanoparticles	[31]
siRNA (+ intraperitoneal temozolomide)	Chlorotoxin [a]	T98G-bearing mice	Measurement of tumor size by MRI		Dextran coated Fe_3O_4 nanoparticles	[63]
O^6-Benzylguanine (+ oral temozolomide)	Chlorotoxin [a]	GBM6-bearing mice	MRI	Survival monitoring	Chitosan-coated iron oxide cores	[99]

Table 4.1.4. Locally-administered iron-oxide-based nanocarriers for malignant brain tumor nanotheranostics in tumor-bearing rodent models. [p]: passive targeting; [a]: active targeting; [e]:external physical stimuli-responsive targeting.

2.1.2.2. *T2-weighted MRI for image-guided therapy*

Other authors have investigated the combination of MRI contrast enhancement with PDT for malignant brain tumor theranostics [56, 60, 93]. In this regard, some porphyrin-loaded nanocarriers have been designed for brain theranostics and have already provided promising results *in vivo*.

Kopelman et al. [93] incorporated a photosensitizer (Photofrin®) into a polyethylene glycol-coated polyacrylamide (PAA) matrix along with iron oxide nanoparticles as MRI contrast agents. This nanocarrier (particle size: 40 nm) was intravenously administered in rats bearing the orthotopic 9L gliosarcoma xenograft. The efficacy of this therapeutic approach was monitored by non-invasive diffusional MRI to evaluate changes in tumor water diffusion properties. A significant enhancement in the diffusion coefficient of the water surrounding neoplastic cells was evidenced, indicating a decrease in tumor growth and shrinkage of tumor mass. In a subsequent study [56], this system was further functionalized with the F3 peptide for active targeting of the nucleolin receptor on the tumor neovasculature. Compared with their untargeted counterparts, *in vivo* administration of the targeted nanocarriers (particle size: 40 nm) to the aforesaid gliosarcoma murine model showed a 2-fold increase in T2-weighted image contrast at the tumor site. The authors also evidenced a significant improvement in PDT efficacy with targeted theranostics, both in terms of water diffusion by MRI (with an increase of 40% in mean tumor apparent diffusion coefficient 8 days after treatment) and median survival time. Indeed, 40% of the rats treated with F3-targeted Photofrin® nanoparticles were tumor-free 60 days after treatment. More importantly for theranostic purposes, survival times were highly correlated with diffusion MRI results, which confirms the reliability of MRI as an early predictor of treatment outcome. Nonetheless, in both studies, the laser exposure was accomplished through the burr hole that had initially been made to inject the 9L gliosarcoma cells, which, as mentioned before, would limit this approach to the intraoperative setting.

2.2. Other imaging techniques

Although other imaging techniques show high potential for brain imaging, their role for brain theranostics has not been studied yet.

Unfortunately, most studies describing the *in vivo* performance of brain theranostic nanomedicines evaluate either the therapeutic or imaging function, but rarely both [18]. Typically, for a given nanocarrier, imaging and therapeutic agents are loaded separately, and tested in different biodistribution and efficacy studies. In this separate experiments, wider armamentarium of both imaging techniques (radionuclide-based imaging [70] and optical imaging [101-104]) and nanocarrier structures (liposomes [102, 104], polymer nanospheres [101, 103] and solid lipid nanoparticles [70]) have been utilized.

Another promising future line of research is the design of theranostic nanomedicines with multiple imaging functions to improve sensitivity in monitoring tumor response to treatment, and to guide stimulus-responsive therapies and surgical resection of malignant brain tumors. Although some nanocarriers with multiple imaging

functions have already been developed and evaluated in orthotopic malignant brain tumor models [17, 105, 106], their combination with a therapeutic approach remains untested *in vivo*.

3. Conclusions and perspectives

In this review, *in vivo* preclinical advances in theranostic nanomedicine for the management of malignant brain tumors have been discussed.

Although numerous therapeutic and imaging modalities can be combined for theranostic purposes, preclinical studies of nanotheranostics on orthotopic malignant brain tumor models have been mostly limited to MRI. This could be because some nanoplatformss, due to their composition, are inherently active MRI agents [83, 85, 107]; hence these nanocarriers can be easily upgraded to nanotheranostics by loading them with pharmaceutics. Magnetic nanoparticles [83] are therefore the most widely explored nanocarriers for use as theranostic agents for malignant brain tumors, and constitute the first generation of brain nanotheranostics, whereas other “traditional” colloidal systems (such as liposomes) lag far behind [108].

Chemotherapy is potentially the therapeutic approach that could most benefit from nanotheranostics. In fact, the incorporation of MRI and chemotherapeutic functions into nanoplatforms has produced multimodal structures with significant clinical potential [30, 52, 66, 91, 92, 95-97]. Stimulus-responsive strategies, that respond to external stimuli with no tissue-penetrating limitations, specifically magnetic field and focused ultrasound, show the highest potential for clinical applications [65, 97]. Moreover, since these nanotheranostics respond to external physical processes, they would be suitable for the management of any type of brain tumor. Apart from inherently enhancing MRI contrast, iron oxide nanoparticles can also act as therapeutic agents themselves for magnetic hyperthermia [90, 109]. Indeed, NanoTherm® therapy, which consists of the intratumoral administration of magnetic nanoparticles and their subsequent exposure to an alternating magnetic field, is already available for magnetic hyperthermia of malignant gliomas [83]. Interestingly, their iron oxide core could be used as an MRI contrast agent to focus the magnetic field on the tumor and consequently restrict the magnetic hyperthermia to the diseased area.

Nonetheless, despite the conceptual sophistication of the latest nanotheranostic systems, some challenges need to be overcome before brain nanotheranostics can be broadly translated to clinical practice. For instance, solid evidence is needed to support the benefit of this combined approach over separate administration of imaging and therapeutic agents. In this regard, theranostic dose optimization needs to be studied, since both imaging and therapeutic functions have different dosage requirements. In contrast to nanotheranostics designed to simultaneously treat and monitoring disease status, nanoformulations intended for imaging should be administered in a single shot, or at least in less frequent dosage regimens [10]. An additional concern in the management of brain tumors with intravascular administration of nanotheranostic systems intended is the need for strategies to enhance distribution across the cerebral vasculature, which has traditionally been regarded as a bottleneck in drug delivery [32].

Moreover, the safety of most brain nanotheranostics systems in humans has not yet been evaluated. Whereas nanomedicines derived chiefly from biocompatible and biodegradable excipients with proven clinical safety might present fewer obstacles for clinical translation [110, 111], the brain tumor nanotheranostics that have proved more successful due to their intrinsic imaging capabilities are mostly metal-based nanomedicines. These have been made more biocompatible and water-soluble with a polymer coating. Importantly, unlike their gadolinium counterparts, iron oxide nanoparticles appear to be processed by the cellular iron metabolism pathway [11]. However, the long-term effects of their accumulation in the brain are not entirely clear. Deeper insight into the clearance mechanisms of these particles would prompt regulatory agencies to authorize for clinical trials of brain nanotheranostics [112].

In conclusion, recent advances in nanomedicines intended for nanoimaging or nanotherapy separately have led to the creation of nanotheranostics. However, nanocarriers with separate functions are still struggling to advance to the clinical trial stage for brain tumor conditions [27, 111], and brain nanotheranostics, as a combination of both, lags far behind. Nonetheless, nanotheranostics is now a research hotspot thanks to advances made in nanotechnology and the demand for individualized therapy. Studies on biomarkers for tumor targeting or for monitoring response to therapy will shape the future direction of research into brain nanotheranostics to tailor treatments to the individual needs of patients. Given the growing incidence of rapidly progressing and so far untreatable malignant brain tumors, brain nanotheranostics is here to stay.

Acknowledgements

This work was partially supported by the Research Group GR35/10 Santander-UCM, Group: Parenteral Administration of Drugs. Juan Aparicio-Blanco would like to thank the Spanish Ministry of Education for his contract within the Professor Training Program FPU (Ref. FPU13/02325). The authors would like to thank Pablo Jiménez-Romero for providing assistance with the figures.

References

[1] Louis DN, Perry A, Reifenberger G, von Deimling A, Figarella-Branger D, Cavenee WK, Ohgaki H, Wiestler OD, Kleihues P, Ellison DW. The 2016 World Health Organization Classification of Tumors of the Central Nervous System: a summary. Acta Neuropathol 2016;131:803-20.

[2] Miranda A, Blanco-Prieto M, Sousa J, Pais A, Vitorino C. Breaching barriers in glioblastoma. Part I: Molecular pathways and novel treatment approaches. Int J Pharm 2017;531:372-88.

[3] Au K, Meng Y, Suppiah S, Nater A, Jalali R, Zadeh G. Current Management of Brain Metastases: Overview and Teaching Cases. In: Morgan LR, editor. New Approaches to the Management of Primary and Secondary CNS Tumors: InTech; 2017.

[4] Alifieris C, Trafalis DT. Glioblastoma multiforme: Pathogenesis and treatment. Pharmacol Ther 2015;152:63-82.

[5] Stupp R, Mason WP, van den Bent MJ, Weller M, Fisher B, Taphoorn MJB, Belanger K, Brandes AA, Marosi C, Bogdahn U, Curschmann J, Janzer RC, Ludwin SK, Gorlia T, Allgeier A, Lacombe D, Cairncross JG, Eisenhauer E, Mirimanoff RO, Van Den Weyngaert D, Kaendler S, Krauseneck P, Vinolas N, Villa S, Wurm RE, Maillot MHB, Spagnolli F, Kantor G, Malhaire JP, Renard L, De Witte O, Scandolaro L, Vecht CJ, Maingon P, Lutterbach J, Kobierska A, Bolla M, Souchon R, Mitine C, Tzuk-Shina T, Kuten A, Haferkamp G, de Greve J, Priou F, Menten J, Rutten I, Clavere P, Malmstrom A, Jancar B, Newlands E, Pigott K, Twijnstra A, Chinot O, Reni M, Boiardi A, Fabbro M, Campone M, Bozzino J, Frenay M, Gijtenbeek J, Brandes AA, Delattre JY, Bogdahn U, De Paula U, van den Bent MJ, Hanzen C, Pavanato G, Schraub S, Pfeffer R, Soffietti R, Weller M, Kortmann RD, Taphoorn M, Torrecilla JL, Marosi C, Grisold W, Huget P, Forsyth P, Fulton D, Kirby S, Wong R, Fenton D, Fisher B, Cairncross G, Whitlock P, Belanger K, Burdette-Radoux S, Gertler S, Saunders S, Laing K, Siddiqui J, Martin LA, Gulavita S, Perry J, Mason W, Thiessen B, Pai H, Alam ZY, Eisenstat D, Mingrone W, Hofer S, Pesce G, Curschmann J, Dietrich PY, Stupp R, Mirimanoff RO, Thum P, Baumert B, Ryan G, European Org Res Treatment Canc B. Radiotherapy plus concomitant and adjuvant temozolomide for glioblastoma. N Engl J Med 2005;352:987-96.

[6] Orive G, Ali OA, Anitua E, Pedraz JL, Emerich DF. Biomaterial-based technologies for brain anti-cancer therapeutics and imaging. Biochim Biophys Acta-Rev Cancer 2010;1806:96-107.

[7] Mura S, Couvreur P. Nanotheranostics for personalized medicine. Adv Drug Deliv Rev 2012;64:1394-416.

[8] Lammers T, Rizzo LY, Storm G, Kiessling F. Personalized Nanomedicine. Clin Cancer Res 2012;18:4889-94.

[9] Patil R, Ljubimov AV, Gangalum PR, Ding H, Portilla-Arias J, Wagner S, Inoue S, Konda B, Rekechenetskiy A, Chesnokova A, Markman JL, Ljubimov VA, Li DB, Prasad RS, Black KL, Holler E, Ljubimova JY. MRI Virtual Biopsy and Treatment of Brain Metastatic Tumors with Targeted Nanobioconjugates: Nanoclinic in the Brain. ACS Nano 2015;9:5594-608.

[10] Jo SD, Ku SH, Won YY, Kim SH, Kwon IC. Targeted Nanotheranostics for Future Personalized Medicine: Recent Progress in Cancer Therapy. Theranostics 2016;6:1362-77.

[11] Tam VH, Sosa C, Liu R, Yao N, Priestley RD. Nanomedicine as a non-invasive strategy for drug delivery across the blood brain barrier. Int J Pharm 2016;515:331-42.

[12] Terreno E, Uggeri F, Aime S. Image guided therapy: The advent of theranostic agents. J Control Release 2012;161:328-37.

[13] Chen Q, Ke HT, Dai ZF, Liu Z. Nanoscale theranostics for physical stimulus-responsive cancer therapies. Biomaterials 2015;73:214-30.

[14] Chen QW, Wen J, Li HJ, Xu YQ, Liu FY, Sun SG. Recent advances in different modal imaging-guided photothermal therapy. Biomaterials 2016;106:144-66.

[15] Rutka JT, Kim B, Etame A, Diaz RJ. Nanosurgical Resection of Malignant Brain Tumors: Beyond the Cutting Edge. ACS Nano 2014;8:9716-22.

[16] Su XH, Cheng K, Wang C, Xing L, Wu H, Cheng Z. Image-guided resection of malignant gliomas using FLuorescent nanoparticles. Wiley Interdiscip Rev-Nanomed Nanobiotechnol 2013;5:219-32.

[17] Kircher MF, de la Zerda A, Jokerst JV, Zavaleta CL, Kempen PJ, Mittra E, Pitter K, Huang RM, Campos C, Habte F, Sinclair R, Brennan CW, Mellinghoff IK,

Holland EC, Gambhir SS. A brain tumor molecular imaging strategy using a new triple-modality MRI-photoacoustic-Raman nanoparticle. Nat Med 2012;18:829-U235.

[18] Muthu MS, Leong DT, Mei L, Feng SS. Nanotheranostics - Application and Further Development of Nanomedicine Strategies for Advanced Theranostics. Theranostics 2014;4:660-77.

[19] Lammers T, Aime S, Hennink WE, Storm G, Kiessling F. Theranostic Nanomedicine. Accounts Chem Res 2011;44:1029-38.

[20] Overchuk M, Zheng G. Overcoming obstacles in the tumor microenvironment: Recent advancements in nanoparticle delivery for cancer theranostics. Biomaterials 2018;156:217-37.

[21] Cheng Y, Morshed RA, Auffinger B, Tobias AL, Lesniak MS. Multifunctional nanoparticles for brain tumor imaging and therapy. Adv Drug Deliv Rev 2014;66:42-57.

[22] Hartshorn CM, Bradbury MS, Lanza GM, Nel AE, Rao JH, Wang AZ, Wiesner UB, Yang L, Grodzinski P. Nanotechnology Strategies To Advance Outcomes in Clinical Cancer Care. ACS Nano 2018;12:24-43.

[23] Ding H, Wu F. Image Guided Biodistribution and Pharmacokinetic Studies of Theranostics. Theranostics 2012;2:1040-53.

[24] Bhaskar S, Tian FR, Stoeger T, Kreyling W, de la Fuente JM, Grazu V, Borm P, Estrada G, Ntziachristos V, Razansky D. Multifunctional Nanocarriers for diagnostics, drug delivery and targeted treatment across blood-brain barrier: perspectives on tracking and neuroimaging. Part Fibre Toxicol 2010;7:25.

[25] Kelkar SS, Reineke TM. Theranostics: Combining Imaging and Therapy. Bioconjugate Chem 2011;22:1879-903.

[26] Shi JJ, Kantoff PW, Wooster R, Farokhzad OC. Cancer nanomedicine: progress, challenges and opportunities. Nat Rev Cancer 2017;17:20-37.

[27] Aparicio-Blanco J, Torres-Suárez AI. Managing CNS Tumors: The Nanomedicine Approach. In: Morgan LR, editor. New Approaches to the Management of Primary and Secondary CNS Tumors: InTech; 2017.

[28] Karim R, Palazzo C, Evrard B, Piel G. Nanocarriers for the treatment of glioblastoma multiforme: Current state-of-the-art. J Control Release 2016;227:23-37.

[29] Choi KY, Liu G, Lee S, Chen XY. Theranostic nanoplatforms for simultaneous cancer imaging and therapy: current approaches and future perspectives. Nanoscale 2012;4:330-42.

[30] Bernal GM, LaRiviere MJ, Mansour N, Pytel P, Cahill KE, Voce DJ, Kang SJ, Spretz R, Welp U, Noriega SE, Nunez L, Larsen G, Weichselbaum RR, Yamini B. Convection-enhanced delivery and in vivo imaging of polymeric nanoparticles for the treatment of malignant glioma. Nanomed-Nanotechnol Biol Med 2014;10:149-57.

[31] Hadjipanayis CG, Machaidze R, Kaluzova M, Wang LY, Schuette AJ, Chen HW, Wu XY, Mao H. EGFRvIII Antibody-Conjugated Iron Oxide Nanoparticles for Magnetic Resonance Imaging-Guided Convection-Enhanced Delivery and Targeted Therapy of Glioblastoma. Cancer Res 2010;70:6303-12.

[32] Aparicio-Blanco J, Martin-Sabroso C, Torres-Suarez AI. In vitro screening of nanomedicines through the blood brain barrier: A critical review. Biomaterials 2016;103:229-55.

[33] Peluffo H, Unzueta U, Negro-Demontel ML, Xu ZK, Vaquez E, Ferrer-Miralles N, Villaverde A. BBB-targeting, protein-based nanomedicines for drug and nucleic acid delivery to the CNS. Biotechnol Adv 2015;33:277-87.

[34] Kievit FM, Zhang MQ. Cancer Nanotheranostics: Improving Imaging and Therapy by Targeted Delivery Across Biological Barriers. Adv Mater 2011;23:H217-H47.

[35] Ali IU, Chen XY. Penetrating the Blood-Brain Barrier: Promise of Novel Nanoplatforms and Delivery Vehicles. ACS Nano 2015;9:9470-4.

[36] Maeda H. Toward a full understanding of the EPR effect in primary and metastatic tumors as well as issues related to its heterogeneity. Adv Drug Deliv Rev 2015;91:3-6.

[37] Suk JS, Xu QG, Kim N, Hanes J, Ensign LM. PEGylation as a strategy for improving nanoparticle-based drug and gene delivery. Adv Drug Deliv Rev 2016;99:28-51.

[38] Kobayashi H, Watanabe R, Choyke PL. Improving Conventional Enhanced Permeability and Retention (EPR) Effects; What Is the Appropriate Target? Theranostics 2014;4:81-9.

[39] van Tellingen O, Yetkin-Arik B, de Gooijer MC, Wesseling P, Wurdinger T, de Vries HE. Overcoming the blood-brain tumor barrier for effective glioblastoma treatment. Drug Resist Update 2015;19:1-12.

[40] Oller-Salvia B, Sanchez-Navarro M, Giralt E, Teixido M. Blood-brain barrier shuttle peptides: an emerging paradigm for brain delivery. Chem Soc Rev 2016;45:4690-707.

[41] Aparicio-Blanco J, Torres-Suarez AI. Glioblastoma Multiforme and Lipid Nanocapsules: A Review. J Biomed Nanotechnol 2015;11:1283-311.

[42] Hu KL, Li JW, Shen YH, Lu W, Gao XL, Zhang QZ, Jiang XG. Lactoferrin-conjugated PEG-PLA nanoparticles with improved brain delivery: In vitro and in vivo evaluations. J Control Release 2009;134:55-61.

[43] Cui YN, Xu QX, Chow PKH, Wang DP, Wang CH. Transferrin-conjugated magnetic silica PLGA nanoparticles loaded with doxorubicin and paclitaxel for brain glioma treatment. Biomaterials 2013;34:8511-20.

[44] Zhang Y, Zhang YF, Bryant J, Charles A, Boado RJ, Pardridge WM. Intravenous RNA interference gene therapy targeting the human epidermal growth factor receptor prolongs survival in intracranial brain cancer. Clin Cancer Res 2004;10:3667-77.

[45] Yue PJ, He L, Qiu SW, Li Y, Liao YJ, Li XP, Xie D, Peng Y. OX26/CTX-conjugated PEGylated liposome as a dual-targeting gene delivery system for brain glioma. Mol Cancer 2014;13:13.

[46] Wei XL, Zhan CY, Shen Q, Fu W, Xie C, Gao J, Peng CM, Zheng P, Lu WY. A D-Peptide Ligand of Nicotine Acetylcholine Receptors for Brain-Targeted Drug Delivery. Angew Chem-Int Edit 2015;54:3023-7.

[47] Zhan CY, Wei XL, Qian J, Feng LL, Zhu JH, Lu WY. Co-delivery of TRAIL gene enhances the anti-glioblastoma effect of paclitaxel in vitro and in vivo. J Control Release 2012;160:630-6.

[48] Xin HL, Sha XY, Jiang XY, Zhang W, Chen LC, Fang XL. Anti-glioblastoma efficacy and safety of paclitaxel-loading Angiopep-conjugated dual targeting PEG-PCL nanoparticles. Biomaterials 2012;33:8167-76.

[49] Huang SX, Li JF, Han L, Liu SH, Ma HJ, Huang RQ, Jiang C. Dual targeting effect of Angiopep-2-modified, DNA-loaded nanoparticles for glioma. Biomaterials 2011;32:6832-8.

[50] Byeon HJ, Thao LQ, Lee S, Min SY, Lee ES, Shin BS, Choi HG, Youn YS. Doxorubicin-loaded nanoparticles consisted of cationic- and mannose-modified-albumins for dual-targeting in brain tumors. J Control Release 2016;225:301-13.

[51] Jiang XY, Xin HL, Ren QY, Gu JJ, Zhu LJ, Du FY, Feng CL, Xie YK, Sha XY, Fang XL. Nanoparticles of 2-deoxy-D-glucose functionalized poly(ethylene glycol)-co-poly(trimethylene carbonate) for dual-targeted drug delivery in glioma treatment. Biomaterials 2014;35:518-29.

[52] Su CH, Tsai CY, Tomanek B, Chen WY, Cheng FY. Evaluation of blood-brain barrier-stealth nanocomposites for in situ glioblastoma theranostics applications. Nanoscale 2016;8:7866-70.

[53] Shi KR, Long Y, Xu CQ, Wang Y, Qiu Y, Yu QW, Liu YY, Zhang QY, Gao HL, Zhang ZR, He Q. Liposomes Combined an Integrin alpha(v)beta(3)-Specific Vector with pH-Responsible Cell-Penetrating Property for Highly Effective Antiglioma Therapy through the Blood-Brain Barrier. ACS Appl Mater Interfaces 2015;7:21442-54.

[54] Jiang XY, Sha XY, Xin HL, Xu XM, Gu JJ, Xia WY, Chen S, Xie YK, Chen LC, Chen YZ, Fang XL. Integrin-facilitated transcytosis for enhanced penetration of advanced gliomas by poly(trimethylene carbonate)-based nanoparticles encapsulating paclitaxel. Biomaterials 2013;34:2969-79.

[55] Kang T, Gao XL, Hu QY, Jiang D, Feng XY, Zhang X, Song QX, Yao L, Huang M, Jiang XG, Pang ZQ, Chen HZ, Chen J. iNGR-modified PEG-PLGA nanoparticles that recognize tumor vasculature and penetrate gliomas. Biomaterials 2014;35:4319-32.

[56] Reddy GR, Bhojani MS, McConville P, Moody J, Moffat BA, Hall DE, Kim G, Koo YEL, Woolliscroft MJ, Sugai JV, Johnson TD, Philbert MA, Kopelman R, Rehemtulla A, Ross BD. Vascular targeted nanoparticles for imaging and treatment of brain tumors. Clin Cancer Res 2006;12:6677-86.

[57] Hu QY, Gu GZ, Liu ZY, Jiang MY, Kang T, Miao DY, Tu YF, Pang ZQ, Song QX, Yao L, Xia HM, Chen HZ, Jiang XG, Gao XL, Chen J. F3 peptide-functionalized PEG-PLA nanoparticles co-administrated with tLyp-1 peptide for anti-glioma drug delivery. Biomaterials 2013;34:1135-45.

[58] Guo JW, Gao XL, Su LN, Xia HM, Gu GZ, Pang ZQ, Jiang XG, Yao L, Chen J, Chen HZ. Aptamer-functionalized PEG-PLGA nanoparticles for enhanced anti-glioma drug delivery. Biomaterials 2011;32:8010-20.

[59] Gao HL, Qian J, Cao SJ, Yang Z, Pang ZQ, Pan SQ, Fan L, Xi ZJ, Jiang XG, Zhang QZ. Precise glioma targeting of and penetration by aptamer and peptide dual-functioned nanoparticles. Biomaterials 2012;33:5115-23.

[60] Bechet D, Auger F, Couleaud P, Marty E, Ravasi L, Durieux N, Bonnet C, Plenat F, Frochot C, Mordon S, Tillement O, Vanderesse R, Lux F, Perriat P, Guillemin F, Barberi-Heyob M. Multifunctional ultrasmall nanoplatforms for vascular-targeted interstitial photodynamic therapy of brain tumors guided by real-time MRI. Nanomed-Nanotechnol Biol Med 2015;11:657-70.

[61] Wang BY, Lv LY, Wang ZY, Zhao Y, Wu L, Fang XL, Xu QW, Xin HL. Nanoparticles functionalized with Pep-1 as potential glioma targeting delivery system via interleukin 13 receptor alpha 2-mediated endocytosis. Biomaterials 2014;35:5897-907.

[62] Yang FY, Wong TT, Teng MC, Liu RS, Lu M, Liang HF, Wei MC. Focused ultrasound and interleukin-4 receptor-targeted liposomal doxorubicin for enhanced targeted drug delivery and antitumor effect in glioblastoma multiforme. J Control Release 2012;160:652-8.

[63] Yoo B, Ifediba MA, Ghosh S, Medarova Z, Moore A. Combination Treatment with Theranostic Nanoparticles for Glioblastoma Sensitization to TMZ. Mol Imaging Biol 2014;16:680-9.

[64] Serwer LP, James CD. Challenges in drug delivery to tumors of the central nervous system: An overview of pharmacological and surgical considerations. Adv Drug Deliv Rev 2012;64:590-7.

[65] Kong SD, Lee J, Ramachandran S, Eliceiri BP, Shubayev VI, Lal R, Jin S. Magnetic targeting of nanoparticles across the intact blood-brain barrier. J Control Release 2012;164:49-57.

[66] Hua MY, Liu HL, Yang HW, Chen PY, Tsai RY, Huang CY, Tseng IC, Lyu LA, Ma CC, Tang HJ, Yen TC, Wei KC. The effectiveness of a magnetic nanoparticle-based delivery system for BCNU in the treatment of gliomas. Biomaterials 2011;32:516-27.

[67] Carpentier A, Canney M, Vignot A, Reina V, Beccaria K, Horodyckid C, Karachi C, Leclercq D, Lafon C, Chapelon JY, Capelle L, Cornu P, Sanson M, Hoang-Xuan K, Delattre JY, Idbaih A. Clinical trial of blood-brain barrier disruption by pulsed ultrasound. Sci Transl Med 2016;8:8.

[68] Horvath A, Varallyay CG, Schwartz D, Toth GB, Netto JP, Barajas R, Varallyay P, Szidonya L, Firkins J, Youngers E, Fu R, Ambady P, Bogner P, Neuwelt EA. Quantitative comparison of delayed ferumoxytol T1 enhancement with immediate gadoteridol enhancement in high grade gliomas. Magnetic resonance in medicine 2018;80:224-30.

[69] Li CY, Cao LM, Zhang YJ, Yi PW, Wang M, Tan B, Deng ZW, Wu DM, Wang QB. Preoperative Detection and Intraoperative Visualization of Brain Tumors for More Precise Surgery: A New Dual-Modality MRI and NIR Nanoprobe. Small 2015;11:4517-25.

[70] Banerjee I, De K, Mukherjee D, Dey G, Chattopadhyay S, Mukherjee M, Mandal M, Bandyopadhyay AK, Gupta A, Ganguly S, Misra M. Paclitaxel-loaded solid lipid nanoparticles modified with Tyr-3-octreotide for enhanced anti-angiogenic and anti-glioma therapy. Acta Biomater 2016;38:69-81.

[71] Wang JTW, Rubio N, Kafa H, Venturelli E, Fabbro C, Menard-Moyon C, Da Ros T, Sosabowski JK, Lawson AD, Robinson MK, Prato M, Bianco A, Festy F, Preston JE, Kostarelos K, Al-Jamal KT. Kinetics of functionalised carbon nanotube distribution in mouse brain after systemic injection: Spatial to ultra-structural analyses. J Control Release 2016;224:22-32.

[72] Shang WT, Zeng CT, Du Y, Hui H, Liang X, Chi CW, Wang K, Wang ZL, Tian J. Core-Shell Gold Nanorod@Metal-Organic Framework Nanoprobes for Multimodality Diagnosis of Glioma. Adv Mater 2017;29:8.

[73] Schiff D, Jaeckle KA, Anderson SK, Galanis E, Giannini C, Buckner JC, Stella P, Flynn PJ, Erickson BJ, Schwerkoske JF, Kaluza V, Twohy E, Dancey J, Wright J, Sarkaria JN. Phase 1/2 Trial of Temsirolimus and Sorafenib in the Treatment of Patients With Recurrent Glioblastoma: North Central Cancer Treatment Group Study/Alliance N0572. Cancer 2018;124:1455-63.

[74] Buckner JC, Shaw EG, Pugh SL, Chakravarti A, Gilbert MR, Barger GR, Coons S, Ricci P, Bullard D, Brown PD, Stelzer K, Brachman D, Suh JH, Schultz CJ, Bahary JP, Fisher BJ, Kim H, Murtha AD, Bell EH, Won M, Mehta MP, Curran WJ. Radiation plus Procarbazine, CCNU, and Vincristine in Low-Grade Glioma. N Engl J Med 2016;374:1344-55.

[75] Cikankowitz A, Clavreul A, Tetaud C, Lemaire L, Rousseau A, Lepareur N, Dabli D, Bouchet F, Garcion E, Menei P, Couturier O, Hindre F. Characterization of the

distribution, retention, and efficacy of internal radiation of Re-188-lipid nanocapsules in an immunocompromised human glioblastoma model. J Neuro-Oncol 2017;131:49-58.

[76] Shen S, Wang S, Zheng R, Zhu XY, Jiang XG, Fu DL, Yang WL. Magnetic nanoparticle clusters for photothermal therapy with near-infrared irradiation. Biomaterials 2015;39:67-74.

[77] Langen KJ, Galldiks N, Hattingen E, Shah NJ. Advances in neuro-oncology imaging. Nat Rev Neurol 2017;13:279-89.

[78] Lee DE, Koo H, Sun IC, Ryu JH, Kim K, Kwon IC. Multifunctional nanoparticles for multimodal imaging and theragnosis. Chem Soc Rev 2012;41:2656-72.

[79] Cui LY, Lin QY, Jin CS, Jiang WL, Huang H, Ding LL, Muhanna N, Irish JC, Wang F, Chen J, Zheng G. A PEGylation-Free Biomimetic Porphyrin Nanoplatform for Personalized Cancer Theranostics. ACS Nano 2015;9:4484-95.

[80] Cheng L, Wang C, Feng LZ, Yang K, Liu Z. Functional Nanomaterials for Phototherapies of Cancer. Chem Rev 2014;114:10869-939.

[81] Luo DD, Carter KA, Miranda D, Lovell JF. Chemophototherapy: An Emerging Treatment Option for Solid Tumors. Adv Sci 2017;4:24.

[82] Ding Q, Liu DF, Guo DW, Yang F, Pang XY, Che BRE, Zhou NZ, Xie J, Sun JF, Huang ZH, Gu N. Shape-controlled fabrication of magnetite silver hybrid nanoparticles with high performance magnetic hyperthermia. Biomaterials 2017;124:35-46.

[83] Gobbo OL, Sjaastad K, Radomski MW, Volkov Y, Prina-Mello A. Magnetic Nanoparticles in Cancer Theranostics. Theranostics 2015;5:1249-63.

[84] Liu YJ, Zhang N. Gadolinium loaded nanoparticles in theranostic magnetic resonance imaging. Biomaterials 2012;33:5363-75.

[85] Villaraza AJL, Bumb A, Brechbiel MW. Macromolecules, Dendrimers, and Nanomaterials in Magnetic Resonance Imaging: The Interplay between Size, Function, and Pharmacokinetics. Chem Rev 2010;110:2921-59.

[86] Lux F, Sancey L, Bianchi A, Cremillieux Y, Roux S, Tillement O. Gadolinium-based nanoparticles for theranostic MRI-radiosensitization. Nanomedicine 2015;10:1801-15.

[87] Kunz-Schughart LA, Dubrovska A, Peitzsch C, Ewe A, Aigner A, Schellenburg S, Muders MH, Hampel S, Cirillo G, Iemma F, Tietze R, Alexiou C, Stephan H, Zarschler K, Vittorio O, Kavallaris M, Parak WJ, Madler L, Pokhrel S. Nanoparticles for radiooncology: Mission, vision, challenges. Biomaterials 2017;120:155-84.

[88] Miladi I, Alric C, Dufort S, Mowat P, Dutour A, Mandon C, Laurent G, Brauer-Krisch E, Herath N, Coll JL, Dutreix M, Lux F, Bazzi R, Billotey C, Janier M, Perriat P, Le Duc G, Roux S, Tillement O. The In Vivo Radiosensitizing Effect of Gold Nanoparticles Based MRI Contrast Agents. Small 2014;10:1116-24.

[89] Le Duc G, Miladi I, Alric C, Mowat P, Brauer-Krisch E, Bouchet A, Khalil E, Billotey C, Janier M, Lux F, Epicier T, Perriat P, Roux S, Tillement O. Toward an Image-Guided Microbeam Radiation Therapy Using Gadolinium-Based Nanoparticles. ACS Nano 2011;5:9566-74.

[90] Chertok B, Moffat BA, David AE, Yu FQ, Bergemann C, Ross BD, Yang VC. Iron oxide nanoparticles as a drug delivery vehicle for MRI monitored magnetic targeting of brain tumors. Biomaterials 2008;29:487-96.

[91] Liu HL, Hua MY, Yang HW, Huang CY, Chu PC, Wu JS, Tseng IC, Wang JJ, Yen TC, Chen PY, Wei KC. Magnetic resonance monitoring of focused

ultrasound/magnetic nanoparticle targeting delivery of therapeutic agents to the brain. Proc Natl Acad Sci U S A 2010;107:15205-10.

[92] Fan CH, Ting CY, Lin HJ, Wang CH, Liu HL, Yen TC, Yeh CK. SPIO-conjugated, doxorubicin-loaded microbubbles for concurrent MRI and focused-ultrasound enhanced brain-tumor drug delivery. Biomaterials 2013;34:3706-15.

[93] Kopelman R, Koo YEL, Philbert M, Moffat BA, Reddy GR, McConville P, Hall DE, Chenevert TL, Bhojani MS, Buck SM, Rehemtulla A, Ross BD. Multifunctional nanoparticle platforms for in vivo MRI enhancement and photodynamic therapy of a rat brain cancer. J Magn Magn Mater 2005;293:404-10.

[94] Laurent S, Forge D, Port M, Roch A, Robic C, Elst LV, Muller RN. Magnetic iron oxide nanoparticles: Synthesis, stabilization, vectorization, physicochemical characterizations, and biological applications. Chem Rev 2008;108:2064-110.

[95] Chen PY, Liu HL, Hua MY, Yang HW, Huang CY, Chu PC, Lyu LA, Tseng IC, Feng LY, Tsai HC, Chen SM, Lu YJ, Wang JJ, Yen TC, Ma YH, Wu T, Chen JP, Chuang JI, Shin JW, Hsueh C, Wei KC. Novel magnetic/ultrasound focusing system enhances nanoparticle drug delivery for glioma treatment. Neuro-Oncology 2010;12:1050-60.

[96] Xu HL, Mao KL, Huang YP, Yang JJ, Xu J, Chen PP, Fan ZL, Zou S, Gao ZZ, Yin JY, Xiao J, Lu CT, Zhang BL, Zhao YZ. Glioma-targeted superparamagnetic iron oxide nanoparticles as drug-carrying vehicles for theranostic effects. Nanoscale 2016;8:14222-36.

[97] Fan CH, Cheng YH, Ting CY, Ho YJ, Hsu PH, Liu HL, Yeh CK. Ultrasound/Magnetic Targeting with SPIO-DOX-Microbubble Complex for Image-Guided Drug Delivery in Brain Tumors. Theranostics 2016;6:1542-56.

[98] Agemy L, Friedmann-Morvinski D, Kotamraju VR, Roth L, Sugahara KN, Girard OM, Mattrey RF, Verma IM, Ruoslahti E. Targeted nanoparticle enhanced proapoptotic peptide as potential therapy for glioblastoma. Proc Natl Acad Sci U S A 2011;108:17450-5.

[99] Stephen ZR, Kievit FM, Veiseh O, Chiarelli PA, Fang C, Wang K, Hatzinger SJ, Ellenbogen RG, Silber JR, Zhang MQ. Redox-Responsive Magnetic Nanoparticle for Targeted Convection-Enhanced Delivery of O-6-Benzylguanine to Brain Tumors. ACS Nano 2014;8:10383-95.

[100] Messaoudi K, Clavreul A, Lagarce F. Toward an effective strategy in glioblastoma treatment. Part I: resistance mechanisms and strategies to overcome resistance of glioblastoma to temozolomide. Drug Discov Today 2015;20:899-905.

[101] Zhang B, Shen S, Liao ZW, Shi W, Wang Y, Zhao JJ, Hu Y, Yang JR, Chen J, Mei H, Hu Y, Pang ZQ, Jiang XG. Targeting fibronectins of glioma extracellular matrix by CLT1 peptide-conjugated nanoparticles. Biomaterials 2014;35:4088-98.

[102] Chen CT, Duan ZQ, Yuan Y, Li RX, Pang L, Liang JM, Xu XC, Wang JX. Peptide-22 and Cyclic RGD Functionalized Liposomes for Glioma Targeting Drug Delivery Overcoming BBB and BBTB. ACS Appl Mater Interfaces 2017;9:5864-73.

[103] Wang XZ, Zhang Q, Lv LY, Fu JJ, Jiang Y, Xin HL, Yao QZ. Glioma and microenvironment dual targeted nanocarrier for improved antiglioblastoma efficacy. Drug Deliv 2017;24:1401-9.

[104] Zhou JE, Yu J, Gao LP, Sun L, Peng T, Wang J, Zhu JZ, Lu WY, Zhang L, Yan ZQ, Yu L. iNGR-Modified Liposomes for Tumor Vascular Targeting and Tumor Tissue Penetrating Delivery in the Treatment of Glioblastoma. Mol Pharm 2017;14:1811-20.

[105] Ni DL, Zhang JW, Bu WB, Xing HY, Han F, Xiao QF, Yao ZW, Chen F, He QJ, Liu JN, Zhang SJ, Fan WP, Zhou LP, Peng WJ, Shi JL. Dual-Targeting Upconversion Nanoprobes across the Blood-Brain Barrier for Magnetic Resonance/Fluorescence Imaging of Intracranial Glioblastoma. ACS Nano 2014;8:1231-42.

[106] Yan HH, Wang L, Wang JY, Weng XF, Lei H, Wang XX, Jiang L, Zhu JH, Lu WY, Wei XB, Li C. Two-Order Targeted Brain Tumor Imaging by Using an Optical/Paramagnetic Nanoprobe across the Blood Brain Barrier. ACS Nano 2012;6:410-20.

[107] Cole AJ, Yang VC, David AE. Cancer theranostics: the rise of targeted magnetic nanoparticles. Trends Biotechnol 2011;29:323-32.

[108] Al-Jamal WT, Kostarelos K. Liposomes: From a Clinically Established Drug Delivery System to a Nanoparticle Platform for Theranostic Nanomedicine. Accounts Chem Res 2011;44:1094-104.

[109] Kumar C, Mohammad F. Magnetic nanomaterials for hyperthermia-based therapy and controlled drug delivery. Adv Drug Deliv Rev 2011;63:789-808.

[110] Luk BT, Fang RH, Zhang LF. Lipid- and Polymer-Based Nanostructures for Cancer Theranostics. Theranostics 2012;2:1117-26.

[111] Hare JI, Lammers T, Ashford MB, Puri S, Storm G, Barry ST. Challenges and strategies in anti-cancer nanomedicine development: An industry perspective. Adv Drug Deliv Rev 2017;108:25-38.

[112] Cupaioli FA, Zucca FA, Boraschi D, Zecca L. Engineered nanoparticles. How brain friendly is this new guest? Prog Neurobiol 2014;119:20-38.

Discussion

This thesis project focuses on the design, development and pre-clinical evaluation of a targeted lipid nanocarrier for brain delivery following intravenous administration. It is presented as a compendium of research articles with stand-alone entity for publication. The dissertation is structured in chapters, each of which deals with a specific aim of the thesis project.

Diseases affecting the central nervous system (CNS) should be regarded as a major health challenge of the twenty-first century due to their steadily rising incidences and to the current lack of effective treatments in most cases, since brain drug delivery is truly hindered by the presence of the blood-brain barrier (BBB) [1, 2]. The BBB consists of the endothelial cell monolayer of the brain capillaries closely associated with pericytes and astrocytes and is physiologically responsible for the maintenance of CNS homeostasis. The key features of the brain endothelium that account for the severe restriction to brain drug delivery are both the lack of fenestrations and the presence of tight intercellular junctions. Therefore, there is a dire need for developing effective brain drug delivery strategies that overcome the biodistribution and pharmacokinetic limitations that account for treatment failure [3].

Some of the described delivery strategies to circumvent the BBB such as the direct intracerebral administration and the artificial disruption of the tight junctions by chemical or physical stimuli involve high risk of neurological damage and even of widespread tumor dissemination in the case of brain tumors. Hence, every effort is currently being devoted to achieving efficient transport across the brain endothelium with targeted drug carriers following minimally-invasive intravenous injection. In this regard, the use of nanocarriers arises as an alternative to enhance the passage across the BBB [4-6].

Intravenously-administered nanomedicines have already reached clinical trials for the treatment of different CNS diseases (with a focus on brain tumors, but also including neurodegenerative diseases such as multiple sclerosis). Noticeably, given their non-toxic, biocompatible and biodegradable nature, most of the launched clinical trials evaluate lipid-based carriers and, particularly, liposomes, as their potential was acknowledged much earlier than any other alternative (ClinicalTrials.gov Identifiers:

NCT00734682, NCT02861222, NCT00019630, NCT00944801, NCT01222780, NCT01386580, NCT02048358 and NCT02340156 as detailed in Table 1.0.1)[7].

On account of the aforementioned context, in the first chapter entitled "Nanomedicine and central nervous system: on-demand development of lipid nanocapsules", we have analyzed the possibilities and technological challenges ahead to improve the chances of success in the development of nanomedicines for CNS pathologies. The focus has been put on three major aspects as discussed hereunder.

Firstly, whereas the empirical development of delivery systems and later assignment to a specific disease has led to high attrition rates in clinical trials, the transition towards a rational disease-driven approach, whereby the nanomedicine features are thoroughly defined beforehand on the basis of the pathophysiology of a specific disease is introduced as a novel therapeutic strategy more likely to succeed.

As discussed in the first chapter, one of the major features that certainly influence the *in vivo* behavior of nanomedicines is particle size since their effect mainly relies on the unique interactions of materials at the nanoscale with biological structures. For instance, the plasma circulation time of nanomedicines depends on the extent of recognition by the reticuloendothelial system and of renal clearance, both of them size-dependent phenomena. Furthermore, the size of nanomedicines can account for the release rate of their payloads. Remarkably, a size-driven extravasation at tumor and/or inflammatory sites based on their pathophysiological features (namely, the enhanced permeation and retention (EPR) effect) has been sought. However, the EPR effect in CNS disorders is relatively weak due to the presence of the BBB, with a cut-off size of only 10-100 nm. In these cases, a much finer control on particle size will certainly improve the potential therapeutic benefits. Moreover, the mechanisms that mediate the internalization of nanocarriers in target cells often follow a size-dependent pattern within this size range [8] and particle size reversely correlates with the attained extravasation distance and interstitial diffusion. Hence, rational disease-driven design of nanocarriers can only be achieved with the ascertainment of the parameters that accurately control their size distribution.

Under this assumption, in the research article of the first chapter we have thoroughly revisited the parameters controlling the size distribution of lipid nanocapsules (LNCs) prepared by the phase inversion temperature (PIT) method. The PIT method is a low-energy nanoemulsification method wherein the physicochemical properties of surfactants are exploited to lower the interfacial tension between the aqueous and oily phases so that the required energy input for nanoemulsification can be achieved by simple stirring. To this end, the PIT method profits from the negligible interfacial tension achieved when the surfactant curvature is inverted by changes in temperature. Therefore, surfactants whose hydrophilic-lipophilic balance (HLB) follows a temperature-dependent pattern must be utilized (namely, non-ionic ethoxylated surfactants). Certainly, increasing temperatures reduce the extent of hydration of the poly (oxyethylene) moieties of non-ionic ethoxylated surfactants, which ultimately leads to an inversion in the surfactant curvature. At the "phase inversion temperature", the affinity for both phases is balanced, the surfactant curvature is negligible and a

minimum in interfacial tension is achieved [9]. The final formulation is obtained then following a thermal quench below the surfactant melting point as schemed in Figure 1.2.1. Hence, being stabilized by the rigid surfactant shell, nanoemulsion droplets eventually adopt the form of nanocapsules with a liquid oily core.

The parameters that determine the properties of nanocarriers can be divided into formulation or preparation variables. In particular, for low-energy methods, the formulation variables, and particularly the relative proportion of excipients, are the most influencing parameters, as these methods do not rely either on physical energy input or on shear forces.

Since Morales et al [10] evidenced that the size of O/W nanoemulsions is independent on the water concentration because water only acts as a dilution medium for the dispersed phase, we hypothesized that surfactant and oil should be regarded as the key formulation-driving parameters. On the one hand, the particle size is expected to be reduced with increasing amounts of surfactant due to the decrease in interfacial tension. On the other hand, the particle size is expected to grow with increasing amounts of oil, as it represents the liquid core of the colloid capsules. Hence, the mass ratio of oily phase to surfactant seems a suitable variable for prediction of the particle size of nanocapsules prepared by the PIT method.

In this regard, we have evidenced herein that the oily phase: surfactant ratio is effectively the major parameter that drives the nanocapsule formation for different oil-surfactant combinations (namely, Labrafac WL1349®-Kolliphor HS15®, Labrafac WL1349®-Kolliphor ELP®, Labrafil MS 1944 CS®-Kolliphor HS15®). These combinations exhibited distinct oil: surfactant affinities as summarized in Table 1.2.2 in terms of HLB. Biocompatible excipients have been chosen in order to envisage the nanocapsules for parenteral administration. As shown in Figure 1.2.6, the plot of the average volume diameters versus the oil: surfactant ratio was linear within the ratio range between 0.08 and 3. Hence, the global linear trend between particle size and oil: surfactant ratio is consistent through distinct surfactant-oil affinities. According to the high coefficient of determination observed for the different combinations tested (R^2>0.99), these univariate linear mathematical models are well-suited to predict the particle size of the nanocapsules prepared by the PIT method (Table D1). As hypothesized, the particle size increased along with the oil:surfactant ratio: higher ratios represent a decrease in surfactant relative concentration, and ultimately lead to bigger capsules. For ratios above 3-4, the linearity is lost, although monodisperse LNCs are still obtained. The estimation of particle size with a univariate mathematical model is of the utmost significance as it will enlighten formulators on how to tailor particle size of LNCs prepared by the PIT method to the therapeutic needs imposed by a specific disease.

Importantly, highly monodisperse LNCs were obtained: for the Labrafac WL1349®-Kolliphor HS15® and Labrafac WL1349®-Kolliphor ELP® tandems, the polydispersity indexes (PdI) were not statistically modified among the different ratios tested ($p>0.05$, as shown in Figures 1.2.4b and 1.2.S1a, respectively); whereas for the Labrafil MS1944 CS®-Kolliphor HS15® some statistically significant differences among

the PdIs along the linear region were observed, but the indexes were maintained below 0.06 in all cases regardless the particle size (as shown in Figure 1.2.S1b). It is worth mentioning that the most broadly utilized upper limit for monodisperse criteria is a PdI = 0.1.

To validate the linear univariate model that predicts the average volume diameter as a function of the oily phase: surfactant mass ratio, we utilized the Labrafac WL1349®-Kolliphor HS15® tandem. In particular, we prepared formulations with the same oil: surfactant ratio but different total amount of both excipients as detailed in Table 1.2.S3. To compare the size distribution profiles of the test and reference formulations, the similarity factor f_2, defined by Equation 1.2.2 and traditionally used for dissolution testing, is utilized herein. This parameter was chosen on the grounds of simultaneously evaluating the contribution of average volume diameter and polydispersity index, as for f_2 calculation not only the mean values but also the different percentiles must be considered. This ultimately enables a more detailed comparison of size distribution profiles. Size distributions were considered identical for f_2-values above 50. As shown in Figure 1.2.5, the calculated f_2 factor was above this 50% similarity threshold for both oil: surfactant ratios tested (namely, 65.34% for the ratio 0.4374 and 70.25% for the ratio 1.2151). These results validated that the oil: surfactant weight ratio is the leading parameter that controls size distribution of the final suspension. More precisely, and taking into account the results of Anton and Saulnier [11], who described that it was the water:surfactant ratio which determined the particle size of W/O nanocapsules, the key driving parameter seems to be the dispersed phase:surfactant weight ratio.

Importantly, as shown in Figure 1.2.6, a comparison among the linear plots for the different oil-surfactant tandems can be drawn. On the one hand, there are not statistically significant differences in the Y-intercept (Table D1), which means that there exists a lower limit of particle size to be obtained with the PIT method and this limit equals 10 nm. On the other hand, we observe significant differences in the slopes (***: $p<0.001$). As shown in Table D1, the steepest slope was achieved for the Labrafac®-Kolliphor HS15® tandem ($b = 28.16$), whereas the lowest value corresponded to the Labrafil®-Kolliphor HS15® ($b = 11.11$). This difference in the slopes of the linear plots can be attributed to the difference between the HLB values of the poly-ethoxylated surfactants and the triglycerides utilized as oily phase (shown in Table 1.2.2 as provided by supplier). The slopes follow the pattern: the closer the HLB affinity between the surfactant and the oily phase, the lower the slope of the linear plot.

Moreover, this linearization strategy accounts for the variation of particle size from a wide variety of experimental data available in the literature and originally evaluated following other parameters. Remarkably, this linearization does not only serve to predict the particle size of nanocapsules prepared by the PIT method [12, 13], but also by other phase inversion methods [14, 15], which emphasizes the link between the governing phenomena of all these techniques. The results from the first chapter seem to indicate that there is no need for establishing the complex phase diagrams traditionally utilized to define the suitable conditions for the formulation of nanocarriers.

Table D1: Parameters of the univariate linear regression between the average volume diameter and the oil: surfactant ratio for the different combinations tested.

Oil :surfactant tandem	Y-intercept (a)	Slope (b)	Coefficient of determination (R^2)
Labrafac lipophile WL1349®-Kolliphor® HS15	8.83	28.16	0.9983
Labrafac lipophile WL1349®-Kolliphor® ELP	9.59	22.13	0.9996
Labrafil M1944 CS®- Kolliphor® HS15	11.23	11.11	0.9939

Figure D1: Analysis of the formulation possibilities from the mathematical univariate linear models obtained in the first chapter.

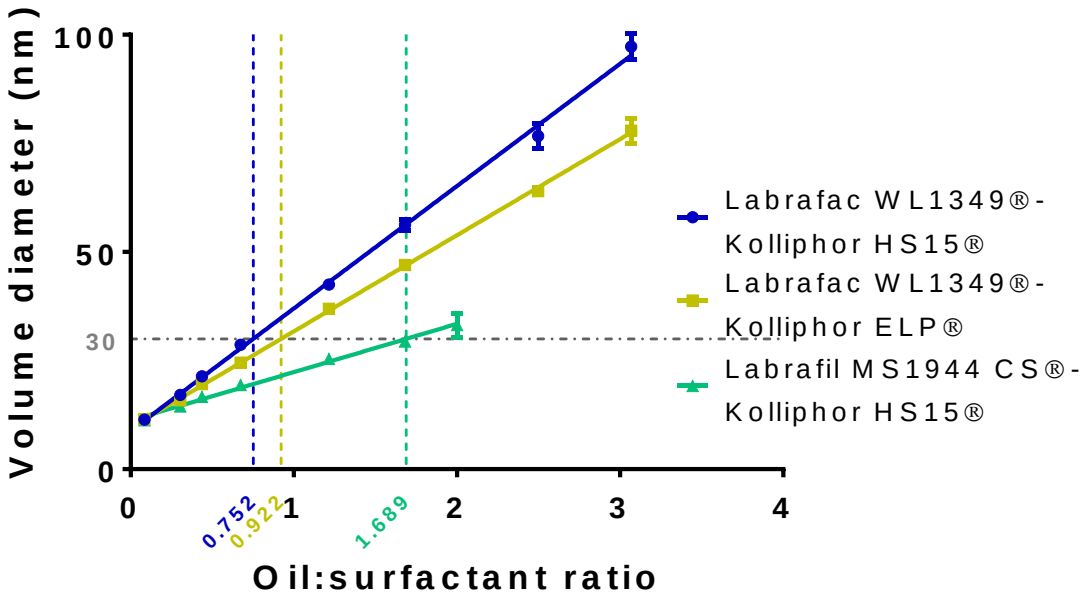

As a result, the size of nanocapsules can be accurately tailored to each particular therapeutic purpose within the range 10-100 nm. Importantly, since the univariate linear model has been established for surfactants and oily phases with different affinities, this tailoring can also be made in terms of adjusting the excipients to the therapeutic needs. For instance, solubility issues imposed by the drug substance could be addressed presumably by changing the oily phase to another one that fully solubilizes the drug substance. Alternatively, toxicological concerns associated with some surfactants could be overcome as nanocarriers of the same size can be obtained at lower surfactant concentration by switching to an emulsifier with lower HLB or by switching to an oily phase with higher HLB. This can eventually contribute to increasing the maximum tolerated dose. These latter cases are illustrated in Figure D1. For a given volume diameter, fixed in 30 nm, a formulation with a 0.752 ratio for the Labrafac WL1349®-Kolliphor HS15® tandem can be utilized. However, according to the results from the first chapter, there are other alternatives. On the one hand, the Kolliphor

HS15® with a HLB of 15 can be switched to another poly ethoxylated surfactant with lower HLB (namely, Kolliphor ELP® with a HLB of 13 and this change will imply a reduction in the surfactant amount, as it will require a higher oil: surfactant ratio 0.922. On the other hand, the oily phase can likewise be modified to ultimately reduce the amount of surfactants. The replacement of Labrafac WL1349® with a HLB of 1 to Labrafil MS1944 CS® with a HLB of 9 will enable 30-nm sized nanocapsules to be obtained at an oil: surfactant ratio of 1.689, which halves the required amount of surfactant.

This finding refutes the broadly-agreed requirement of a surfactant with an optimum HLB number for a given oily phase. The reason may lie in the fact that the HLB number concept, defined at 25ºC, only considers the surfactant molecule itself and overlooks the interactions with the aqueous and oily phases under the influence of external parameters.

Another aspect worthy of mention is that by varying the oil-surfactant affinity, the PIT can be modulated. The tuning of the PIT is relevant for industrial applications where optimal PIT is required, especially in the case of thermo-sensitive components. Additionally, if the PIT can be modulated to temperatures slightly above the physiological body temperature, the application of local hyperthermia can be envisaged as a strategy to promote the release of the cargo at the target site, as mentioned in the review articles of the first and fourth chapters.

Secondly, despite holding great promise for improving the efficacy of many drug substances, manufacturing of nanomedicines on a large scale is still a major obstacle for their market access [16]. This technical challenge for scale-up is greatly due to the lack of comprehensive understanding of the role played by the critical factors involved in the formulation of nanomedicines. Hence, investment in the fundamental principles of nanoscience will help provide clearer guidance for rational scale-up. Currently, nanocarriers are mostly manufactured using high-pressure homogenization, a high-energy nanoemulsification method wherein the required energy input is achieved by agitation of the dispersion medium with a mechanical device. As a result, from an industrial point of view, there is much room for improvement in terms of energetic yield, especially for small-sized nanocarriers, as the energy requirement for nanoemulsification negatively correlates with droplet size in accordance with the Laplace equation (Equation 1.2.1). In this regard, low-energy methods, with improved formulation yields, are energetically more efficient and suitable for large-scale production because they utilize the physicochemical properties of surfactants to lower the interfacial tension and consequently the energy requirement for nanoemulsification. Interestingly, the gentle emulsification conditions also help prevent the potential degradation of drug substances.

Specifically concerning the nanocapsules prepared by the PIT method, there seems to be some controversy on the relevance of the number of temperature cycles around the phase inversion region. Anton et al. [17] have reported that the number of temperature cycles is associated with a decrease in both particle size and polydispersity index. In a subsequent study, when Malzert-Fréon et al. replaced one of

the excipients by Labrasol®, they evidenced that the number of temperature cycles does not improve the size distribution [18]. However, they exclusively attributed this temperature cycle-independence to the presence of Labrasol®. More recently, Klassen et al. switched the nature of both the oily phase and the surfactant to test the role of temperature cycles [19]. This time, they concluded that the contribution of the temperature cycle was only significant at low surfactant concentrations, but had no influence at higher surfactant concentrations. Given these misleading results, we have comprehensively addressed this phenomenon in the first chapter. Indeed, this is not a trivial issue, since as long as the technical complexity of formulation procedures is kept to a minimum; the manufacturing criteria are more likely to be fulfilled.

From the rationale of the mechanism behind the PIT method, we hypothesized that the surfactant concentration at the interface is constant throughout the process and the curvature inversion responsible for driving the emulsification is the same regardless of the number of temperature cycles applied. Hence, there seems not to be scientific support for expecting an improvement in size distribution with the number of cycles for any potential combination of excipients. In this line, we have evaluated the influence of the number of temperature cycles (up to five) on the size distribution of the Labrafac WL1349®-Kolliphor HS15® system. In particular, we have tested three different sizes that could be categorized into high, medium and low-surfactant formulations (Table 1.2.1).

Noticeably, as shown in Figure 1.2.2, monodisperse LNCs were obtained in all cases. Notably, we have demonstrated that, as hypothesized, neither the average volume diameter (Figure 1.2.2a) nor the polydispersity index (Figure 1.2.2b) were significantly modified with the number of temperature cycles for any of the formulations tested ($p>0.05$). These results evidence that, contrary to the traditionally postulated three temperature cycles necessary to achieve monodisperse populations, LNCs have been obtained in a single-step process, as a single temperature cycle around the phase inversion region is required for their formation as evidenced both by dynamic light scattering and transmission electron microscopy (Figure 1.2.3). These results show great interest for the industrial relevance of the PIT method: the simplification of the formulation procedure paves the way for the encapsulation of thermosensitive cargos thanks to the reduced exposure to heating conditions, increases its energetic yield and greatly shortens preparation times.

Thirdly, the stability upon storage has been traditionally another flaw of many nanocarriers (such as liposomes) to achieve global translational impact. In this regard, as thermodynamically unstable systems, nanoemulsions eventually tend to separate into the constituent phases to achieve the minimal interfacial area. Nonetheless, given their inherent features, nanoemulsions, and nanocarriers from them derived, can be kinetically stable over several months [20]. The potential breakdown mechanisms are discussed in the first chapter to rule out their contribution in the case of the LNCs.

In the first instance, their size on the nanoscale provides stability against sedimentation and creaming as the Brownian motion wherein nanocarriers are involved outweighs the gravity force [21]. Other breakdown mechanisms that can be precluded

are flocculation and coalescence thanks to the steric stabilization provided by the surfactant layer [22]. This steric stabilization is particularly relevant in nanocarriers, where the thickness of the surfactant layer is significantly high in comparison with the particle size. Importantly, around the PIT, given the minimal interfacial tension, coalescence is favored unless the temperature is rapidly removed from the PIT. For this reason, we applied a thermal quench to obtain monodisperse LNCs.

In this context, Ostwald ripening represents the potential major source of instability for nanocarriers [23, 24]. Ostwald ripening consists of the diffusion of the liquid core through the dispersion medium from the smaller to the larger particles due to their different Laplace pressures. As shown in Equation 1.2.3, the contribution of Ostwald ripening as breakdown mechanism can be inferred from linear plots of the cube of particle radius versus time since the slope of this linear plot is the Ostwald ripening rate (ω_0), which is dependent on temperature since both solubility and diffusivity follows an Arrhenius behavior. Hence, we have studied herein the kinetic stability of three differently-sized formulations of LNCs (20 nm, 40 nm and 80nm, Table 1.2.1) stored in suspension over 6 months by monitoring the changes in size distribution with time.

Interestingly, as shown in Figure 1.2.7, in no case could Ostwald ripening be inferred as a source of instability because the slopes (ω_0) were not statistically different from zero ($p>0.05$). Consequently, it can be concluded that LNCs prepared by the PIT method are kinetically stable in suspension over 6 months regardless of the oily core: surfactant mass ratio. Unlike Malzert-Fréon et al. [18], we have observed high kinetic stability both at 25ºC (Figure 1.2.7a) and at 4ºC (Figure 1.2.7b), which further serves to rule out Ostwald ripening rate as breakdown mechanism of LNCs as it does not follow an Arrhenius pattern. This is highly relevant, especially if taking into account that our results are evaluated over a much longer period of time than other results reported in the literature (6 months versus 2-4 weeks) [19, 23] .

This high kinetic stability is likely to lie, on the one hand, in the presence of a solid thick surfactant layer that noticeably precludes the passage of the liquid oily core through the interface, and on the other hand, in the low polydispersity indexes that prevent significant differences in Laplace pressures that ultimately account for the occurrence of Ostwald ripening. Moreover, as deduced from Equation 1.2.3, low ripening rates should be expected for oily phases such as Labrafac lipophile WL1349® with negligible solubility in the aqueous dispersion medium.

Alternatively, we have tested if the size distribution of three formulations categorized into high, medium and low-surfactant LNCs (Table 1.2.1) is kept unaltered after water removal by freeze-drying and subsequent extemporaneous reconstitution. As shown in Figure 1.2.8, only the 20 nm-sized nanocapsules with the highest surfactant content were kept unaltered after freeze-drying, exhibiting a similarity factor between their size distributions before and after freeze-drying above 50% (f_2 = 72.72). Overall, the inclusion of trehalose as cryoprotectant did not significantly improve the maintenance of the size distribution after freeze-drying. These results outline that the prevention of leakage of the oily phase during freeze-drying is closely related to the

thickness of the surfactant layer relative to the diameter of the colloid capsules as indicated in Equation 1.2.4. Accordingly, an estimation of the thickness of the surfactant shell relative to the capsule diameter represents a 33% for the smallest capsules, with the other two lagging far behind (19.2% and 11.9%, respectively). This conclusion supports that the surfactant crystallization following the temperature quench of the PIT method below its melting point confers rigidity to the shell of the LNCs. Notably, the size distribution features of the lyophilisate of the LNCs that had been kept unaltered after freeze-drying were maintained over 12 months ($p > 0.05$, Figure 1.2.S2) under storage at 25ºC and 75% relative humidity. However, the alteration of the size distribution of some LNCs after freeze-drying does not represent a relevant constraint as they were kinetically stable in suspension.

Altogether, the results presented serve to envisage LNCs prepared by the PIT method as auspicious candidates for further research as drug carriers for the treatment of CNS diseases with potential for energetically-efficient industrial manufacturing to ultimately achieve broad market access. This delivery system overcomes some drawbacks inherent to other colloid systems such as liposomes (namely, the low drug payloads and the reduced stability on storage). On the one hand, thanks to its liquid lipid core of triglyceride oils, an increase in loading of hydrophobic drugs can be achieved. On the other hand, the formation of a solid shell formed by poly (ethoxylated) surfactants that confers rigidity to the system extends the stability of the carrier upon storage. Moreover, the linear univariate mathematical model validated herein will ultimately enable monodisperse LNCs to be obtained “on-demand” to meet the disease-driven criteria in terms of particle size for specific therapeutic purposes and ultimately increase their chances of success.

With around a quarter of a million new cases of brain and other CNS tumors being diagnosed every year, these pathologies illustrate the best archetype of brain disorders that could take great advantage of LNCs. Since around 95% of malignant CNS tumors occur in the brain, the focus henceforth will be on malignant brain tumors. In particular, malignant primary brain tumors typically originate from glial cells (being thus referred to as gliomas). Brain tumors are stratified according to a ‘malignancy scale’ closely related to clinical prognosis [25]. The current standard approach in high grade brain tumors combines maximal surgical resection (if eligible) with radiotherapy and chemotherapy; as well as symptomatic treatment. Unfortunately, the efficacy of this treatment remains questionable, since recurrence happens within months after diagnosis, with a poor median survival of 14.6 months and 2-year survival rate of 26.5% [26]. Brain targeting of nanocarriers would be chiefly germane to the field of brain chemotherapy wherein dose availability at the target site cannot be enhanced by dose increase for fear of severe side effects [27, 28]. Moreover, whereas most anticancer drugs are hydrophobic and often require to be solubilized in organic solvents for administration, LNCs provide alternative formulations to administer chemotherapy without the need to use toxic solvents.

In the search for novel antitumor agents, the therapeutic potential of several cannabinoids has become a research hotspot as cannabinoids have been reported to

not only palliate cancer-related symptoms (such as nausea, pain or anorexia) but also promote apoptotic cancer cell death through the production of reactive oxygen species, impair tumor angiogenesis and reduce cell migration [29, 30]. Cannabinoids are pharmacologically-active terpenophenols that interact with cannabinoid receptors among others and that can be ascribed to three distinct categories: phytocannabinoids (produced by the glandular trichomes of the herbaceous plant *Cannabis sativa* [31]), endocannabinoids (produced naturally by animals and humans) and synthetic cannabidomimetics [32]. However, the therapeutic potential of cannabinoids has been truly constrained heretofore due to two main issues: their strong psychoactive effects and their high lipophilicity.

Precisely due to this lack of psychoactive effects, CBD arises as the phytocannabinoid with the most auspicious therapeutic potential for the treatment of various pathologies, namely inflammatory and neurodegenerative diseases, mental disorders, neuropathic pain, epilepsy and cancer [33]. CBD can serve to widen the therapeutic armamentarium for the treatment of malignant brain tumors thanks to its synergistic effects with the currently available drugs and radiotherapy [30]. As a proof of it, CBD has already reached the clinical trials stage in combination with chemo and/or radiotherapy for patients with glioblastoma (NCT01812616, NCT01812603, NCT03246113 and NCT03529448).

Herein, we have evaluated the monodisperse LNCs developed in the first chapter as biocompatible and biodegradable carriers for CBD. In particular, in the third chapter hereof, we have encapsulated CBD into the oily core of LNCs at a concentration of 15 % CBD/Labrafac lipophile WL1349® (w/w) under the assumption that it contributes to overcome classical formulation problems associated with cannabinoids [34] and attain a prolonged-release platform for this drug. The choice of the oily phase was made on the grounds of the solubility of CBD to achieve both high encapsulation efficiencies and drug loading (as shown in Table 3.2.2).

CBD-loaded LNCs in three different sizes have been prepared and for all of them there was a statistically significant increase in particle size that progressively augmented with the initial size of blank LNCs (Figure 3.2.1 a, $p<0.05$). These results positively correlated with the respective percentage of CBD loading, which ranged from 4.30% for the smallest LNCs to 9.78% for the biggest ones. So as to evidence if the oily phase: surfactant mass ratio is also the major parameter that drives the formation of CBD-loaded LNCs, we have plotted their average volume diameters versus the oil: surfactant ratio, including in this case the drug content as part of the oily phase. As shown in Figure D2, there was a linear correlation between both variables and according to the high coefficient of determination (R^2=0.9991) this novel univariate linear mathematical model is well-suited to predict the particle size of the CBD-loaded LNCs prepared by the PIT method.

Importantly, as occurred with unloaded LNCs with different surfactants an oily phases, a comparison between the linear plots for the drug-loaded and blank LNCs can be drawn (Figure D2). On the one hand, there are not statistically significant differences in the Y-intercept, which means that the lower limit in particle size is

maintained after drug loading. On the other hand, we observe significant differences in the slopes ($p<0.01$): a steeper slope was achieved for the drug-loaded LNCs (b = 33.37), whereas the lower value corresponded to the blank LNCs (b = 28.16). This difference in the slopes of the linear plots can be attributed to shifts in the HLB value of the oily phase upon CBD addition that were also observed in terms of changes in the "phase inversion temperature" towards lower values (as evidenced from the shift in the point of inflection in the plot of conductivity against temperature shown in Figure D3). As a consequence, the size of CBD-loaded LNCs can likewise be accurately tailored.

Figure D2: Univariate linear regression between the volume diameter and the oil:surfactant ratio for CBD-loaded and blank LNCs (Labrafac WL1349®-Kolliphor HS15® tandem).

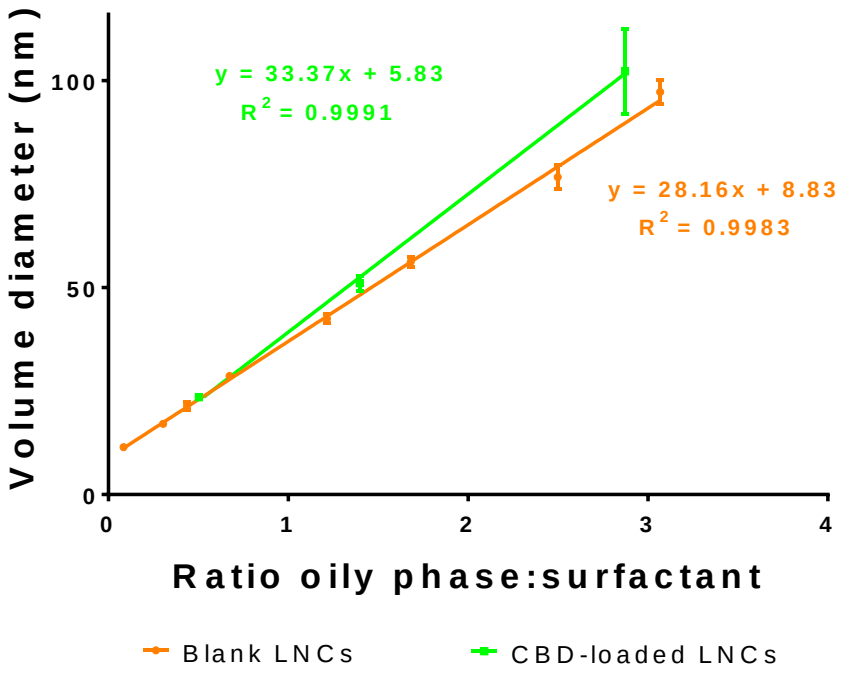

Interestingly, the encapsulation of CBD did not significantly alter the PdI of the LNCs in comparison with their blank counterparts (Figure 3.2.1 b, $p>0.05$). Moreover, in agreement with the hypothesized encapsulation within the oily core, no changes in the zeta potential profiles were evidenced (Figure 3.2.1 c-h): values close to neutrality with high profile width were obtained in all cases, as it might be expected from a shell made of a complex mixture of poly (ethoxylated) surfactants (namely, Kolliphor HS15®). Consistently, the width of the zeta potential distribution was progressively reduced with a decrease in the surfactant percentage (from the smallest (Figure 3.2.1 c-d) to the biggest LNCs (Fig. 3.2.1 g-h)).

The *in vitro* efficacy of CBD-loaded LNCs as extended-release carriers against the human glioblastoma cell line U373MG (the most prevalent and aggressive type of glioma) has been tested, along with the role played by the size of LNCs in CBD release and cytotoxicity. Blank LNCs have been used as controls for their CBD-loaded counterparts. As shown in Figure D4, none of the blank LNCs showed significant cytotoxicity against the U373MG cell line within the concentration range tested (cell

viability above 70% versus untreated cells according to the ISO 10993-5 Biological evaluation of medical devices, Part 5: Tests for in vitro cytotoxicity). Hence, all changes observed in the percentage of cell viability following treatment with CBD-loaded LNCs were attributed to the extent of CBD released from the LNCs at each time point.

Figure D3: Comparison of the conductivity against temperature for CBD-loaded and blank LNCs throughout the PIT method.

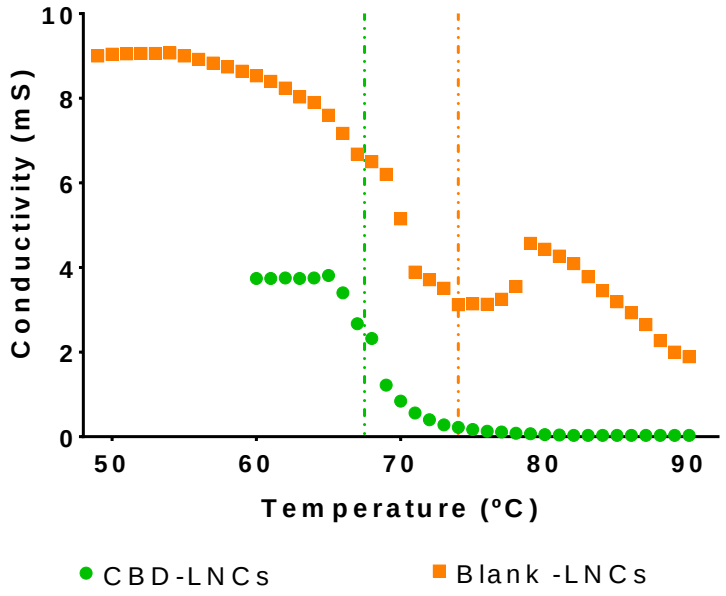

Figure D4: Cytotoxicity of blank LNCs against the U373MG cell line. (a) Cytotoxicity of 20 nm-sized blank LNCs after 48 (orange) and 96 hours (blue). (b) Cytotoxicity of 40 nm-sized blank LNCs after 48 (orange) and 96 hours (blue).

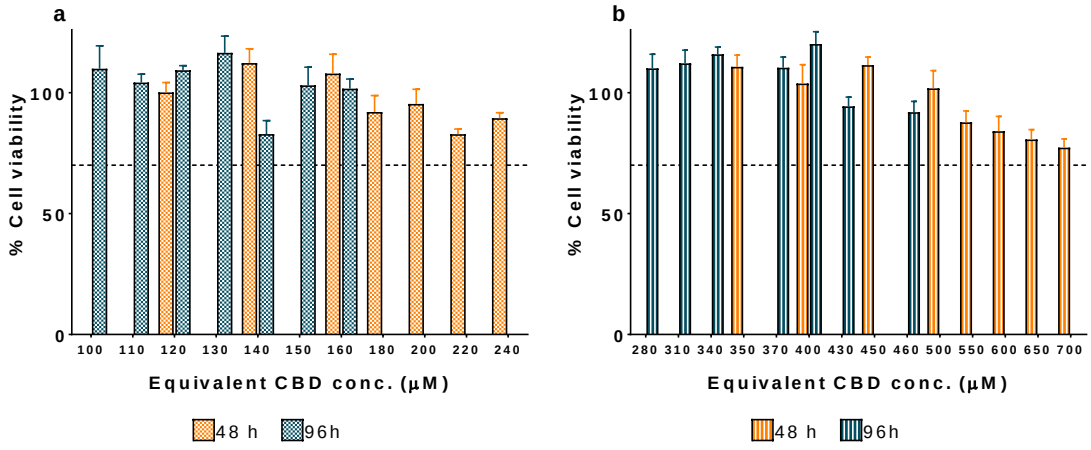

As shown in Figure 3.2.5, both free CBD and CBD-loaded LNCs reduced the viability of U373MG cells in a concentration-dependent manner, confirming thereby the *in vitro* antitumor effect of CBD against human glioblastoma.

Free CBD exhibited the strongest antiproliferative effect against the U373MG cells (Table 3.2.3), since free CBD, as a small molecule is readily available to be internalized by glioma cells, whereas encapsulated CBD must be first released from the oily core of LNCs to exert its cytotoxicity. Similar trends have recently been observed by other authors for other combinations of drug substances and carriers [35-37].

In particular, the size of LNCs played a pivotal role in the extent of CBD release: 20 nm-sized CBD-loaded LNCs reduced by 3.0-fold the IC_{50} value achieved with 50-nm sized CBD-loaded LNCs both after 48 (202.6 μM versus 615.4 μM) and 96 hours (129.1 μM versus 375.4 μM). Moreover, as deduced from the reduction in the IC_{50} values from 48 to 96 hours, both formulations continued to release CBD from their oily cores; accordingly, LNCs could serve as efficient prolonged-release carriers of CBD.

Hence, CBD-loaded LNCs are extended-release carriers with potential for the treatment of glioma. However, to be efficacious following intravenous administration, these carriers must be able to passage across the BBB to ultimately reach the tumor cells. Unfortunately, although the paracellular permeability of the brain endothelium is altered in most CNS diseases, this alteration only occurs substantially in advanced stages of disease and in the most affected areas [38, 39] .Therefore, efficient brain targeting of nanomedicines should not solely rely on passive targeting. To remedy this shortcoming, brain active targeting is being explored with the purpose of boosting transcellularly the delivery efficiency across the BBB [40].

Brain active targeting is based on the modification of nanocarriers with moieties capable of triggering receptor-mediated transcytosis into the CNS through specific binding with endogenous transporters overexpressed on the brain endothelium. Various receptors highly expressed on the cerebral endothelial cells have been utilized to develop brain active targeting strategies with the purpose of effectively improving the selective distribution across the BBB. However, the translational impact of brain active targeting in clinical trials remains modest, as only three actively-targeted liposomes have made their way to clinical trials for distinct brain conditions following intravenous administration (ClinicalTrials.gov identifiers: NCT01386580, NCT02048358 and NCT02340156). This is greatly due to the flaws that currently available targeting moieties have: on the one hand, the use of physiological ligands as targeting moieties can develop competitive phenomena with their endogenous counterparts and consequently dysregulate brain homeostasis; whereas on the other hand, the use of targeting peptides must ensure non-immunogenicity [41, 42]. Hence, research on novel exogenous non-immunogenic ligands for brain targeting has become a research hotspot.

Since any ligand for which a receptor exists on the cerebral endothelial cells may be potentially used for brain targeting, research on innovative exogenous non-immunogenic ligands are likely to thrive in the near future. In this regard, CBD has been postulated to bind to various receptors located on the brain endothelium environment, as detailed in Table D2. Hence, we hypothesized that this cannabinoid holds great promise for brain active targeting (Figure 2.0.1).

Table D2: Summary of the distinct receptors in the CNS environment to which CBD has been postulated to bind. CB_1: cannabinoid receptor type 1, CB_2: cannabinoid receptor type 2, 5-HT_{1A}: serotoninergic receptor, $TRPV_{1–2}$: transient potential vanilloid receptors, A_{2A}: adenosine receptor, GPR55: G-protein-coupled receptor 55, D_2: dopamine receptor.

Receptor	Activity	Ref.
CB_1	Negative allosteric modulator	[43]
CB_2	Negative allosteric modulator	[44]
5-$HT1_A$	Agonist	[45]
TRPV receptors	Agonist	[46]
Glycine receptor	Agonist	[47]
A_{2A}	Agonist	[48]
GPR55	Antagonist	[49]
D_2	Partial agonist	[50]

In particular, in the case of gliomas, the blood-brain tumor barrier (BBTB) closely resembles the non-fenestrated endothelium of healthy brain capillaries in low grade and along the infiltrative areas of high grade gliomas [51, 52]. As detailed in Table 2.0.1, some other receptors apart from those normally overexpressed on the brain endothelium can be used for active targeting of brain tumors. For instance, receptors that are overexpressed on tumor cells can be used to promote the selective distribution to glioma cells.

In this regard, the expression of some of the receptors to which the cannabinoids bind has been reported to be increased in glioma (namely, cannabinoid receptors 1 and 2 (CB_1 and CB_2) [53], transient potential vanilloid receptor type 2 (TRPV2) [46] and G-protein-coupled receptor 55 (GPR55 [54]). Therefore, we hypothesized that CBD can likewise act as a glioma-targeting molecule for nanocarriers.

Hence, we have introduced herein a pioneering strategy for brain tumor targeting with CBD under the assumption that, if existing, this double BBB- and glioma-targeting effect will ultimately enable a dual-targeting strategy for intravenous treatment of glioma to be designed. Dual-actively-targeted nanomedicines have already been designed to target simultaneously the BBB, the BBTB and the brain tumor cells by either attaching multiple targeting moieties [35, 36, 55, 56], or by conjugating a single ligand that targets both the brain endothelia and the brain tumor cells [57-59]. In broad terms, the preclinical studies with these dual-targeted nanomedicines have shown more extended survival times over their mono-targeted counterparts [35, 36, 56, 59]. The functionalization of LNCs with CBD is technologically described and characterized in detail in the third chapter of this dissertation due to formatting reasons. The evaluation of the potential of this active targeting strategy is addressed both in the second and third chapters: whereas the second chapter is devoted to exploring *in vitro* and *in vivo* its BBB-targeting efficiency, the third chapter focuses on the potential of this phytocannabinoid to target any of the cannabinoid receptors overexpressed in glioma cells. Since the transcytosis mechanisms that drive the distinct active targeting

strategies may follow a size-dependent pattern, the role played by the particle size of LNCs in the extent of targeting has concomitantly been evaluated in both chapters.

As detailed in the third chapter, preformed LNCs were functionalized with CBD at two different concentrations (2.5 and 5 mg/mL, respectively) following incubation with a CBD solution in methanol. As shown in Figure 2.2.S1, the incubation of LNCs with pure solvent did not contribute to any increase in particle size. Hence, all changes observed in the characterization of LNCs were attributed to the cannabinoid itself.

As enumerated in Table 3.2.2, we have achieved high binding efficiencies with this strategy of functionalization, which nearly doubled those achieved by [Balzeau13] with a targeting peptide following an analogous procedure. These results could be explained by the lower aqueous solubility of CBD than peptides, which ultimately favors its adsorption at the amphiphilic surfactant interface. The functionalization with CBD increased the particle size of blank LNCs (Figure 3.2.2a, $p<0.05$). This increase in the average volume diameter followed an inverse size-related pattern: the greatest percentage of size increase was observed with the smallest LNCs (75%) and vice versa (33% increase for medium-sized LNCs and 16% increase for the biggest LNCs). The higher specific surface area and the higher surfactant density at the particle interface of the smallest LNCs could account for this trend observed upon CBD functionalization. This analysis based on DLS data was highly corroborated with the particle sizes observed through transmission electron microscopy (TEM) for the different formulations (Figure 3.2.3 a, c, d, f, g, i). The PdIs in the smallest and medium-sized LNCs were significantly increased in comparison with their blank counterparts (Figure 3.2.2b, $p<0.01$). Furthermore, the zeta potential profiles of CBD-decorated LNCs were remarkably smoothed in comparison to the ones previously obtained both for blank and CBD-loaded LNCs (Figure 3.2.2 c-h versus Figure 3.2.1 c-h). These profiles are consistent with a shell dominated by a single entity instead of the former mixture of poly (ethoxylated) surfactants. Altogether, our results invariably support the superficial location of CBD on LNCs.

The BBB-targeting ability of this functionalization strategy, along with the role played by the particle size of LNCs in their BBB-transcytosis efficiency, has been evaluated in the second chapter of this thesis wherein cell viability, uptake and permeability experiments have been conducted with the human brain endothelial cell line hCMEC/D3. The results obtained with the *in vitro* cell-based BBB model have also been validated in the second chapter with *in vivo* biodistribution data in healthy mice.

The first cell viability experiment with differently-sized blank LNCs (20, 40 and 80-nm) at a normalized concentration of 10^{13} LNCs/mL (see Equation 2.2.4 for calculation) to determine the most suitable size of LNCs for conducting the uptake and permeability experiments evidenced a size-dependent toxicity pattern on hCMEC/D3 cells. Whereas none of the formulations of LNCs showed significant cytotoxicity after 1 hour (Figure 2.2.2a, $p>0.05$), 40-nm sized LNCs exhibited substantial toxicity at 24 hours and 80-nm sized started causing significant toxicity already at 4 hours (Figure 2.2.2a). This correlation between particle size and cytotoxic effect on cerebral endothelial cells had not been studied previously. Hence, we ruled out the most cytotoxic particle size against the hCMEC/D3 cells (namely, 80-nm sized LNCs).

In a subsequent cell viability experiment, we evaluated the cytotoxicity of 20-nm and 40-nm sized LNCs at an equivalent concentration of 110 μg of oily phase/mL of suspension to ultimately normalize the *in vitro* studies as a function of the different payloads. In particular, this payload for both uptake and permeability experiments has been the fluorescent dye 3,3'-dioctadecyloxacarbocyanine perchlorate (DiO). Remarkably, in this case no toxicity was observed for any of the LNCs at any time point (Figure 2.2.2b, $p>0.05$). Therefore, these two formulations at these non-toxic concentrations (that corresponded to an equivalent concentration of 1.65 μg of DiO/mL for the fluorescently-labeled LNCs) have been used for all subsequent *in vitro* experiments.

Hence, for *in vitro* particle tracking purposes, we have developed both undecorated and CBD-functionalized DiO-labeled LNCs. To prepare the dye-loaded LNCs, the fluorescent dye was firstly dissolved in the oily core of the LNCs at a weight ratio of 15 mg of dye/ g of Labrafac lipophile WL1349®. As shown in Figure 2.2.1, whereas the inclusion of the fluorescent dye did not significantly vary the size distribution of their blank counterparts (having obtained monodisperse 20 and 40 nm-sized DiO-labeled LNCs), the modification of dye-loaded LNCs with CBD increased the particle size from 20 to 40 nm and from 40 to 60 nm, respectively. This increase is in agreement with the size distribution observed for fluorescently-unlabeled CBD-decorated LNCs and was solely due to the presence of the cannabinoid. Therefore, on the one hand, the role played by particle size in the BBB targeting properties will be assessed separately in undecorated and in CBD-decorated fluorescently-labeled LNCs, and on the other hand, the influence of CBD-decoration will be evaluated for equally-sized LNCs so as to maintain all the variables constant except the one being studied in each case.

The *in vitro* BBB targeting efficiency of the different fluorescently-labeled LNCs has been quantified by flow cytometry. As shown in Figure 2.2.3a, the internalization of LNCs by the hCMEC/D3 cells followed a time-dependent pattern. Moreover, results consistently demonstrated a significantly higher BBB-targeting effect for smaller LNCs (Figures 2.2.3b and c,) and for CBD-decorated LNCs (Figure 2.2.3d). Importantly, the differences in the targeting effect achieved with the reduction in particle size and the functionalization with CBD were more significantly evidenced at 4 hours than at 24 hours. The images taken by confocal microscopy further evidenced qualitatively the efficient internalization of LNCs (Figure 2.2.4). In particular, the 3D reconstructions of the Z-stacks of these images executed with the IMARIS software support a perinuclear localization of the LNCs within the hCMEC/D3 cells (Figure D5).

For permeability experiments, the human brain endothelial cell line hCMEC/D3 was used as the *in vitro* BBB model given both their human origin (Table 2.1.5) and their better barrier properties in comparison with other commonly used cerebral endothelial cell lines [60]. Additionally, to enhance the differentiation of hCMEC/D3 cells into tighter monolayers, some strategies among those thoroughly discussed in the review article of chapter 2 (and summarized in Table 2.1.3) have been implemented to establish this *in vitro* BBB model. First, the filter surface has been coated with rat tail type I collagen and fibronectin to mimic the basal lamina, which *in vivo* contributes to

the development of a functional BBB. Secondly, culture media has been supplemented with hydrocortisone to upregulate the monolayer tightness. Thirdly, time in culture has been prolonged to accomplish a confluent monolayer, since it determines the extent of both tight junction formation and cell differentiation. Moreover, for all experiments, cells between passage 25 and 30 were used.

Figure D5: 3D reconstructions of the Z-stacks of confocal images executed with the IMARIS software: undecorated (left) and CBD-decorated DiO-labeled LNCs.

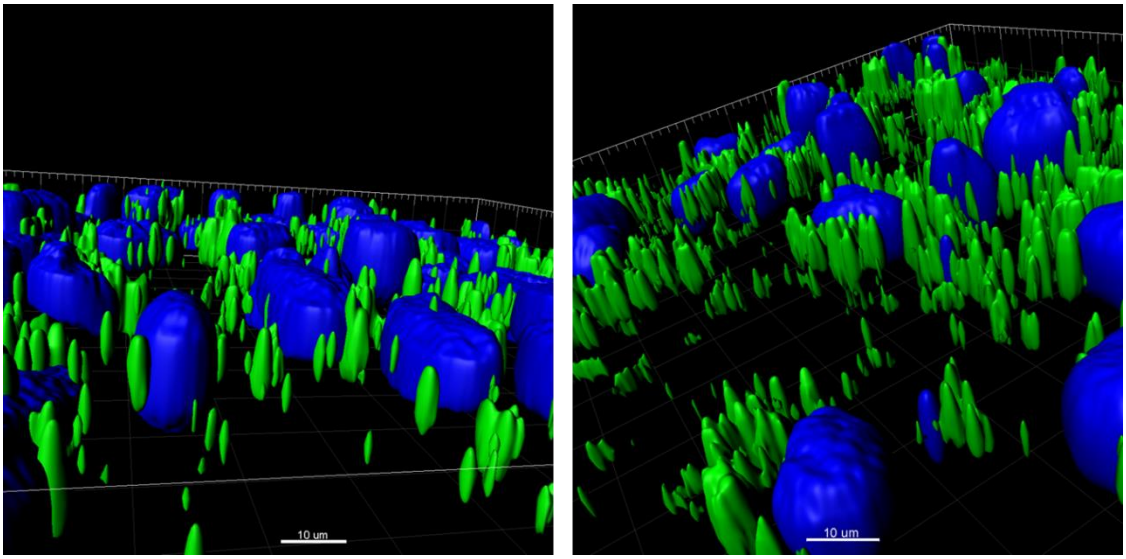

The monolayer integrity of the model was assessed by determining the permeability coefficient of the hydrophilic tracer tetramethyl-rhodamine-isothiocyanate–dextran (TRITC-dextran, MW 150 kDa) across the hCMEC/D3 monolayer both in the presence and the absence of LNCs to confirm that the nanocapsules themselves do not alter the barrier properties. For this experiment, the culture media was switched to DMEM without phenol red supplemented with 0.1% (v/v) FBS to avoid signal overlap with TRITC-dextran and ultimately enable permeability coefficients to be determined. The experiment was conducted in parallel in cell-seeded and non-seeded filters to take into account the contribution of the filter itself to the overall resistance to the passage of TRITC-dextran. The permeability coefficients have been calculated in each case using Equations 2.2.1 and 2.2.2, both of which have been deduced from first principles in the first article of chapter 2. The concentrations of TRITC-dextran in the basolateral compartment at the different time points have been used to evidence the linear region within which the permeability coefficients can be calculated (Figure D6).

Importantly, we have not observed any statistically significant differences between the calculated permeability coefficients of TRITC-dextran across the cell monolayer in the presence and the absence of LNCs (Figure 2.2.5b, $p>0.05$). Consequently, during the period evaluated, LNCs do not significantly alter the monolayer properties of hCMEC/D3 cells. These results ultimately demonstrated the integrity of the BBB model throughout the 24 hours that lasted the permeability experiments. As a result, the *in vitro* BBB model was suitable for evaluating the transport ability of the different LNCs.

Figure D6: Determination of the linear region in the clearance rate of TRITC-dextran across cell-seeded and non-seeded inserts both in the presence and the absence of blank LNCs.

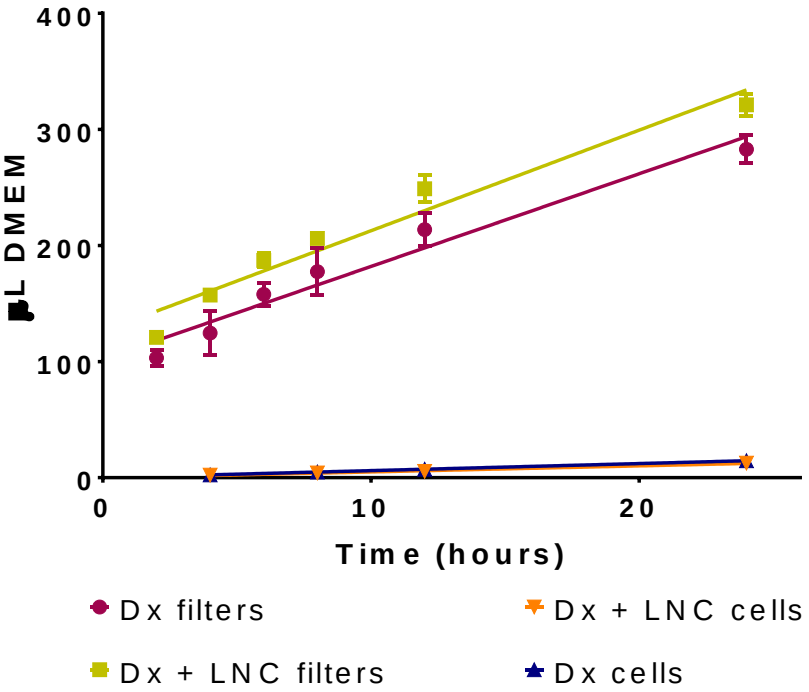

Hence, this *in vitro* BBB model with the hCMEC/D3 monolayer has been utilized to evaluate *in vitro* the BBB transcytosis ability of the different DiO-labeled LNCs. The BBB transcytosis efficiency of each formulation across the *in vitro* BBB model has been quantified with their permeability coefficients, which have been calculated similarly as described for TRITC-dextran. Only in those cases wherein less than 90% of the DiO dose was recovered between both apical and basolateral chambers, have we replaced Equation 2.2.1 by Equation 2.2.3 to take the retention factor (R) into account (as deduced from first principles in the first article of chapter 2).

The results from the permeability experiments are consistent with those obtained with uptake studies. On the one hand, the permeability coefficients across the endothelial monolayer are significantly higher for smaller LNCs (2.46-fold increase for undecorated LNCs and 2.48-fold increase for CBD-decorated LNCs as shown in Figures 2.2.6a and b, respectively). On the other hand, the functionalization with CBD also enhanced the permeability coefficients of LNCs in comparison with equally-sized undecorated LNCs by 4.32 fold (Figure 2.2.6c).

Importantly, we have calculated herein the permeability coefficient as a robust parameter that readily enables the comparison of the different transport efficiencies. This is not the case for the transport ratio expressed as percentage of passage across the endothelial monolayer. Although this ratio is being broadly utilized to express transport efficiencies [35, 36, 61-64], it varies with the different time points and does not take into account important experimental parameters such as the filter surface area or the volumes of the acceptor and the donor chambers to normalize the data. For this

reason, the efficiency of different brain active targeting strategies cannot be readily compared with transport ratios calculated as percentage.

The *in vitro* BBB-targeting and penetrating properties across the hCMEC/D3 monolayers have been validated with biodistribution studies in male ICR mice aging 4-5 weeks following intravenous administration via the tail vein of 150 μL of different fluorescently-labeled LNCs (Ref. PROEX 111/14 supplied as annex of this thesis). Although brain targeting efficiency has often been evaluated in pathophysiological models, given that BBB dysfunction only occurs in the most damaged brain regions, we aimed at evidencing targeting properties at earlier stages of the CNS diseases with biodistribution studies in healthy mice.

For *in vivo* experiments, we switched to the near-infrared dye 1,1′-dioctadecyl-3,3,3′,3′-tetramethylindodicarbocyanine 4-chlorobenzenesulfonate salt (DiD), as it is excited and emits within the wavelength window of 640−800 nm (namely, the wavelength range with the lowest absorption in tissue). Overall, the size distribution features of DiD-labeled LNCs were analogous to their DiO-labeled counterparts (Figure 2.2.1). Hence the same comparisons as those drawn *in vitro* to evaluate the role played by particle size and functionalization with cannabinoids in the extent of passage across the BBB have been made *in vivo*. We have determined the percentage of the injected dose of the different DiD-labeled LNCs located in each organ (namely, blood, brain, lungs, kidneys, heart, spleen and liver) to be able to draw comparisons with *in vivo* results reported by different authors.

The *in vivo* results 90 minutes after their intravenous injection strongly confirmed the auspicious results obtained with the *in vitro* BBB model as, on the one hand, a decrease in particle size yielded a higher transcytosis rate to brain (1.6-fold increase for unmodified LNCs and 2.5-fold increase for CBD-decorated LNCs, Figure 2.2.8a and b, respectively) and, on the other hand, the modification of LNCs with CBD showed higher brain targeting properties *in vivo* (2.5-fold increase for equally sized LNCs, Figure 2.2.8c). The increase in brain levels highly correlated with the higher available plasma concentration and lower recognition by the reticuloendothelial organs (liver and spleen) observed for these formulations (Figure 2.2.7).

The biodistribution of LNCs on a longer term (4 hours after administration) has also been assessed for the formulations that achieved the highest levels in plasma 90 minutes after administration. The percentage of the injected dose in blood and brain decreased with time, whereas the levels in the reticuloendothelial organs progressively augmented (Figures 2.2.9 and 2.2.10).

As discussed in the original research article in the second chapter hereof, a comparison with those scarce studies that explored the brain targeting properties of carriers within the here tested size range and expressed their results as percentage of the injected dose per gram of brain overall revealed brain levels in the same order as those obtained herein [65, 66]. In particular, in [65] the maximal percentage of injected dose per gram of brain tissue (slightly below 0.3% for the targeted nanocarrier) was accomplished at a much later time point (t_{max} around 24h) than the reported herein (0.6% of injected dose per gram of brain tissue at only 90 minutes following

intravenous injection). However, all these studies evaluated the biodistribution in glioma-bearing rodent models. Hence, whereas in our study only transcellular routes can be exploited for brain targeting, in the glioma-bearing models the transcellular routes can be supplemented with paracellular pathways across the blood-brain barrier to enhance the targeting properties (the extent of this contribution will highly depend on the disease stage). As a result, the evaluation of our nanocarrier system in an animal model of disease is expected to exhibit values even higher than those reported herein. Apart from that, Luo et al. had to utilize a double targeting strategy to achieve higher percentage of injected dose per gram of brain tumor [66]. More importantly, the enhancement in brain targeting achieved with the conjugation of CBD to LNCs with regards to nude nanocapsules outperformed the enhancement observed for the gluthatione functionalization strategy (not statistically significant) tested in a seminal study with healthy mice that laid the foundations for the G-Technology® (the main brain active strategy that have already entered clinical trials for the treatment of CNS diseases) [67].

The most likely mechanism of the observed brain targeting ability of CBD-decorated LNCs is receptor-mediated transcytosis across the brain endothelium [68]. As aforementioned, CBD binds to many receptors preferentially located at the CNS level, and among those, dopamine receptor has been postulated to specifically locate at the BBB and has recently started being tested as a potential receptor to mediate brain targeting of nanomedicines with exogenous ligands [36].

Altogether, the consistency between the *in vitro* and *in vivo* results served to validate our *in vitro* BBB model with the human brain endothelial cell line hCMEC/D3 as a versatile screening method to evaluate the passage of nanocarriers across the BBB that meets the high-throughput demands in the early stages of the development of a new drug product (Table 2.1.6) and lacks ethical constraints (Table 2.1.4). Noteworthy, *in vitro* BBB models may also serve in the future to verify batch-to-batch variability in terms of BBB permeation, a critical attribute for the regulation of nanomedicines to promote their translation to the market.

Analogously, the ability of the CBD functionalization strategy to target *in vitro* any of the cannabinoid receptors overexpressed in glioma cells, along with the role played by the particle size of LNCs in their glioma-targeting efficiency, has been evaluated in the third chapter wherein uptake experiments have been conducted with the human glioblastoma cell line U373MG. To this end, we have utilized the same undecorated and CBD-functionalized DiO-labeled LNCs used in chapter 2 (Figure 3.2.4).

The *in vitro* glioma targeting efficiency of the DiO-labeled LNCs has been quantified by flow cytometry. As shown in Figure 3.2.6, a decrease in particle size consistently yielded an increase in *in vitro* uptake by human glioblastoma cells (by 3.02-fold for undecorated LNCs (Figure 3.2.6a, $p<0.05$) and by 3.53-fold CBD-functionalized LNCs (Figure 3.2.6b, $p<0.001$) for CBD-modified LNCs. Moreover, the functionalization with CBD also enhanced the *in vitro* glioma targeting properties of LNCs, with a 3.37-fold increase over the fluorescence intensity from their equally-sized

undecorated counterparts (Figure 3.2.6c, $p<0.001$). The images taken by confocal microscopy further evidenced qualitatively the more efficient internalization of CBD-decorated LNCs (Figure 3.2.7). In particular, the Z-stacks from the maximal projections that have been shown in chapter 3 support the intracellular localization of the LNCs within the U373MG cells (Figure D7).

Figure D7: Confocal microscopy images of U373Mg after incubation with DiO-labeled undecorated (left series of images) and CBD-decorated LNCs (right series of images). The samples were optically sectioned in the x-y plane at regularly spaceddistances along the z-axis. The top images represent sections closest to the apical membrane and the bottom images represent the intracellular space toward the basolateral side.

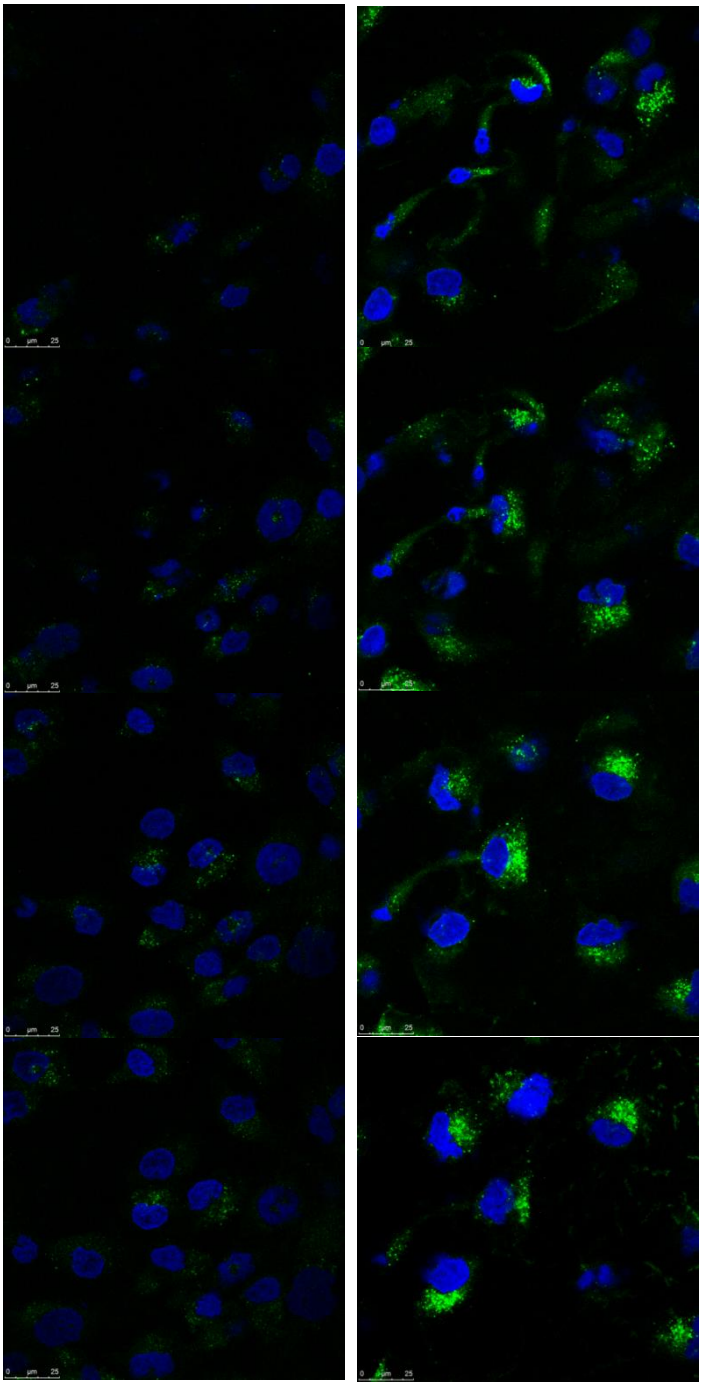

These auspicious *in vitro* glioma-targeting properties demonstrated for the CBD-functionalization strategy are in the same order of magnitude than those observed with other glioma targeting moieties [65, 66]. For instance, the aptamer AS1411 that binds to nucleolin, a protein overexpressed in highly proliferative cells yielded a 3-fold increase in *in vitro* glioma-targeting properties of poly glutamylglutamine nanoconjugates when tested in the human glioblastoma U87MG cell line [65]. With this same cell line, angiopep-2 (a targeting moiety currently in clinical trials for different brain tumor conditions that promotes receptor-mediated transcytosis across the low density lipoprotein receptor LRP1) enhanced the cellular uptake of poly (lactic-co-glycolic) acid nanoparticles by 3.6-fold [66]. Unlike angiopep-2, the non-peptide nature of CBD makes it less prone to cause immunogenicity. Interestingly, CBD performed better than other tested glioma-targeting moieties. In this regard, two different ligands of the transferrin receptor highly expressed in glioma cells yielded a 1.73-fold and 2.28-fold increase (for transferrin [69] and T7 peptide [70], respectively) in cellular uptake of liposomes and core-shell nanoparticles into the C6 and U87MG cell lines. Analogously, mannose as ligand targeting the glucose transporter only achieved a 1.18-fold increase in cellular uptake of liposomes into the rat glioma C6 cell line [69].

A comparison of the uptake experiments from chapters 2 and 3 with both cell lines (namely, hCMEC/D3 and U373MG) after 24 hours reveal that LNCs were internalized to a higher extent by the human glioblastoma cells as may be expected from the tumorigenic nature. Furthermore, the reduction in particle size was proven to be more relevant in glioma-targeting properties than in BBB-targeting properties (3.02 and 3.53-fold increase versus 1.76 and 2.03-fold increase, respectively; Figure D8). More interestingly, the functionalization with CBD was even more efficient as glioma-targeting than as BBB-targeting strategy (3.37-fold increase for U373MG cells versus 1.35-fold increase for hCMEC/D3 cells, Figure D8).

Lastly, given the enhancement in *in vitro* glioma-targeting properties of the CBD-decorated LNCs evidenced by flow cytometry and confocal microscopy, in the third chapter hereof, we have tested if the functionalization of CBD-loaded LNCs with CBD, with the ensuing enhanced internalization extent, could further reduce the IC_{50} values achieved for their undecorated counterparts. Similarly to what had occurred with blank and dye-loaded LNCs, the functionalization with CBD significantly increased the average volume diameter and the polydispersity index in comparison with their untargeted CBD-loaded LNCs counterparts (Figure 3.2.4). This time, the influence of CBD-decoration on the enhancement of the *in vitro* cytotoxicity of CBD-loaded LNCs has been tested for LNCs with the same volume of internal oily phase, wherefrom CBD is released over an extended timeframe. As shown in Figure 3.2.8, CBD-functionalized CBD-loaded LNCs outperformed the cytotoxicity of undecorated CBD-loaded LNCs against the U373MG cell line following 48 hours treatment (namely, in terms of IC_{50} values, 158.6 μM versus 202.6 μM and 513.2 μM versus 615.4 μM for the decorated versus unmodified LNCs for each of the two pairs of formulations tested, Table 3.2.3). These results can be accounted for by the differences in the drug release rate as a function of the distinct location of the CBD in each formulation. Whereas CBD-decorated LNCs exhibit part of the cannabinoid on their surface, and hence more prone to faster release due to the smaller distances for diffusion, undecorated CBD-loaded

LNCs have the totality of the drug encapsulated within the oily core, wherein CBD has higher solubility and calls for a longer distance for diffusion.

Figure D8: Comparison of the efficiency of particle size reduction and functionalization with CBD as strategies to enhance the BBB and glioma *in vitro* targeting properties of LNCs. *: p<0.05, **: p<0.01, ***: p<0.001.

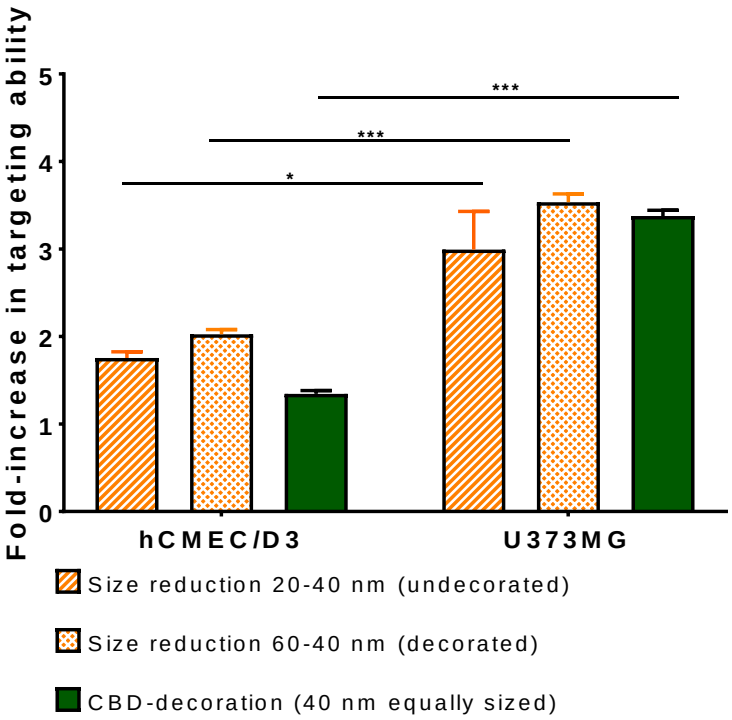

Altogether, all results from the present thesis are highly interrelated. On the one hand, it has been demonstrated that the BBB-transcytosis ability of LNCs follows a size-dependent pattern within the range 20-60 nm and so does their *in vitro* glioma targeting ability. Moreover, the size of LNCs plays a pivotal role in the extent of CBD release. Hence, both the BBB and glioma targeting ability and the drug release rate that ultimately leads to greater cytotoxicity can be tailored by varying the particle size of the LNCs. This is ultimately correlated with the fine size-tailoring of LNCs by the PIT method described in the first chapter. On the other hand, the functionalization of LNCs with CBD enhanced the *in vitro* glioma targeting properties and the functionalization of CBD-loaded LNCs further reduced the IC_{50} values. These results, added to the enhancement in BBB-targeting observed in chapter 2, make of the pioneering active targeting strategy with non-immunogenic and non-psychotropic CBD an auspicious dual-targeting strategy with great potential for intravenous treatment of glioma that deserves subsequent *in vivo* evaluation.

To conclude the present dissertation with an outline on future research directions within the field of the nanomedicine applied to the treatment of CNS neoplasms, in the fourth chapter hereof we have analyzed the possibilities that nanocarriers offer to achieve a personalized follow-up of brain tumors by means of theranostics, a research hotspot that integrates treatment with imaging diagnosis [71].

Firstly, simultaneous imaging and therapy could provide non-invasive monitoring of drug distribution and accumulation at the tumor site together with early feedback on disease progression to speed up triage of those patients most likely to respond to the treatment and to avoid overdosing non-responders[72].

Secondly, theranostics can provide a valuable platform for image-guided cancer therapy with unprecedented spatiotemporal control, because in novel physical stimulus-responsive therapies, an external stimulus must be applied locally to selectively activate the therapeutic agents in the tumorigenic area, thereby greatly reducing toxicity in healthy tissues [73, 74].

Thirdly, theranostics could also be beneficial in the intraoperative setting [75]. The imaging function of theranostics could help identify the boundaries between neoplastic and healthy tissue for complete surgical resection [76] and the therapeutic function of theranostics would serve to eradicate inoperable tumor margins.

References

[1] Silberberg D, Anand NP, Michels K, Kalaria RN. Brain and other nervous system disorders across the lifespan - global challenges and opportunities. Nature. 2015;527:S151-S4.

[2] Banks WA. From blood-brain barrier to blood-brain interface: new opportunities for CNS drug delivery. Nat Rev Drug Discov. 2016;15:275-92.

[3] Oberoi RK, Parrish KE, Sio TT, Mittapalli RK, Elmquist WF, Sarkaria JN. Strategies to improve delivery of anticancer drugs across the blood-brain barrier to treat glioblastoma. Neuro-Oncology. 2016;18:27-36.

[4] Tsou YH, Zhang XQ, Zhu H, Syed S, Xu XY. Drug Delivery to the Brain across the Blood-Brain Barrier Using Nanomaterials. Small. 2017;13:17.

[5] Zhou YQ, Peng ZL, Seven ES, Leblanc RM. Crossing the blood-brain barrier with nanoparticles. J Control Release. 2018;270:290-303.

[6] Kaushik A, Jayant RD, Bhardwaj V, Nair M. Personalized nanomedicine for CNS diseases. Drug discovery today. 2018;23:1007-15.

[7] Miranda A, Blanco-Prieto MJ, Sousa J, Pais A, Vitorino C. Breaching barriers in glioblastoma. Part II: Targeted drug delivery and lipid nanoparticles. Int J Pharm. 2017;531:389-410.

[8] Pan RH, Liu GQ, Li YS, Wei Y, Li SR, Tao L. Size-dependent endocytosis and a dynamic-release model of nanoparticles. Nanoscale. 2018;10:8269-74.

[9] Roger K. Nanoemulsification in the vicinity of phase inversion: Disruption of bicontinuous structures in oil/surfactant/water systems. Curr Opin Colloid Interface Sci. 2016;25:120-8.

[10] Morales D, Gutierrez JM, Garcia-Celma MJ, Solans YC. A study of the relation between bicontinuous microemulsions and oil/water nano-emulsion formation. Langmuir. 2003;19:7196-200.

[11] Anton N, Saulnier P. Adhesive water-in-oil nano-emulsions generated by the phase inversion temperature method. Soft Matter. 2013;9:6465-74.

[12] Anton N, Vandamme TF. The universality of low-energy nano-emulsification. Int J Pharm. 2009;377:142-7.

[13] Roger K, Cabane B, Olsson U. Formation of 10-100 nm Size-Controlled Emulsions through a Sub-PIT Cycle. Langmuir. 2010;26:3860-7.

[14] Morral-Ruiz G, Melgar-Lesmes P, Garcia ML, Solans C, Garcia-Celma MJ. Polyurethane and polyurea nanoparticles based on polyoxyethylene castor oil derivative surfactant suitable for endovascular applications. Int J Pharm. 2014;461:1-13.

[15] Elgammal M, Schneider R, Gradzielski M. Preparation of latex nanoparticles using nanoemulsions obtained by the phase inversion composition (PIC) method and their application in textile printing. Colloid Surf A-Physicochem Eng Asp. 2015;470:70-9.

[16] Hare JI, Lammers T, Ashford MB, Puri S, Storm G, Barry ST. Challenges and strategies in anti-cancer nanomedicine development: An industry perspective. Adv Drug Deliv Rev. 2017;108:25-38.

[17] Anton N, Gayet P, Benoit JP, Saulnier P. Nano-emulsions and nanocapsules by the PIT method: An investigation on the role of the temperature cycling on the emulsion phase inversion. Int J Pharm. 2007;344:44-52.

[18] Malzert-Freon A, Saint-Lorant G, Hennequin D, Gauduchon P, Poulain L, Rault S. Influence of the introduction of a solubility enhancer on the formulation of lipidic nanoparticles with improved drug loading rates. Eur J Pharm Biopharm. 2010;75:117-27.

[19] Klassen PL, George Z, Warwick J, Georgiadou S. PIT tuning effects of hydrophobic co-surfactants and drugs. Colloid Surf A-Physicochem Eng Asp. 2014;455:1-10.

[20] Anton N, Benoit JP, Saulnier P. Design and production of nanoparticles formulated from nano-emulsion templates - A review. J Control Release. 2008;128:185-99.

[21] Gupta A, Eral HB, Hatton TA, Doyle PS. Nanoemulsions: formation, properties and applications. Soft Matter. 2016;12:2826-41.

[22] Rahn-Chique K, Puertas AM, Romero-Cano MS, Rojas C, Urbina-Villalba G. Nanoemulsion stability: Experimental evaluation of the flocculation rate from turbidity measurements. Adv Colloid Interface Sci. 2012;178:1-20.

[23] Koroleva M, Nagovitsina T, Yurtov E. Nanoemulsions stabilized by non-ionic surfactants: stability and degradation mechanisms. Phys Chem Chem Phys. 2018;20:10369-77.

[24] Singh Y, Meher JG, Raval K, Khan FA, Chaurasia M, Jain NK, et al. Nanoemulsion: Concepts, development and applications in drug delivery. J Control Release. 2017;252:28-49.

[25] Louis DN, Perry A, Reifenberger G, von Deimling A, Figarella-Branger D, Cavenee WK, et al. The 2016 World Health Organization Classification of Tumors of the Central Nervous System: a summary. Acta Neuropathol. 2016;131:803-20.

[26] Alifieris C, Trafalis DT. Glioblastoma multiforme: Pathogenesis and treatment. Pharmacol Ther. 2015;152:63-82.

[27] del Burgo LS, Hernandez RM, Orive G, Pedraz JL. Nanotherapeutic approaches for brain cancer management. Nanomed-Nanotechnol Biol Med. 2014;10:905-19.

[28] Ganipineni LP, Danhier F, Preat V. Drug delivery challenges and future of chemotherapeutic nanomedicine for glioblastoma treatment. J Control Release. 2018;281:42-57.

[29] Velasco G, Hernandez-Tiedra S, Davila D, Lorente M. The use of cannabinoids as anticancer agents. Prog Neuro-Psychopharmacol Biol Psychiatry. 2016;64:259-66.

[30] Fowler CJ. Delta(9)-Tetrahydrocannabinol and Cannabidiol as Potential Curative Agents for Cancer: A Critical Examination of the Preclinical Literature. Clin Pharmacol Ther. 2015;97:587-96.

[31] Andre CM, Hausman JF, Guerriero G. Cannabis sativa: The Plant of the Thousand and One Molecules. Front Plant Sci. 2016;7:17.

[32] Russo EB. Beyond Cannabis: Plants and the Endocannabinoid System. Trends Pharmacol Sci. 2016;37:594-605.

[33] Pisanti S, Malfitano AM, Ciaglia E, Lamberti A, Ranieri R, Cuomo G, et al. Cannabidiol: State of the art and new challenges for therapeutic applications. Pharmacology & therapeutics. 2017;175:133-50.

[34] Holgado MA, Martin-Banderas L, Alvarez-Fuentes J, Fernandez-Arevalo M. Neuroprotective effect of cannabinoids nanoplatforms in neurodegenerative diseases. J Drug Deliv Sci Technol. 2017;42:84-93.

[35] Chen CT, Duan ZQ, Yuan Y, Li RX, Pang L, Liang JM, et al. Peptide-22 and Cyclic RGD Functionalized Liposomes for Glioma Targeting Drug Delivery Overcoming BBB and BBTB. ACS Appl Mater Interfaces. 2017;9:5864-73.

[36] Belhadj Z, Ying M, Cao X, Hu XF, Zhan CY, Wei XL, et al. Design of Y-shaped targeting material for liposome-based multifunctional glioblastoma-targeted drug delivery. J Control Release. 2017;255:132-41.

[37] Wei XL, Gao J, Zhan CY, Xie C, Chai ZL, Ran D, et al. Liposome-based glioma targeted drug delivery enabled by stable peptide ligands. J Control Release. 2015;218:13-21.

[38] Liebner S, Dijkhuizen RM, Reiss Y, Plate KH, Agalliu D, Constantin G. Functional morphology of the blood-brain barrier in health and disease. Acta Neuropathol. 2018;135:311-36.

[39] Sweeney MD, Sagare AP, Zlokovic BV. Blood-brain barrier breakdown in Alzheimer disease and other neurodegenerative disorders. Nat Rev Neurol. 2018;14:133-50.

[40] Bertrand N, Wu J, Xu XY, Kamaly N, Farokhzad OC. Cancer nanotechnology: The impact of passive and active targeting in the era of modern cancer biology. Adv Drug Deliv Rev. 2014;66:2-25.

[41] Oller-Salvia B, Sanchez-Navarro M, Giralt E, Teixido M. Blood-brain barrier shuttle peptides: an emerging paradigm for brain delivery. Chem Soc Rev. 2016;45:4690-707.

[42] Peluffo H, Unzueta U, Negro-Demontel ML, Xu ZK, Vaquez E, Ferrer-Miralles N, et al. BBB-targeting, protein-based nanomedicines for drug and nucleic acid delivery to the CNS. Biotechnol Adv. 2015;33:277-87.

[43] Laprairie RB, Bagher AM, Kelly MEM, Denovan-Wright EM. Cannabidiol is a negative allosteric modulator of the cannabinoid CB1 receptor. Br J Pharmacol. 2015;172:4790-805.

[44] Martinez-Pinilla E, Varani K, Reyes-Resina I, Angelats E, Vincenzi F, Ferreiro-Vera C, et al. Binding and Signaling Studies Disclose a Potential Allosteric Site for Cannabidiol in Cannabinoid CB2 Receptors. Front Pharmacol. 2017;8:10.

[45] Espejo-Porras F, Fernandez-Ruiz J, Pertwee RG, Mechoulam R, Garcia C. Motor effects of the non-psychotropic phytocannabinoid cannabidiol that are mediated by 5-HT1A receptors. Neuropharmacology. 2013;75:155-63.

[46] Nabissi M, Morelli MB, Amantini C, Liberati S, Santoni M, Ricci-Vitiani L, et al. Cannabidiol stimulates Aml-1a-dependent glial differentiation and inhibits glioma

stem-like cells proliferation by inducing autophagy in a TRPV2-dependent manner. Int J Cancer. 2015;137:1855-69.

[47] Xiong W, Cui TX, Cheng KJ, Yang F, Chen SR, Willenbring D, et al. Cannabinoids suppress inflammatory and neuropathic pain by targeting alpha 3 glycine receptors. J Exp Med. 2012;209:1121-34.

[48] Mecha M, Feliu A, Inigo PM, Mestre L, Carrillo-Salinas FJ, Guaza C. Cannabidiol provides long-lasting protection against the deleterious effects of inflammation in a viral model of multiple sclerosis: A role for A(2A) receptors. Neurobiol Dis. 2013;59:141-50.

[49] Sylantyev S, Jensen TP, Ross RA, Rusakov DA. Cannabinoid- and lysophosphatidylinositol-sensitive receptor GPR55 boosts neurotransmitter release at central synapses. Proc Natl Acad Sci U S A. 2013;110:5193-8.

[50] Seeman P. Cannabidiol is a partial agonist at dopamine D2High receptors, predicting its antipsychotic clinical dose. Transl Psychiatr. 2016;6:4.

[51] Sarkaria JN, Hu LS, Parney IF, Pafundi DH, Brinkmann DH, Laack NN, et al. Is the blood-brain barrier really disrupted in all glioblastomas? A critical assessment of existing clinical data. Neuro-Oncology. 2018;20:184-91.

[52] van Tellingen O, Yetkin-Arik B, de Gooijer MC, Wesseling P, Wurdinger T, de Vries HE. Overcoming the blood-brain tumor barrier for effective glioblastoma treatment. Drug Resist Update. 2015;19:1-12.

[53] Wu XY, Han LJ, Zhang XL, Li L, Jiang CZ, Qiu Y, et al. Alteration of endocannabinoid system in human gliomas. J Neurochem. 2012;120:842-9.

[54] Andradas C, Caffarel MM, Perez-Gomez E, Salazar M, Lorente M, Velasco G, et al. The orphan G protein-coupled receptor GPR55 promotes cancer cell proliferation via ERK. Oncogene. 2011;30:245-52.

[55] Kim JS, Shin DH, Kim JS. Dual-targeting immunoliposomes using angiopep-2 and CD133 antibody for glioblastoma stem cells. J Control Release. 2018;269:245-57.

[56] Wang XZ, Zhang Q, Lv LY, Fu JJ, Jiang Y, Xin HL, et al. Glioma and microenvironment dual targeted nanocarrier for improved antiglioblastoma efficacy. Drug Deliv. 2017;24:1401-9.

[57] Jiang XY, Xin HL, Ren QY, Gu JJ, Zhu LJ, Du FY, et al. Nanoparticles of 2-deoxy-D-glucose functionalized poly(ethylene glycol)-co-poly(trimethylene carbonate) for dual-targeted drug delivery in glioma treatment. Biomaterials. 2014;35:518-29.

[58] Hu JG, Zhang X, Wen ZH, Tan Y, Huang N, Cheng S, et al. Asn-Gly-Arg-modified polydopamine-coated nanoparticles for dual-targeting therapy of brain glioma in rats. Oncotarget. 2016;7:73681-96.

[59] Kang T, Zhu QQ, Jiang D, Feng XY, Feng JX, Jiang TZ, et al. Synergistic targeting tenascin C and neuropilin-1 for specific penetration of nanoparticles for anti-glioblastoma treatment. Biomaterials. 2016;101:60-75.

[60] Toman P, Lien CF, Ahmad Z, Dietrich S, Smith JR, An Q, et al. Nanoparticles of alkylglyceryl-dextran-graft-poly(lactic acid) for drug delivery to the brain: Preparation and in vitro investigation. Acta Biomaterialia. 2015;23:250-62.

[61] Cui Y, Zhang M, Zeng F, Jin HY, Xu Q, Huang YZ. Dual-Targeting Magnetic PLGA Nanoparticles for Codelivery of Paclitaxel and Curcumin for Brain Tumor Therapy. ACS Appl Mater Interfaces. 2016;8:32159-69.

[62] Byeon HJ, Thao LQ, Lee S, Min SY, Lee ES, Shin BS, et al. Doxorubicin-loaded nanoparticles consisted of cationic- and mannose-modified-albumins for dual-targeting in brain tumors. J Control Release. 2016;225:301-13.

[63] Huang YK, Liu WC, Gao F, Fang XL, Chen YZ. c(RGDyK)-decorated Pluronic micelles for enhanced doxorubicin and paclitaxel delivery to brain glioma. Int J Nanomed. 2016;11:1629-41.

[64] Su CH, Tsai CY, Tomanek B, Chen WY, Cheng FY. Evaluation of blood-brain barrier-stealth nanocomposites for in situ glioblastoma theranostics applications. Nanoscale. 2016;8:7866-70.

[65] Luo ZM, Yan ZQ, Jin K, Pang Q, Jiang T, Lu H, et al. Precise glioblastoma targeting by AS1411 aptamer-functionalized poly (L-gamma-glutamylglutamine)-paclitaxel nanoconjugates. J Colloid Interface Sci. 2017;490:783-96.

[66] Luo ZM, Jin K, Pang Q, Shen S, Yan ZQ, Jiang T, et al. On-Demand Drug Release from Dual-Targeting Small Nanoparticles Triggered by High-Intensity Focused Ultrasound Enhanced Glioblastoma-Targeting Therapy. ACS Appl Mater Interfaces. 2017;9:31612-25.

[67] Gaillard PJ, Appeldoorn CCM, Dorland R, van Kregten J, Manca F, Vugts DJ, et al. Pharmacokinetics, Brain Delivery, and Efficacy in Brain Tumor-Bearing Mice of Glutathione Pegylated Liposomal Doxorubicin (2B3-101). PLoS One. 2014;9:10.

[68] Bih CI, Chen T, Nunn AVW, Bazelot M, Dallas M, Whalley BJ. Molecular Targets of Cannabidiol in Neurological Disorders. Neurotherapeutics. 2015;12:699-730.

[69] Ying X, Wen H, Lu WL, Du J, Guo J, Tian W, et al. Dual-targeting daunorubicin liposomes improve the therapeutic efficacy of brain glioma in animals. J Control Release. 2010;141:183-92.

[70] Wei L, Guo XY, Yang T, Yu MZ, Chen DW, Wang JC. Brain tumor-targeted therapy by systemic delivery of siRNA with Transferrin receptor-mediated core-shell nanoparticles. Int J Pharm. 2016;510:394-405.

[71] Overchuk M, Zheng G. Overcoming obstacles in the tumor microenvironment: Recent advancements in nanoparticle delivery for cancer theranostics. Biomaterials. 2018;156:217-37.

[72] Mura S, Couvreur P. Nanotheranostics for personalized medicine. Adv Drug Deliv Rev. 2012;64:1394-416.

[73] Chen Q, Ke HT, Dai ZF, Liu Z. Nanoscale theranostics for physical stimulus-responsive cancer therapies. Biomaterials. 2015;73:214-30.

[74] Terreno E, Uggeri F, Aime S. Image guided therapy: The advent of theranostic agents. J Control Release. 2012;161:328-37.

[75] Rutka JT, Kim B, Etame A, Diaz RJ. Nanosurgical Resection of Malignant Brain Tumors: Beyond the Cutting Edge. ACS Nano. 2014;8:9716-22.

[76] Xu HL, Yang JJ, Zhuge DL, Lin MT, Zhu QY, Jin BH, et al. Glioma-Targeted Delivery of a Theranostic Liposome Integrated with Quantum Dots, Superparamagnetic Iron Oxide, and Cilengitide for Dual-Imaging Guiding Cancer Surgery. Adv Healthc Mater. 2018;7:18.

Conclusions

1. Diseases affecting the central nervous system (CNS) are a major health challenge due to their steadily rising incidences and to the presence of the blood-brain barrier (BBB) that truly hinders brain drug delivery. Therefore, there is a dire need for developing effective brain drug delivery strategies. In this context, intravenously-administered lipid-based nanomedicines have already reached clinical trials for the treatment of CNS diseases. However, the empirical development of delivery systems and later assignment to an existing clinical challenge has led to high attrition rates in clinical trials. Alternatively, a disease-driven rational approach, whereby the nanomedicine features are carefully designed on the basis of the pathophysiology of a specific disease is more likely to succeed.

2. Since particle size certainly influences the *in vivo* behavior, rational disease-driven design of nanocarriers can only be achieved with the ascertainment of the parameters that accurately control their size distribution. Lipid nanocapsules (LNCs) are auspicious candidates for disease-driven tailoring as their particle size can be accurately predicted by a validated linear univariate mathematical model as a function of the oily phase: surfactant ratio for various oily phase-surfactant combinations. In particular, there exists a lower limit of particle size to be predicted (10 nm) and the slope of the linear model correlates with the affinity between the poly-ethoxylated surfactants and the triglycerides utilized as oily phase: the closer the HLB affinity between them, the lower the slope. Importantly, this univariate mathematical model serves to obtain not only size-tailored blank LNCs but also drug-loaded LNCs. The phase inversion temperature (PIT) method whereby LNCs are prepared can be carried out in a single-step, as only one temperature cycle is required for their formation, with the ensuing potential for industrial manufacturing. Moreover, the LNCs are kinetically stable in suspension against the main breakdown mechanisms over six months both at 25ºC and at 4ºC regardless of the oil: surfactant mass ratio.

3. Although the paracellular permeability of the brain endothelium is altered in most CNS diseases, the BBB disruption is only substantial in advanced stages of disease and in the most affected areas. Therefore, brain targeting of nanomedicines should not solely rely on passive targeting. Brain active targeting seeks to boost

transcellularly the delivery efficiency across the BBB. Hence, the BBB permeability of targeted nanomedicines is a key ADME feature and researchers have been endeavoring to develop *in vitro* screening methods that reliably predict the *in vivo* BBB permeability of nanomedicines to early triage the most promising targeting strategies. In this regard, the permeability coefficient calculated in *in vitro* BBB models is a robust parameter that enables readily comparisons among different transport strategies. The *in vitro* BBB model with the human cerebral endothelial cell line hCMEC/D3 has been designed and validated with *in vivo* data as a versatile screening method to evaluate the passage of nanocarriers across the BBB. This *in vitro* model meets the high-throughput demands in the early stages of drug discovery and lacks ethical constraints.

4. The BBB-transcytosis ability of LNCs follows a size-dependent pattern within the range 20-60 nm. Moreover, cannabidiol (CBD), the major non-psychotropic phytocannabinoid, represents a pioneering non-immunogenic BBB-targeting molecule for LNCs. As a proof of it, the smallest LNCs functionalized with CBD consistently exhibit the highest BBB-targeting ability both in permeability experiments across the hCMEC/D3 monolayer and in biodistribution experiments in healthy mice. In particular, on the one hand, a decrease in the particle size of LNCs yielded a 2.5- and 1.6-2.5--fold higher transcytosis rate across the BBB *in vitro* and *in vivo*, respectively and, on the other hand, the functionalization of LNCs with CBD increased the brain targeting properties by 4.3- and 2.5-fold *in vitro* and *in vivo*, respectively.

5. Malignant brain tumors are the best archetype of brain disorders that could take great advantage of LNCs. In the search for novel antitumor agents, the therapeutic potential of several cannabinoids, traditionally constrained due to their strong psychoactive properties and their high lipophilicity, has become a research hotspot. Hence, precisely due to the lack of psychoactive effects, CBD is the lead cannabinoid that can profit from nanomedicine-based formulation strategies for the treatment of gliomas. LNCs can encapsulate CBD at high drug loading within their oily core and act as extended-release carriers for this cannabinoid with *in vitro* activity against the human glioblastoma cell line U373MG. The size of LNCs plays a pivotal role in the extent of CBD release: 20 nm-sized CBD-loaded LNCs reduce by 3.0-fold the IC_{50} value achieved with 50-nm sized CBD-loaded LNCs both after 48 and 96 hours.

6. The *in vitro* glioma targeting ability of LNCs also follows a size-dependent pattern within the range 20-60 nm. Analogously, CBD enhances the active targeting of LNCs to glioma cells. As a proof of it, the smallest LNCs functionalized with CBD consistently exhibit the highest glioma-targeting ability in uptake experiments with the human glioblastoma cell line U373MG, the most prevalent and aggressive type of malignant brain tumor. In particular, on the one hand, a decrease in particle size yields an increase in *in vitro* uptake by human glioblastoma cells (by 3.0-fold for undecorated LNCs and by 3.5-fold for CBD-decorated LNCs) and on the other hand, the functionalization of LNCs with CBD enhances the *in vitro* glioma targeting properties by 3.4-fold in comparison with their equally-sized unmodified counterparts. These in vitro glioma-targeting properties are in the same order of magnitude of other targeting strategies that have already reached the clinical trials stage.

7. Given the extremely heterogeneous nature of malignant brain tumors, the assumption that a single therapy could be beneficial for all patients is no longer plausible. At best, each treatment would only be effective for certain target populations at certain stages of disease. In this context, at the intersection between imaging and therapy, theranostic nanomedicine holds tremendous promise for tracking tumor responses to treatment and for guiding stimulus-activated therapies and surgical resection of malignant brain tumors to ultimately help tailor therapies to each patient's individual needs. Currently, magnetic nanoparticles exploiting brain targeting strategies represent the first generation of preclinical theranostic nanomedicines for the personalized management of malignant brain tumors.

8. Altogether, the results presented herein serve to envisage LNCs, prepared by the PIT method and loaded with CBD in their oily core and functionalized with CBD on their surface, as auspicious dually-targeted candidates for intravenous treatment of glioma. Consequently, they deserve subsequent *in vivo* evaluation in an animal model of disease. In particular, both the BBB and glioma targeting ability and the drug release rate can be tailored by varying the particle size of LNCs. This fine size-tailoring of LNCs can be achieved by the PIT method to increase the chances of success in the development of nanomedicines for the treatment of CNS diseases.

Abbreviations

Abbreviation	Meaning	Abbreviation	Meaning
AMT	.Adsorptive-mediated transcytosis	IGF	Insulin growth factor
BBB	Blood-brain barrier	LNC	Lipid nanocapsule
BBTB	Blood-brain tumor barrier	MGMT	O6-methylguanine-DNA methyltransferase
BCNU	Carmustine	MRI	Magnetic resonance imaging
CBD	Cannabidiol	MTT	3-(4,5-dimethyl-2-thiazolyl)-2,5-diphenyl-2H-tetrazolium bromide
CCNU	Lomustine	MWCO	Molecular weight cut-off
CED	Convection-enhanced delivery	NIR	Near-infrared dye
CNS	Central nervous system	PAMPA	Parallel Artificial Membrane Permeability Assay
CSF	Cerebrospinal fluid	PdI	Polydispersity index
DAPI	4′,6-Diamidino-2-phenylindole dihydrochloride	PDT	Photodynamic therapy
DC	Drug content	PEG	Polyethylene glycol
DiD	1,1′-dioctadecyl-3,3,3′,3′-tetramethy-lindodicarbocyanine 4-chloro-benzene-sulfonate salt	PET	Positron-emission tomography
DiO	3,3'-dioctadecyl-oxa-carbocyanine perchlorate	PIC	Phase inversion composition
DLS	Dynamic light scattering	PIT	Phase inversion temperature
DMEM	Dulbecco's Modified Eagle Medium	PTT	Photothermal therapy
DMSO	Dimethyl-sulfoxide	RES	Reticulo-endothelial system
EBM	Endothelial Cell Basal Medium	RMT	Receptor-mediated transcytosis
EGF	Epidermal growth factor	SD	Standard deviation

Abbreviation	Meaning	Abbreviation	Meaning
EGFR	Epidermal growth factor receptor	SEM	Standard error of the mean
EPR	Enhanced permeability and retention	TEER	Transendothelial electrical resistance
FBS	Foetal bovine serum	TEM	Transmission electron microscopy
FDA	Food and Drug Administration	TRPV	Transient potential vanilloid receptor
FGF	Fibroblast growth factor	THC	Tetrahydrocannabinol
GBM	Glioblastoma multiforme	TRITC	Tetramethyl-rhodamine-isothiocyanate
GPR55	G protein-coupled receptor 55	UWL	Unstirred water layer
HBSS	Hank's Balanced Salt Solution	VEGF	Vascular endothelial growth factor
HLB	Hydrophilic-lipophilic balance	WHO	World Health Organisation
IE	Incorporation efficiency		

Annex

Dirección General del Medio Ambiente
CONSEJERÍA DE MEDIO AMBIENTE
Y ORDENACIÓN DEL TERRITORIO
Comunidad de Madrid

REGISTRO DE SALIDA
Ref:10/171413.9/14 Fecha:17/07/2014 15:12
Cons. Medio Ambiente y Orden. Territorio
Reg C.Medio Amb.y Ord.T.(ALC)
Destino: Ana Isabel Torres Suárez

Vista la solicitud presentada por ANA ISABEL TORRES SUÁREZ, para la autorización del proyecto de memoria técnica titulada NANOPARTICULAS POLIMERICAS Y LIPIDICAS FUNCIONALIZADAS PARA EL TRATAMITENO DE ENFERMEDADES EN EL SISTEMA NERVIOSO CENTRAL: a desarrollar en el centro usuario UNIVERSIDAD COMPLUTENSE DE MADRID con código de registro ES280790000086 y siendo el responsable del proyecto ANA ISABEL TORRES SUÁREZ.

Visto el informe del Área de Protección Animal.

Considerando que el citado proyecto se ajusta a lo establecido en el Real Decreto 53/2013 de 1 de febrero por el que se establecen las normas básicas aplicables para la protección de los animales utilizados en experimentación y otros fines científicos, incluyendo la docencia.

Esta Dirección General ha resuelto: autorizar la realización del proyecto referenciado siempre que se mantengan las condiciones que dieron lugar a la autorización y que el personal que intervenga tenga la preparación y formación adecuada que se especifica en el citado Real Decreto.

Tal y como se establece en el informe de evaluación aportado, este proyecto no deberá ser sometido a la realización de una evaluación retrospectiva.

La presente Resolución no pone fin a la vía administrativa y contra la misma podrá interponer recurso de Alzada en el plazo de un mes a partir del día siguiente al de la recepción de esta notificación, ante el Consejero de Medio Ambiente y Ordenación del Territorio (C/ Alcalá 16, 28014 Madrid), o ante el Director General del Medio Ambiente (C/ Alcalá 16, 28014 Madrid), o en cualquiera de las formas previstas en el artículo 38.4 de la Ley 30/1992, de Régimen Jurídico de las Administraciones Públicas y del Procedimiento Administrativo Común de conformidad con lo previsto en los artículos 107, 114 y 115 de dicha Ley.

Madrid, 14 de julio de 2014.
EL DIRECTOR GENERAL DEL MEDIO AMBIENTE

Fdo.: Ricardo Riquelme y Sánchez de la Viña.

Ref PROEX 111/14